Synthesis, Characterization, and Micellar Properties of Dendritic Amphiphiles

Richard Vincent Macri

Dissertation submitted to the faculty of the Virginia Polytechnic Institute and State University in partial fulfillment of the requirements for the degree of

Doctor of Philosophy

In

Chemistry

Richard D. Gandour, Committee Chair
Paul R. Carlier
David G.I. Kingston
Timothy E. Long
James M. Tanko

May 6, 2009
Blacksburg, VA 24061

Keywords: amphiphile, CMC, critical micelle concentration, pendent drop, surfactant

Synthesis, Characterization, and Micellar Properties of Dendritic Amphiphiles

Richard Vincent Macri

ABSTRACT

Two new homologous series of amphiphiles—five long-chain, three-headed amphiphiles [**3CCb14, 3CCb16, 3CCb18, 3CCb20, 3CCb22**; $CH_3(CH_2)_{n-1}OCONHC(CH_2CH_2COOH)_3$, **n** = 14, 16, 18, 20, 22], and six branched-chain, three-headed amphiphiles [**3CCb1(7,7), 3CCb1(8,8), 3CCb1(9,9), 3CCb1(10,10), 3CCb1(11,11), 3CCb1(12,12)**; $(CH_3(CH_2)_{n-1})_2CHOCONHC(CH_2CH_2COOH)_3$, **n** = 7, 8, 9, 10, 11, 12]—were synthesized. The synthesis of the **3CCbn** series was accomplished in two steps from Weisocyanate™ and the long chain alcohol in good yields of chromatographed products (65–81%). The **3CCb1(n,n)** series was similarly synthesized from Weisocyanate™ and the two-tailed symmetric alcohol (produced from a reaction of alkyl magnesium bromide and ethyl formate) in good yields of chromatographed products (71–84%).

CMC data were collected by pendent-drop technique for the **3CAmn, 3CCbn, 3CUrn,** and **3CCb1(n,n)** series of amphiphiles to establish the concentration required for detergency. The triethanolammonium salt provided better solubility and higher CMCs of these amphiphiles than the potassium salt. All amphiphilic series tested lowered the solution surface tension from ~ 72 mN/m to ~ 50–55 mN/m, indicating that these amphiphiles are less surface active than typical surfactants such as sodium dodecyl sulfate. The CMCs for the **3CAmn** series were found to decrease in value from 2×10^{-2} M (**3CAm15)** to 2×10^{-3} M (**3CAm21**) in a linear fashion. The CMCs for the **3CCbn** series were found to decrease in value from 7×10^{-3} M (**3CCb16)** to 0.4×10^{-3} M

(**3CCb22**) in a linear fashion. The CMCs for the **3CUrn** series were found to decrease in value from 2×10^{-3} M (**3CUr18)** to 1×10^{-3} M (**3CUr22**) in a linear fashion.

Due to discrepancies in several of the IFT vs. log concentration plots for the previous homologous series of amphiphiles, the CMC data was collected using a pyrene fluorescence measurement technique. The data from the pyrene fluorescence technique seems likely to be more accurate, indicating that surface tension may not be the most reliable method for determining the CMC of these amphiphiles. The CMCs (as determined by pyrene fluorescence) for the **3CAmn** series were found to decrease in value from 2×10^{-2} M (**3CAm15)** to 2×10^{-3} M (**3CAm21**) in a linear fashion. The CMCs for the **3CCbn** series were found to decrease in value from 7×10^{-3} M (**3CCb16)** to 0.3×10^{-3} M (**3CCb22**) in a linear fashion. The CMCs for the **3CUrn** series were found to decrease in value from 7×10^{-3} M (**3CUr16)** to 0.2×10^{-3} M (**3CUr22**) in a linear fashion. In both the surface tension and the pyrene fluorescence techniques, the shortest chain length homologues (**3CAm13**, **3CCb14**, and **3CUr14**) did not show a break up to the limits of solubility.

The CMCs as determined by surface tension for the **3CCb1(n,n)** series were found to decrease in value from 0.5×10^{-3} M (**3CCb1(9,9)**) to 0.02×10^{-3} M (**3CCb1(12,12)**) in a linear fashion. The **3CCb1(8,8)** and **3CCb1(7,7)** amphiphiles did not show a CMC break up to the limits of solubility. The **3CCb1(12,12)** showed an unusually steep decrease in surface tension over a very narrow range of concentration. There is considerable doubt as to the accuracy of the **3CCb1(11,11)** data, and the CMCs for these two-tailed amphiphiles needs to be measured by a second method as was done for the single-tail series to verify the CMCs of all the two-tail homologues.

Activity (minimal inhibitory concentrations, MICs) for the **3CAmn, 3CCbn, 3CUrn, 3CCb1(n,n), 2CAmn,** and **2CCbn** series was measured against several different bacteria, mycobacteria, yeast, and fungi. Additionally, anti-HIV and cytotoxicity data was collected for the **3CAmn, 3CCbn,** and **3CUrn** series. Greatest inhibition was typically seen from the 18–20 carbon tail length homologues of each series (**3CAm19–3CAm21, 3CCb18–3CCb20, 3CUr18–3CUr20, 2CAm19–2CAm21,** and **2CCb18–2CCb20**).

Inoculum density affected the activity of our earlier studies, and selected organisms were retested to obtain the intrinsic activity. **3CUr18** and **3CAm19** proved most effective against *Mycobacterium smegmatis*, with MIC_{99} = 6.3 μM @ 10^5 CFU/mL inoculum density. **3CCb20** was most effective against *Mycobacterium marinum* with MIC_{99} = 16 μM @ 10^5 CFU/mL inoculum density. **3CAm19, 3CCb18,** and **3CUr18** all showed equivalent activity against *Mycobacterium chelonae* with MIC_{99} = 17 μM @ 10^5 CFU/mL inoculum density. Against *Staphylococcus aureus*, the **2CAm21** was most effective, with MIC_{90} = 2.0 μM @ 10^5 CFU/mL inoculum density. **3CCb20** was most effective against MRSA with MIC_{90} = 2.9 μM @ 10^5 CFU/mL inoculum density. The two-tailed analogs (**3CCb1(n,n)**, **3CUr(n,n)**, and **3CUr1(n,n)**) typically showed little to no activity against the tested microorganisms. Comparison of MIC to CMC is a relative measure of safety of a drug candidate. All single-tail amphiphiles showed ratios of MIC/CMC of 16–126, with a ratio of 100 or better being optimal. The ratios for the two-tail amphiphiles ranged from 0.39 to 2.9.

Acknowledgements

I would like to thank my family: my wife and son, Barbara and Stephen; my father and mother, Richard and Carolyn Macri; my brother, Robert; my grandparents, Joe and Fay Macri, and Roy and Jean Mitchell; my aunt and uncle Rita and Howard Mitchell, and finally my cousin Katie Kegg. Your love, patience, and support have made me who I am today, and I am grateful for the time you took to help me be a better person.

I would like to thank my advisor, Dr. Richard Gandour, whose guidance, patience, knowledge, love of chemistry, and willingness to help gave me all the tools I needed to succeed in graduate school. A special thank you goes to Dr. Alan Esker for all his time and effort in helping me to understand the physical principles of surface chemistry and CMC, and to Dr. Carla Slebodnik for her help with the collection and interpretation of the X-ray crystallography data. I would also like to thank my advisory committee for their open-door policies whenever I had a question, especially Dr. Tanko who was never far off with a well-timed and well-needed quip.

I would like to thank my lab mates Dr. Brett Kite, Dr. Winny Sugandhi, Dr. Andre Williams, Shauntrece Hardrict, Marcelo Actis, and Brad Maisuria. You made it fun to come to lab everyday and were always willing to be a springboard for ideas or a sympathetic ear when something, inevitably, went wrong.

Finally, I would like to thank my peers, specifically Dr. Stephanie MacQuarrie-Hunter, Dr. Casey Elkins, Dr. Jason Harmon, Dr. Mike Zalich, Susan Mitroka, Jared Spencer, Charles Carfagna, and Josh Hartsel. Without you the years I spent in graduate school would have been much less bearable. You made me feel accepted and welcomed; I am eternally grateful for having you in my life.

Dedication

I would like to dedicate this document in the loving memory of my mother, Carolyn, and to my father, Richard, for the undying support and unconditional love only a parent can show.

I also dedicate this work to my son, Stephen, and my wife, Barbara, without either of whom my life would be only a shell of what it is now. My son has re-introduced me to the wonder that is childhood, and I approach each day with a new outlook because of him. Thank you, Stephen. I love you!

Barbara, you are an inspiration to all the people whose lives you touch, including my own. You have been a constant source of companionship, love, and hope for me over these many years, and I look forward to our next great adventure.

TABLE OF CONTENTS

LIST OF FIGURES

LIST OF TABLES

LIST OF SCHEMES

CHAPTER 1 – INTRODUCTION

1.1 – PROJECT GOALS

The purpose of this research project is the synthesis of a new homologous series of three-headed, long chain amphiphiles, having both one and two tails consisting of *n*-alkyl and branched-alkyl units. We have synthesized five new single-tail, dendritic, tricarboxylato amphiphiles (**3CCbn** series, **2**) and six new two-tail, dendritic, tricarboxylato amphiphiles (**3CCb1(n,n)** series, **4**), shown in Figure 1-1. Additionally, the critical micelle concentrations (CMCs) of the surfactants shown in Figure 1-1 have been measured via pendent-drop analysis to determine the micellization point of these amphiphiles and also to help determine if detergency is playing a role as a possible mechanism of action for the biological activity of the series.

Biological activity against several bacteria, fungi, and yeasts has been measured for potential use of these amphiphiles as topical microbicides. The focus of this particular dissertation is the synthesis of **2** and **4** and the determination of the CMCs of all the amphiphiles shown. The biological activity studies have been conducted by (Dr.) Andre A. Williams, (Dr.) Eko W. Sugandhi, Ms. Shauntrece Hardrict, and Ms. Myra Williams. HIV and cytotoxicity data have been collected by the research group of Dr. Gustavo Doncel at the Eastern Virginia Medical School.

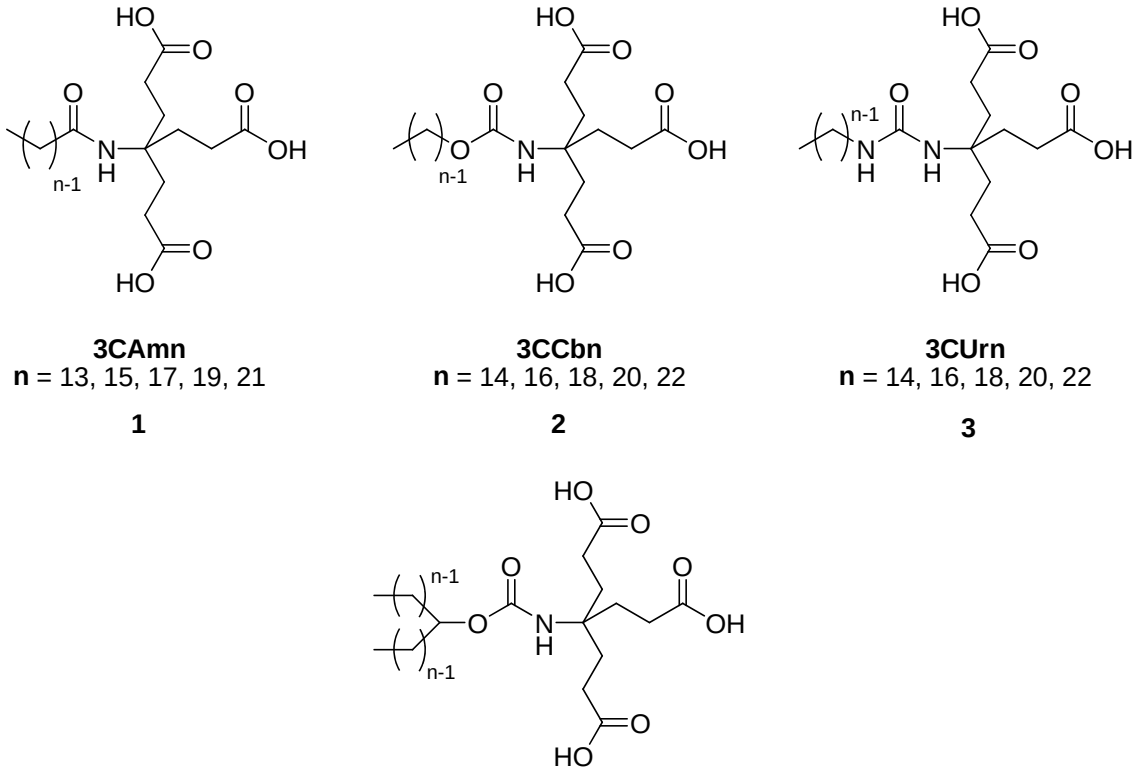

3CAmn
n = 13, 15, 17, 19, 21

1

3CCbn
n = 14, 16, 18, 20, 22

2

3CUrn
n = 14, 16, 18, 20, 22

3

3CCb1(n,n)
n = 7, 8, 9, 10, 11, 12

4

Figure 1-1 Chemical structure of the amphiphiles synthesized and tested, where **3C** = three carboxyl groups, **Am** = amido linker, **Cb** = carbamato linker, **Ur** = ureido linker, and **n** = number of carbons in alkyl chain.

1.2 – INTRODUCTION TO AMPHIPHILES

1.2.1 – What Are Amphiphiles?

Amphiphiles are chemical compounds belonging to a general class of materials called surfactants. The term surfactant is a blend of "surface-active agent", and was first used in the 1950s to describe any material that adsorbs onto surfaces or interfaces in a system, thereby altering the free energies of those surfaces/interfaces.[2] An interface is defined as a boundary between any two immiscible phases; a surface is an interface in which one phase is a gas (usually air).[2]

Typically, researchers think of surfactants as possessing detergent-like properties. However, it is known that detergency is associated with cytotoxicity, inflammation, and irritation towards cells, leading to increased chances of infection.[3,4] Therefore, we prefer to use the term amphiphile to describe these materials to prevent the (in this case) negative association of the concept of detergency. We have designed these amphiphiles with the intention of possession of very high critical micelle concentration (CMC; cf. section 1.4) values in relation to their minimal inhibitory concentrations (MIC), so that any antimicrobial activity associated with these amphiphiles is due to specific interactions and not due to detergency.

1.2.2 – General Applications of Surfactants and Amphiphiles

Surfactant materials are major industrial products. Table 1-1 shows the consumption of surfactants broken down by headgroup (Table 1-1, A.) and further by the actual surfactant itself (Table 1-1, B.). Worldwide consumption numbers range in the millions of metric tons annually.[5]

Table 1-1 Surfactant Consumption–United States and Canada (excluding soap), 2000 (recreated from reference 5)

A. Surfactant, by Charge Type	
TYPE	**%**
Anionics	59
Cationics	10
Nonionics	24
Zwitterionics/Amphoterics	7
TOTAL	**100**

B. Major Surfactants, by Tonnage	
SURFACTANT	**THOUSAND METRIC TONS**
Linear alkylbenzene sulfonates	420
Alcohol ethoxysulfates	380
Alcohol sulfates	140
Alcohol ethoxylates	275
Alkylphenol ethoxylates	225
Other	1,625
TOTAL	**3,065**

Surfactants have been used for at least 2,300 years, starting with alkali metal soaps produced by the treatment of animal fats with wood ash in a saponification reaction.[6] These materials were used by the Phoenicians as trade goods as early as 600 B.C.E. The first documented use of a synthetic surfactant material employed for their surface-active qualities were sulfonated oils used in the late nineteenth century as a dyeing aid.[6] Since the late nineteenth century, surfactants have found uses in a variety of applications including detergents, shampoos, crude oil recovery enhancers, cosmetics, chelating agents, and antimicrobial agents, to name a few.[7-10] As the focus of this work is on the determination of the CMC and how it compares to the MICs of amphiphiles **1–4**, the remainder of the discussion will be limited to the use of amphiphiles as antimicrobial agents.

1.2.3 – Amphiphilic Structure

An amphiphile is physically composed of two separate parts—a lyophobic ("solvent-hating") group and a lyophilic ("solvent-loving") group, as represented in Figure 1-2.[11] In the vast majority of cases where water is the solvent, the typical terms used are hydrophobic and hydrophilic, respectively.

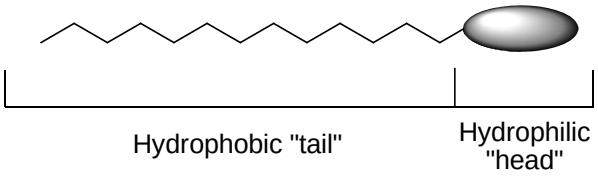

Figure 1-2 Generic depiction of a surfactant for use in water-based applications

A typical amphiphile's molar mass will be in excess of 300 g/mol since, in order to demonstrate the typical properties associated with amphiphiles in general, they are necessarily large molecules.[12] The hydrophobic and hydrophilic groups must be sufficiently separated from one another so that their interactions with surfaces and solvent molecules are independent of one another. Due to their dual nature, each amphiphile is designed or especially suited for a specific application as the lyophilic/lyophobic groups will interact with solvents and other materials in a unique fashion.[11] This means that a "universal surfactant" that is applicable to all situations and applications is not likely to ever exist.

Amphiphiles designed for use in water-based applications are typically classified according to the nature of the hydrophilic headgroup because it is the nature of the headgroup which determines the solubility of the amphiphile as a whole.[13] The general headgroup classifications can then be further subdivided by the nature of the hydrophobic "tail" to further distinguish among molecules in the same classification. The four major

classifications of amphiphiles according to their headgroups for water-based applications are as follows:

1. Anionic – the hydrophilic headgroup is a negatively-charged functional group with associated counterion. The most common types of these groups are carboxylates ($RCOO^- M^+$), sulfonates ($RSO_3^- M^+$), sulfates ($ROSO_3^- M^+$), and phosphates ($ROPO_3^- M^+$).
2. Cationic – the headgroup bears a positive charge, such as the quaternary ammonium salts ($R_4N^+ X^-$). The four R-groups may or may not be the same.
3. Nonionic – the headgroup has no charge associated with it, but instead derives its water solubility from highly polar groups, such as polyoxyethylenes (R—OCH_2CH_2O—) or R–polyol groups, which include sugars.
4. Amphoteric/Zwitterionic – the molecule contains both a negative and positive charge, the most well-known of which are the sulfo-betaines ($RN^+(CH_3)_2CH_2CH_2SO_3^-$).

Generally, the hydrophobic groups tend to be significantly more varied than the hydrophilic headgroups.[13] In general, the hydrophobic "tails" tend to be long-chain hydrocarbons, although there is great variation among this generality to include straight- and branched-chain alkyls, unsaturated alkyl chains, alkylbenzenes and alkylnaphthalenes, fluroroalkyls, dimethylsiloxanes, polypropylene glycol derivatives, biosurfactants, and derivatives of synthetic and natural polymers.[13] The amphiphiles designed and tested in this work are all classified as anionic, *n*-alkyl (**3CAmn, 3CCbn, 3CUrn)** and anionic, branched-alkyl (**3CCb1(n,n)**) surfactants.

1.3 – Aqueous Solubility of Amphiphiles

Due to their dual nature, amphiphiles have unique properties with respect to solubility in aqueous media. The solubility of any given amphiphile and its ability to form aggregate structures is affected by changes in temperature, pH, carbon chain length, number and types of headgroups, addition of salts and organics, and the types of counterions.

1.3.1 – Factors Affecting Solubility

As touched on in section 1.2.3, an amphiphile's unique structure causes it to naturally adsorb at interfaces. For water-based applications, the amphiphile must possess a highly polar headgroup in order to dissolve. Typically, ionic headgroups are better at solubilizing a long-chain hydrocarbon than a polar headgroup.[14] As an example, a sulfate or quaternary ammonium headgroup is readily able to solubilize a C_{12} hydrocarbon chain, whereas it would take ten ethylene oxide units in a nonionic headgroup to provide the same solubility. While the headgroup is extremely soluble in aqueous media when considered in isolation, it is attached to a carbon chain that has little, if any, affinity for water. Therefore the amphiphile will attempt to solubilize the hydrophobic tail portion in any nonpolar phase that is available (air, oil, adsorption to a solid surface, etc.) while the headgroup remains in the aqueous phase. When no other interfaces are available an amphiphile will form phases for itself to minimize their energy. This self-assembly is the formation of aggregates, called micelles. The factors affecting aggregate formation will be looked at further in section 1.3.2.

Amphiphilic solubility also varies with pH as shown in Table 1-2.[14] Strongly dissociating groups, such as sulfates, will be soluble over the entire pH range, whereas weak anionics are only soluble in alkaline solutions and weak cationics are soluble in

acidic solutions. Nonionic groups are typically soluble over a wide pH range as their solubility is based on hydrogen-bonding interactions and not the formation of ions. Amphoteric groups, having both a positive and negative charge, are soluble over wide pH ranges at high and low pH.

Table 1-2 Surfactant Solubility Ranges (recreated from reference 14)

Headgroup Type	pH
Anionic	5–14
Nonionic	3–12
Cationic (weak)	1–8
Cationic (quaternary)	1–14
Amphoteric	1–6, 9–14

Nonionics lose their solubility at the extremes of the pH range due to competition with the electrolyte for hydrogen bonding sites with water.[14] Amphoterics lose their solubility near their isoelectric points due to "tail biting" between the ionic headgroups, as shown in Figure 1-3.

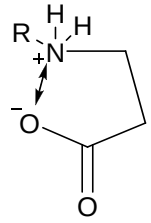

Figure 1-3 "Tail Biting" (recreated from Reference 14)

1.3.2 – Factors Affecting Aggregate Formation

The formation of aggregates, or micelles, is driven by the relative solubility of the headgroup and tailgroup and is counterbalanced by the interplay of the repulsion of the hydrophilic headgroups versus attraction of the hydrophobic tails.[15] With ionic headgroups, the solubility of the amphiphile is markedly increased over nonionics.

However, as solution concentration of the amphiphile increases there will be an increase in the ionic repulsion between headgroups of different molecules of surfactants. This repulsion is also seen with nonionics, but the repulsion is steric in nature, as opposed to electronic.[15]

Additionally, as amphiphile concentration increases, there is an increase in the hydrophobic attraction of the tails. This attractive force is entropy driven and serves to minimize the effect of the hydrophobic tail on the hydrogen bonding network of the water molecules.[15] When these forces are correctly balanced, the individual molecules of amphiphile will aggregate into micellar structures. If the hydrophilic repulsion of the headgroup is small compared with the hydrophobic attraction of the tails, the amphiphile will aggregate at low concentrations, thereby producing a low CMC.[15] Conversely, large hydrophilic repulsion in relation to hydrophobic attraction will prevent the amphiphiles from aggregating, thereby delaying the point at which micelles form and producing a higher CMC value. With this in mind, we can begin to look at the factors that affect aggregate formation of an amphiphile.

1.3.2.1 – The Hydrophobic Group

The number of carbon atoms in the chain of a homologous series of amphiphiles affects the CMC.[16,17] As we are increasing the hydrophobic attraction when we add methylene groups to the tail, the effect is a decrease in the CMC. The decrease is logarithmic as the number of carbons in the chain increases. For straight-chain tails of 16 or fewer carbon atoms attached to a single ionic headgroup, the CMC is typically reduced by approximately one-half with the addition of each methylene group.[18] For nonionic surfactants the decrease is usually much larger, with a change of a factor of 10 from the

addition of two methylene groups. The relationship between hydrocarbon chain length and CMC can be expressed mathematically by the Klevens equation, eq 1,

$$\log_{10}(CMC) = A - Bn_c \quad (1)$$

where *A* and *B* are constants specific to the homologous series under conditions of constant temperature, pressure, and other factors, and n_c is the number of carbons in the tail. Generally, the value of *A* is approximately constant for a given ionic headgroup, and *B* is constant and approximately equal to $\log_{10} 2$ (~0.3) for all paraffin chain amphiphiles with a single ionic headgroup. Above 18 carbons the CMC may remain substantially unchanged with increased chain length.[19] The introduction of branching in the tail appears to have about one-half of the effect of carbon atoms in a straight-chain compound, and unsaturation in the tail generally produces higher CMCs than corresponding saturated compounds.[19] The cis isomer typically has a higher CMC than the trans isomer, due to steric bulk increasing the difficulty of incorporation of the tail into the interior of the micelle.

1.3.2.2 – The Hydrophilic Group

Ionic surfactants have much higher CMC values than nonionic surfactants with the equivalent number of hydrophobic groups.[20,21] For ionic surfactants, the hydrophilic repulsion is increased compared to nonionics, so an increase in CMC is the expected behavior. By way of an example, a 12-carbon straight-chain ionic surfactant has a CMC of approximately 1×10^{-2} M, whereas CMCs of nonionics are on the order of 1×10^{-4} M.[20,21] Zwitterionics appear to have slightly smaller CMCs than ionics with identical hydrophobic groups.[20] As the hydrophilic group is moved from the terminal position of a hydrophobic chain to a more centralized position (as seen in the **3CCbn** series vs. the

3CCb1(n,n) series), the CMC begins to increase.[20,21] The hydrophobic group acts as if it has become branched at the position at which the hydrophilic headgroup is attached.

The CMC is higher when the charge on the ionic headgroup is closer to the α-carbon of the hydrophobic group.[22] The explanation for this phenomenon is that as the amphiphile is added to the micelle, it takes work to move the ionic headgroup closer to the hydrophobic core of the micelle and out of the solvent water, which has a higher dielectric constant and can therefore stabilize the ionic charge more effectively. A charge that is closer to the hydrophobic core of the micelle will require more work to incorporate that molecule into the micelle than an amphiphile in which the charge is located further from the α-carbon of the hydrophobic group.

As expected, an amphiphile with multiple hydrophilic groups have larger CMCs than those with one hydrophilic group.[20] This is due to larger hydrophilic repulsion from increased electronic repulsion as well as increase in the work needed to move the amphiphile into the micellar structure, as described above. The nature of the headgroup has a rather small effect on the CMC when compared to changes in the hydrophobic chain.[21,23] This effect is expected when we consider that the driving force for micellization is the energy gain due to the reduction of water–hydrophobe interactions. The effect of the ionic group, aside from the impact on water solubility, is to work against the aggregation process.

1.3.2.3 – Counterion Effects

The counterion of an amphiphile will decrease hydrophilic repulsion, and therefore the CMC decreases as well.[24] The degree of ionization, α, of the micelle near its CMC can be obtained from the ratio of the slopes above and below the break that

indicates the CMC when specific conductivity is plotted against concentration (see Figure 1-4).[25,26]

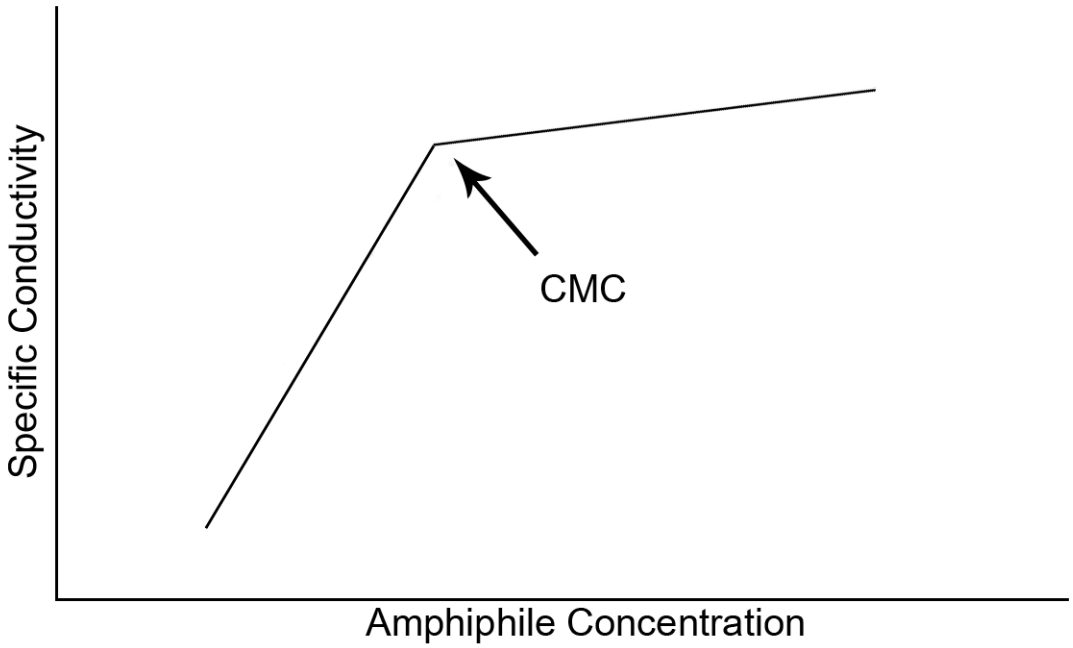

Figure 1-4 Plot of specific conductivity vs. concentration (recreated from Reference 25)

The degree of binding is then found, for a surfactant with one ionic headgroup, from (1-α). Anionic surfactants with a headgroup structure of $RC(O)N(R^1)CH_2CH_2COO^-Na^+$ (effectively the single-headed analog of **1** in Figure 1-1), show binding values much smaller than surfactants that do not contain the amide linkage.[27-29] This is due to the anion of the headgroup hydrogen-bonding to the hydrogen of the amide group, thereby releasing the sodium ion upon micellization, as shown in Figure 1-5.[27-29]

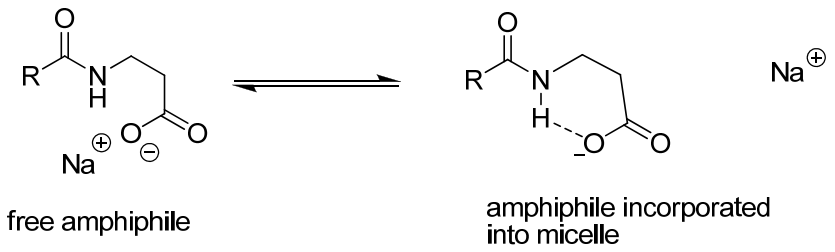

Figure 1-5 Depiction of hydrogen bonding that occurs during micellization

The CMC and the degree of binding are related such that as the degree of binding of the counterion increases, the CMC will decrease. A higher charge density on the counterion will lead to greater hydrophilic repulsion (therefore Mg^{2+} will have a greater effect on the CMC than Na^+, for example). The degree of binding of the counterion to the micelle is related to the hydrated radius, polarizability, and charge of the counterion. Counterions with larger hydrated radii show weaker degrees of binding to the micelle, so that $NH_4^+ > K^+ > Na^+ > Li^+$ for anionic amphiphiles.[25] Counterions with increased polarizability and charge show increased degrees of binding. For lauryl sulfates, the CMC decreases in the order $Li^+ > Na^+ > K^+ > Cs^+ > N(CH_3)_4^+ > N(C_2H_5)_4^+ > Ca^{2+} \approx Mg^{2+}$, which is the same order as the increase in the degree of binding for the counterions as measured by Robb[25,30] using NMR spin relaxation rates. Changes to counterion valency have a more profound effect on the CMC than changes to hydrated radii among counterions of similar valency.[31] These various effects are summarized in Table 1-3 for salts of dodecyl sulfate.

Table 1-3 Effect on CMC with Various Salts of Dodecyl Sulfate (recreated from reference 31)

Counterion	Temperature (°C)	CMC (mM)
Li^+	25	8.8
	40	10.5
Na^+	25	8.1
	40	8.9
K^+	40	7.8
Cs^+	40	6.9
$(CH_3)_4N^+$	25	5.6
½ Ca^{2+}	54	2.6
½ Mg^{2+}	25	1.6
½ Zn^{2+}	60	2.1

1.3.2.4 – Electrolyte Effects

Addition of electrolytes (in the form of salts such as NaCl) causes a change to the CMC of amphiphiles based on the nature of the headgroup. As would be expected, the effect is more pronounced for highly charged headgroups, such that the CMC decrease is greater for cationics and anionics than for zwitterionics, and greater for zwitterionics than nonionics.[32,33] For cationic and anionic amphiphiles, the electrolyte causes a screening effect in which the electrical repulsion of the headgroups is decreased. This decrease in hydrophilic repulsion leads to a lower CMC. Experimental data produced by Corrin[34] shows that for cationic and anionic amphiphiles the effect of the concentration of added electrolyte on the amphiphile's CMC is given by eq 2

$$\log CMC = -a \log C_i + b \tag{2}$$

where a and b are constants for the ionic headgroup at a particular temperature and C_i is the total counterion concentration in equivalents per liter.[32,34]

For zwitterionics and nonionics, the effect of electrolyte is better described by eq 3

$$\log CMC = -KC_s + const. \qquad (C_s < 1) \tag{3}$$

where K is a constant for a particular amphiphile, electrolyte, and temperature and C_s is the concentration of electrolyte expressed as molarity.[32,35,36] Studies by Mukerjee and Ray attribute the change in CMC to the "salting out" or "salting in" of the hydrophobic groups of the amphiphile by added electrolyte, rather than the electrolyte's effect on the hydrophilic headgroup.[32,37,38] Whether the electrolyte salts in or salts out the amphiphile depends on the effect of the electrolyte on the bulk structure of the solvent, water. Ions with a large ionic charge/radius ratio, such as fluoride (F^-), are highly hydrated and help

to form structured water; these ions are called "water structure makers" by Rosen.[32] This has the effect of salting out the hydrophobic groups of the amphiphile and therefore causes a decrease in the CMC. Conversely, ions with small charge/radii ratios, such as CNS^-, are "water structure breakers" and salt in the hydrophobic groups, thereby increasing the CMC.

Myers and Rosen describe this phenomenon in terms of solution energy—a water structure maker serves to decrease the entropy of the solution by forcing the water molecules into ordered solvation shells.[33,39] This means that the amount of work necessary for the solvation of the hydrophobic group of the amphiphile must be increased for solvation to occur, and therefore the CMC decreases in response because the monomeric form of the amphiphile is now less soluble in solution. The opposite effect is seen with the water structure breakers, which serve to increase solution entropy and disrupt the ordered water molecules. The hydrocarbon chain of the surfactant is believed to create the structure in the liquid water, and removal of this nonpolar group from the bulk water during micelle formation produces a consequential increase in the solution entropy which favors the micellization process. As the structure breakers decrease the order of the water molecules, they also decrease the entropy gain upon micellization. This means that the amphiphile now needs less energy for solvation, and a consequential increase in the CMC is observed because a higher monomeric amphiphile concentration is necessary for micelle formation.

1.3.2.5 – Organic Additive Effects

Small amounts of organic materials can produce experimentally noticeable changes in the CMC of amphiphiles.[39,40] As seen in the work done by Lin, [40] the types of materials which can cause these changes can be found as byproducts from the

manufacture of the amphiphile itself, and it therefore becomes a matter of importance to understand how these impurities will affect the CMC. Rosen[39] divides the types of organic materials into two groups: Type 1 materials affect the CMC by being incorporated into the micelle itself, while Type 2 materials affect the CMC by changing the nature of the solvent–micelle or solvent–monomer interactions.

1.3.2.5.1 – Type I Materials

The types of materials that fit into this group are typically polar organic compounds, such as alcohols and amides.[39] These compounds reduce the CMC by decreasing the hydrophilic repulsion of the headgroups, which leads to a decrease in the work required to form the micelle. The shorter chain alcohols and amides will typically incorporate into the micelle towards the water–micelle interface, with the molecule moving closer to the outer portion of the core of the micelle as the chain length increases.

Data of the depression in the CMC for these additives suggest that straight-chain compounds have a greater effect than branched-chain additives, with a maximum effect on CMC depression occurring when the length of the hydrocarbon portion of the additives is approximately equal to that of the amphiphile. The physical explanation for this behavior comes from Schick and Fowkes.[41] The molecules that are most effective at reducing the CMC are solubilized in the outer portion of the micelle's core and are under pressure from the amphiphiles that make up the micelle to move towards the interior of the core of the micelle. This is visually demonstrated in Figure 1-4 with sodium dodecyl sulfate (SDS) as the amphiphile and dodecan-1-ol as the impurity.

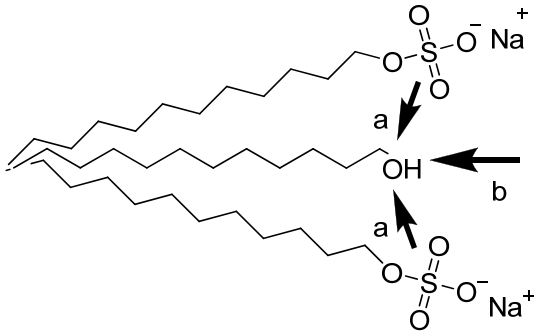

Figure 1-4 Impurity solubilization. Arrows (a) represent the lateral pressure on the impurity from the amphiphiles, with the net force (b) directing the impurity deeper into the interior of the micelle.

The pressure from the neighboring monomers of the amphiphile increases as the cross-sectional area of the impurity increases. This means that straight-chain impurities, which have a smaller cross-sectional area than branched-chain impurities, will tend to remain closer to the outer portion of the core and therefore affect the CMC to a greater degree than the branched-chain impurities, which are forced deeper into the core of the micelle. This also helps to explain the maximum CMC depression seen when the chain length of the impurity nears that of the amphiphile—when the chain length of the impurity and the amphiphile are nearly equal, the non-polar groups have maximum van der Waals interactions, which tends to keep the impurity in the outer portion of the micelle.

Additives with more than one hydrogen-bonding polar terminal group appear to produce greater depressions in the CMC than impurities with single hydrogen-bonding groups.[39,41] The increased hydrogen-bonding of the multiple polar groups helps to more effectively counterbalance the force that is attempting to drive the impurity into the micellar core, thereby reducing the CMC further than impurities with a single hydrogen-bonding group. Pure hydrocarbons, which penetrate deep into the micellar core, have

little effect on the CMC in the same way polar impurities that penetrate deep into the core do.[39]

1.3.2.5.2 – Type II Materials

The Type II materials also change the CMC, typically at higher bulk solution concentrations than the Type I materials.[39] As stated previously, these materials modify the interaction of the micelle or the monomeric form of the amphiphile with bulk water. This is accomplished by modification of the bulk structure of water, changing the dielectric constant, or by changing the solubility parameter. Molecules that exhibit this behavior are ureas, formamide, guanidinium salts, short-chain alcohols, ethylene glycol, water-soluble esters, and polyols such as fructose and xylose.[39]

Ureas, formamide, and guanidinium salts are thought to disrupt the structure of water which increases the hydration of the hydrophilic group. This effect is much more noticeable for nonionic amphiphiles than for ionic ones. This increase in hydration opposes micellization, which thereby increases the CMC.[42] It may also be that these impurities act as water structure breakers and cause an increase in the CMC by decreasing the entropy effect that accompanies micellization (cf. Section 1.3.2.4). Materials such as xylose and fructose decrease the CMC of the amphiphile because they act as water structure makers.

Ethylene glycol, water-soluble esters, and the short-chain alcohols cause an increase in the CMC due to decreasing the solubility parameter of water. This increases the solubility of the monomeric form of the amphiphile and therefore increases the CMC as well.[42] An alternative explanation proposed by Herzfeld is that, for ionic surfactants, these impurities cause a decrease in the dielectric constant of the aqueous phase.[43] This

would cause an increase in hydrophilic repulsion of the headgroups of the amphiphile with concomitant increase of the CMC.

1.3.2.6 – Temperature Effects

The effect on the CMC of amphiphilic systems due to temperature changes is quite complex.[44,45] As the temperature of the system increases, the CMC begins to decrease until reaching some minimum, at which point the CMC then begins to increase.[45] Temperature increases cause decreased hydration of the hydrophilic group, which in turn favors micellization.[45] Simultaneously, the temperature increase also serves to disrupt the structured water around the hydrophobic group of the amphiphile, thereby disfavoring micellization. The relative magnitudes of these two opposing effects serve to dictate whether the CMC will increase or decrease over a given temperature range.[45] The data would suggest that at lower temperatures the disruption of the structured water has a greater effect, as the experimental observation is that the CMC decreases at first. At higher temperatures, the decreased hydration of the headgroup becomes the dominant effect and the CMC increases as a result. The minimum in the temperature–CMC curve appears around 25 °C for ionic amphiphiles and around 50 °C for nonionics.[46-48] Data concerning zwitterionics are limited and inconclusive.

For many ionic amphiphiles it is found that as the temperature increases so does the overall solubility.[49] This effect is due to the physical characteristics of the material, namely the heat of hydration and the crystal lattice energy. Figure 1-5 shows a generic concentration vs. temperature dependency curve for ionic amphiphiles.

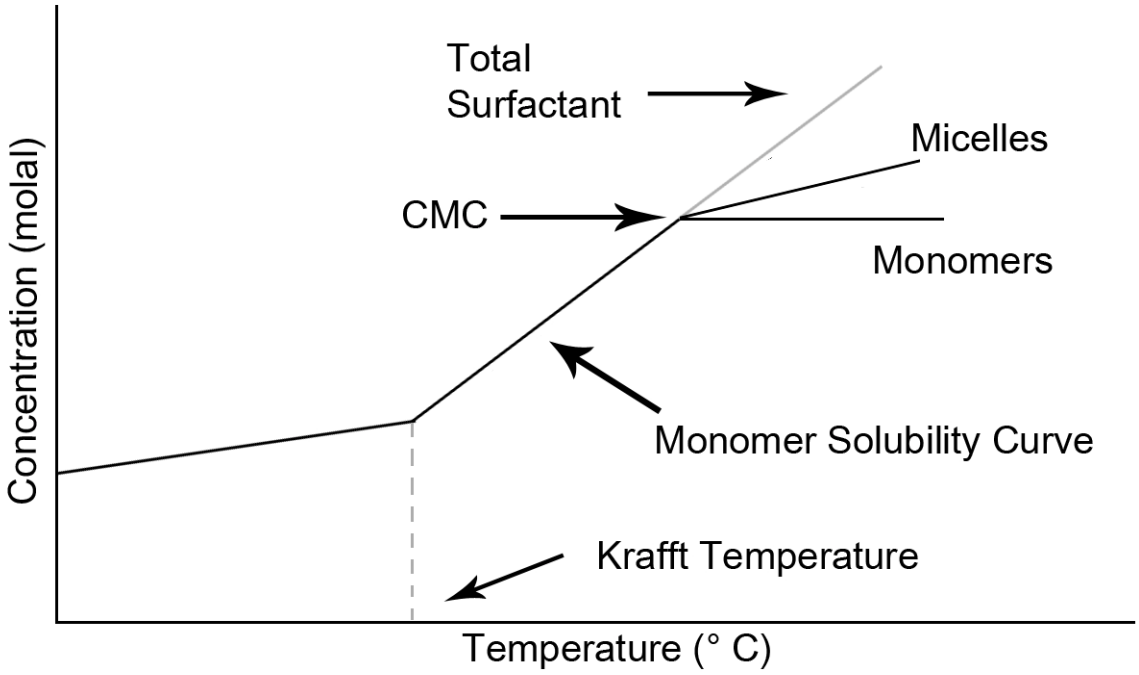

Figure 1-5 Concentration-Temperature relationship curve for typical ionic amphiphiles (recreated from Reference 49)

We see that the solubility of an amphiphile will typically undergo a sharp, discontinuous increase at a temperature that is characteristic of the amphiphile in question. This point is called the Krafft temperature, or Krafft point (T_K). The Krafft temperature is the solution temperature at which the CMC and the surfactant solubility are equal.

Below the T_K, the solubility of the amphiphile is dependent on the crystal lattice energy and the heat of hydration of the system. The concentration of the monomeric form of the amphiphile will be limited to some equilibrium value as determined by those system properties. Above T_K, the solubility increases until aggregate formation begins, and the micelle then becomes the thermodynamically favored form in solution. At this point the monomer concentration in solution becomes effectively constant as increased concentration of monomer is used to produce the more thermodynamically stable micelle.

The increase in solubility is accompanied by a decrease in the surface tension of the solution until aggregate formation begins, at which time the surface tension remains constant.[50] If the CMC exceeds the solubility of an amphiphile at a given temperature, the minimum in the surface tension will be achieved at the point of maximum monomer solubility, rather than at the CMC.[50] The Krafft point increases as the number of carbon atoms in the hydrophobic group increases, and decreases with branching or unsaturation. The Krafft point also depends on the counterion, increasing in the order $Li^+ < NH_4^+ < Na^+ < K^+$ for anionic surfactants. Changing from trimethyl- to triethylammonium cations leads to reduction in the Krafft point,[51] as does changing from oxyethylenation to oxypropylenation of alkyl sulfates. For amphiphiles being used above the Krafft point, maximum reduction in the surface tension and maximum monomer solubility is reached at the CMC.

1.4 – Critical Micelle Concentration (CMC) Measurements

1.4.1 – Introduction

The CMC is the concentration at which a solution of surfactant molecules self-assembles to create a micro-phase in which the surfactant has a minimal energy effect on the bulk solution.[52] Micellar formation is associated with detergency, which is one possible mechanism of antimicrobial activity.[3] However, detergency has also been shown to increase mucosal tissue irritation and cause damage.[3] Therefore, we would like to know at what point these amphiphiles form micelles with the aim of combining high CMC with low MIC to produce a surfactant that is biologically active against the targeted microbes of interest, yet relatively non-irritating to a user's mucosal tissues.

1.4.2 – Surface Chemistry

Surface chemistry is the branch of chemistry that studies processes occurring at interfaces between phases (especially those between liquid and gas). We will determine the CMC of solutions of the amphiphiles that we will synthesize. By knowing the CMC of these amphiphiles **1–4**, we can begin to gain an understanding of how these compounds function as microbicides as defined by the limits of inhibitory activity versus the point at which micellization occurs.[1]

Typically, solutions of surfactants that have a concentration at or above the CMC function as microbicides via detergent action, in which the surfactant ruptures the microbial cell membrane.[3] This detergency also affects non-pathogenic cells (such as host mucosal tissue membranes and beneficial microorganisms) in a similar fashion, the end result of which is dryness and irritation. In our work to design topical microbicides, side effects such as irritation, dryness, and possible minor hemorrhaging are not desired.

Therefore, a major design goal of this work is to create surfactants that have good efficacy towards target pathogens while maintaining little to no deleterious side-effects. The CMC data when compared to the MIC data give us a more holistic view of the surfactant in terms of not only efficacy in inhibiting pathogen growth, but also in terms of safety of the amphiphile.[1]

A surfactant that is a good pathogen inhibitor at concentrations well below the CMC tends to indicate that the surfactant is functioning via some specific mechanism of action (cell signal protein disruption, ion channel blocking, etc.). As there is a large difference between the makeup of mammalian and bacterial cell structures, this tends to indicate that, in theory, the surfactant itself will be relatively safe because a compound that will function specifically against one will tend to be relatively non-functional against

the other. For instance, bacterial cells have a cell "wall" that is made up of a polysaccharide "capsule", a cell wall composed of a polymer of disaccharides cross-linked by short chains of amino acids, and finally a phospholipid bilayer membrane.[53] In contrast, a mammalian cell "wall" is composed of only the phospholipid bilayer membrane. Therefore a compound that will act against a bacterial cell will encounter the capsule and cell wall first, and must be active against those structures that a mammalian cell does not possess. Any compound that specifically targets the phospholipid bilayer membrane of a bacterial cell will most likely affect a mammalian cell in a similar manner, thereby preventing its use in a clinical fashion.

The following sections will present a basic introduction into the theory behind the CMC and how it is determined experimentally.

1.4.2.1 – Surface Tension Defined

Surface tension is defined as the energy difference between the molecules in the bulk phase versus those at the interfacial surface.

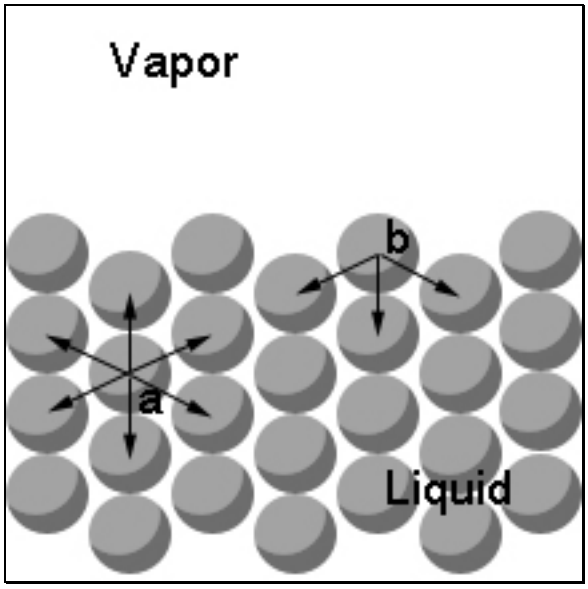

Figure 1-6 Intermolecular forces acting on molecules in the bulk (a) vs. the interface (b) (recreated from Reference 54)

In a pure liquid, as seen in Figure 1-6, the molecules in the bulk phase (a) interact with more of their neighbors than those at the surface (b). This molecular interaction is due to various intermolecular forces including van der Waals or hydrogen bonding, dependent of course on the solvent in question.[54] The existence of a bulk phase provides evidence that these intermolecular interactions are indeed energetically favorable. If the interactions of molecules with each other were not energetically favorable no condensed phase would exist; there would only be a vapor phase.

Therefore, moving a molecule from the bulk to the surface—in other words, moving a molecule from a low energy state to a high energy state—requires work. The work required (W) is proportional to the new surface area (A) created by moving a molecule to the surface, times some proportionality constant (eq 1).

$$dW = \gamma \cdot dA \tag{1}$$

The proportionality constant in question (γ) in (1) is the surface tension. From eq 1, the surface tension must have units of force/length, expressed as Newtons/meter. Most surface tension values range from 0.02–0.08 N/m, and the surface tension is typically expressed in practice as milliNewtons/meter (mN/m). As would be expected the surface tension of a liquid is temperature dependent. For water the nominal surface tension value is 72.8 mN/m at 20 °C.

The phenomenon of surface tension is most readily observable in a water drop adopting a spherical shape in the absence of outside forces (e.g.: gravity). The surface tension of the droplet works to minimize the surface area of the drop, and therefore minimize the work required to form that drop, so that the energy difference between the molecules in the bulk and those at the surface is kept as small as possible.

1.4.2.2 – Surfactant Effect on Surface Tension

It is an observable phenomenon that as a surfactant is added to water, the surface tension of the solution decreases.[55] This decrease is due to the differences in intermolecular forces between a surfactant molecule and bulk water versus a water molecule and bulk water.[56] When a surfactant molecule is dissolved in solution, an energy cost is paid in terms of solvation of the tail. As the tail is a non-polar hydrocarbon chain, it costs energy to break up the hydrogen bonding network of the bulk water molecules in order to solvate the tail.[57] There is a way that the system can minimize this energy cost: by moving the surfactant molecule to the surface. The hydrophobic tail is infinitely more "soluble" in the vapor phase than it is in the bulk, and in this case some of the energy cost paid to solvate the tail is recovered by moving the molecule to the interface.

The effect on the surface tension is that the surface tension is decreased. Moving a (relatively) high energy surfactant from the bulk to the interface causes a decrease in the surface energy (surface tension) from what is seen when moving a relatively low energy water molecule from the bulk to a higher-energy interfacial position. Hence, we see a decrease in the surface tension as surfactant concentration increases.

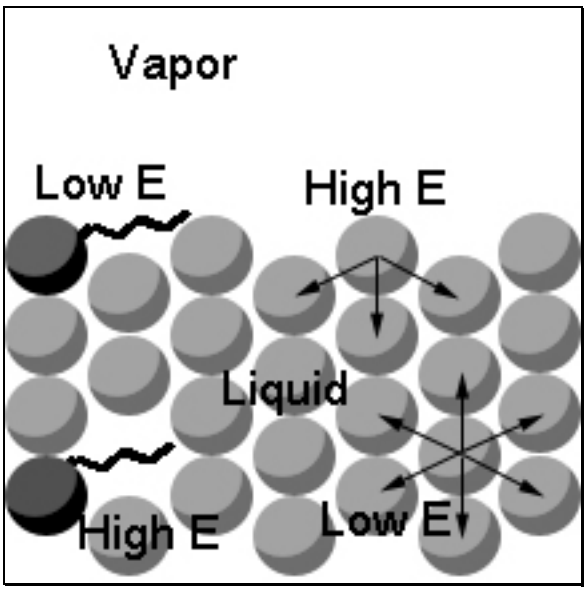

Figure 1-7 Comparison of energy differences between solvent and surfactant molecules

1.4.2.3 – Micellar Formation

But what is the effect of continually adding more and more surfactant to a solution? Will the surface tension continue to decrease indefinitely? As it turns out, the answer to this question is no. What is observed is that as the surfactant concentration increases, the surface tension of the solution continues to decrease up to a specific point, and then no longer changes (or changes very slowly) when additional surfactant is added to the solution.[55] The point at which the surface tension stops changing is dependent on the physical structure of the surfactant itself.

This point where the surface tension ceases to change is called the CMC, and is the point at which individual surfactant molecules begin to spontaneously aggregate into self-assembled structures known as micelles. These micellar structures are a compromise between a phase-separated and molecularly dispersed system.[52] We have already explored how a surfactant molecule will move to the air/water interface to minimize its energy effect on the solution. In the same way, formation of a separate phase (as is seen

with nonpolar or apolar compounds such as hexane or octanol) is not energetically viable because then the polar headgroups would be increasing the energy of the system by being forced to be "soluble" in the non-polar environment of the long-chain tails. The compromise is the formation of the micelle, in which both the hydrophobic and hydrophilic parts of the surfactant can minimize their energy effect on the solution simultaneously.[52] The classic system used for the study of surfactant behavior and micellar formation involves a solution of sodium dodecylsulfate (SDS) in water, shown in Figure 1-8.

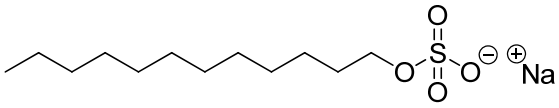

Figure 1-8 Molecular representation of SDS

Some of the most common micellar structures are shown below.

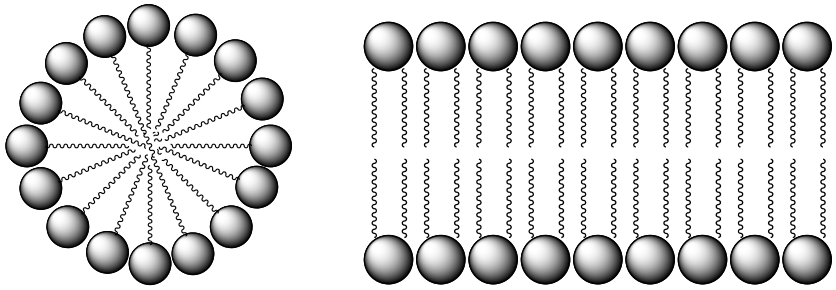

Figure 1-9 2-D representations of micellar structures, spherical (left) and bilayer (right)

The shape of the micelle formed is based upon the volume of the hydrophobic tail, the length of the tail, and the effective area per headgroup. The interrelation of these parameters gives a value known as the surfactant number, N_s.

$$N_s = \frac{v}{l * a_0} \tag{2}$$

In eq 2, *v* is the volume of the tail, *l* is the length of the tail, and a_0 is the effective area of the headgroup. The surfactant number relates the physical properties of the surfactant molecules to the preferred curvature properties of the micelle formed.[58] For $N_s = 0.33$, spherical micelles are typically formed. $N_s = 0.5$ produces infinite cylinders and surfactant number values of ~ 1 means that the surfactant tends to produce planar bilayers. The surfactant number gives reasonable approximate models for micellar structure, and the values cited above are not fixed.[58] Surfactant number values between the cited values above may produce aggregates that are "slightly off" from ideal, or produce aggregates of lower symmetry. The power of the aggregation number is in predicting the shape of an aggregate based on the physical parameters of the surfactant molecule. For instance, adding a second "tail" to a single-tail surfactant (such as SDS) will cause the volume parameter to nearly double, while the l and a_0 values remain essentially unchanged. The result is that the N_s value changes from less than 0.5 to 0.5–1, meaning that the aggregate will now form planar bilayers or cylinders instead of spherical constructs.

In Figure 1-10 we present a theoretical graph of a surfactant's surface tension vs. the log of its concentration to illustrate the key steps in micellar formation.

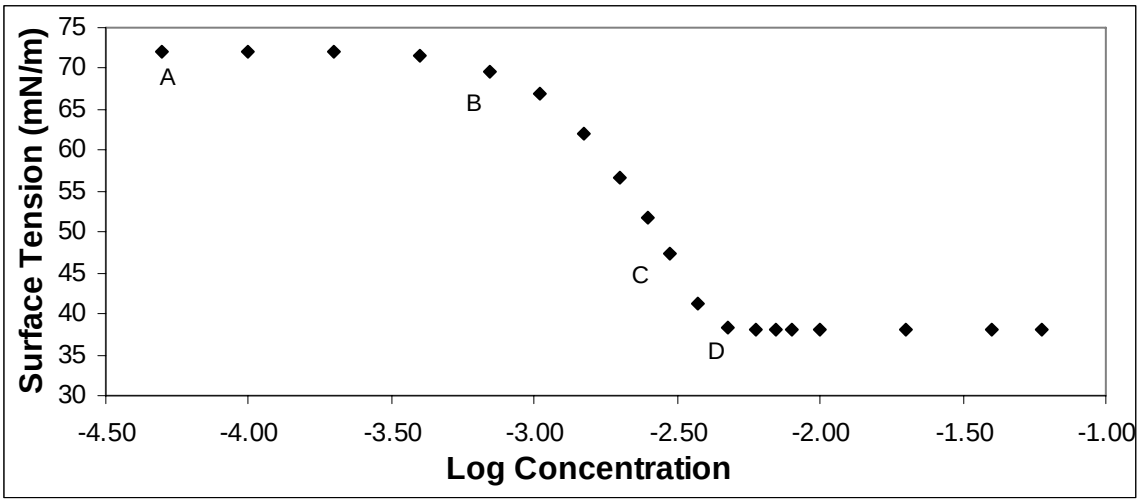

Figure 1-10 Theoretical plot of surface tension vs. surfactant concentration

Figure 1-11 shows a nanoscale view of each of the indicated regions in Figure 1-10 (solvent molecules omitted for clarity):

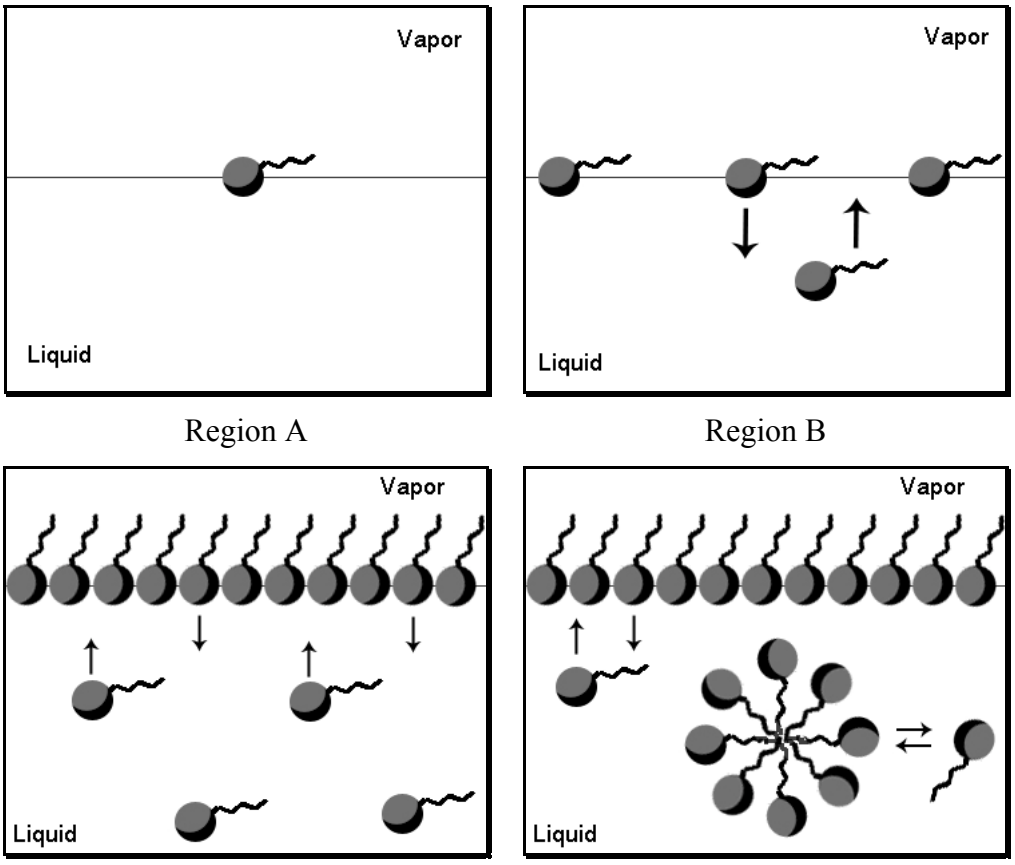

Figure 1-11 Nanoscale view of regions (A-D) indicated in Figure 1-10

Region A in Figure 1-11 depicts the point at which there is very little surfactant in solution. At this point there is almost no surfactant in solution, as it is more energetically favorable for the surfactant molecule to move to the surface. The tail of the surfactant tends to "lie down" on the interface, due to the weak van der Waals interactions between the hydrocarbon chain and the water molecules of the solvent. While these are not the strongest intermolecular forces, these interactions are generally more stabilizing (i.e. less energetic) than having the tail standing straight up away from the surface atoms of the liquid phase.

Additionally, the surfactant molecules tend to move as far apart from one another as possible, due to unfavorable headgroup interactions. How far the headgroup penetrates into the liquid phase is dependent on the atoms that make up the headgroup and their interactions with the atoms of the liquid phase. As the number of surfactant molecules is much less than the number of molecules comprising the liquid phase, there tends to be little, if any, effect on the surface tension at this point.

In Region B we begin to measurably see the effect of increasing surfactant concentration on the surface tension of the solution. A dynamic equilibrium is beginning to be established between the surfactant molecules in the bulk and those at the surface, although the vast majority of surfactant molecules are still located at the surface. The surfactant molecules are beginning to interact with one another, although the effect of this interaction will not readily be noticeable until the surfactant concentration approaches the CMC.

Region C is the point just before the CMC, and the solution surface is almost completely comprised of surfactant molecules. The hydrophobic tails of the surfactants at the interface are now standing more or less vertically. The van der Waals interactions of the tails are now functioning to help stabilize the molecules' destabilizing headgroup interactions. At this point there is a fairly high concentration of individual surfactant molecules in solution, although the molecules are not readily interacting with one another. The dynamic equilibrium of surfactant molecules moving to and from the interface that began in region B is still occurring, but to a greater extent.

Point D is the CMC. The tails of the surfactant molecules orient themselves towards the interior of the aggregate, with the headgroups pointed out toward the solvent

of the liquid phase (for an aqueous solution). The self-assembly of surfactant molecules into well-defined micellar structures is a physicochemical process, meaning that the surfactant molecules are associated through physical interactions, not chemical bonds, and can therefore change size or shape depending on variations in solution ionic strength, pH, temperature, etc.[52]

The formation of the micelle is a spontaneous start–stop process; for any given surfactant only a set number of molecules are needed to make an aggregate.[52] For SDS, this is approximately 60 molecules. For any given micellar aggregate, there are two competing forces that determine when the aggregate forms and the number of molecules comprising the micelle.[52] The removal of the hydrocarbon chains of the surfactant molecules from the bulk water by solubilizing the hydrophobic tails in the oily micellar interior drives the micellization process. This energy decrease is counterbalanced by an energy increase from the electrostatic repulsion between headgroups of the micelle. Due to these competing forces, the growth of a micelle has specific limits in terms of micellar aggregation number and as surfactant concentration continues to increase above the CMC (region E in Figure 1-10) these two competing forces produce new micelles rather than adding additional surfactant molecules to already existing micelles.[52]

Additionally, micellar structures are not static. The free molecules in solution migrate into the micelle and other molecules dissociate from the micelle to move into solution. This dynamic process is controlled to a large extent by the structure of the surfactant, particularly the size of the hydrophobic tail. For SDS, which has 12 carbons in its tail, the average residence time of a single molecule inside a micelle is 6 μs at 25

°C.[59] Increasing or decreasing the number of carbons by two methylene groups in either direction changes the residence time value to 83 μs and 0.5 μs, respectively.

It is tempting to assert that the formation of the micellar aggregate is the result of the buildup of surfactant molecules in the bulk because they can no longer occupy the more energetically favorable interface—the entire interface is already saturated with surfactant molecules. However, this assertion is incorrect. The reason for the relatively unchanging surface tension above the CMC is due to the chemical potential of the surfactant itself.[60] Below the CMC, the surfactant chemical potential changes logarithmically with increasing solution concentration. To obtain the same change in chemical potential above the CMC as that seen below the CMC, the total surfactant concentration would have to change by 2^N (where N is the aggregation number—the number of individual molecules making up a micelle) For typical aggregation numbers of micellar structures (recall SDS has an aggregation number of approximately 60 monomers), this amount of increase is not possible and we see a relatively small, if any, effect on the chemical potential of the surfactant and hence the surface tension.

1.4.3 – Measuring Surface Tension

The surface tension, and thereby the CMC, is able to be measured by using several different physical techniques.[52,61] The most common of these include the optical measurement of a sessile or pendent droplet or bubble, Du-Noüy ring tensiometry, and the Wilhelmy-plate technique. In addition to surface tension measurements, the CMC can also be determined using conductance and surface ion electrode measurements.

Both the Du-Noüy ring tensiometry method and the Wilhelmy-plate technique function in similar manners.

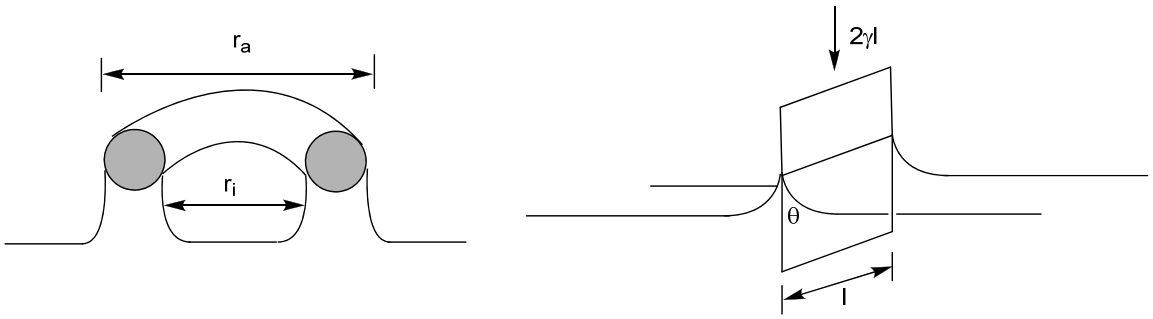

Figure 1-12 The Du-Noüy ring tensiometry (left, cutaway view) and Wilhelmy-plate method (right) (recreated from Reference 61)

In the Wilhelmy-plate technique a thin plate is lowered into the solution to be tested and then slowly withdrawn. As the surface tension of the liquid exerts a downward force on the plate in an attempt to submerge the plate, this force is recorded with a force balance. The force (F) exerted on the plate relates to the surface tension (γ) via eq 3,

$$F = 2 \cdot (l + t) \cdot \cos\theta \cdot \gamma \tag{3}$$

where l and t are the length and thickness of the plate in question, respectively. Making the assumption that the thickness of the plate is negligible ($l >> t$), that the contact angle θ is near zero, and then solving for γ simplifies eq 3 to

$$\gamma = \frac{F}{2l} \tag{4}$$

The contact angle, depicted in Figure 1-13, is the angle that is formed where a liquid and solid surface meet, measured from inside the liquid up to the liquid/vapor interface. A contact angle of zero means that the surface is completely wetted by the liquid. A contact angle of 180 indicates that the surface is completely non-wetted (think of a perfect sphere of liquid resting on the surface).

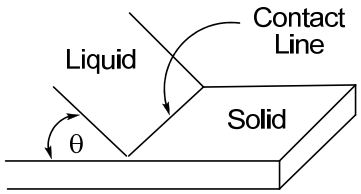

Figure 1-13 Graphical depiction of the contact angle θ measured between a drop (Liquid) and a surface (Solid). The contact angle is always measured from inside the drop up to the liquid/vapor interface (recreated from Reference 61)

In the Du-Noüy ring tensiometry technique, a ring is lowered into the solution to be tested and then lifted slowly. The maximal force being exerted on the ring by the surface tension of the liquid attempting to draw the ring back down into the solution is again recorded using a force balance. This force (F) relates to the surface tension (γ) via eq 5

$$F = 2\Pi \cdot \left(r_i + r_a\right) \cdot \gamma \tag{5}$$

where r_i and r_a are the radii as shown in Fig. 1-12. Solving for the surface tension (γ) gives us eq 6

$$\gamma = \frac{F}{2\Pi \cdot (r_i + r_a)} \tag{6}$$

These methods have several inherent problems associated with them. For one, these techniques are extremely sensitive to solution surface contamination by dust or other foreign particles. Additionally, both the ring and the plate used in these techniques must be fully wetting ($\theta \approx 0$) so that there is no angular component to the force of the surface tension acting on the ring/plate. Finally, the ring tensiometer method tends to need a correction factor to produce the correct values. While the Wilhelmy plate technique does not need a correction factor, care must be taken to ensure the plate remains clean.

The optical techniques suffer from few, if any, of these drawbacks and are usually an easier method to use to determine surface tension values, although as we will see the theoretical underpinnings of the optical techniques are much more advanced. All optical techniques function on the same basic physical principle centered on the equation of Laplace and Young (eq 7).

$$\Delta P = \gamma \cdot \left(\frac{1}{R_1} + \frac{1}{R_2} \right) + \rho g h \tag{7}$$

When a liquid surface is curved (as in a pendent or sessile drop), the Young–Laplace equation relates the pressure difference across the interface (ΔP) to the surface tension (γ). ρ is the density of the solution, g is the acceleration due to gravity, and h is the height. R_1 and R_2 are the two principle radii of curvature of the drop.

The surface tension of the pendent drop is determined by eq 8

$$\gamma = \Delta\rho g R_0^2 / \beta \tag{8}$$

where $\Delta\rho$ is the density difference between the solution and the surroundings (typically air), g is the gravitational constant, R_0 is the radius of curvature at the drop apex, and β the so-called shape factor.[62] The equations that are actually used to determine the drop profile are derived from the Young–Laplace equation.

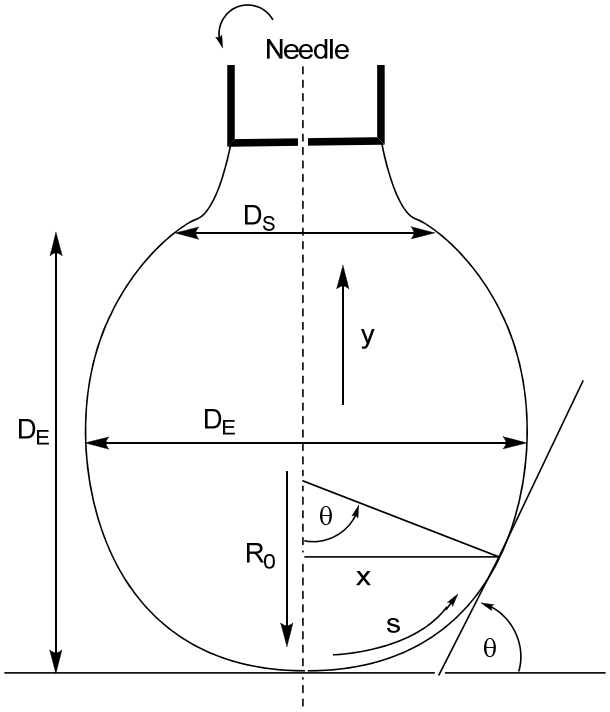

Figure 1-14 Pendent drop geometry (recreated from Reference 62)

The Young–Laplace equation can be expressed as three dimensionless first-order differential equations as shown in eqs 9–11

$$\frac{d\theta}{dS} = 2 - \beta Y - \frac{\sin\theta}{X} \tag{9}$$

$$\frac{dX}{dS} = \cos\theta \tag{10}$$

$$\frac{dY}{dS} = \sin\theta \tag{11}$$

s, *y*, *x*, and θ are shown in Figure 1-14. *S*, *Y*, and *X* are derived by dividing *s*, *y*, and *x*, respectively, by R_0. By solving these differential equations in terms of β, the surface tension can ultimately be determined.

As can be expected, the determination of the surface tension via pendent-drop method was an arduous task to perform by hand when first developed, and was not very

accurate. However the advent of the personal computer has largely done away with the need to perform these calculations by hand and software has been written that iteratively determines the value for β and then solves for the surface tension via eq 8.

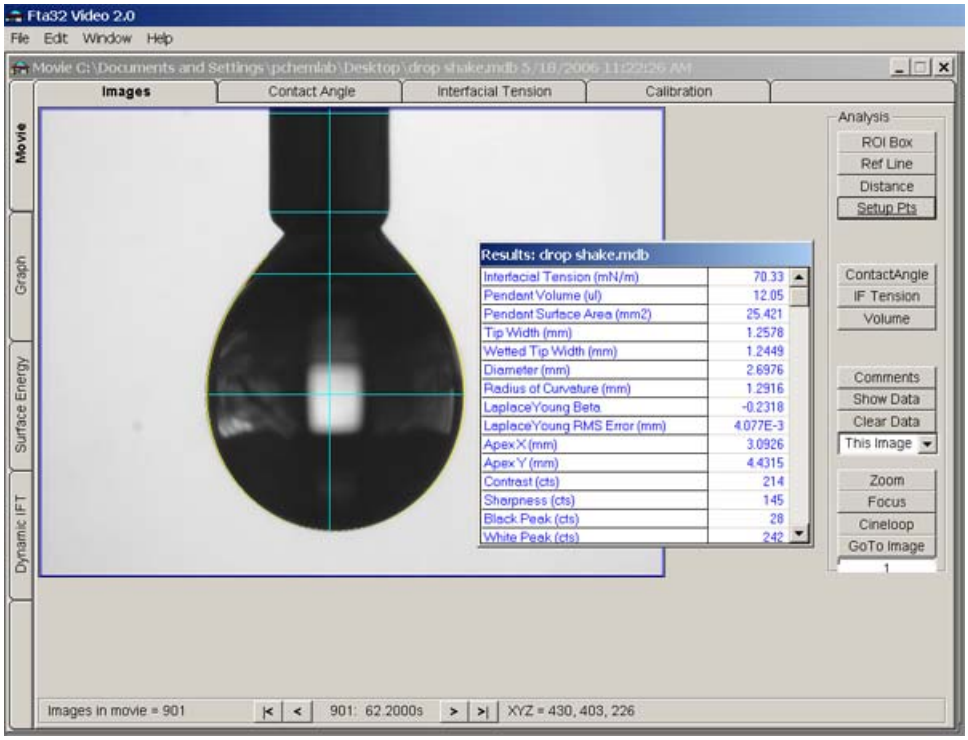

Figure 1-15 Pendent drop showing the geometry lines as drawn by computer software

This method requires very little material for a measurement, typically on the order of 10-15 microliters per drop, as compared to the tensiometer methods, which typically require several milliliters. If there is a drawback to the pendent-drop method, it lies in the need to have the drop remain completely motionless and at a constant volume. Both of these issues can be minimized or eliminated by use of a humidity chamber. A typical humidity chamber is constructed from a standard cuvette with a hole in the lid to accommodate the needle. The chamber is then filled with a small amount of the test solution so that the air inside the chamber becomes saturated by solvent molecules and helps to prevent the evaporation of the drop from the needle tip. The chamber also serves

to eliminate any potential air currents that may cause the drop to move, which would degrade the software's ability to determine the drop's profile. A second source of vibrations comes from normal low-frequency vibrations found in buildings above ground floor. It is recommended that surface tension measurements made with a pendent-drop instrument be performed at ground level or on a vibration isolation table to eliminate these vibrations.

1.4.4 – Solubility and Critical Micelle Concentration Values of Fatty Acids

Vorum[63] and Robb[64] showed that the aqueous solubility of the fatty acids is limited to chain lengths of fewer than 20 carbons. Above 18 carbons, the fatty acids do not possess enough hydrophilicity to enable them to be soluble in water to any measurable extent. The solubility and the CMC of an amphiphile are directly related to the number of headgroups—the greater the number of headgroups the more water soluble the amphiphile and the higher the CMC.[65-69] Shinoda[65,66] has observed that the CMCs for the following malonate-derived amphiphiles (Figure 1-16, **6** and **7)** were 3.5–15 times higher than the corresponding fatty acid (Figure 1-16, **5**).

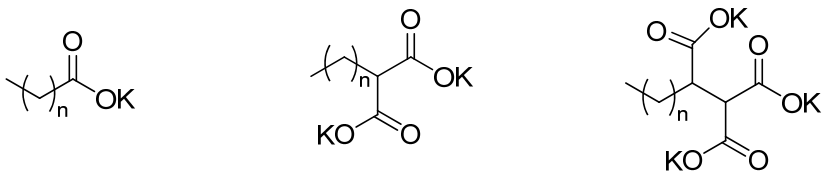

5 **6** **7**

Figure 1-16 Potassium salts of fatty acids and Malonate-derived fatty acids

Additionally, Shinoda noted that as the carbon chain length of the homologous series increased, the CMC decreased.[65] As the number of headgroups increased the CMC increased as well.[16] These data would suggest that the triheaded amphiphiles (Figure 1-1,

1–4) should show good water solubility. The hope is that increasing the water solubility of these amphiphiles will lead to more effective inhibitory properties.

1.5 – MINIMAL INHIBITORY CONCENTRATION (MIC) MEASUREMENTS

1.5.1 – Introduction to Fatty Acid Antimicrobial Activity and the Cutoff Effect

Fatty acids (**5**) have been known to possess antimicrobial activity since the 1920s.[70-72] The rising number of antibiotic-resistant strains of microorganisms ensures that the discovery of new compounds aimed at inhibiting organism growth will not slow for the foreseeable future. Fatty acids are known to show activity against a broad spectrum of bacteria (both Gram-positive and, to a lesser extent, Gram-negative[73,74]), fungi, yeast, mycobacteria, and certain viruses.[73,75-83] The activity of the fatty acids increases with increasing chain length[84,85] and then begins to decrease. This decrease is thought to be due to limited aqueous solubility of the longer chain homologues,[17] although micellization or some other physical process could be at work as well. A theoretical plot of log MIC vs. chain length is shown in Figure 1-17 to illustrate this phenomenon. This phenomenon is known as the cutoff effect.[84]

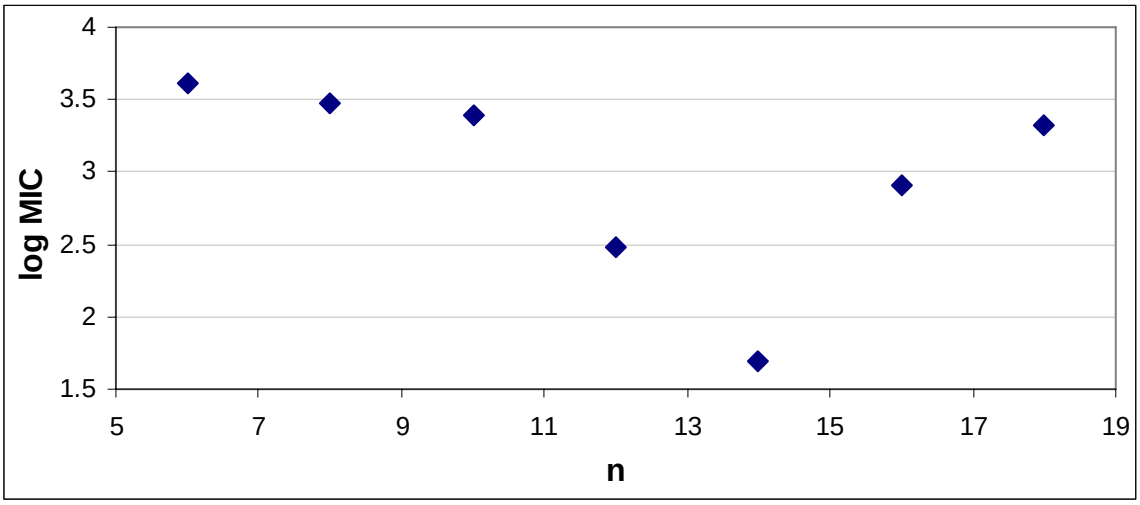

Figure 1-17 Theoretical plot of log MIC vs. number of carbons in tail (n) for an amphiphile

As the carbon chain length increases so does hydrophobicity, and therefore the solubility decreases for a given amphiphile.[17] Along with a decrease in solubility as the carbon chain length increases, the antimicrobial properties of a given amphiphile increase as well.[84,85] Work done previously in the Gandour group has shown a direct correlation between the inhibitory ability of an amphiphile (in this case anti-HIV and spermicidal activity) and the chain length of the tail.[86,87]

One reason given for the cutoff effect is the decrease in amphiphile concentration at the site of inhibition due to the limited solubility of longer chain tails. By designing multi-headed amphiphiles with three ionizable groups, we are aiming to remove solubility as a possible cause for the cutoff effect. Multi-headed ionic amphiphiles have higher aqueous solubility than single-headed amphiphiles,[88] and we therefore expect the multi-headed amphiphiles to improve the aqueous solubility of the longer chains in the homologous series.

Balgavý and Devínsky have proposed a few theories for the cutoff effect: size discrimination, limited aqueous solubility of amphiphiles, kinetic effects, and free volume.[84] Size discrimination refers to the physical size of the amphiphile binding site on the cell itself. The binding site has a fixed size depending on the organism in question. As the amphiphile chain length increases, the tail fills the available space until maximum activity is seen. As the chain continues to increase in length the receptor volume becomes too small, causing a decrease in activity.

Most studies of fatty acid inhibitory activity do not include fatty acids above 18 carbons in the tail due to the limited solubility. For instance, Vorum[63] measured the solubility of fatty acids in a pH 7.4 solution, and found that the C_{16} homologue had a solubility of ~ 1 μM, as opposed to 20–30 μM for the C_{14} homologue. The C_{20} and C_{22} homologues were too low to be measured. Robb obtained similar results.[64] The addition of the multi-head functionality to these amphiphiles is an attempt to remove limited aqueous solubility as a possible cause of the cutoff effect. This will also have the added benefit of allowing us to determine if longer chain homologues are indeed more active than the medium chain fatty acids.

Kinetic effects refer to the ability of the amphiphile to pass through the cell membrane of a target organism. This theoretical model assumes that the target receptor for the amphiphile is located within the cell itself, and not on the surface of the cell membrane. In order for the amphiphile to reach the target receptor, it must be hydrophobic enough to pass through the microbe's bilayer membrane, yet hydrophilic enough to be soluble in the aqueous media of the body or cell interior to reach the receptor site. Shorter chain amphiphiles would not be hydrophobic enough to cross the

lipid bilayer of the membrane, and longer chain amphiphiles will not be hydrophilic enough to pass through the aqueous environments of the cell interior.

Free volume is a theoretical model in which the amphiphile interacts with the microbial cell membrane itself. An amphiphile that inserts its tail into the cell membrane causes open space to appear. This open space is referred to as free volume. The lipids that naturally make up the cell membrane spread out to fill this free space. This causes the cellular membrane to become thinner, possibly leading to changes in functionality of cell membrane-bound proteins, cell leakage, or a complete rupturing of the cell itself. An amphiphile with too short a carbon chain (i.e. one that is relatively hydrophilic) would not cause antimicrobial activity. Even though a relatively large free volume is created, this amphiphile would be too hydrophilic to properly partition into the cell membrane. An amphiphile with too long a carbon chain (relatively hydrophobic) will not cause antimicrobial activity either. As the amphiphile carbon chain length approaches that of the phospholipids making up the cell membrane, the free volume goes to zero, thereby preventing the thinning of the cell membrane because the phospholipids do not have any free volume to fill.

1.5.2 – Fatty Acid Inhibition of Microorganisms

1.5.2.1 – Fatty Acid Activity Against non-Viral Organisms

Although fatty acid inhibitory activity has been known for over a century, very little is known about the mechanism(s) of action of fatty acids against target organisms.[76,77,82,84,89-93] In general, fatty acids are known to inhibit the growth of Gram-positive bacteria more effectively than Gram-negative.[73,74] The reason for the difference is thought to be the construction of the cell itself—Gram-positive bacteria cell walls are much less complex and are thinner than Gram-negative bacteria and mycobacteria.

However, this generalization does have exceptions. Fatty acids are active against *Neisseria gonorrhoeae*—a Gram-negative bacterium.[76]

While the mechanism(s) of action of fatty acid inhibition are relatively unknown, several theories have been proposed. The most prevalent possible mechanisms of action are destabilization of the cell membrane, inhibition of enzymatic activities, inhibition of oxygen uptake, uncoupling of the electron transport chain and oxidative phosphorylation, changes in turgor (osmotic) pressure, changes in lipid bilayer thickness, inhibition of cell wall synthesis, and inhibition of protein myristoylation.[76,77,82,84,89-93]

1.5.2.2 – Fatty Acid Activity Against Viruses

Fatty acids are also known to inhibit the growth of enveloped viruses.[94-96] Fatty acids typically do not inhibit non-enveloped viruses, which tends to suggest that the viral envelope is the site of attack.[95,97] Antiviral activity is usually dependent on chain length of the fatty acid tail[94,95] and the number of double bonds in the fatty acid.[94,95,98] Polyanionic compounds have been demonstrated to be effective against HIV[99-103] by blocking the binding of HIV to cell surfaces, thereby inhibiting the replication of this retrovirus. More specifically, Cushman and coworkers[104] have demonstrated that polycarboxylates are effective at preventing HIV attachment. This work has prompted us to test the multi-headed anionic surfactants we have designed as possible inhibitors of HIV.[105]

The mechanism(s) of action of fatty acids against viruses are even less well understood than their action against other microorganisms; however, a few theories have been presented. Anti-viral activity is believed to be due to the disruption of the viral envelope and cell membranes leading to the disintegration of the viral envelope. The mechanism for the disintegration of the viral envelope has not been clearly identified.

Both chain length and unsaturation probably affect the degree at which fatty acids can penetrate the viral envelope.[95] fatty acids are typically believed to inhibit viruses by destabilization of the viral envelope, prevention of myristolylation, and destabilizing viral proteins.

1.6 – SUMMARY AND CONCLUSIONS

The focus of this research is the synthesis and characterization of two new series of homologous dendritic tricarboxylato amphiphiles, **3CCbn** and **3CCb1(n,n)** (**2** and **4** in Figure 1-1, respectively). Once these amphiphiles have been synthesized and characterized, the CMC of these amphiphiles will be determined via pendent drop measurement to determine at what concentration micelles begin to form. Due to the number of ionizable headgroups in these amphiphiles, we expect that they will be more water soluble than a fatty acid of comparable chain length and will not form micelles as easily. This should allow us to test the activity of longer chain amphiphiles than have been previously studied. The best type of counterion will need to be determined in order to provide the maximum solubility for these amphiphiles.

Inhibitory activity of these series of amphiphiles will be collected and compared to the micellization data. This will help us determine whether these amphiphiles are inhibiting growth due to detergency or via some possible specific mechanism of action. Inhibitory activity occurring at concentrations below the CMC tends to indicate that the activity is based on some specific mechanism of action, because detergency is a function of micelles. The broad screen inhibition testing will also help develop leads for which microorganisms these amphiphiles should be tested against, as well as provide ideas for

future experimental direction. We have also determined whether making the isosteric changes between compounds **1**, **2**, and **3** has any effect on the CMC or inhibitory activity.

1.7 – REFERENCES

(1) Vieira, O. V.; Hartmann, D. O.; Cardoso, C. M. P.; Oberdoerfer, D.; Baptista, M.; Santos, M. A. S.; Almeida, L.; Ramalho-Santos, J. o.; Vaz, W. L. C. *PLoS ONE* **2008**, *3*, e2913.

(2) Rosen, M. J. In *Surfactants and Interfacial Phenomena*; 3 ed.; John Wiley & Sons, Inc.: Hoboken, New Jersey, 2004, p 1.

(3) D'Cruz, O. J.; Uckun, F. M. *Curr. Pharm. Des.* **2004**, *10*, 315-336.

(4) Fichorova, R. N.; Tucker, L. D.; Anderson, D. J. *J. Infect. Dis.* **2001**, *184*, 418-428.

(5) Rosen, M. J. In *Surfactants and Interfacial Phenomena*; 3 ed.; John Wiley & Sons, Inc.: Hoboken, New Jersey, 2004, p 6.

(6) Myers, D. In *Surfactant Science and Technology*; 3 ed.; John Wiley & Sons, Inc.: Hoboken, New Jersey, 2006, p 3.

(7) Cross, J. In *Surfactant Science*; Cross, J., Ed.; Marcel Dekker, Inc.: New York, New York, 1994; Vol. 53, p 7-14.

(8) Lawrence, C. A. In *Surfactant Science*; Jungermann, E. E., Ed.; Marcel Dekker, Inc.: New York, New York, 1970; Vol. 4, p 491-495.

(9) Myers, D. In *Surfactant Science and Technology*; 3 ed.; John Wiley & Sons, Inc.: New York, New York, 2006, p 7-17.

(10) Urizzi, P.; Souchhard, J. P.; Nepvue, F. *Tet. Lett.* **1996**, *37*, 4685.

(11) Myers, D. In *Surfactant Science and Technology*; 3 ed.; John Wiley & Sons, Inc.: Hoboken, New Jersey, 2006, p 6.

(12) Cross, J. In *Anionic Surfactants: Analytical Chemistry*; 2 ed.; Cross, J., Ed.; Marcel Dekker, Inc.: New York, New York, 1998; Vol. 73, p 2.

(13) Myers, D. In *Surfactant Science and Technology*; 3 ed.; John Wiley & Sons, Inc.: Hoboken, New Jersey, 2006, p 31.

(14) Lomax, E. G. In *Amphoteric Surfactants*; Lomax, E. G., Ed.; Marcel Dekker, Inc.: New York, 1996; Vol. 59, p 3.

(15) Lomax, E. G. In *Amphoteric Surfactants*; Lomax, E. G., Ed.; Marcel Dekker, Inc.: New York, 1996; Vol. 59, p 10-11.

(16) Shinoda, K.; Nakagawa, T.; Tamamushi, B.-I.; Isemura, T. In *Physical Chemistry: A Series of Monographs*; Loebl, E. M., Ed.; Academic Press, Inc.: New York and London, 1963, p 42-44.

(17) Klevens, H. B. *Chem. Rev.* **1950**, *47*, 1-74.

(18) Myers, D. In *Surfactant Science and Technology*; 3 ed.; John Wiley & Sons, Inc.: Hoboken, New Jersey, 2006, p 131.

(19) Rosen, M. J. In *Surfactants and Interfacial Phenomena*; 3 ed.; John Wiley & Sons, Inc.: Hoboken, New Jersey, 2004, p 121.

(20) Rosen, M. J. In *Surfactants and Interfacial Phenomena*; 3 ed.; John Wiley & Sons, Inc.: Hoboken, New Jersey, 2004, p 138-139.

(21) Myers, D. In *Surfactant Science and Technology*; 3 ed.; John Wiley & Sons, Inc.: Hoboken, New Jersey, 2006, p 140-142.

(22) Stigter, D. *J. Phys. Chem.* **1974**, *78*, 2480-2485.

(23) Shinoda, K.; Nakagawa, T.; Tamamushi, B.-I.; Isemura, T. In *Physical*

Chemistry: A Series of Monographs; Loebl, E. M., Ed.; Academic Press, Inc.: New York and London, 1963, p 54-55.
(24) Lomax, E. G. In *Amphoteric Surfactants*; Lomax, E. G., Ed.; Marcel Dekker, Inc.: New York, 1996; Vol. 59, p 13-14.
(25) Rosen, M. J. In *Surfactants and Interfacial Phenomena*; 3 ed.; John Wiley & Sons, Inc.: Hoboken, New Jersey, 2004, p 139-144.
(26) Yiv, S.; Zana, R. *J. Colloid Interface Sci.* **1980**, *77*, 449-455.
(27) Tsubone, K.; Arakawa, Y.; Rosen, M. J. *J. Colloid Interface Sci.* **2003**, *262*, 516-524.
(28) Tsubone, K.; Ogawa, T.; Mimura, K. *J. Surfactants Detgts.* **2003**, *6*, 39-46.
(29) Tsubone, K.; Rosen, M. J. *J. Colloid Interface Sci.* **2001**, *244*, 394-398.
(30) Robb, I. D.; Smith, R. *J. Chem. Soc., Faraday Trans. 1* **1974**, *70*, 287-292.
(31) Myers, D. In *Surfactant Science and Technology*; 3 ed.; John Wiley & Sons, Inc.: Hoboken, New Jersey, 2006, p 142-143.
(32) Rosen, M. J. In *Surfactants and Interfacial Phenomena*; 3 ed.; John Wiley & Sons, Inc.: Hoboken, New Jersey, 2004, p 144-146.
(33) Myers, D. In *Surfactant Science and Technology*; 3 ed.; John Wiley & Sons, Inc.: Hoboken, New Jersey, 2006, p 144-145.
(34) Corrin, M. L.; Harkins, W. D. *J. Am. Chem. Soc.* **1947**, *69*, 683-688.
(35) Shinoda, K.; Yamaguchi, T.; Hori, R. *Bull. Chem. Soc. Japan* **1961**, *34*, 237-241.
(36) Ray, A.; Nemethy, G. *J. Am. Chem. Soc.* **1971**, *93*, 6787-6793.
(37) Ray, A. *Nature (London)* **1971**, *231*, 313-315.
(38) Mukerjee, P. *Adv. Colloid Interface Sci.* **1967**, *1*, 242-275.
(39) Rosen, M. J. In *Surfactants and Interfacial Phenomena*; 3 ed.; John Wiley & Sons, Inc.: Hoboken, New Jersey, 2004, p 146-148.
(40) Lin, S.-Y.; Lin, Y.-Y.; Chen, E.-M.; Hsu, C.-T.; Kwan, C.-C. *Langmuir* **1999**, *15*, 4370.
(41) Schick, M. J.; Fowkes, F. M. *J. Phys. Chem.* **1957**, *61*, 1062-1068.
(42) Schick, M. J.; Gilber, A. H. *J. Colloid Sci.* **1965**, *20*, 464-472.
(43) Herzfeld, S. H.; Corrin, M. L.; Harkins, W. D. *J. Phys. Chem.* **1950**, *54*, 271-283.
(44) Myers, D. In *Surfactant Science and Technology*; 3 ed.; John Wiley & Sons, Inc.: Hoboken, New Jersey, 2006, p 149-150.
(45) Rosen, M. J. In *Surfactants and Interfacial Phenomena*; 3 ed.; John Wiley & Sons, Inc.: Hoboken, New Jersey, 2004, p 149.
(46) Flockhart, B. D. *J. Colloid Sci.* **1961**, *16*, 484-492.
(47) Crook, E. H.; Fordyce, D. B.; Trebbi, G. F. *J. Phys. Chem.* **1963**, *67*, 1987-1994.
(48) Chen, L.-J.; Lin, S.-Y.; Huang, C.-C.; Chen, E.-M. *Coll. Surfs. A* **1998**, *135*, 175-181.
(49) Myers, D. In *Surfactant Science and Technology*; 3 ed.; John Wiley & Sons, Inc.: Hoboken, New Jersey, 2006, p 108-112.
(50) Rosen, M. J. In *Surfactants and Interfacial Phenomena*; 3 ed.; John Wiley & Sons, Inc.: Hoboken, New Jersey, 2004, p 214-215.

(51) Davey, T. M.; Ducker, W. A.; Hayman, A. R.; Simpson, J. *Langmuir* **1998**, *14*, 3210-3213.
(52) Evans, D. F.; Wennerstrom, H. In *The Colloidal Domain: Where Physics, Chemistry, and Biology Meet*; 2nd ed.; Wiley-VCH: New York, 1999, p 7-10.
(53) Todar, K., *BACTERIAL STRUCTURE IN RELATIONSHIP TO PATHOGENICITY*, 2008, http://textbookofbacteriology.net/BSRP.html, last accessed December 15th, 2008
(54) Butt, H.-J.; Graf, K.; Kappl, M. In *Physics and Chemistry of Interfaces*; 2nd ed.; Wiley-VCH: Weinheim, 2006, p 7.
(55) Evans, D. F.; Wennerstrom, H. In *The Colloidal Domain: Where Physics, Chemistry, and Biology Meet*; 2nd ed.; Wiley-VCH: New York, 1999, p 5-8.
(56) Butt, H.-J.; Graf, K.; Kappl, M. In *Physics and Chemistry of Interfaces*; 2nd ed.; Wiley-VCH: Weinheim, 2006, p 4-7.
(57) Hartley, G. S. *Aqueous Solutions of Paraffin-chain Salts: A Study in Micelle Formation*; Hermann & Co.: Paris, 1936.
(58) Evans, D. F.; Wennerstrom, H. In *The Colloidal Domain: Where Physics, Chemistry, and Biology Meet*; 2nd ed.; Wiley-VCH: New York, 1999, p 13-18.
(59) Aniansson, E. A. G.; Wall, S. N.; Almgren, M.; Hoffmann, H.; Kielmann, I.; Ulbricht, W.; Zana, R.; Lang, J.; Tondre, C. *J. Phys. Chem.* **1976**, *80*, 905.
(60) Evans, D. F.; Wennerstrom, H. In *The Colloidal Domain: Where Physics, Chemistry, and Biology Meet*; 2nd ed.; Wiley-VCH: New York, 1999, p 166.
(61) Butt, H.-J.; Graf, K.; Kappl, M. In *Physics and Chemistry of Interfaces*; 2nd ed.; Wiley-VCH: Weinheim, 2006, p 12-15.
(62) Hansen, F. K.; Rodsrud, G. *J. Coll. Inter. Sci.* **1991**, *141*, 1-12.
(63) Vorum, H.; Brodersen, R.; Kragh-Hansen, U.; Pedersen, A. O. *Biochim. Biophyis. Acta.* **1992**, *1126*, 135-142.
(64) Robb, I. D. *Aust. J. Chem. Rev.* **1966**, *19*, 2281-2284.
(65) Shinoda, K. *J. Phys. Chem.* **1954**, *58*, 1136-1141.
(66) Shinoda, K. *J. Phys. Chem.* **1955**, *59*, 432-435.
(67) Shinoda, K. *J. Phys. Chem.* **1956**, *60*, 1439-1441.
(68) Haldar, J.; Aswal, V. K.; Goyal, P. S.; Bhattacharya, S. *Angew. Chem. Int. Ed.* **2001**, *40*, 1228-1232.
(69) Bhattacharya, S.; Haldar, J. *Colloids Surf., A* **2002**, *205*, 119-126.
(70) Walker, J. E. *J. Infect. Dis.* **1924**, *35*.
(71) Nieman, C. *Bacteriol. Rev.* **1954**, *18*, 147-163.
(72) Bayliss, M. *J. Bacteriol.* **1936**, *31*, 489-504.
(73) Kanai, K.; Kondo, E. *Jpn. J. Med. Sci. Biol.* **1979**, *32*, 135-174.
(74) Thormar, H.; Bergsson, G. *Recent Dev. Antiviral Res.* **2001**, *1*, 157-173.
(75) Kabara, J. J. *J. Soc. Cosmet Chem.* **1978**, *29*, 733-741.
(76) Miller, R. D.; Brown, K. E.; Morse, S. A. *Infect. Immun.* **1977**, *17*, 303-312.

(77) McGaw, L. J.; Jager, A. K.; van Staden, J. *South African J. Botany* **2002**, *68*, 417-423.
(78) Kabara, J. J. *Nutr. Rev.* **1980**, *38*, 65-73.
(79) Kabara, J. J.; Vrable, R.; Liekenjie, M. S. F. *Lipids* **1977**, *12*, 753-759.
(80) Kabara, J. J.; Swieczkowski, D. M.; Conley, A. J.; Truant, J. P. *Antimicrob. Agents Chemother.* **1972**, *2*, 23-28.
(81) Kondo, E.; Kanai, K. *Jpn J. Med. Sci. Biol.* **1972**, *25*, 1-13.
(82) Saito, H.; Tomioka, H.; Yoneyama, T. *Antimicrob. Agents Chemother.* **1984**, *26*, 164-169.
(83) Bergsson, G.; Arnfinnsson, J.; Steingrimsson, O.; Thormar, H. *Antimicrob. Agents Chemother.* **2001**, *45*, 3209-3212.
(84) Balgavy, P.; Devinsky, F. *Adv. Colloid Interface Sci.* **1996**, *66*, 23-63.
(85) Devinsky, F.; Kopecka-Leitmanova, A.; Sersen, F.; Balgavy, P. *J. Pharm. Pharmacol.* **1990**, *42*, 790-794.
(86) Wong, Y.-L.; Hubieki, M. P.; Curfman, C. L.; Doncel, G. F.; Dudding, T. C.; Savle, P. S.; Gandour, R. D. *Bioorg. Med. Chem.* **2002**, *10*.
(87) Wong, Y.-L.; Curfman, C. L.; Doncel, G. F.; Hubieki, M. P.; Dudding, T. C.; Savle, P. S.; Gandour, R. D. *Tetrahedron* **2002**, *58*, 45-54.
(88) Lindman, B.; Wennerstrom, H. In *Topics in Current Chemistry*; Springer-Verlag: New York, 1980; Vol. 87, p 10.
(89) Bergsson, G.; Arnfinnsson, J.; Steingrimsson, O.; Thormar, H. *Apmis* **2001**, *109*, 670-678.
(90) Galbraith, H.; Miller, T. B. *J. Appl. Bacteriol.* **1973**, *36*, 635-646.
(91) Galbraith, H.; Miller, T. B. *J. Appl. Bacteriol.* **1973**, *36*, 647-658.
(92) Saito, H.; Tomioka, H. *Antimicrob. Agents Chemother.* **1988**, *32*, 400-402.
(93) Niwano, M.; Mirumachi, E.; Uramoto, M.; Isono, K. *Agric. Biol. Chem.* **1984**, *48*, 1359-1360.
(94) Stock, C. C.; Francis, T. *J. Exp. Med.* **1940**, *71*, 661-681.
(95) Thormar, H.; Isaacs, C. E.; Brown, H. R.; Barshatzky, M. R.; Pessolano, T. *Antimicrob. Agents Chemother.* **1987**, *31*, 27-31.
(96) Horowitz, B.; Piet, M. P. J.; Prince, A. M.; Edwards, C. A.; Lippin, A.; Walakovits, L. A. *Vox Sanguinis* **1988**, *54*, 14-20.
(97) Hilmarsson, H.; Kristmundsdottir, T.; Thormar, H. *Apmis* **2005**, *113*, 58-65.
(98) Kohn, A.; Gitelman, J.; Inbar, M. *Antimicrob. Agents Chemother.* **1980**, *18*, 962-968.
(99) deClercq, E. *J. Med. Chem.* **1986**, *29*, 1562-1569.
(100) deClercq, E. *J. Med. Chem.* **1995**, *38*, 2491-2517.
(101) deClercq, E. *Curr. Med. Chem.* **2001**, *8*, 1543-1572.
(102) deClercq, E. *Biochim. Biophys. Acta* **2002**, *1587*, 258-275.
(103) Leydet, A.; Barthelemy, P.; Boyer, B.; Lamaty, G.; Roque, J. P.; Witvrouw, M.; deClercq, E. *Bioorg. Med. Chem. Lett.* **1996**, *6*, 397-402.
(104) Cushman, M.; Shabana, I.; Ruell, J. A.; Schaeffer, C. A.; Rice, W. G. *Bioorg. Med. Chem. Lett.* **1998**, *8*, 833-836.

(105) Macri, R. V.; Karlovská, J.; Doncel, G. F.; Du, X.; Maisuria, B. B.; Williams, A. A.; Sugandhi, E. W.; III, J. O. F.; Esker, A. R.; Gandour, R. D. *Bioorg. Med. Chem.* **2009**, *Accepted for Publication*.

CHAPTER 2 – 3CCbn SERIES SYNTHESIS AND CHARACTERIZATION

2.1 – SYNTHETIC STRATEGY

The synthesis of the target compounds (**3CCbn, n=14, 16, 18, 20, and 22**) was envisioned utilizing a synthetic strategy wherein the long chain, hydrophobic tail was coupled with the triheaded, hydrophilic carboxylato functionality to produce the desired amphiphile in the final step of the synthesis (Scheme 2-1). For this series of reactions, **3E** and **3C** refer to the triester and tricarboxylate headgroups, respectively, **Cb** refers to the carbamido linker group, and **n** is the total number of carbons in the hydrophobic tail.

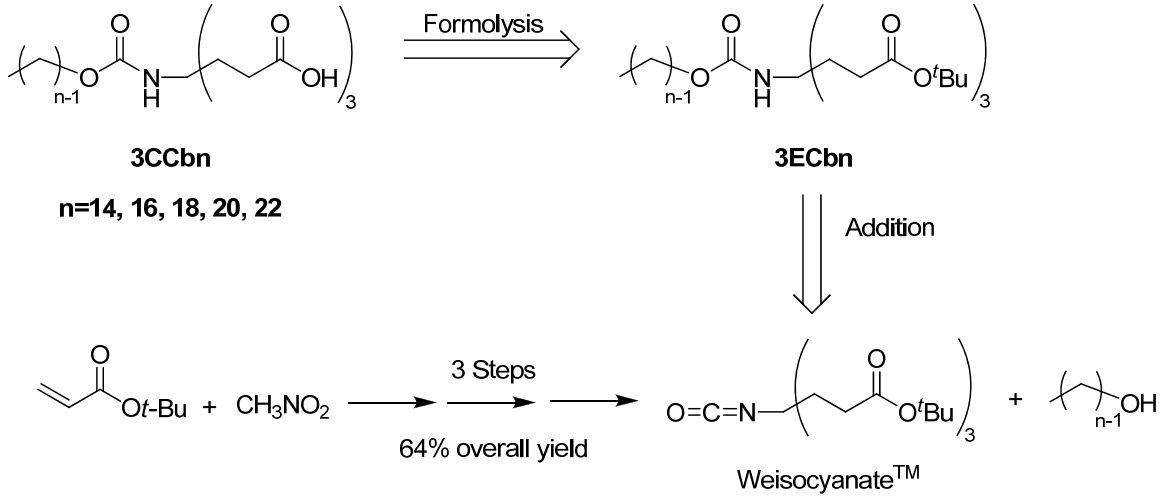

Scheme 2-1 Retrosynthetic analysis of **3CCbn** material

The hydrophobic moiety of the **3CCbn** series was derived from simple alkan-1-ols. The alcohols were all commercially available in high purity, leaving only the synthesis of the triheaded acid functionality to be elucidated. Newkome's isocyanate-based dendritic building blocks[1] proved to be an excellent starting point for the formation of the triheaded acid functionality, beginning with simple starting materials

(nitromethane and *tert*-butyl acrylate) to produce Weisocyanate™ in good overall yields (64 %).[2]

As noted by Newkome,[3] Weisocyanate™ is an extraordinarily stable isocyanate, requiring no special handling considerations as is typical with isocyanate functional groups. This unusual stability does have an adverse side effect on the chemistry – it makes the isocyanate rather unreactive towards non-nucleophilic alcohols. Work done in our research group[4-6] has shown that a more nucleophilic species, such as a primary or secondary amine, is much more reactive towards Weisocyanate™, requiring much milder conditions for the reaction to take place. Therefore, the majority of our synthetic endeavors were devoted towards developing optimal reaction conditions for the addition reaction.

2.2 – CARBAMATE FORMATION – SYNTHESIS OF THE 3ECbn SERIES

2.2.1 – Initial Alcohol Addition Attempts

While there are several literature examples[3,7-19] of reactions involving alcohols with tertiary isocyanates, none could be found for the coupling of long-chain alkan-1-ols (greater than 12 carbons) to tertiary isocyanates. Several literature examples of carbamate formation are displayed in Table 1.

Table 2-1 Reactions of alcohols with tertiary isocyanates

Entry	Alcohol	Isocyanate	Conditions	Reference
1	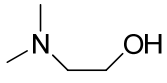	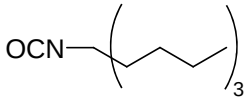	Xylene, reflux, 64%	Sperber et al.[17]
2	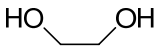	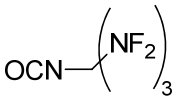	25 h, rt, 96% dicarbamate	Firth and Frank[8]
3	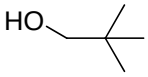	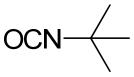	$Ti(Ot\text{-}Bu)_4$, benzene, 1 h, rt, 70%	Spino et al.[18]
4	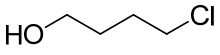	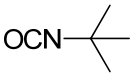		Yamakazi et al.[19]
5	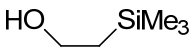	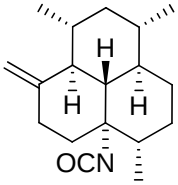	TEA, Toluene, 60 h, 100 °C, no yield given	Piers and Llinas-Brunet[12]
6	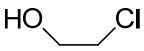	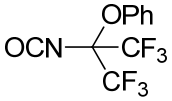	Et_2O, rt	Korenchenko et al.[10]
7	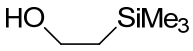	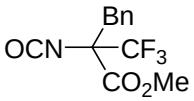	TEA, $CHCl_3$, 80 °C	Hollweck et al.[9]
8	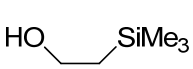	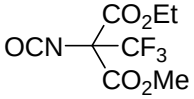	TEA, $CHCl_3$, 6 h, reflux	Pozzo et al.[13]
9	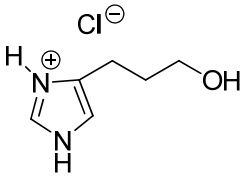	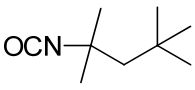	CH_3CN, heat, no yield given	Sasse et al.[15]
10	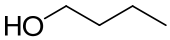	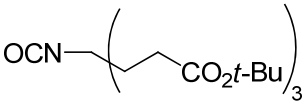	95%, no conditions given	Newkome et al.[3]
11	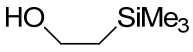	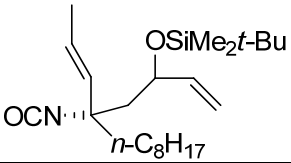	NaH, THF, 20 min., 0 °C, 97%	Roulland et al.[14]

We note that several of these examples show reactive functional groups in addition to the isocyanate (Table 1, entries 5, 7, 8, 10, 11), yet the major product is that in which the alcohol and isocyanate react to form the carbamate. Additionally, a wide range of reaction conditions have been used for the addition reaction. The varying conditions are most likely based around the reactivity of the isocyanate, with more reactive isocyanates requiring milder reaction conditions (Table 1, entries 2, 6).[8,10] Specifically, the strongly electron withdrawing groups present would pull electron density away from the isocyanate, making the carbon more electropositive, and thereby requiring milder conditions for the addition reaction to occur.

Our procedure required some optimization as our initial attempt in refluxing dichloromethane, based on a literature procedure[20] for addition of 1-dodecanol to a primary isocyanate, resulted in recovery of the starting materials. We noted that the literature procedure utilized a liquid isocyanate, which precluded the need for solvent, whereas the starting materials we are using are all solids at room temperature. We also noted that the reaction was run at 80 °C; the solvent was therefore switched to toluene to allow the reaction mixture to be heated to temperatures higher than those obtainable with dichloromethane.

The results of the addition reaction with toluene as a solvent at 80 °C were disappointing, producing only 26% crude yield. The reaction was next attempted neat at 80 °C—a temperature at which the starting materials would melt—in order to more closely mirror the literature procedure, which produced only 21% crude yield of desired product.

2.2.2 – Base-Catalyzed Addition–A Mechanistic Interpretation

Following the precedent[21] that a base could potentially catalyze the addition of the alcohol to the isocyanate, heating the mixture to reflux (95 °C oil bath) in triethylamine as the solvent gave high crude yields (>90%) of a colorless product. Under these conditions, the addition of alkan-1-ols to Weisocyanate™ gave triesters (**3ECbn**) in good yields of chromatographed products (Scheme 2-2).

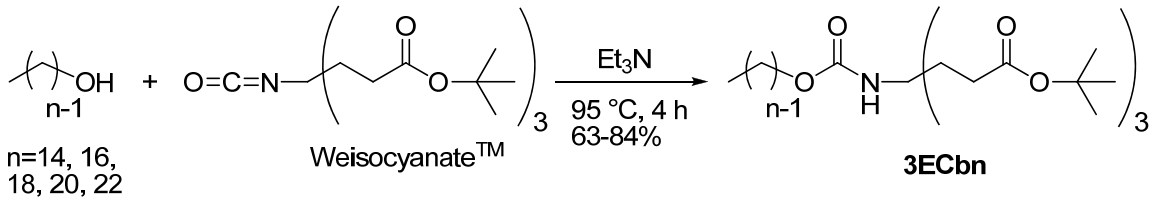

Scheme 2-2 Synthesis of **3ECbn** material

The reaction likely proceeds through a multi-step addition mechanism,[21] with overall proton transfer from the oxygen of the alcohol to the nitrogen of the isocyanate, catalyzed by the presence of the organic base (Scheme 2-3).

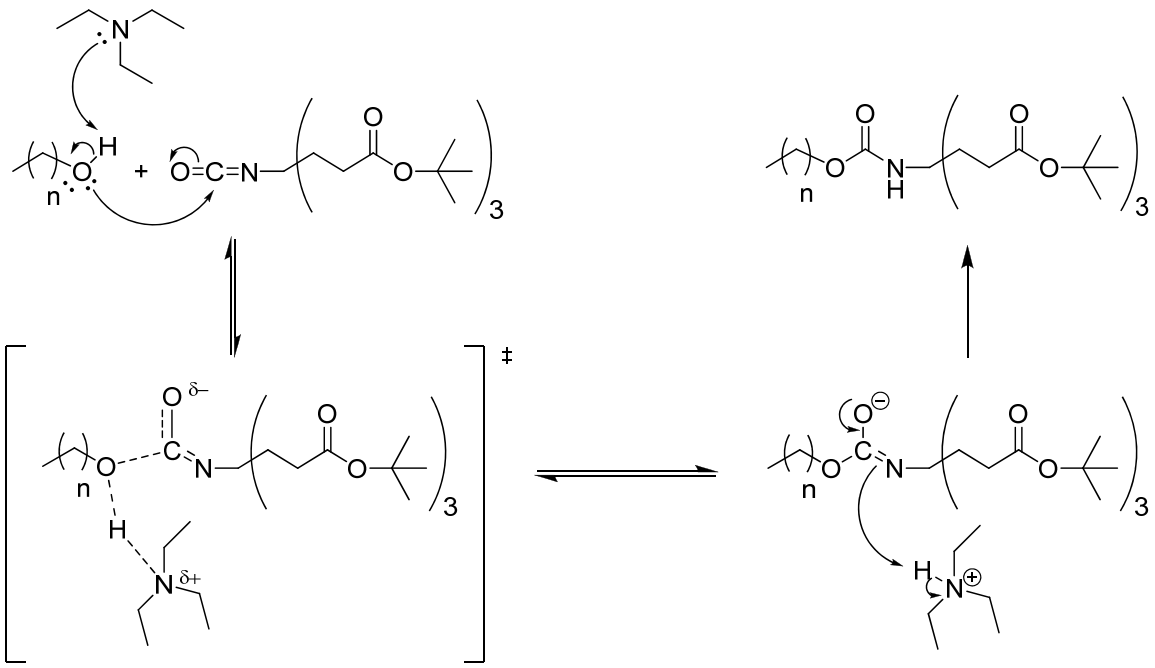

Scheme 2-3 Proposed mechanism of action of base-catalyzed addition

This proton transfer is greatly enhanced by the presence of the base, and the lack of efficiency of proton transfer is the most likely reason for the first few experimental failures before the use of a basic solvent.

According to Schwetlick et al.,[21] the mechanism of action of addition of hydrogen acidic compounds (i.e. alcohols) to isocyanates is a two-step process, with the initial addition of the alcohol to the isocyanate, along with the corresponding proton transfer, being the rate-limiting step (1, Figure 2-1).

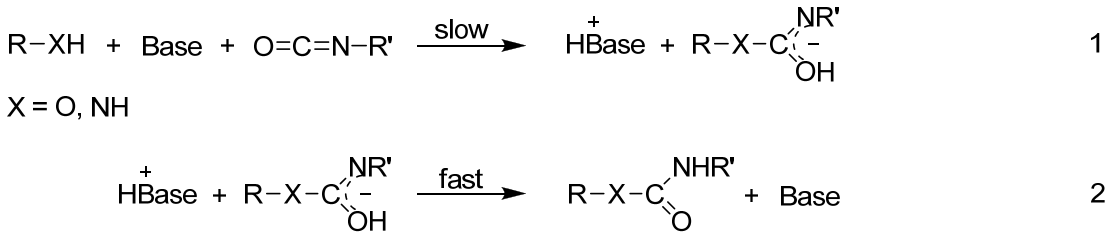

Figure 2-1 Overall mechanism of base-catalyzed addition of alcohols and amines to isocyanates

The timing of the rate-limiting step of these two processes is the essential problem in these reactions, and may follow any of three different mechanistic pathways which are heavily dependent on solvent.

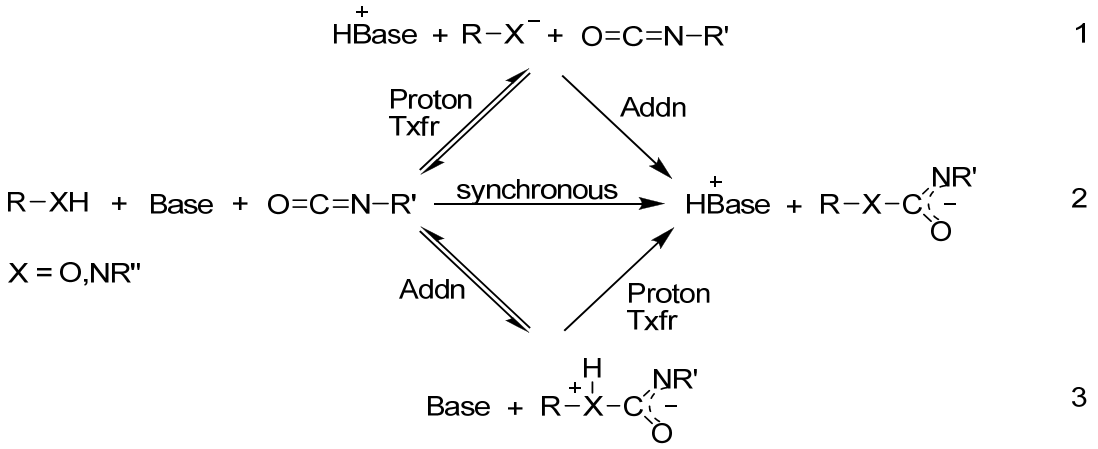

Figure 2-2 Mechanistic pathways for proton transfer of Step 1 in Figure 2-1

The most likely reaction pathway for our reaction series is that of reaction 2 (synchronous addition with corresponding proton transfer) in Figure 2-2 (X = O), as the reaction is being run in a solvent of intermediate polarity (triethylamine) with a relatively non-acidic alcohol. Reaction pathway 1 typically holds for acidic alcohols and phenols (X = O), and reaction pathway 3 is typical of ureido formation by nucleophilic amines (X = N). The rates of the reactions in pathways 2 and 3 should both be affected by steric bulk in R-XH.[21] As the steric bulk of R-XH increases, the rate of the reaction should decrease; therefore if this reaction is functioning by reaction 2 as supposed above, we should see a change in the rate of the reaction by going to sterically bulkier alcohols. Chapter 3 deals with the synthesis of two-tailed alcohols and their addition to isocyanates, and we see from that work that the rate of the reaction does in fact decrease when the only change is to the steric bulk of the alcohol. This suggests that our supposition that this reaction is occurring by reaction pathway 2 is probably correct.

2.2.3 – Reaction Workup

The initial workup for this set of reaction conditions constituted a simple concentration of the product by rotary evaporation to remove the bulk of the triethylamine, followed by high vacuum to remove the remaining solvent. However, this did not remove all of the triethylamine from the reaction flask, even after three days under high vacuum. Optimal workup conditions were found by diluting the reaction mixture with diethyl ether, followed by washing with an aqueous solution of hydrochloric acid (2*M*) to convert the triethylamine into its highly water-soluble salt. The acid wash was followed by washes with solutions of saturated sodium bicarbonate and finally saturated sodium chloride. One experiment was performed in which the $NaHCO_3$ and NaCl washes were omitted, and the ^1H NMR of the recovered product showed an unacceptable level of impurities.

2.2.4 – Characterization

All compounds were fully characterized by melting point, 1-D ^1H and ^{13}C NMR, IR, high-resolution mass spectrometry, and elemental analysis. The ^1H NMR showed the characteristic signals associated with carbamate formation at ~ 4.7 δ (representing the NH signal of the carbamate). The signal produced by the α-protons to the carbamate oxygen has shifted downfield from that produced by the free alcohol from ~3.6 δ to ~ 4.0 δ. All other NMR signals were consistent with the addition of the alcohol to the isocyanate functionality, and not to one of the *tert*-butyl esters (the stretch at 1.4 δ integrated to 27 protons, which indicates that all *tert*-butyl esters remained intact). The ^{13}C NMRs showed weak single peaks at ~ 155 δ, representing the carbamate carbonyl group. The ester carbonyls show a much stronger signal at ~ 172 δ. Due to longer T1 relaxation

times and almost no NOE, carbons without hydrogen attached tend to have weak NMR signals. The supposed reason for the stronger ester carbonyl signal versus the carbamate carbonyl is due to faster relaxation time of the ester, more ester groups contributing to the signal, or both. IR data indicate the loss of the isocyanate signal at 2250 cm^{-1}, and shows the presence of two carbonyl peaks, corresponding to the carbamate at 1702 cm^{-1} and *tert*-butyl esters at 1728 cm^{-1}.

2.3 – TRIACID FORMATION

Formolysis of the triesters produced the triacids (**3CCbn**) in good yields of recrystallized products (Scheme 2-4).

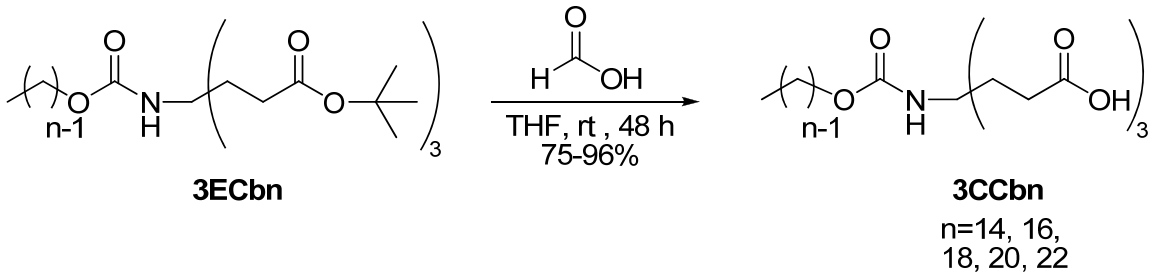

Scheme 2-4 Synthesis of **3CCbn** material

THF was added to all of the reactions to help dissolve the esters in formic acid. All reactions formed a white precipitate after approximately 24 hours, and the reactions were given an additional 24 hours to ensure complete formolysis. The formolysis reaction supposedly follows an E1 elimination pathway, producing 2-methylpropene as a byproduct (Scheme 2-5).

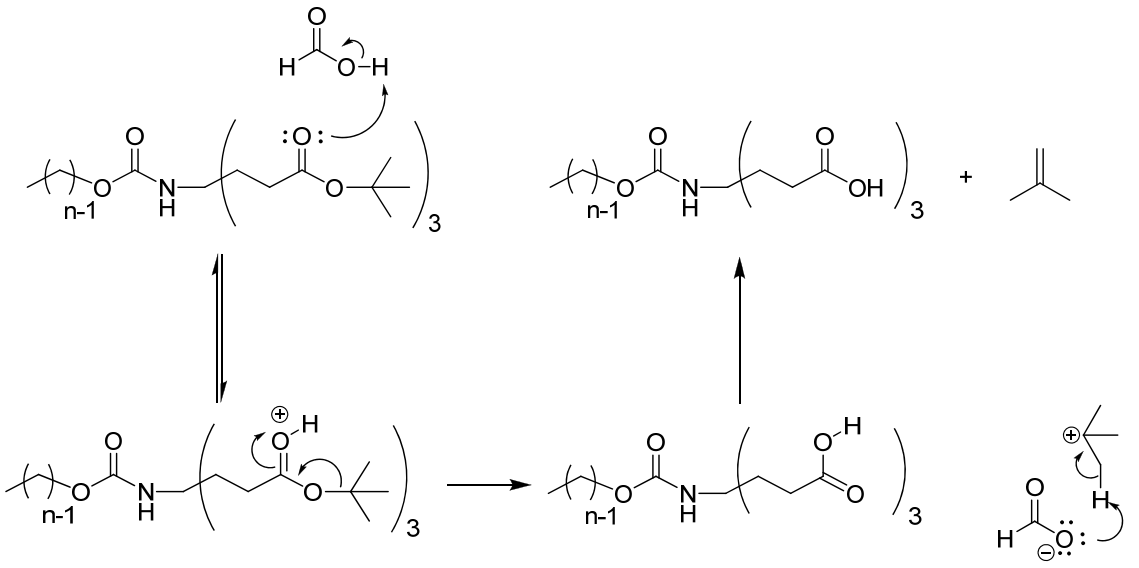

Scheme 2-5 Mechanism of action of formolysis reaction

Workup consisted of removal of the formic acid by rotary evaporation. Due to its extremely hydrophilic nature, the **3CCbn** material had to be recrystallized to purify it. Any attempt at normal-phase column chromatography would have resulted in unacceptable losses of material, due to the triheaded acid sticking to the silica gel on the column. Reverse phase chromatography can be employed in these instances, but due to the cost of reverse-phase silica, recrystallization of the material (using acetonitrile or ethanol/water) was preferable.

2.3.1 – Characterization

All compounds were fully characterized by melting point, 1-D ^{1}H and ^{13}C NMR, IR, high-resolution mass spectrometry, and elemental analysis. The ^{1}H NMR showed that the characteristic signals associated with carbamate formation at ~4.7 δ (representing the NH absorption of the carbamate) for the **3ECbn** series have now shifted upfield to ~6.7 δ for the **3CCbn** series. This chemical shift could be attributed to the formation of hydrogen bonds between the NH of the carbamate and the carboxylic oxygen of the

hydrophilic headgroup (via a 7-membered ring, Figure 2-3) leading to a more deshielded nucleus for the NH proton.

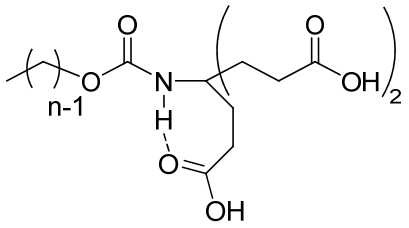

Figure 2-3 Hydrogen bond formation of **3CCbn** series compounds

We note the loss of the *tert*-butyl signals in the ^{1}H spectrum at ~ 1.4 δ and that there is now a characteristic broad carboxylic acid signal at ~ 12 δ. The ^{13}C NMRs showed weak single peaks at ~ 155 δ, indicating that the carbamate is still intact after the formolysis reaction. Additionally, the carbonyl signal due to the carbamate linker has grown in intensity from that seen in the **3ECbn** series. The ^{13}C NMR shows that the carbonyl groups making up the headgroup have shifted slightly downfield to ~ 174 δ supporting the ^{1}H NMR data showing the conversion of the *tert*-butyl esters into acids.

2.4 – EXPERIMENTAL

2.4.1 – 3ECbn & 3CCbn Series – General Methods

Unless specified, solvents and reagents were used as received. Weisocynate™ was prepared as described.[22,23] Analytical thin layer chromatography was performed on aluminum-coated silica gel 60 Å and detected by dipping in a solution of 10% ethanolic phosphomolybdic acid reagent (20 wt. % solution in ethanol) and then heated with a heat gun until the spots were visualized. The R_f for **3ECbn** in hexane:THF (6:1 v:v) was 0.32–0.41. Flash column chromatography was carried out on silica gel (60 Å). The samples were introduced as concentrated solutions in hexane:THF (6:1 v:v). After eluting the solvent mixture (100 mL), fractions (25 mL) were collected. The flow rate (~64 mL/min) was controlled by compressed air. The product appeared in fractions 3 to 12. Solutions were concentrated by rotary evaporation. Melting points were determined in open capillary tubes at 1°/min and uncorrected. NMR spectra were recorded at 400 and 100 MHz for ^{1}H and ^{13}C, respectively, and reported in ppm. References in ^{1}H and ^{13}C spectra were TMS and DMSO-d_6, respectively. IR spectra were recorded on neat samples with an FTIR equipped with a diamond ATR system, and reported in cm^{-1}. HRMS data were obtained on a dual-sector mass spectrometer in FAB mode with 2-nitrobenzylalcohol as the proton donor. Elemental analyses were performed by a commercial vendor.

2.4.2 – 3ECbn Synthetic Methodology – General Procedure

Alkan-1-ol (1.05 mol equivalents), Weisocyanate™ (1.00 mol equivalent), and Et_3N (to create a 1 M solution of Weisocyanate) were combined in a 50-mL round bottom flask and stirred at 95 °C for 4 h. The mixture was allowed to cool to rt and diluted with Et_2O (40 mL). The resulting solution was washed with 2-*M* HCl (3×5 mL), then saturated $NaHCO_3$ (3×5 mL), and finally saturated NaCl (1×5 mL). The solution was dried with $MgSO_4$, filtered and concentrated to a white solid. The resulting solid was purified via flash chromatography (6:1 v/v hexane/THF) to give a white solid.

2.4.3 – 3ECbn Synthetic Methodology – Synthetic Details

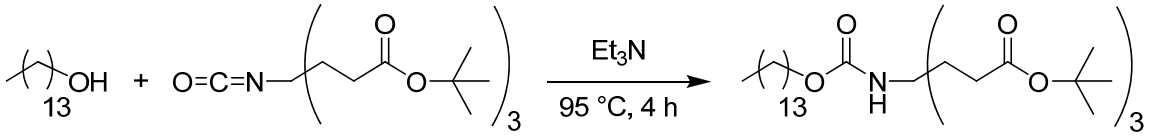

2.4.3.1 – Di-*tert*-butyl 4-(2-(*tert*-Butoxycarbonyl)ethyl)-4-(3-tetradecyloxycarbonylamino)heptanedioate, 3ECb14.

Following the general procedure outlined above, tetradecan-1-ol (0.7289 g, 3.399 mmol), Weisocyanate™ (1.424 g, 3.224 mmol), and Et_3N (3.2 mL) produced a waxy white solid (1.9874 g, 92%), which was purified via flash chromatography to give a white solid (1.7658 g, 84 %).

mp 54.3–54.9 °C

^{1}H NMR ($CDCl_3$) δ 0.88 (t, 3H), 1.25 (m, 22H), 1.42 (s, 27H), 1.57 (broad p, 2H), 1.91 (m, 6H), 2.21 (m, 6H), 3.96 (broad t, 2H), 4.69 (broad s, 1H)

^{13}C NMR ($CDCl_3$) δ 14.1, 22.7, 25.9, 28.08, 28.99, 29.35, 29.37, 29.58, 29.62, 29.67, 29.69, 29.72, 30.2, 31.9, 56.4, 64.6, 80.6, 154.6, 172.6

IR 3372, 2916, 1728, 1704, 1526, 1363, 1249, 1142

HRMS (FAB+) calcd for $C_{37}H_{70}NO_8$ $[M+H]^+$ 656.5101, found 656.5105

anal. calcd for $C_{37}H_{69}NO_8$: C, 67.75; H, 10.60; N, 2.14. Found: C, 67.75; H, 10.84; N, 2.27.

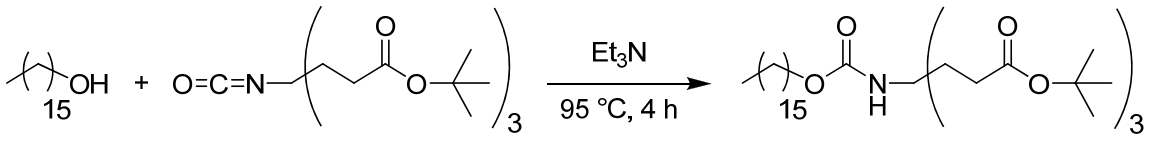

2.4.3.2 – Di-*tert*-butyl 4-(2-(*tert*-Butoxycarbonyl)ethyl)-4-(3-hexadecyloxycarbonylamino)heptanedioate, 3ECb16

Following the general procedure outlined above, hexadecan-1-ol (0.7889 g, 3.254 mmol) and Weisocyanate™ (1.438 g, 3.255 mmol) produced a waxy white solid (2.106 g, 95 %), which was purified via flash chromatography to give a white solid (1.8781 g, 84 %).

mp 60.8–61.4 °C

^{1}H NMR ($CDCl_3$) δ 0.89 (t, 3H), 1.27 (m, 26H), 1.45 (s, 27H), 1.59 (broad p, 2H), 1.92 (m, 6H), 2.23 (m, 6H), 3.99 (broad t, 2H), 4.70 (broad s, 1H)

^{13}C NMR ($CDCl_3$) δ 14.1, 22.7, 25.9, 28.08, 28.99, 29.33, 29.37, 29.56, 29.62, 29.66, 29.70, 30.2, 31.9, 56.4, 64.6, 80.6, 154.6, 172.6

IR 3357, 2921, 1727, 1708, 1531, 1363, 1258, 1143

HRMS (FAB+) calcd for $C_{39}H_{74}NO_8$ $[M+H]^+$ 684.5414, found 684.5427

anal. calcd for $C_{39}H_{73}NO_8$: C, 68.48; H, 10.76; N, 2.05. Found: C, 68.37; H, 10.83; N, 2.18.

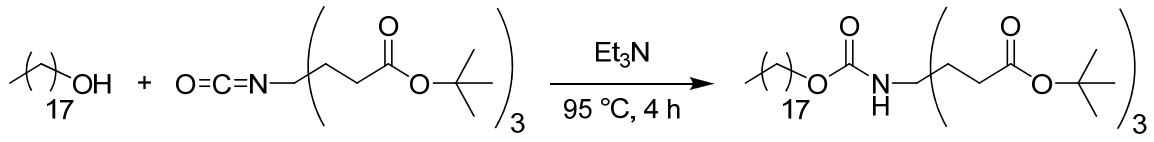

2.4.3.3 – Di-*tert*-butyl 4-(2-(*tert*-Butoxycarbonyl)ethyl)-4-(3-octadecyloxycarbonylamino)heptanedioate, 3ECb18

Following the general procedure outlined above, octadecan-1-ol (0.9072 g, 3.354 mmol) and Weisocyanate™ (1.4113 g, 3.1961 mmol) produced a waxy white solid (1.9694 g, 85 %), which was purified via flash chromatography to give a white solid (1.7988 g, 79 %).

mp 58.6–59.1 °C

^{1}H NMR ($CDCl_3$) δ 0.88 (t, 3H), 1.26 (m, 30H), 1.44 (s, 27H), 1.58 (broad p, 2H), 1.91 (m, 6H), 2.22 (m, 6H), 3.98 (broad t, 2H), 4.70 (broad s, 1H)

^{13}C NMR ($CDCl_3$) δ 14.1, 22.7, 25.9, 28.1, 28.99, 29.34, 29.36, 29.57, 29.61, 29.67, 29.71, 30.2, 31.9, 56.4, 64.6, 80.6, 154.6, 172.6

IR 3357, 2921, 1728, 1708, 1531, 1363, 1253, 1143

HRMS (FAB+) calcd for $C_{41}H_{78}NO_8$ $[M+H]^+$ 712.5727, found 712.5710

anal. calcd for $C_{41}H_{77}NO_8$: C, 69.16; H, 10.90; N, 1.97. Found: C, 69.10; H, 11.10; N, 2.13.

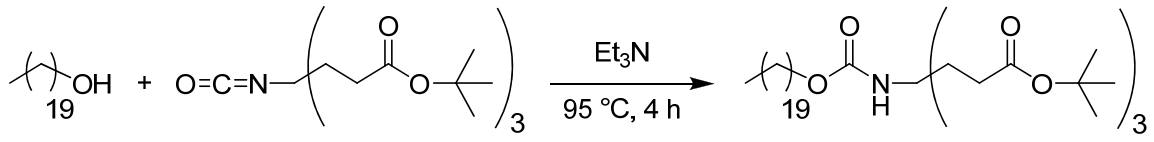

2.4.3.4 – Di-*tert*-butyl 4-(2-(*tert*-Butoxycarbonyl)ethyl)-4-(3-eicosadecyloxycarbonylamino)heptanedioate, 3ECb20

Following the general procedure outlined above, icosan-1-ol (1.0153 g, 3.4007 mmol) and Weisocyanate™ (1.5093 g, 3.2110 mmol) produced a white solid (2.2112 g, 91 %), which was purified via flash chromatography to give a white solid (1.5093 g, 63 %).

mp 59.0–59.6 °C

^{1}H NMR ($CDCl_3$) δ 0.88 (t, 3H), 1.25 (m, 34H), 1.44 (s, 27H), 1.57 (broad p, 2H), 1.90 (m, 6H), 2.21 (m, 6H), 3.97 (broad t, 2H), 4.69 (broad s, 1H)

^{13}C NMR ($CDCl_3$) δ 14.2, 22.8, 26.0, 28.2, 29.11, 29.46, 29.48, 29.69, 29.75, 29.83, 30.3, 32.0, 56.5, 64.7, 80.7, 154.7, 172.7

IR 3338, 2916, 1728, 1704, 1526, 1363, 1255, 1143

HRMS (FAB+) calcd for $C_{43}H_{82}NO_8$ $[M+H]^+$ 740.6040, found 740.6021

anal. calcd for $C_{43}H_{81}NO_8$: C, 69.78; H, 11.03; N, 1.89. Found: C, 69.73; H, 11.27; N, 2.05.

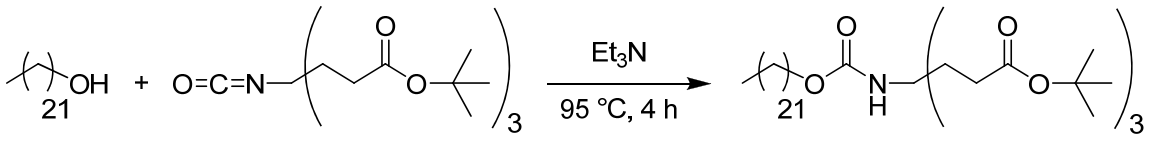

2.4.3.5 – Di-*tert*-butyl 4-(2-(*tert*-Butoxycarbonyl)ethyl)-4-(3-docosadecyloxycarbonylamino)heptanedioate, 3ECb22

Following the general procedure outlined above, docosan-1-ol (1.1070 g, 3.3894 mmol) and Weisocyanate™ (1.4231 g, 3.2228 mmol) produced a white solid (2.3928 g, 97 %), which was purified via flash chromatography to give a white solid (1.7017 g, 69 %).

mp 65.8–66.3 °C

^{1}H NMR ($CDCl_3$) δ 0.88 (t, 3H), 1.25 (m, 38H), 1.44 (s, 27H), 1.59 (broad p, 2H), 1.90 (m, 6H), 2.21 (m, 6H), 3.98 (broad t, 2H), 4.69 (broad s, 1H)

^{13}C NMR ($CDCl_3$) δ 14.3, 22.9, 26.1, 28.3, 29.17, 29.51, 29.54, 29.75, 29.80, 29.89, 30.3, 32.1, 56.5, 64.8, 80.8, 154.8, 172.8

IR 3338, 2916, 1728, 1704, 1531, 1464, 1363, 1251, 1142

HRMS (FAB+) calcd for $C_{45}H_{86}NO_8$ $[M+H]^+$ 768.6353, found 768.6356

anal. calcd for $C_{45}H_{85}NO_8$: C, 70.36; H, 11.15; N, 1.82. Found: C, 70.33; H, 11.25; N, 1.89.

2.4.4 – 3CCbn Synthetic Methodology – General Procedure

3ECbn (~ 3 mmol) was combined with THF (4 mL) in a 50-mL round bottom flask and all solids were allowed to dissolve. HCO_2H (15 mL) was added and the solution stirred at rt for 48 h. The solution was concentrated to a white solid and then crystallized from acetonitrile or ethanol/water to give a white powder.

2.4.5 – 3CCbn Synthetic Methodology – Synthetic Details

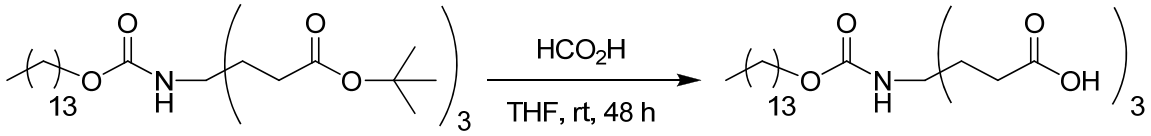

2.4.5.1 – 4-(2-Carboxyethyl)-4-(3-tetradecyloxycarbonylamino)heptanedioic acid, 3CCb14.

Following the general procedure outlined above, **3ECb14** (3.42 g, 5.21 mmol) produced a white solid and was then crystallized from acetonitrile to give a white powder (1.96 g, 77%).

mp 121.4–121.9 °C

^{1}H NMR (DMSO-d_6) δ 0.80 (t, 3H), 1.19 (broad m, 22H), 1.43 (broad p, 2H), 1.65 (m, 6H), 2.05 (m, 6H), 3.81 (t, 2H), 6.62 (broad s, 1H), 11.98 (broad s, 3H)

^{13}C NMR (d6-DMSO) δ 13.9, 22.1, 25.3, 28.06, 28.68, 28.69, 28.96, 28.98, 29.02, 29.20, 31.3, 55.6, 63.1, 154.5, 174.3

IR 3429, 3165, 2916, 1725, 1678, 1520, 1237, 1090

HRMS (FAB+) calcd for $C_{25}H_{46}NO_8$ $[M+H]^+$ 488.3223, found 488.3234

anal. calcd for $C_{25}H_{45}NO_8$: C, 61.58; H, 9.30; N, 2.87. Found: C, 61.58; H, 9.51; N, 2.84.

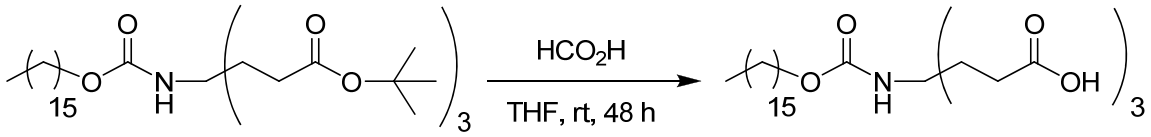

2.4.5.2 – 4-(2-Carboxyethyl)-4-(3-hexadecyloxycarbonylamino)heptanedioic acid, 3CCb16

Following the general procedure outlined above, **3ECb16** (4.11 g, 6.01 mmol) produced a white solid and was then crystallized from acetonitrile to give a white powder (2.79 g, 90%).

mp 123.9–124.7 °C

^{1}H NMR (DMSO-d_6) δ 0.85 (t, 3H), 1.23 (broad m, 26H), 1.50 (broad p, 2H), 1.76 (m, 6H), 2.10 (m, 6H), 3.88 (t, 2H), 6.72 (broad s, 1H), 11.98 (broad s, 3H)

^{13}C NMR (DMSO-d_6) δ 13.9, 22.1, 25.4, 28.07, 28.70, 28.71, 28.98, 28.99, 29.03, 29.19, 31.3, 55.6, 63.1, 154.5, 174.3

IR 3429, 3156, 2916, 1723, 1675, 1521, 1234, 1090

HRMS (FAB+) calcd for $C_{27}H_{50}NO_8$ $[M+H]^+$ 516.3536, found 516.3521

anal. calcd for $C_{27}H_{49}NO_8$: C, 62.89; H, 9.58; N, 2.72. Found: C, 62.67; H, 9.79; N, 2.76.

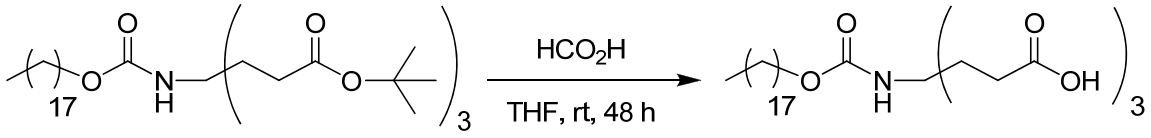

2.4.5.3 – 4-(2-Carboxyethyl)-4-(3-octadecyloxycarbonylamino)heptanedioic acid, 3CCb18

Following the general procedure outlined above, **3ECb18** (2.93 g, 4.11 mmol) produced a white solid and was then crystallized from acetonitrile to give a white powder (1.68 g, 75%).

mp 125.3–126.3 °C

^{1}H NMR (DMSO-d_6) δ 0.85 (t, 3H), 1.23 (broad m, 30H), 1.50 (broad p, 2H), 1.76 (m, 6H), 2.10 (m, 6H), 3.88 (t, 2H), 6.71 (broad s, 1H), 12.05 (broad s, 3H)

^{13}C NMR (DMSO-d_6) δ 13.9, 22.1, 25.4, 28.05, 28.69, 28.71, 29.02, 29.17, 31.3, 55.5, 63.1, 154.5, 174.3

IR 3431, 3163, 2918, 1725, 1677, 1523, 1236, 1030

HRMS (FAB+) calcd for $C_{29}H_{54}NO_8$ $[M+H]^+$ 544.3849, found 544.3855

anal. calcd for $C_{29}H_{53}NO_8$: C, 64.06; H, 9.82; N, 2.58. Found: C, 64.02; H, 10.06; N, 2.54.

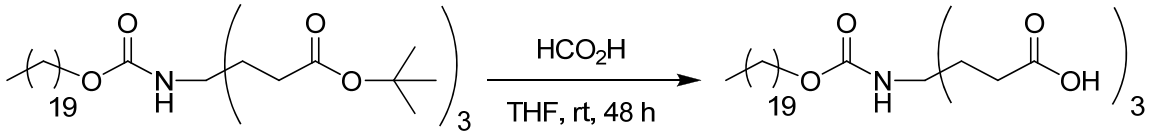

2.4.5.4 – 4-(2-Carboxyethyl)-4-(3-eicosadecyloxycarbonylamino)heptanedioic acid, 3CCb20

Following the general procedure outlined above, **3ECb20** (2.68 g, 3.62 mmol) produced a white solid and was then crystallized from methanol/water to give a white powder (1.99 g, 96%).

mp 124.1–124.8 °C

^{1}H NMR (DMSO-d_6) δ 0.85 (t, 3H), 1.23 (broad m, 34H), 1.50 (broad p, 2H), 1.76 (m, 6H), 2.10 (m, 6H), 3.87 (t, 2H), 6.71 (broad s, 1H), 12.06 (broad s, 3H)

^{13}C NMR (DMSO-d_6) δ 13.9, 22.1, 25.4, 28.06, 28.68, 28.71, 29.00, 29.17, 31.3, 55.6, 63.1, 154.5, 174.3

IR 3429, 3165, 2916, 1723, 1675, 1521, 1239, 1028

HRMS (FAB+) calcd for $C_{31}H_{58}NO_8$ $[M+H]^+$ 572.4162, found 572.4153

anal. calcd for $C_{31}H_{57}NO_8$: C, 65.12; H, 10.05; N, 2.45. Found: C, 64.82; H, 10.16; N, 2.49.

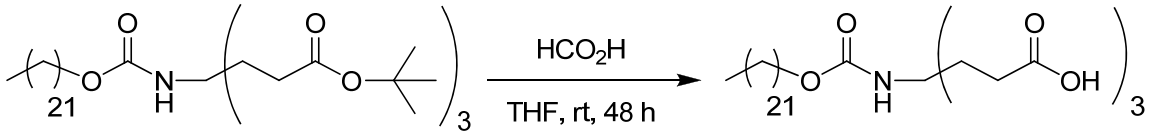

2.4.5.5 – 4-(2-Carboxyethyl)-4-(3-docosadecyloxycarbonylamino)heptanedioic acid, 3CCb22

Following the general procedure outlined above, **3ECb22** (1.52 g, 1.98 mmol) produced a white solid and was then crystallized from methanol/water to give a white powder (1.05 g, 89%).

mp 125.9–126.6 °C

^{1}H NMR (DMSO-d_6) δ 0.85 (t, 3H), 1.23 (broad m, 38H), 1.50 (broad p, 2H), 1.76 (m, 6H), 2.10 (m, 6H), 3.87 (t, 2H), 6.71 (broad s, 1H), 12.06 (broad s, 3H)

^{13}C NMR (DMSO-d_6) δ 13.9, 22.1, 25.4, 28.07, 28.71, 28.74, 29.01, 29.18, 31.3, 55.6, 63.1, 154.5, 174.3

IR 3429, 3161, 2916, 1723, 1680, 1521, 1239, 1028

HRMS (FAB+) calcd for $C_{33}H_{62}NO_8$ $[M+H]^+$ 600.4475, found 600.4476

anal. calcd for $C_{33}H_{61}NO_8$: C, 66.08; H, 10.25; N, 2.34. Found: C, 65.96; H, 10.49; N, 2.37.

2.5 – REFERENCES

(1) Newkome, G. R.; Weis, C. D.; Moorefield, C. N.; Baker, G. R.; Childs, B. J.; Epperson, J. *Angew. Chem., Int. Ed. Engl.* **1998**, *37*, 307–310.

(2) Sugandhi, E. W. Synthesis, Characterization, and Antimicrobial Activity of Water-soluble, Tri-carboxylato Amphiphiles. Ph.D. Dissertation, Department of Chemistry, Virginia Polytechnic Institute and State University, Blacksburg, VA, 2007.

(3) Newkome, G. R.; Weis, C. D.; Moorefield, C. N.; Fronczek, F. R. *Tetrahedron Lett.* **1997**, *38*, 7053-7056.

(4) Sugandhi, E. W.; Kite, B. L.; Macri, R. V.; Slebodnick, C. F., J., III; Gandour, R. D. *J. Org. Chem.* **2007**, *72*, Submitted for Review.

(5) Sugandhi, E. W.; Macri, R. V.; Williams, A. A.; Kite, B. L.; Slebodnick, C.; Falkinham, J. O., III; Esker, A. R.; Gandour, R. D. *J. Med. Chem.* **2007**, *50*, 1645 – 1650.

(6) Sugandhi, E. W.; Falkinham, I., Joseph O.; Gandour, R. D. *Bioorg. Med. Chem.* **2007**, *15*, 3842–3853.

(7) Benalil, A.; Roby, P.; Carboni, B.; Vaultier, M. *Synthesis* **1991**, 787-788.

(8) Firth, W. C.; Frank, S. *J. Org. Chem.* **1973**, *38*, 1083-1088.

(9) Hollweck, W.; Sewald, N.; Michel, T.; Burger, K. *Liebigs Ann., Recl.* **1997**, 2549-2552.

(10) Korenchenko, O. V.; Aksinenko, A. Y.; Sokolov, V. B.; Pushin, A. N. *Russ. Chem. Bull.* **1995**, *44*, 381-383.

(11) Nikiforov, A.; Jirovetz, L.; Buchbauer, G. *Liebigs Ann. Chem.* **1989**, 489-492.

(12) Piers, E.; Llinas-Brunet, M. *J. Org. Chem.* **1989**, *54*, 1483-1484.

(13) Pozzo, A. D.; Dikovskaya, K.; Moroni, M.; Fagnoni, M.; Vanini, L.; Bergonzi, R.; Castiglione, R. d.; Bravo, P.; Zanda, M. *J. Chem. Res. Miniprint* **1999**, 1980-1991.

(14) Roulland, E.; Monneret, C.; Florent, J.-C.; Bennejean, C.; Renard, P.; Leonce, S. *J. Org. Chem.* **2002**, *67*, 4399-4406.

(15) Sasse, A.; Stark, H.; Reidemeister, S.; Huels, A.; Elz, S.; Ligneau, X.; Ganellin, C. R.; Schwartz, J.-C.; Schunack, W. *J. Med. Chem.* **1999**, *42*, 4269-4274.

(16) Schmittel, M.; Peters, K.; Peters, E.-M.; Haeuseler, A.; Trenkle, H. *J. Org. Chem.* **2001**, *66*, 3265-3276.

(17) Sperber, N.; Fricano, R.; Schwenk, E.; Papa, D. *J. Am. Chem. Soc.* **1951**, *73*, 2965-2966.

(18) Spino, C.; Joly, M.-A.; Godbout, C.; Arbour, M. *J. Org. Chem.* **2005**, *70*, 6118-6121.

(19) Yamazaki, T.; et al. *Bull. Chem. Soc. Jpn.* **1977**, *50*, 1094-1096.

(20) Humphlett, W. J.; Wilson, C. V. *J. Org. Chem.* **1961**, *26*, 2511-2515.

(21) Schwetlick, K.; Noack, R.; Stebner, F. *J. Chem. Soc., Perk. 2* **1994**, 599–608.

(22) Newkome, G. R.; Behera, R. K.; Moorefield, C. N.; Baker, G. R. *J. Org. Chem.* **1991**, *56*, 7162-7167.

(23) Newkome, G. R.; Weis, C. D.; Childs, B. J. *Designed Monomers and Polymers* **1998**, *1*, 3-14.

CHAPTER 3 – 3CCb1(n,n) SERIES SYNTHESIS AND CHARACTERIZATION

3.1 – SYNTHETIC STRATEGY

The synthesis of the two-tailed triacids followed a similar synthetic strategy to that of the single-tailed **3CCbn** series of compounds.

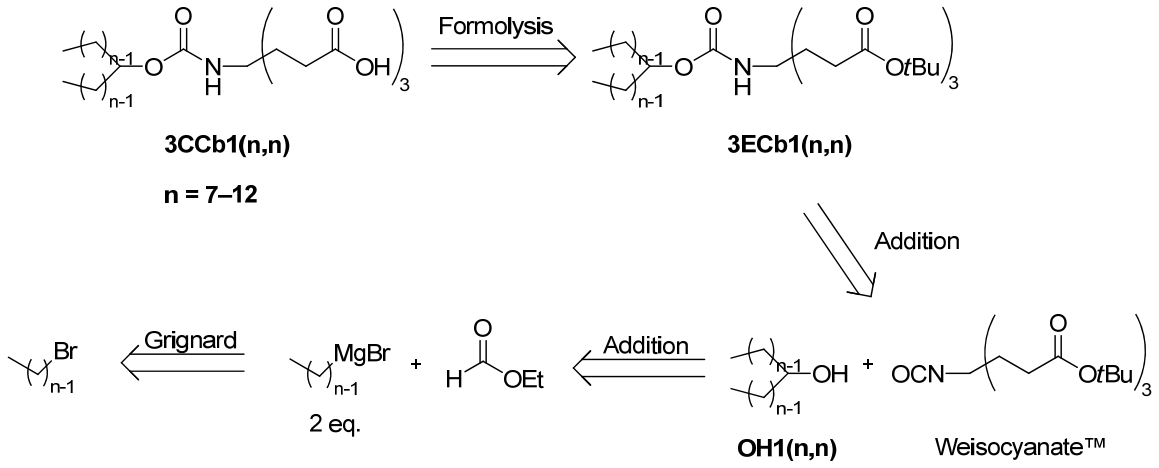

Scheme 3-1 Retrosynthetic analysis of **3CCb1(n,n)** series

The nomenclature for this series of compounds follows the standard set for the **3CCbn** series of compounds, where **3E** and **3C** correspond to the triester and triacid functionality of the head group, respectively, **Cb** refers to the carbamido linker connecting the hydrophobic and hydrophilic ends of the molecule, and **1(n,n)** refers to the two tails **(n,n)** of the alcohol, both connected to the same methine carbon attached to the carbamato group.

Additional steps were needed to synthesize the two-tailed alcohols as they were either not readily commercially available or in the cases where the material was commercially available the cost was prohibitively expensive. Literature searches for the synthesis of two-tailed alcohols yielded several different methods as shown in Table 3.1.

Table 3-1 Literature procedures for the synthesis of two-tailed alcohols

Entry #	Starting Material	Reaction Conditions	Product	Reference
1	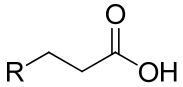	1. Phosphorus anhydride, 210 °C, 30-50% yield 2. Na (s), EtOH	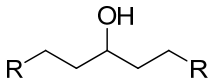	Kipping[1]
2	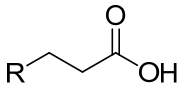	1. ThO_2, 450 °C, 53% yield 2. Al(Oi-Pr) in i-PrOH or Raney Ni in EtOH, H_2	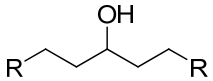	Carrington and Evans;[2] Meakins and Sack[3]
3	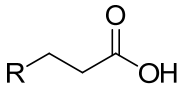	1. Fe cat., 285 °C, 4 h, 75% 2. Na (s), amyl alcohol, reflux, 2 h*	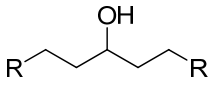	Piper et al.[4]
4	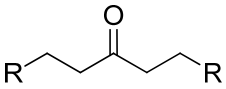	$LiAlH_4$, Et_2O	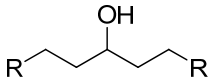	Breusch;[5] Baykut and Oezeris[6]
5	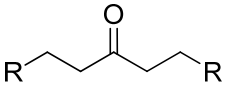	H_2, Raney Ni	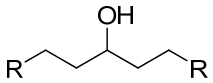	Lenne et al.[7]
6	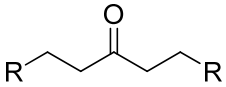	Sodium, amyl alcohol	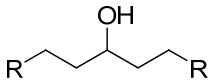	Kirrmann and Geiger;[8] Easterfield and Taylor[9]
7	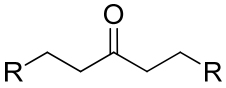	$LiAlH_4$, THF, 3 d, 20%	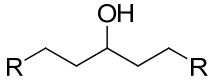	Claypool et al.[10]
8	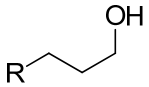	1. Chromic oxide, 400 °C, 55% yield 2. Ni/silica, 120 °C, 80 atm, H_2	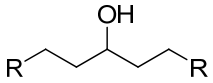	Komarewsky and Coley[11]
9	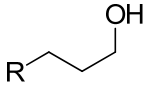	KOH, boric anhydride 300 °C, 5 h, 79%	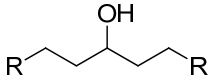	Sulzbacher[12]
10	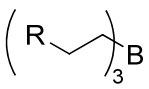	1. $Li^{+}{}^{-}CH(SPh)_2$, $HgCl_2$, 0 °C 2. H_2O_2, OH^-	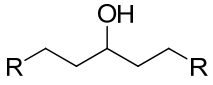	Hughes et al.[13]
11	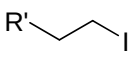	RCHO, $CrCl_2$, cat. CoPc, DMF, 30 °C, 89%	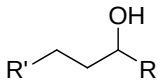	Takai et al.[14]
12	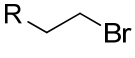	1. Mg (s), Et_2O 2. HCO_2Et, Et_2O, reflux, 1 h, 94%	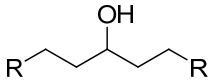	Overmars et al.[15]
13	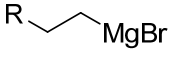	HCO_2Et, THF, -78 °C to rt, 18 h, 84%	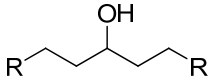	Boal et al.[16]

14	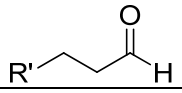	RMgBr, Et_2O, reflux, 1.5 h, 92%	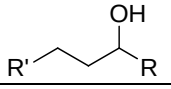	Guedj et al.[17]

* Need to repeat step 2 in some cases

As seen in Table 3.1, there are many different types of specific reactions and reagents that could be used to produce the two-tailed alcohol, and as the final alcohol is symmetrical there would be no need to use asymmetric reductions, which typically require expensive catalysts. However, there are practical limitations to most of these reactions.

Conceptually, the easiest method to produce a two-tailed alcohol would be via a simple reduction of a symmetrical ketone of the appropriate chain length. The problem that arises is that the required ketones are typically not commercially available. This problem is solved in the literature examples by generating the ketone by various methods as shown above. The majority of these methods use extreme temperatures (entries 1, 2, 3, 8, and 9 as examples), specialized catalysts (entries 2, 3, 8, and 10 as examples) or both. Additionally, the yields for the various methods of generating the ketone are all rather low (≤ 55% yield). Once the ketone is formed, we see that the reduction is usually done via standard reducing agents, such as $LiAlH_4$, Raney Ni, or solid sodium metal, usually in ether or alcoholic solvents.

The main focus of interest for our synthesis was found with examples 12 – 14 in the above table. These reactions use a Grignard reaction of an alkyl bromide with an aldehyde to form the required symmetrical alcohol.

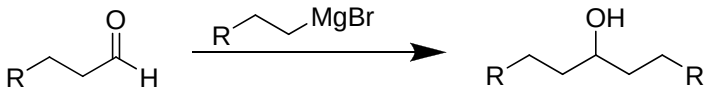

Scheme 3-2 Grignard reaction of aldehydes with alkyl magnesium bromides

This chemistry was attractive for several reasons. Both of the listed reactions produced outstanding yields in relatively short amounts of time with no requirements for expensive catalysts or high temperatures. The starting materials for this transformation were all commercially available and were relatively inexpensive. Additionally, the reaction itself was simple enough to not require extensive preparation or perfect laboratory technique, meaning that these reactions (once conditions had been worked out) could be taught to, and successfully run by, anyone with limited synthetic experience (e.g.: undergraduates working in our lab).

To preclude the need to purchase all of the various aldehydes and alkyl bromides that would be required to use the method shown in entry 12, it was decided that the reaction shown in entries 13 and 14 would be used for our chemistry, in which two equivalents of alkyl magnesium bromide react with ethyl formate.

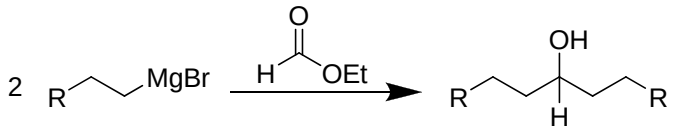

Scheme 3-3 Grignard reaction of alkyl magnesium bromides with ethyl formate

This further simplified the synthesis of these homologous series because we would now only require the alkyl bromides of differing chain lengths, instead of the need for both aldehyde and alkyl bromide of each separate chain length. The ethyl formate would serve as an inexpensive, readily available, common electrophile for all of the reactions we would run in this homologous series.

Once the necessary alcohols were synthesized, the remaining chemistry for the addition of the alcohol to Weisocyanate™ and the removal of the *tert*-butyl esters to form the triacids would follow that of the single-tailed series (cf. Chapter 2).

3.2 – FORMATION OF TWO-TAILED, LONG-CHAIN ALCOHOLS

The two-tailed, long-chain alcohols were synthesized with a modification of a procedure by Boal et al. (literature conditions as shown).[16]

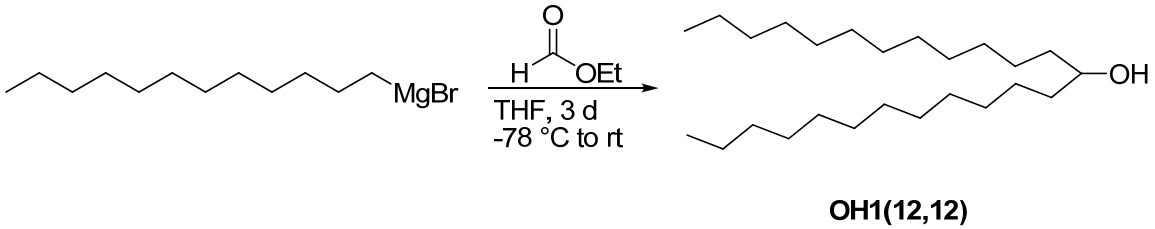

OH1(12,12)

Scheme 3-4 Literature procedure for production of two-tailed alcohols, **OH1(n,n)**

The literature procedure called for the addition of the Grignard reagent (20 mmol, 20 mL of a 1 M solution in THF) to ethyl formate (6.67 mmol in 10 mL of THF) at -78 °C in one portion. The reaction mixture was then allowed to warm to room temperature and stirred for 3 nights to produce the 12 carbon, two-tailed alcohol (pentacosan-13-ol, 84% yield).

In our initial experiments to reproduce the literature results, the alkyl Grignard reagent was synthesized from the necessary 1-bromoalkane and solid magnesium turnings with dry, deoxygenated THF (stored under N_2) as a solvent, rather than purchasing a prepared solution of Grignard reagent in THF. Solvent volumes and reagent masses were calculated so as to produce identical concentrations of Grignard reagent as that used in the literature procedure.

Initial attempts at formation of the Grignard reagent were sluggish at best, so two crystals of I_2 were added to help catalyze the reaction of magnesium with the alkyl bromide. The activation of the magnesium is thought to occur by formation of magnesium (I) iodide, which is more reactive than elemental magnesium itself and is

regenerated during the reaction, allowing for catalytic amounts of iodine to be used.[18] Additionally, the reaction was heated to 45 °C to allow the THF to reflux when the 1-bromoalkane and the magnesium began to exothermically react. The characteristic dark grey color associated with the formation of a Grignard reagent was not readily noticeable in the experiments conducted before we began heating the solution.

As the Grignard reagent needed to be generated, it was decided to reverse the order of addition of materials for the reaction, and add the ethyl formate to the Grignard reagent in situ, as opposed to the reverse as done in the literature. This allowed us to synthesize the secondary alcohol and maintain dry, oxygen free conditions throughout the entire process, with no need to transfer the Grignard reagent and risk possible atmospheric oxygen/water exposure.

The addition of the ethyl formate to the Grignard reagent was done at room temperature, instead of -78 °C. The change was made to avoid the need for a dry ice/acetone bath setup, considering the flask needed to be heated to generate the Grignard reagent. To offset this change, it was decided to add the ethyl formate dropwise to the room temperature solution, thereby allowing the reaction to proceed at a slower rate and with lower exothermicity. The final modified reaction to produce the two-tailed alcohol (pentacosan-13-ol, **OH1(12,12)**)from 1-bromododecane is shown in Scheme 3-5.

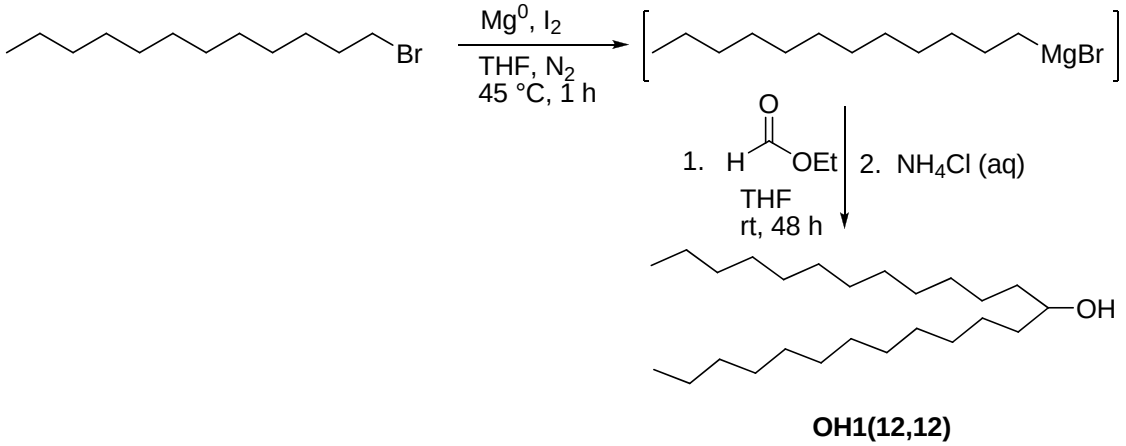

OH1(12,12)

Scheme 3-5 Initial synthesis for two-tailed alcohols

A change in recrystallization solvent was necessary for the alcohols with fewer than 11 carbons per branch. These alcohols were too soluble in ethyl acetate for it to be useful as a recrystallization solvent, so acetonitrile was used for alcohols **OH1(7,7)** through **OH1(10,10)**. Final recrystallized yields of the series of alcohols were low, ranging from 30–50%. The synthesis was also extremely inconsistent, with different batches of product from the same chain length 1-bromoalkane producing different yields, or not working at all.

Due to these disappointing results, a change of solvent was made from THF to diethyl ether. The lower boiling point of diethyl ether allowed us to visually verify that the Grignard reaction was occurring, due to the copious amounts of bubbles given off during the reaction as the solution began to reflux. These visual cues also simplified the adjustment of the rate of the addition of ethyl formate in order to maintain a gentle reflux. The lack of visual cues for the reactions run in THF made it difficult to determine if the proper reaction temperature had been reached. By simply increasing or decreasing the rate at which the alkyl bromide was added to the magnesium, we could adjust how fast the reaction was occurring, based on how vigorously the reaction bubbled. Additionally,

the gas used to maintain an atmospherically oxygen- and water-free environment was changed from nitrogen to argon. Due to its atomic mass, argon would more readily displace any oxygen or water vapor present in the reaction setup before the formation of the Grignard reagent. A paper by Owens et al. also suggests that Grignard reactions run under argon produce higher yields than those run under nitrogen.[19]

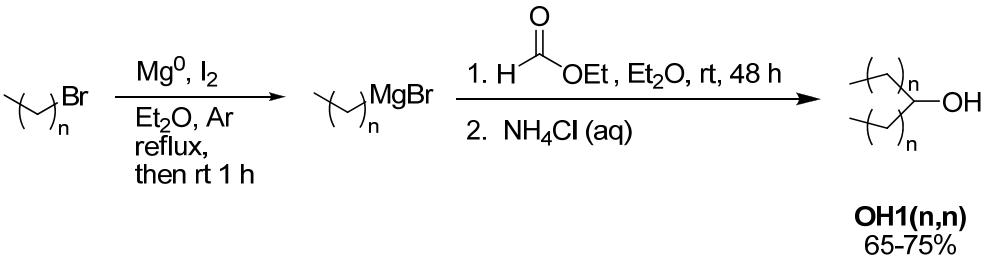

Scheme 3-6 Final two-tailed alcohol synthesis route

3.2.1 – Reaction Workup

Recrystallized yields of the alcohols from the diethyl ether series of reactions increased to 65–75% and were much more consistent from reaction to reaction. The recrystallization solvent was changed to ethanol/water for all alcohols to provide for a uniform solvent system for recrystallization.

Although recrystallization of the two tailed alcohols worked to some extent, enough impurity was left behind so as to cause the products to fail melting point range analysis. It was found that flash column chromatography produced a cleaner final product of the two-tail alcohol and made the second step of the synthesis, generation of the carbamate ester, **3ECb1(n,n)**, much easier to work up after the reaction was completed due to the purity of the starting two-tail alcohol.

3.2.2 – Two-Tail Alcohol Characterization

The purity and structure of the two-tailed alcohols were verified via melting range analysis and 1-D ^{1}H NMR. The experimentally determined melting point ranges were in

good agreement with the literature values.[3,5-7] The NMR data showed the expected results for these compounds, with the methine proton (H_a in Figure 3.1) of the central carbon appearing at approximately 3.6 δ as a broad quintuplet due to the strong deshielding effect of the hydroxyl group. The methylene groups (H_b) appear as a broad signal centered around ~ 1.2 δ, with the methylenes next to the methine carbon (H_c) appearing at ~ 1.45 δ and slightly overlapping with the H_b signal. The methyl groups (H_d) appear as a triplet centered around ~ 0.8 δ. The hydroxyl proton is typically not seen in the NMR experiments.

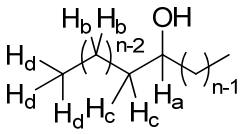

Figure 3-1 Proton locations for ^{1}H NMR of **OH1(n,n)** series

3.3 – SYNTHESIS OF 3ECb1(n,n) AND 3CCb1(n,n) SERIES

3.3.1 – 3ECb1(n,n) Series Synthesis

The synthesis of the two-tailed, triheaded amphiphiles was carried out in a manner analogous to that of the **3ECbn** series, with one minor change. The reflux time necessary to produce high yields of **3ECb1(n,n)** needed to be increased to 48 hours, as compared to the 4.5 hours from the **3ECb1n** series (cf. Chapter 2).

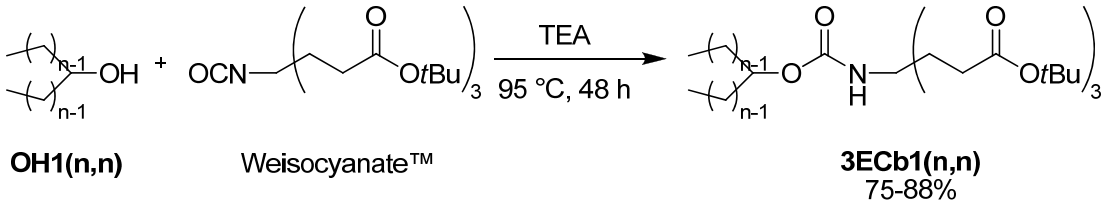

Scheme 3-7 Synthesis of **3ECb1(n,n)** series

Initial experiments showed that a four-hour reaction time at 95 °C gave almost no product. This reduction in reactivity is attributed to the mechanism of addition of the

alcohol to the isocyanate. In this addition mechanism, a primary alcohol should be more reactive than a secondary, due to the increase in steric bulk of a secondary alcohol. Along this line of reasoning, a tertiary alcohol should take longer to undergo reaction than a secondary alcohol.

In a reaction designed to test this theory, a three-tailed alcohol (produced by the same literature precedent[16] as that of the two-tailed alcohols and modified as per the initial modifications made above) with 5 carbons in each chain was allowed to react with the isocyanate. Complete product formation was not seen for approximately 3½ weeks. A second test reaction was run to explore the possibility of attaching the triheaded carboxylate functionality to a β-cholestanol derivative via the isocyanate. As expected for a secondary alcohol, the reaction had reached completion after 48 hours. No product isolation was performed for either test reaction. Reaction completion was monitored by ^{1}H NMR in both cases.

3.3.2 – 3CCb1(n,n) Series Synthesis

The synthesis of the **3CCb1(n,n)** series of compounds was carried out in an analogous manner to that of the **3CCbn** series with another minor change.

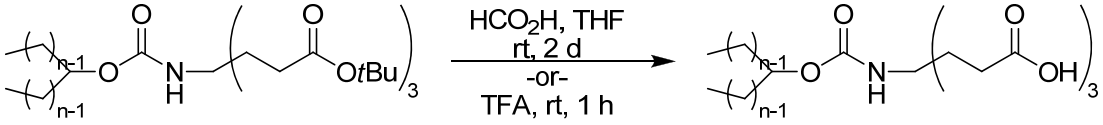

3ECb1(n,n) **3CCb1(n,n)**

Scheme 3-8 Synthesis of **3CCb1(n,n)** series

A literature procedure[20] was found with trifluoroacetic acid (TFA) to effect the removal of the three *tert*-butyl groups, converting the *tert*-butyl esters into acids, in only eleven hours instead of two days. In practice, we found that as little as one hour was necessary to effect the elimination. The TFA is approximately 2,800 times stronger an acid than

formic acid (pK_a TFA = 0.3, pK_a HCOOH = 3.75).[21] If we assume the model for elimination of the *tert*-butyl groups via acid catalyst (cf. section 2.7) is correct, then this increase in the reaction rate suggests that the reversible first step of the mechanism (Figure 3.9) is the rate limiting step of the reaction, as the TFA does not participate in any steps past the first step.

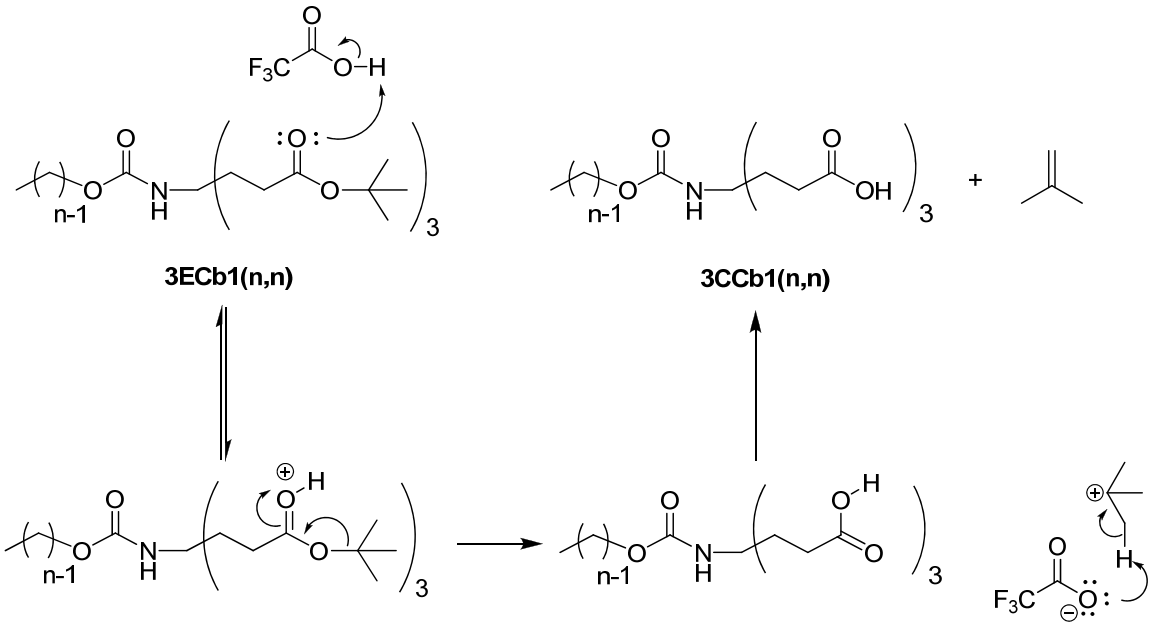

Scheme 3-9 Proposed mechanism for conversion of **3ECb1(n,n)** into **3CCb1(n,n)** series

The observed kinetic effect also fits with reaction theory, as we would expect a stronger acid to more readily donate a proton to an available base (the carbonyl oxygen, in this case) than a weaker acid.

3.4 – 3ECb1(n,n) AND 3CCb1(n,n) CHARACTERIZATION

As with the **3CCbn** series of compounds, the **3ECb1(n,n)** and **3CCb1(n,n)** two-tailed series of compounds were fully characterized by melting range, 1-D ^{1}H and ^{13}C NMR, IR, high-resolution mass spectrometry, and elemental analysis. The ^{1}H NMR of the esters (**3ECb1(n,n)**) showed the characteristic signals associated with carbamate

formation at ~ 4.65 δ (Hc in Figure 3-2). The signal produced by the α–methine proton to the carbamate oxygen (Hb) has shifted downfield from that produced by the free alcohol from ~3.6 δ to ~ 4.6 δ. All other NMR signals were consistent with the addition of the alcohol to the isocyanate functionality, and not to one of the *tert*-butyl esters. The signal at ~1.4 δ integrated to ~31 protons, 27 from the *tert*-butyl esters (Hd) and 4 protons in the aliphatic chains (Ha) β to the carbamate oxygen.

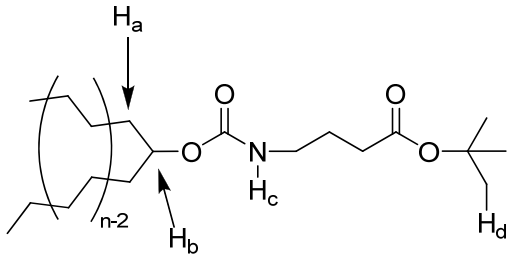

Figure 3-2 Proton locations for ^{1}H NMR of **3ECb1(n,n)** series

The ^{13}C NMRs showed weak single peaks at ~ 155 δ (cf. 2.2.4), representing the carbamate carbonyl group. The ester carbonyls show a much stronger signal at ~ 173 δ. IR data indicates the loss of the isocyanate signal at 2250 cm^{-1}, and shows the presence of two carbonyl peaks, corresponding to the carbamate at 1702 cm^{-1} and *tert*-butyl esters at 1728 cm^{-1}. Melting ranges of the esters followed an even–odd effect to some extent, in that the even-numbered esters (**3ECb1(n,n)**, where n = 8, 10) had a relatively higher melting range than either the preceding or trailing compound in the homologous series. This effect was seen until n = 10, at which point the melting point range leveled off for n = 10 and n = 11, and then dropped sharply for n = 12 (Figure 3-3).

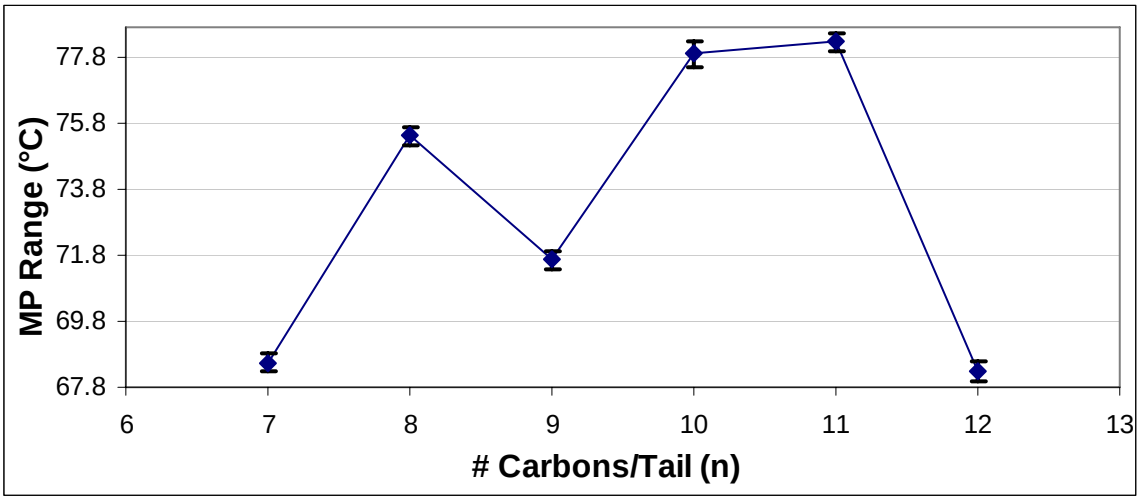

Figure 3-3 Even–Odd Effect of **3ECb1(n,n)** series. Error bars show maximal and minimal extent of melting ranges for each data point.

The **3CCb1(n,n)** series NMR data was nearly identical to that of the **3ECb1(n,n)** series, with the anticipated exception of the missing *tert*-butyl signals at ~ 1.4 δ. Similar variations between the two compounds in the NMR followed the differences noted between the **3ECbn** and **3CCbn** series (cf. 2.2.4 and 2.3.1). Melting ranges for the **3CCb1(n,n)** series do not follow the observed even-odd effect of the esters. Instead, we note a sharp decrease in melting point at first, followed by a gradual decrease as the chain length increases, shown in Table 3-2.

Table 3-2 Melting ranges of the **3CCb1(n,n)** series

Compound	Melting Point Range
3CCb1(7,7)	155.3 – 155.9 °C
3CCb1(8,8)	131.6 – 132.8 °C
3CCb1(9,9)	128.9 – 129.8 °C
3CCb1(10,10)	127.4 – 128.2 °C
3CCb1(11,11)	127.5 – 128.2 °C
3CCb1(12,12)	124.0 – 124.7 °C

We note that for the smallest compound of the series, **3CCb1(7,7)**, the melting range is over 20 °C higher than the next closest homologue. Additionally, the melting point range decreases as molecular weight of the series increases. A possible explanation for these observations is that as the long-chain carbon tail is increased it leads to difficulty in packing in the formation of the crystal lattice, and therefore the melting points decrease.

3.5 – X-Ray Crystallographic Data Analysis

3ECb1(7,7) was obtained as single crystals suitable for X-ray analysis.

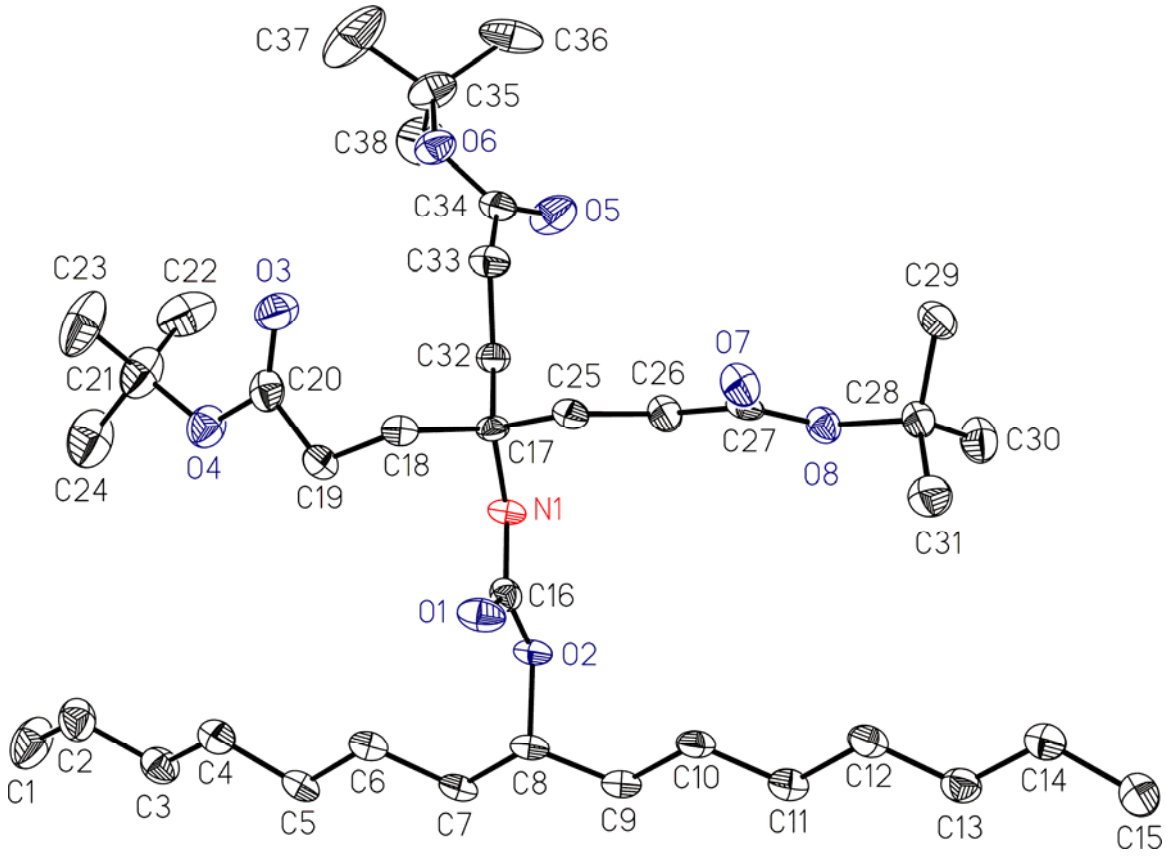

Figure 3-4 Displacement ellipsoid drawing (50%) of **3ECb1(7,7)** (H-atoms are omitted for clarity). Picture obtained from Dr. Carla Slebodnick.

Figure 3-5 depicts the 1-D H-bonding network between O7 and the N1 hydrogen of each neighboring molecule. The H-bonding distance is 2.963 ± 0.002 Å. Figure 3-6 shows the staggered, face-to-face packing of the hydrocarbon chains. The closest packing

distances are between O1 of one molecule and H5/H7 of another, with distances of 2.400 and 2.580 Å, respectively (line a in Figure 3-6). We note that the hydrocarbon chains are aligned in a staggered conformation with a slight displacement of C1–C4 from complete eclipsing due to steric interactions with the neighboring headgroups of the other molecules in the crystal lattice.

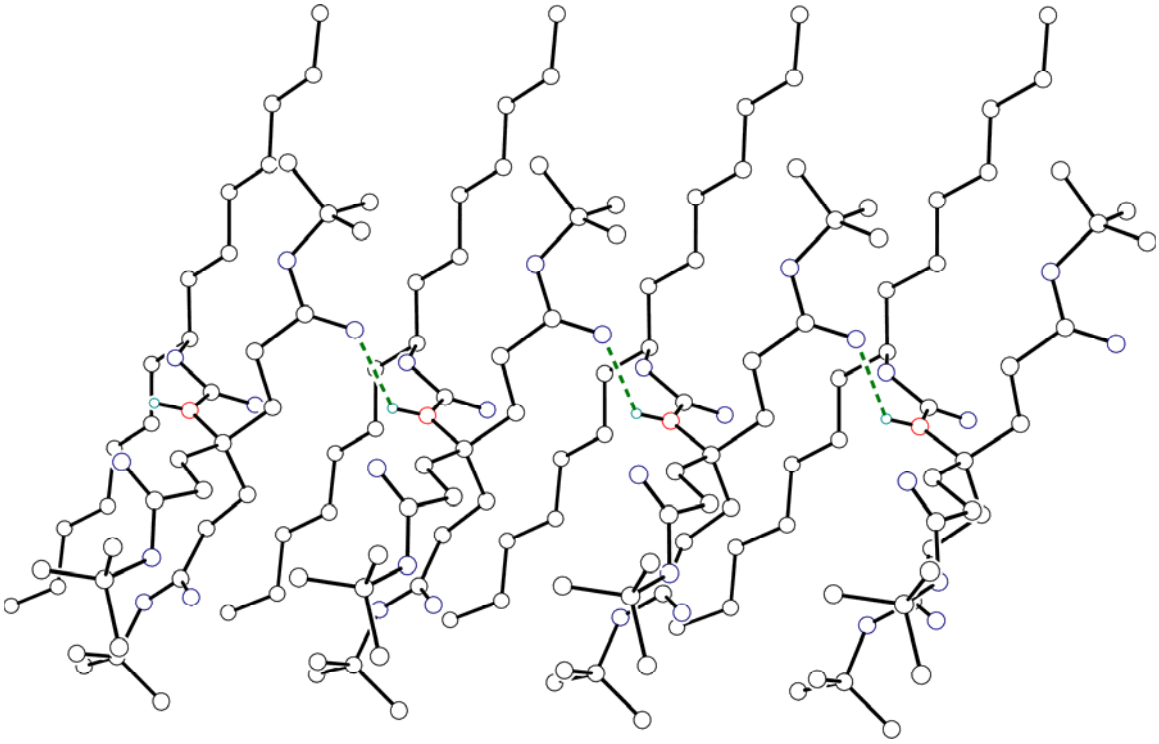

Figure 3-5 Drawing of **3ECb1(7,7)** 1-D H-bonding network. Picture obtained from Dr. Carla Slebodnick.

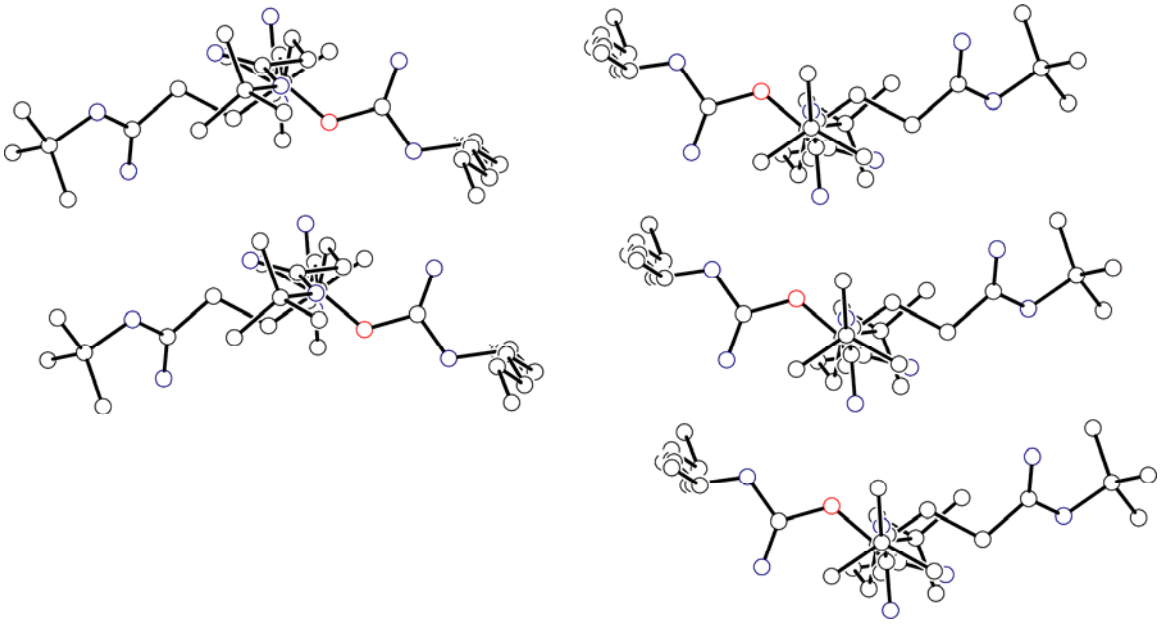

Figure 3-6 Drawing of **3ECb1(7,7)** depicting the face-to-face packing of the hydrocarbon chains. Picture obtained from Dr. Carla Slebodnick.

The steric interaction is more easily viewed in Figure 3-7, where we can see that the spacing between the packed hydrocarbon chains are lined up with the headgroups of neighboring molecules to facilitate tighter packing. The length of the hydrocarbon chain may help to explain the reason for the overall difficulty encountered in growing good crystals for the other homologues, as longer length hydrocarbon chains would not allow the headgroups to fill the interpenetrated space of the crystal lattice as well. This tends to indicate that the longer chain homologues of the series either do not form good crystalline structures, or form crystal structures of a different morphology.

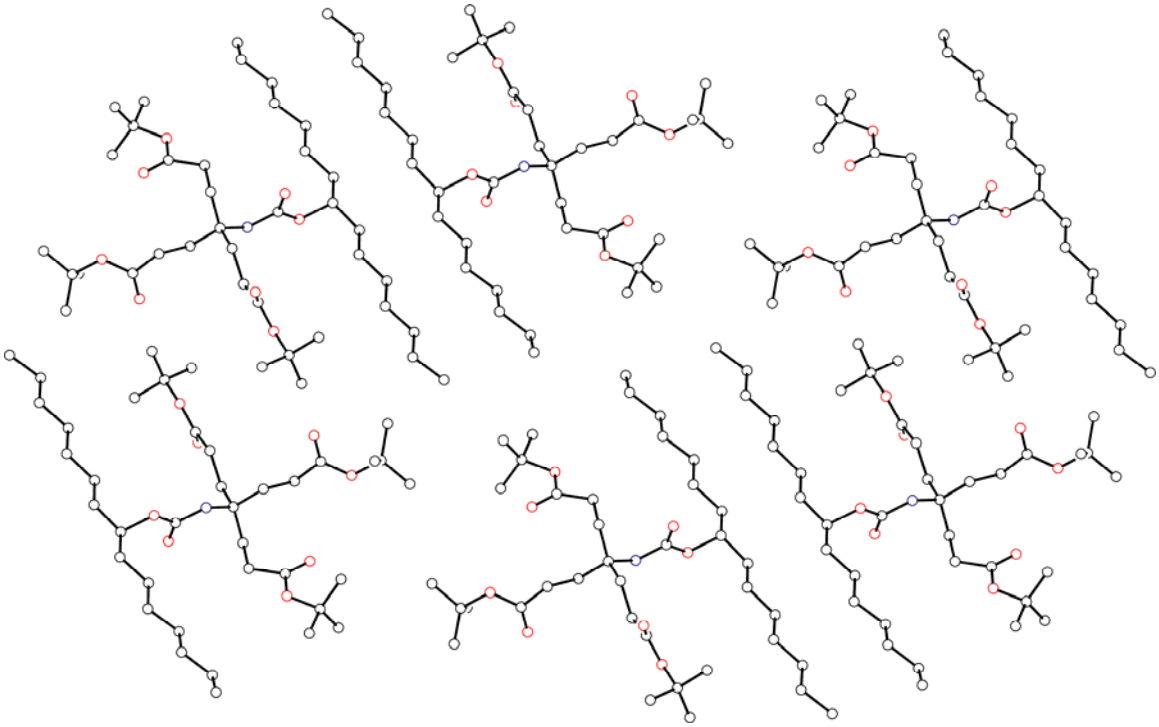

Figure 3-7 View of **3ECb1(7,7)** down the 1D H-bonding chain depicting the interpenetration of neighboring chains. Picture obtained from Dr. Carla Slebodnick.

3.6 – EXPERIMENTAL

3.6.1 – 3CCb1(n,n) Series – General Methods

Unless specified, solvents and reagents were used as received. Weisocynate™ was prepared as described.[22,23] Analytical thin layer chromatography was performed on aluminum-coated silica gel 60 Å and detected by dipping in a solution of 10% ethanolic phosphomolybdic acid reagent (20 wt.% solution in ethanol) and then heated with a heat gun. The R_f for **3ECb1(n,n)** in hexane:ethyl acetate (9:1 v:v) was 0.15. Flash column chromatography was carried out on silica gel (60 Å). The samples were introduced as concentrated solutions in hexane:ethyl acetate (9:1 v:v). After eluting the solvent mixture (125 mL), fractions (25 mL) were collected. The flow rate (~64 mL/min) was controlled by compressed air. The starting two-tailed alcohol appeared in fractions 8–16, and the product was flushed from the column with pure ethyl acetate after the starting material was isolated. Solutions were concentrated by rotary evaporation. Melting point ranges were determined in open capillary tubes at 1°/min and uncorrected. NMR spectra were recorded at 400 and 100 MHz for ^{1}H and ^{13}C, respectively, and reported in ppm. References in ^{1}H and ^{13}C spectra were TMS and DMSO-d_6, respectively. IR spectra were recorded on neat samples with an FTIR equipped with a diamond ATR system, and reported in cm^{-1}. HRMS data were obtained on a dual-sector mass spectrometer in FAB mode with 2-nitrobenzylalcohol as the proton donor. Elemental analyses were performed by a commercial vendor.

3.6.2 – Synthesis of Grignard Reagents

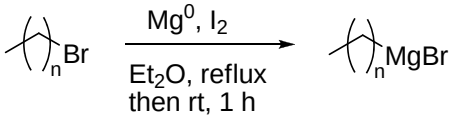

All glassware was oven dried at 110 °C for 48 h prior to use and allowed to cool in a vacuum dessicator. All ground glass joints were wrapped with a single layer of Teflon™ tape prior to assembly. Mg^0 (160 mmol) and two crystals of I_2 were added to the round bottom flask, which was then fitted with a Claisen adapter and a 50-mL dropping funnel. The entire assembly was flame-dried, sealed with rubber septa, and then quickly fitted with a condenser and purged with Argon for 10 min. The Argon stream was stopped, and the crystals of I_2 were sublimed with a heat gun until purple vapors appeared. After 10 min, diethyl ether (20 mL) was added to the round-bottom flask via the dropping funnel. 1-Bromoalkane (80 mmol) and diethyl ether (60 mL) were added to the dropping funnel; 20% of the resulting mixture was added in one portion to the round bottom flask to initiate the reaction, and the remainder was added at a rate which maintained a gentle reflux of the mixture. The mixture was allowed to stir for 1 h once it had cooled to ambient temperature.

3.6.3 – Synthesis of Two-Tailed Alcohols

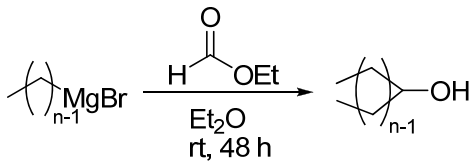

After 1 h of stirring, ethyl formate (30 mmol) and diethyl ether (40 mL) were added to the dropping funnel. The resulting mixture was added dropwise to the round bottom flask from the previous step containing the Grignard reagent and was allowed to stir for 48 h at rt. The liquid was decanted from the remaining Mg^0 into a separatory funnel. CH_2Cl_2 (40 mL) was added to dissolve the organic salts, and the reaction mixture was then washed with saturated aq NH_4Cl soln (5×10 mL), followed by saturated aq NaCl soln (50 mL). The organic layer was then dried over anhyd $MgSO_4$. The mixture was filtered, concentrated under vacuum, and purified via flash column chromatography (8:1 hexane/EtOAc v/v). Analytical data are presented in Table 3.2.

Table 3-3 Two-tailed alcohol melting point ranges compared to literature values

Compound	% Yield	Melting Point Range (°C)	Literature Melting Point Range (°C)
Pentadecan-8-ol, **OH1(7,7)**	89	53.5−54.3	51–51.3 [3] 52−52.6 [5]
Heptadecan-9-ol, **OH1(8,8)**	68	61.7−62.2 °C	59.5−59.8 [7] 60.8−61.2 [5]
Nonadecan-10-ol, **OH1(9,9)**	84	67.0−67.4 °C	65.9−66.1 [3] 65.7−67 [5]
Henicosan-11-ol, **OH1(10,10)**	87	71.1−72.0 °C	71.8−72.4 [6] 71.3−72.5 [5]
Tricosan-12-ol, **OH1(11,11)**	71	76.8−77.6 °C	75.2−75.6 [3] 75.5−75.7 [5]
Pentacosan-13-ol, **OH1(12,12)**	82	80.2−81.0 °C	79.5−80.5 [6]

^{1}H NMR Data ($CDCl_3$, 400 MHz)

OH1(7,7): 0.88 (6H, t), 1.28 (24H, m), 1.42 (1H, m), 3.59 (1H, broad s)

OH1(8,8): 0.88 (6H, t), 1.29 (28H, m), 1.42 (1H, m), 3.58 (1H, broad s)

OH1(9,9): 0.88 (6H, t), 1.28 (32H, m), 1.42 (1H, m), 3.59 (1H, broad s)

OH1(10,10): 0.89 (6H, t), 1.27 (36H, m), 1.42 (1H, m), 3.58 (1H, broad s)

OH1(11,11): 0.89 (6H, t), 1.28 (40H, m), 1.43 (1H, m), 3.59 (1H, broad s)

OH1(12,12): 0.87 (6H, t), 1.27 (44H, m), 1.41 (1H, m), 3.59 (1H, broad s)

3.6.4 – 3ECb1(n,n) Synthetic Methodology

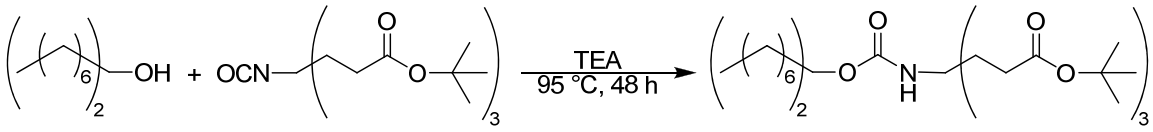

3.6.4.1 – Di-*tert*-butyl 4-(2-(*tert*-butoxycarbonyl)ethyl)-4-(1-heptyloctyloxycarbonylamino)heptanedioate, 3ECb1(7,7)

Pentadecan-8-ol (1.68 g, 7.35 mmol), Weisocyanate™ (3.09 g, 7.00 mmol), and Et_3N (7.3 mL) were combined in a 50-mL round bottom flask and stirred at 95 °C for 48 h. The mixture was allowed to cool to rt, and diluted with Et_2O (40 mL). The resulting solution was washed with 2-M HCl (3×10 mL), then saturated $NaHCO_3$ (3×10 mL), and finally saturated NaCl (1×10 mL). The solution was dried with $MgSO_4$, filtered and concentrated to a yellow-white solid (4.61 g, 98% yield). The resulting solid (2.35 g) was purified via flash column chromatography; after concentration by rotary evaporation and drying under high vacuum a white crystalline solid (2.07 g, 88% yield) formed.

mp 68.3–68.8 °C

^{1}H NMR ($CDCl_3$) δ 0.88 (t, 6H), 1.26 (broad m, 20H), 1.43 (s, 27H), 1.47 (broad m, 4H), 1.90 (broad t, 6H), 2.21 (t, 6H), 4.61 (broad s, 1H), 4.65 (broad m, 1H)

^{13}C NMR ($CDCl_3$) δ 14.3, 22.8, 25.5, 28.2, 29.37, 29.71, 29.82, 30.3, 32.0, 34.5, 56.4, 74.4, 80.6, 154.7, 172.7

IR 3354, 2922, 1729, 1713, 1148 cm^{-1}

HRMS (FAB+) calcd for $C_{38}H_{72}NO_8$ (MH^+) 669.9915, found 670.5266

anal. calcd for $C_{38}H_{71}NO_8$: C, 68.12; H, 10.68; N, 2.09. Found: C, 68.28; H, 10.63; N, 2.15.

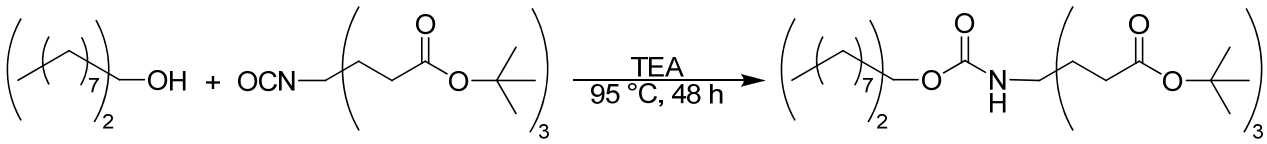

3.6.4.2 – Di-*tert*-butyl 4-(2-(*tert*-butoxycarbonyl)ethyl)-4-(1-octylnonyloxycarbonylamino)heptanedioate, 3ECb1(8,8)

Heptadecan-9-ol (0.822 g, 3.21 mmol) and Weisocyanate™ (1.42 g, 3.20 mmol) produced a white solid (2.04 g, 91%), The resulting solid (1.57 g) was purified via flash column chromatography to give a white crystalline solid (1.29 g, 82%) in an analogous manner to that of **3ECb1(7,7)**.

mp 75.1–75.7 °C;

^{1}H NMR ($CDCl_3$) δ 0.88 (t, 6H), 1.26 (broad m, 24H), 1.44 (s, 27H), 1.478 (broad m, 4H), 1.90 (broad t, 6H), 2.21 (t, 6H), 4.61 (broad s, 1H), 4.65 (broad m, 1H)

^{13}C NMR ($CDCl_3$) δ 14.3, 22.8, 25.5, 28.2, 29.47, 29.71, 29.80, 29.85, 30.3, 32.0, 34.6, 56.4, 74.4, 80.7, 154.8, 172.7

IR 3362, 2916, 1727, 1713, 1142 cm^{-1}

HRMS (FAB+) calcd for $C_{40}H_{76}NO_8$ (MH^+) 698.0457, found 698.5594

anal. calcd for $C_{40}H_{75}NO_8$: C, 68.83; H, 10.83; N, 2.01. Found: C, 69.05; H, 10.87; N, 1.94.

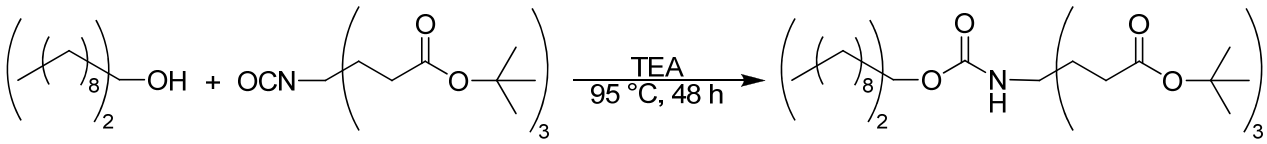

3.6.4.3 – Di-*tert*-butyl 4-(2-(*tert*-butoxycarbonyl)ethyl)-4-(1-nonyldecyloxycarbonylamino)heptanedioate, 3ECb1(9,9)

Nonadecan-10-ol (0.645 g, 2.27 mmol) and Weisocyanate™ (0.954 g, 2.16 mmol) produced a white solid (1.54 g, 98%). The resulting solid (1.02 g) was purified via flash column chromatography to give a white crystalline solid (0.848 g, 83%) in an analogous manner to that of **3ECb1(7,7)**.

mp 71.4–71.9 °C;

^{1}H NMR ($CDCl_3$) δ 0.89 (t, 6H), 1.27 (m, 28H), 1.45 (s, 27H), 1.48 (broad m, 4H), 1.91 (broad t, 6H), 2.22 (t, 6H), 4.62 (broad t, 1H), 4.66 (broad s, 1H)

^{13}C NMR ($CDCl_3$) δ 14.1, 22.7, 25.4, 28.1, 29.32, 29.59, 29.64, 29.68, 30.1, 31.9, 34.4, 37.4, 56.3, 74.2, 80.5, 154.6, 172.7

IR 3357, 2916, 1722, 1708, 1142 cm^{-1}

HRMS (FAB+) calcd for $C_{42}H_{80}NO_8$ (MH^+) 726.0998, found 726.5880

anal. calcd for $C_{42}H_{79}NO_8$: C, 69.48; H, 10.97; N, 1.93. Found: C, 69.51; H, 10.87; N, 1.92.

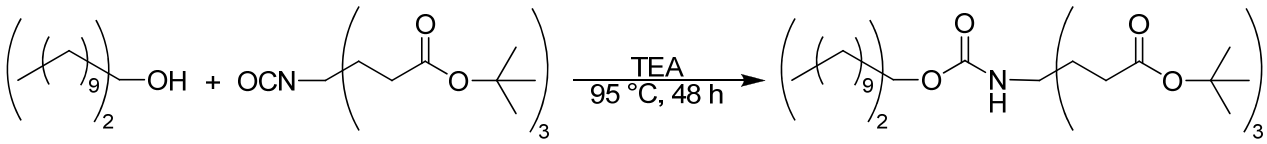

3.6.4.4 – Di-*tert*-butyl 4-(2-(*tert*-butoxycarbonyl)ethyl)-4-(1-decylundecyloxycarbonylamino)heptanedioate, 3ECb1(10,10)

Uncosan-11-ol (1.37 g, 4.37 mmol) and Weisocyanate™ (1.96 g, 4.45 mmol) produced a white solid (3.03 g, 91%). The resulting solid (2.19 g) was purified via flash column chromatography to give a white crystalline solid (1.82 g, 83%) in an analogous manner to that of **3ECb1(7,7)**.

mp 77.5-78.3 °C

^{1}H NMR ($CDCl_3$) δ 0.88 (t, 6H), 1.26 (m, 32H), 1.44 (s, 27H), 1.90 (t, 6H), 2.21 (t, 6H), 4.62 (broad s, 1H), 4.66 (broad s, 1H)

^{13}C NMR ($CDCl_3$) δ 14.3, 22.8, 25.5, 28.2, 29.51, 29.75, 29.78, 29.81, 29.87, 30.3, 32.1, 34.6, 56.4, 74.4, 80.7, 155.1, 172.7

IR 3358, 2918, 1728, 1712, 1146 cm^{-1}

HRMS (FAB+) calcd for $C_{44}H_{84}NO_8$ (MH^+) 754.1540, found 754.6234

anal. calcd for $C_{44}H_{83}NO_8$: C, 70.08; H, 11.09; N, 1.86. Found: C, 70.25; H, 11.11; N, 1.90.

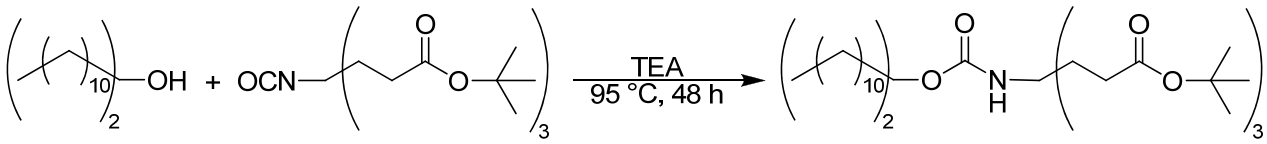

3.6.4.5 – Di-*tert*-butyl 4-(2-(*tert*-butoxycarbonyl)ethyl)-4-(1-undecyldodecyloxycarbonylamino)heptanedioate, 3ECb1(11,11)

Tricosan-12-ol (1.50 g, 4.40 mmol) and Weisocyanate™ (2.00 g, 4.52 mmol) produced a white solid (3.35 g, 96%). The resulting solid (2.16 g) was purified via flash column chromatography to give a white crystalline solid (1.63 g, 75%) in an analogous manner to that of **3ECb1(7,7)**.

mp 78.0-78.5 °C

^{1}H NMR ($CDCl_3$) δ 0.88 (t, 6H), 1.25 (broad s, 36H), 1.43 (s, 27H), 1.48 (broad m, 4H), 1.90 (broad t, 6H), 2.21 (t, 6H), 4.60 (broad s, 1H), 4.65 (broad m, 1H)

^{13}C NMR ($CDCl_3$) δ 14.3, 22.8, 25.5, 28.2, 29.51, 29.73, 29.79, 30.3, 32.1, 34.5, 56.4, 74.4, 80.6, 154.7, 172.7

IR 3353, 2915, 1729, 1713, 1146 cm^{-1}

HRMS (FAB+) calcd for $C_{46}H_{88}NO_8$ (MH^+) 782.2082, found 782.6492

anal. calcd for $C_{46}H_{87}NO_8$: C, 70.64; H, 11.21; N, 1.79. Found: C, 70.77; H, 11.35; N, 1.81.

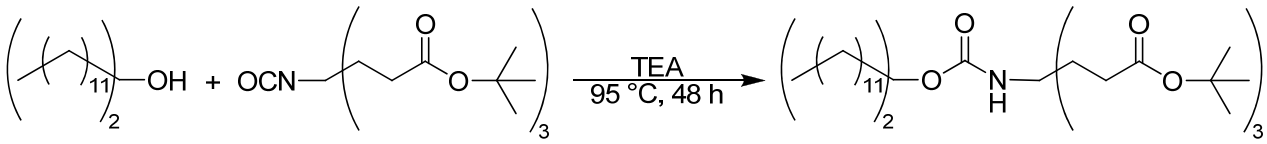

3.6.4.6 – Di-*tert*-butyl 4-(2-(*tert*-butoxycarbonyl)ethyl)-4-(1-dodecyltridecyloxycarbonylamino)heptanedioate, 3ECb1(12,12)

Pentacosan-13-ol (1.10 g, 2.98 mmol) and Weisocyanate™ (1.31 g, 2.98 mmol) produced a white solid (2.27 g, 94%). The resulting solid (1.56 g) was purified via flash column chromatography to give a white crystalline solid (1.24 g, 80%) in an analogous manner to that of **3ECb1(7,7)**.

mp 68.0–68.6 °C

^{1}H NMR ($CDCl_3$) δ 0.88 (t, 6H), 1.25 (broad s, 40H), 1.43 (s, 31H), 1.90 (broad t, 6H), 2.21 (t, 6H), 4.60 (broad s, 1H), 4.65 (broad m, 1H)

^{13}C NMR ($CDCl_3$) δ 14.3, 22.8, 25.5, 28.2, 29.50, 29.73, 29.80, 30.3, 32.1, 34.5, 56.4, 74.4, 80.6, 154.7, 172.7

IR 3357, 2921, 1727, 1708, 1142 cm^{-1}

HRMS (FAB+) calcd for $C_{48}H_{92}NO_8$ (MH^+) 810.2624, found 810.6818

anal. calcd for $C_{48}H_{91}NO_8$: C, 71.15; H, 11.32; N, 1.73. Found: C, 71.37; H, 11.11; N, 1.77.

3.6.5 – 3CCb1(n,n) Synthetic Methodology

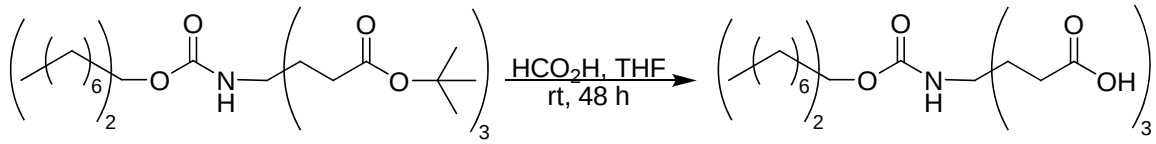

3.6.5.1 – 4-(2-Carboxyethyl)-4-(1-heptyloctyloxycarbonylamino)heptanedioic acid, 3CCb1(7,7)

Compound **3ECb1(7,7)** (1.0189 g, 1.61 mmol) was combined with TFA (2 mL) in a 50 mL round bottom flask and all solids were allowed to dissolve. The solution was then stirred at room temperature for 1 h. The solution was concentrated to a white solid by addition of CH_2Cl_2 (5×20 mL) to help "chase" out the TFA, followed by EtOAc (2×50 mL), and then dried under high vacuum for 48 h to give a white solid (0.7675 g, 95%).

mp 155.3–155.9 °C

^{1}H NMR (CD_3OD) δ 0.89 (t, 6H), 1.29 (m, 20H), 1.50 (broad m, 4H), 1.95 (broad t, 6H), 2.28 (broad t, 6H), 4.66 (broad s, 1H)

^{13}C NMR (CD_3OD) δ 14.5, 23.7, 26.6, 29.2, 30.38, 30.59, 30.66, 32.9, 35.9, 57.2, 74.9, 157.1, 177.1

IR 3352, 2924, 1740, 1701, 1530, 1243 cm^{-1}

HRMS (FAB+) calcd for $C_{26}H_{48}NO_8$ (MH^+) 501.6664, found 502.3370

anal. calcd for $C_{26}H_{47}NO_8$: C, 62.25; H, 9.44; N, 2.79. Found: C, 62.18; H, 9.37; N, 2.79.

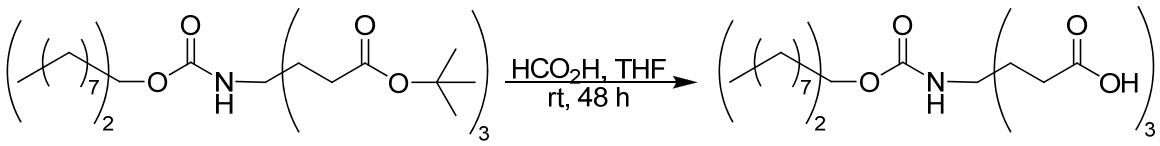

3.6.5.2 – 4-(2-Carboxyethyl)-4-(1-octylnonyloxycarbonylamino)heptanedioic acid, 3CCb1(8,8)

Compound **3ECb1(8,8)** (1.29 g, 1.85 mmol) was used to prepare **3CCb1(8,8)** (1.14 g, 86%) as a white solid in a manner analogous to that of **3CCb1(7,7)**.

mp 131.6–132.8°C

^{1}H NMR (CD_3OD) δ 0.89 (t, 6H), 1.29 (m, 24H), 1.50 (broad m, 4H), 1.95 (broad m, 6H), 2.28 (broad m, 6H), 4.66 (broad s, 1H)

^{13}C NMR (CD_3OD) δ 14.5, 23.7, 26.6, 29.2, 30.40, 30.65, 30.66, 33.0, 35.8, 57.2, 74.8, 157.2, 177.1

IR 3352, 2916, 1737, 1698, 1531, 1238 cm^{-1}

HRMS (FAB+) calcd for $C_{28}H_{52}NO_8$ (MH^+) 529.7206, found 530.3716

anal. calcd for $C_{28}H_{51}NO_8$: C, 63.49; H, 9.70; N, 2.64. Found: C, 63.21; H, 9.78; N, 2.67.

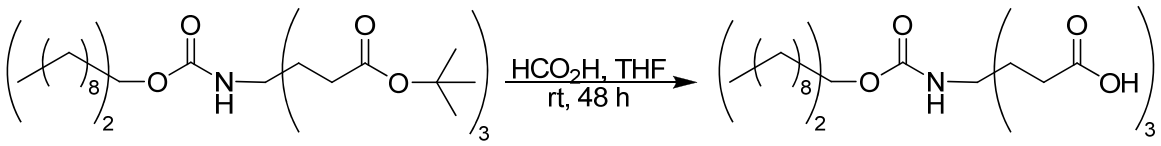

3.6.5.3 – 4-(2-Carboxyethyl)-4-(1-nonyldecyloxycarbonylamino)heptanedioic acid, 3CCb1(9,9)

Compound **3ECb1(9,9)** (0.773 g, 1.06 mmol) was used to prepare **3CCb1(9,9)** (0.576 g, 97%) as a white solid in a manner analogous to that of **3CCb1(7,7)**.

mp 128.9–129.7 °C

^{1}H NMR (CD_3OD) δ 0.86 (t, 6H), 1.25 (m, 28H), 1.46 (broad m, 4H), 1.90 (broad m, 6H), 2.25 (broad m, 6H), 4.62 (broad s, 1H)

^{13}C NMR (CD_3OD) δ 13.0, 22.3, 25.1, 27.7, 29.01, 29.17, 29.23, 29.27, 31.6, 34.4, 55.8, 73.5, 155.7, 174.1

IR 3357, 2921, 1737, 1699, 1531, 1244 cm^{-1}

HRMS (FAB+) calcd for $C_{30}H_{56}NO_8$ (MH^+) 557.7748, found 558.3959

anal. calcd for $C_{30}H_{55}NO_8$: C, 64.60; H, 9.94; N, 2.51. Found: C, 64.48; H, 10.03; N, 2.52.

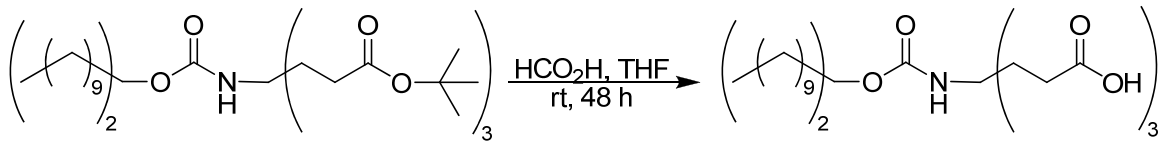

3.6.5.4 – 4-(2-Carboxyethyl)-4-(1-decylundecyloxycarbonylamino)heptanedioic acid, 3CCb1(10,10)

Compound **3ECb1(10,10)** (1.7820 g, 2.36 mmol) was used to prepare **3CCb1(10,10)** (1.38 g, 99%) as a white solid in a manner analogous to that of **3CCb1(7,7)**.

mp 127.4–128.2 °C

^{1}H NMR (CD_3OD) δ 0.90 (t, 6H), 1.29 (m, 32H), 1.50 (broad m, 4H), 1.95 (broad m, 6H), 2.27 (broad m, 6H), 4.66 (broad s, 1H)

^{13}C NMR (CD_3OD) δ 13.0, 22.3, 25.1, 26.9, 27.8, 29.04, 29.16, 29.24, 29.27, 31.6, 34.3, 55.8, 73.4, 155.7, 175.7

IR 3433, 2914, 1741, 1703, 1686, 1514, 1283, 1234 cm^{-1}

HRMS (FAB+) calcd for $C_{32}H_{60}NO_8$ (MH^+) 585.8289, found 586.4304

anal. calcd for $C_{32}H_{59}NO_8$: C, 65.61; H, 10.15; N, 2.39. Found: C, 65.53; H, 10.35; N, 2.38.

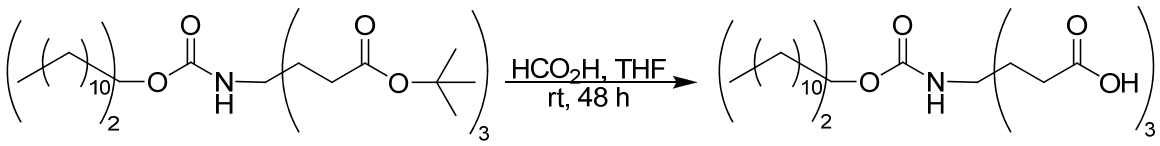

3.6.5.5 – 4-(2-Carboxyethyl)-4-(1-undecyldodecyloxycarbonylamino)heptanedioic acid, 3CCb1(11,11).

Compound **3ECb1(11,11)** (0.508 g, 0.828 mmol) was used to prepare **3CCb1(11,11)** (0.392 g, 98%) as a white solid in a manner analogous to that of **3CCb1(7,7)**.

mp 127.5–128.2 °C

^{1}H NMR (CD_3OD) δ 0.90 (t, 6H), 1.29 (m, 36H), 1.50 (broad m, 4H), 1.95 (broad m, 6H), 2.27 (broad m, 6H), 4.66 (broad s, 1H)

^{13}C NMR (CD_3OD) δ 14.5, 23.8, 26.6, 29.21, 29.24, 30.55, 30.67, 30.76, 30.82, 33.1, 35.8, 57.3, 74.9, 157.2, 177.2

IR 3358, 2916, 1740, 1698, 1691, 1536, 1294, 1267 cm^{-1}

HRMS (FAB+) calcd for $C_{34}H_{64}NO_8$ (MH^+) 613.8831, found 614.4680

anal. calcd for $C_{34}H_{63}NO_8$: C, 66.52; H, 10.34; N, 2.28. Found: C, 66.42; H, 10.53; N, 2.16.

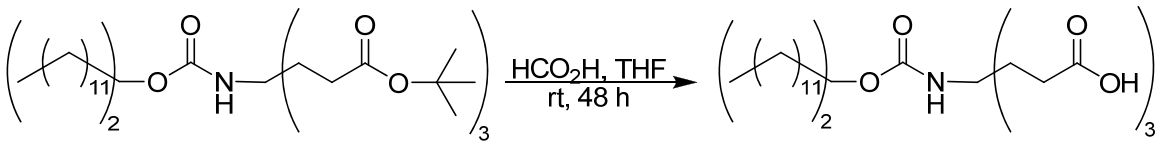

3.6.5.6 – 4-(2-Carboxyethyl)-4-(1-dodecyltridecyloxycarbonylamino)heptanedioic acid, 3CCb1(12,12)

Compound **3ECb1(12,12)** (0.502 g, 0.620 mmol) was used to prepare **3CCb1(12,12)** (0.363 g, 91%) as a white solid in a manner analogous to that of **3CCb1(7,7)**.

mp 124.0–124.7 °C

^{1}H NMR (CD_3OD) δ 0.90 (t, 6H), 1.29 (m, 40H), 1.51 (broad m, 4H), 1.95 (broad m, 6H), 2.28 (broad m, 6H), 4.66 (broad s, 1H)

^{13}C NMR (CD_3OD) δ 14.5, 23.8, 26.6, 29.2, 30.53, 30.62, 30.69, 30.73, 30.79, 30.81, 30.84, 33.1, 35.8, 57.2, 74.8, 157.2, 177.1

IR 3358, 2918, 1741, 1702, 1514, 1266, 1234 cm^{-1}

HRMS (FAB+) calcd for $C_{36}H_{68}NO_8$ (MH^+) 641.9373, found 642.4896

anal. calcd for $C_{36}H_{67}NO_8$: C, 67.36; H, 10.52; N, 2.18. Found: C, 67.27; H, 10.38; N, 2.20.

3.6.6 – X-ray Structure Analysis of 3ECb1(7,7)

Flat colorless needles were crystallized from ethanol/water. The chosen crystal was cut (0.04 x 0.17 x 0.48 mm^3) and centered on the goniometer of an Oxford Diffraction Gemini diffractometer equipped with the Mo-Enhance X-ray source and a Sapphire 3 CCD detector. The data collection routine, unit cell refinement, and data processing were carried out with the program CrysAlis.[24] The Laue symmetry was consistent with the triclinic space group *P*-1. The structure was solved by direct methods and refined using SHELXTL NT.[25] The asymmetric unit of the structure comprises one crystallographically independent molecules. The final refinement model involved anisotropic displacement parameters for non-hydrogen atoms and a riding model for all hydrogen atoms. There was evidence of thermal motion and/or disorder in some of the $-CH_3$ groups. Attempts to model 2-position disorder of the $-CH_3$ groups did not improve the model substantially, so were abandoned.

Table 3-4 Crystal data and structure refinement for **3ECb1(7,7)**. Collected by Dr. Carla Slebodnik.

Identification code	cs999	
Empirical formula	$C_{38}H_{71}NO_8$	
Formula weight	669.96	
Temperature	100(2) K	
Wavelength	0.71073 Å	
Crystal system	Triclinic	
Space group	*P*-1	
Unit cell dimensions	a = 5.7880(13) Å	α= 92.30(2)°.
	b = 18.254(4) Å	β= 90.538(19)°.
	c = 20.041(5) Å	γ= 91.191(19)°.
Volume	2115.1(9) $Å^3$	
Z	2	
Density (calculated)	1.052 Mg/m^3	
Absorption coefficient	0.072 mm^{-1}	
F(000)	740	
Crystal size	0.480 x 0.172 x 0.038 mm^3	
Theta range for data collection	3.71 to 25.15°.	
Index ranges	-6<=h<=4, -21<=k<=21,	
	-23<=l<=21	
Reflections collected	13140	
Independent reflections	7398 [R(int) = 0.0414]	
Completeness to theta = 25.15°	98.0 %	
Absorption correction	None	
Refinement method	Full-matrix least-squares on F^2	
Data / restraints / parameters	7398 / 0 / 435	
Goodness-of-fit on F^2	0.946	
Final R indices [I>2sigma(I)]	R1 = 0.0514, wR2 = 0.1173	
R indices (all data)	R1 = 0.0961, wR2 = 0.1318	
Largest diff. peak and hole	0.254 and -0.231 $e.Å^{-3}$	

3.7 – REFERENCES

(1) Kipping, F. S. *J. Chem. Soc., Trans.* **1893**, *63*, 452-464.
(2) Carrington, R. A. G.; Evans, H. C. *J. Chem. Soc.* **1957**, 1701-1709.
(3) Meakins, R. J.; Sack, R. A. *Aust. J. Sci. Res. Ser. B* **1951**, *4A*, 213-228.
(4) Piper, S. H.; Chibnall, A. C.; Hopkins, S. J.; Pollard, A.; Smith, J. A. B.; Williams, E. F. *Biochem. J.* **1931**, *25*, 2072-2094.
(5) Breusch, F. L.; Sokullu, S. *Chem. Ber.* **1953**, *86*, 678-684.
(6) Baykut, F.; Ozeris, S. *Istanbul Universitesi Fen Fakultesi Mecmuasi, Seri C* **1957**, *22*, 32-38.
(7) Lenne, H. U.; Mez, H. C.; Schlenk, W., Jr. *Justus Liebigs Ann. Chem.* **1970**, *732*, 70-96.
(8) Kirrmann, A.; Geiger-Berschandy, S. *Bull. Soc. Chim. Fr.* **1955**, 991-994.
(9) Easterfield, T. H.; Taylor, C. M. *J. Chem. Soc., Trans.* **1911**, *99*, 2298-2307.
(10) Claypool, C. L.; Faglioni, F.; Matzger, A. J.; Goddard, W. A.; Lewis, N. S. *J. Phys. Chem. B* **1999**, *103*, 9690-9699.
(11) Komarewsky, V. I.; Coley, J. R. *J. Am. Chem. Soc.* **1941**, *63*, 3269-3270.
(12) Sulzbacher, M. *J. Appl. Chem.* **1955**, *5*, 637-641.
(13) Hughes, R. J.; Ncube, S.; Pelter, A.; Smith, K.; Negishi, E.; Yoshida, T. *J. Chem. Soc. Perkin Trans. 1* **1977**, *10*, 1172-1176.
(14) Takai, K.; Nitta, K.; Fujimura, O.; Utimoto, K. *J. Org. Chem.* **1989**, *54*, 4732-4734.
(15) Overmars, F. J. J.; Engberts, J. B. F. N.; Weringa, W. D. *Recl. Trav. Chim. Pays-Bas* **1994**, *113*, 293-296.
(16) Boal, A. K.; Das, K.; Gray, M.; Rotello, V. M. *Chem. Mater.* **2002**, *14*, 2628–2636.
(17) Guedj, C.; Pucci, B.; Zarif, L.; Coulomb, C.; Riess, J. G.; Pavia, A. A. *Chem. Phys. Lipids* **1994**, *72*, 153-174.
(18) Lai, Y.-H. *Synthesis* **1981**, 585-604.
(19) Owens, F. H.; Fellmann, R. P.; Zimmerman, F. E. *J. Org. Chem.* **1960**, *25*, 1808-9.
(20) Stoermer, D.; Caron, S.; Heathcock, C. H. *J. Org. Chem.* **1996**, *61*, 9115-9125.
(21) Jencks, W. P.; Westheimer, F. H., *Compiled pKa Data (R. Williams, Penn State)*, 2008, http://research.chem.psu.edu/brpgroup/pKa_compilation.pdf, last accessed December 30, 2008
(22) Newkome, G. R.; Weis, C. D.; Moorefield, C. N.; Baker, G. R.; Childs, B. J.; Epperson, J. *Angew. Chem., Int. Ed. Engl.* **1998**, *37*, 307–310.
(23) Newkome, G. R.; Behera, R. K.; Moorefield, C. N.; Baker, G. R. *J. Org. Chem.* **1991**, *56*, 7162–7167.
(24) *CrysAlis, v.* 1.171, Oxford Diffraction, Wroclaw, Poland, **2004**
(25) Sheldrick, G. M. *SHELXTL NT, v.* 6.12, Bruker Analytical X-ray Systems, Inc., Madison, WI, **2001**

CHAPTER 4 – CRITICAL MICELLE CONCENTRATION (CMC) MEASUREMENTS

4.1 – INTRODUCTION

As detailed in Chapter 1, the CMC is the concentration at which a solution of surfactant molecules self-assembles to create a micro-phase in which the surfactant has a minimal energy effect on the bulk solution.[1] Micellar formation is associated with detergency, which is one possible mechanism of antimicrobial activity.[2] The standard spermicidal compound, Nonoxynol-9, functions only as a spermicide and antiviral at cytotoxic levels, and is classified as a Class 2-3 toxic substance with toxicity similar to a ~5% solution of household bleach.[2] The detergency action of this compound has been shown to increase the possibility of opportunistic infections due to the harmful effects on epithelial cells and normal vaginal flora.[2] Because of these potential issues, it becomes vital that any compound that is developed as a potential spermicide, virucide, or antibacterial agent for use in contact with human tissues be thoroughly tested to determine at what point the CMC occurs, so that the detergency action of the compound can be limited.

4.2 – AMPHIPHILE SOLUBILITY

As one hypothesis to be tested was whether these compounds were more active than the corresponding fatty acids, we had to ensure that low solubility did not limit antimicrobial activity. Amphiphile **3CAm21** had low solubility in aqueous phosphate buffer (79 μM).[3] Table 5-1 compares the solubility of the fatty acids and the **3CAmn** series in phosphate buffer.

Table 4-1 Comparison of solubilities of long-chain fatty acids with **3CAmn** in phosphate buffer.[3]

	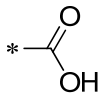 pH 7.4		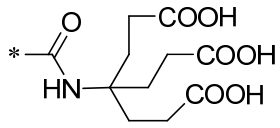 pH 7.2	
Fatty group	**Common Name**	**Solubility[4]**	**3CAmn**	**Solubility**
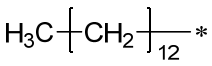	myristic	20–30 μM	**3CAm13**	6900 μM
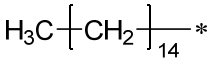	palmitic	~1 μM (visibly clear)	**3CAm15**	3400 μM
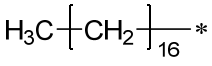	stearic	<<1 μM (visibly clear)	**3CAm17**	1700 μM
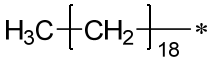	arachidic	Not measured	**3CAm19**	140 μM
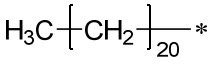	behenic	Not measured	**3CAm21**	79 μM

Triethanolamine (TEA) was chosen as the counterion for these amphiphiles for solubility reasons. Even though the longest chain homologues are soluble whereas the fatty acids are not, we decided to explore different counterions to see if the solubility could be further improved. Kaneko *et al.* found that the bis(triethanolammonium) salt of L-glutamic acid (a diacid) dissolved to a much greater concentration than the dipotassium salt.[5] TEA is a weak base ($pK_a = 7.76$)[6] and stock solutions of the amphiphiles dissolved in TEA/water had pH ranges from 8 to 9. There is no comparable solubility data for the triethanolammonium salts of fatty acids in the literature, but the CMCs of the C_8–C_{18} homologues ranged from 24000 to 92 μM,[7] suggesting that the solubility of the fatty acids in TEA is greater than in phosphate buffer solution. With these results in mind,

solutions of TEA in water were made so as to provide ≥ 6:1 molar equivalents of TEA to amphiphile, with final solubility of **3CAm21** being greater than 22,000 μM. Final solubilities of the **3CCb22** and **3CUr22** amphiphiles were comparable.[3] Maximal solubility beyond this limit was not explored, as any potential drug candidate with MICs beyond this concentration is not worth developing as a lead.[3]

4.3 – Surface Tension and Pyrene Fluorescence Measurements

Initially, CMC data was to be collected using the Wilhelmy-plate technique on a Cahn balance. However, it was determined that the **3CUrn** series was adsorbing to the plate which prevented the collection of accurate data. After the initial attempts to collect CMC data with a Cahn balance setup failed, data collection was done with a pendent-drop analyzer used to record surface tension data at 20 ± 1 °C. The pendent-drop method proved to be much more reproducible in this case due to the surface tension being determined only by the shape of the drop, and not by having a foreign object (i.e. the plate) immersed in the solution. Recall that as the amount of surfactant in solution increases, the surface tension decreases until the CMC is reached, at which point there is little, if any, further change in the surface tension of the solution (cf. section 1.4.2.3).

Plots of interfacial tension (IFT) versus log[amphiphile] were prepared for each amphiphile in the **3CAmn**, **3CUrn**, **3CCbn**, and **3CCb1(n,n)** series. In several cases the surface tension data produced either very weak breaks or no breaks at all (beyond the limits of what could be considered random scatter), which made accurate determination of the CMC from the surface tension data in some cases difficult at best. Due to these results, it was decided to have the CMC of these amphiphiles measured by pyrene fluorescence to verify the CMC point obtained via surface tension. The results shown

below compare and contrast the data obtained via pyrene fluorescence to the surface tension measurements. Pyrene fluorescence measurements were made by Xiaosong Du from Dr. Esker's lab. In both cases, linear least squares regression lines were made on the linear portion of the graphs before and after the break to find the value of the CMC.

The error associated with determination of the correct concentration is variable for each graph, and is mainly indeterminate human error that arises from the selection or rejection of any given data point used to generate the linear regression lines. Error determination is covered further in section 4.4.2.

4.3.1 – Pyrene Fluorescence

Pyrene fluorescence has been used to measure the CMC of various amphiphilic molecules.[8-11] The five emission bands of pyrene undergo significant changes to their vibrational fine structure intensities when fluorescence measurements are made in a polar versus a non-polar environment.[11-14] The first and third bands (hereafter labeled I_1 and I_3) show the greatest relative variation to one another when the microenvironment changes, therefore these two bands are used to determine the fluorescence ratio (I_1/I_3 ratio).[11] The I_1/I_3 ratio is dependent on solvent polarity and the hydrophobicity of the surrounding environment, making it useful for studying aggregation properties.[10]

As amphiphile concentration increases, the I_1/I_3 ratio follows a sigmoid decrease from the typical values seen in polar aqueous media (~ 1.9) to a constant value associated with solubilization of the pyrene in a non-polar environment (~ 1.2). The explanation for this trend is that as more and more amphiphile is added to the solution, the microenvironment of the pyrene changes from an aqueous to a nonpolar one, as the pyrene preferentially interacts with the nonpolar portion of the amphiphile. The I_1/I_3 ratio stops changing at the CMC because the pyrene is preferentially encapsulated within the

micellar core, minimizing hydrophobic interactions of the pyrene with the solvent. The pyrene cannot solubilize into a more non-polar microenvironment than the micellar core, and this represents the limit of the I_1/I_3 ratio decrease.

4.3.2 – 3CAmn Data

All CMC measurements are reported to 1 significant figure. Figure 4-1 shows the IFT vs. log[amphiphile] data for **3CAm21**. Figure 4-2 is the pyrene fluorescence vs. log [amphiphile] data for **3CAm21**. Figure 4-2 shows that the pyrene fluorescence method actually produces a sharper CMC break with less ambiguity in determining the break point, because the data points after the break are more linear. Therefore the determination of the CMC from the pyrene fluorescence measurements should be more accurate. The apparent CMC for **3CAm21** is 1,000 mg/L (2 mM) via surface tension and 900 mg/L (2 mM) via pyrene fluorescence.

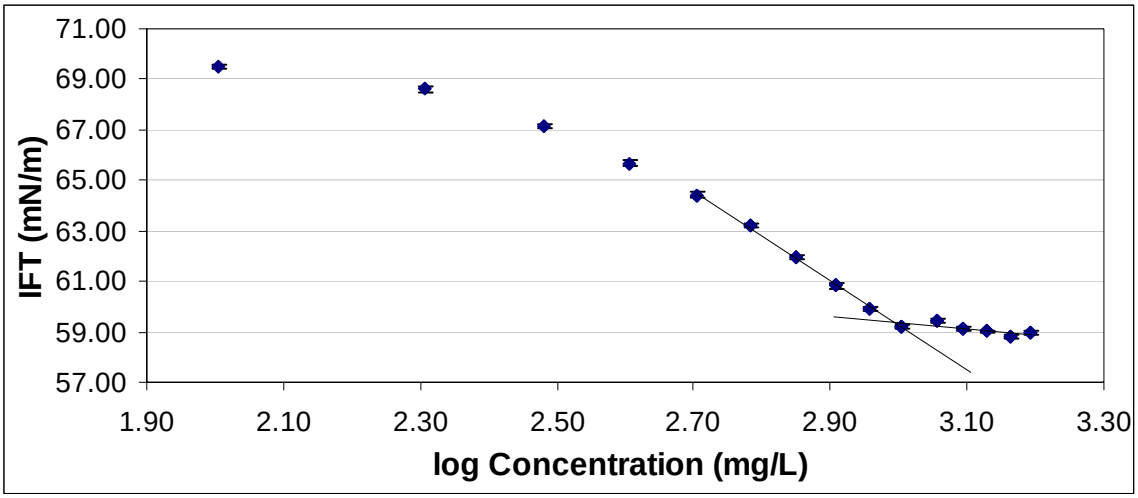

Figure 4-1 IFT vs. log [**3CAm21**]

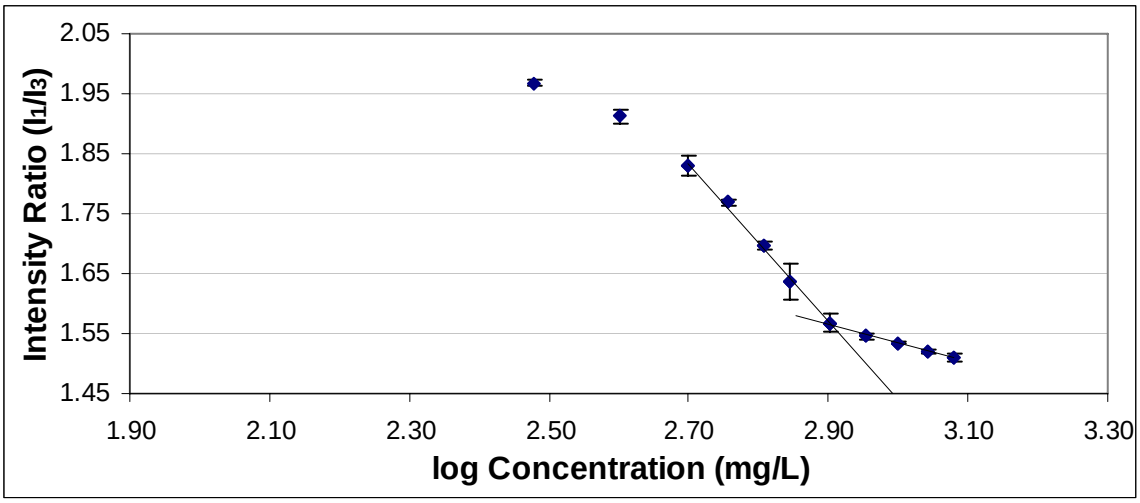

Figure 4-2 Fluorescence Intensity Ratio (I_1/I_3) vs. log [**3CAm21**]

Figure 4-3 is the IFT vs. log[amphiphile] data for **3CAm19**. Figure 4-4 is the pyrene fluorescence vs. log [amphiphile] data for **3CAm19**. The graphs show similar shapes and CMC points, although the lack of linearity before the CMC in the surface tension graph makes accurate determination of the CMC by surface tension difficult. The data are much more linear for the pyrene fluorescence measurements. Despite these issues the CMCs are surprisingly similar when compared, although the results of the CMC determination by pyrene fluorescence are probably more accurate. The data point at log concentration ~ 2.9 is believed to be an outlier from the rest of the data points in the surface tension graph of Figure 4-3. The apparent CMC for **3CAm19** is 2,000 mg/L (3 mM) by surface tension and 2,000 mg/L (3 mM) by pyrene fluorescence.

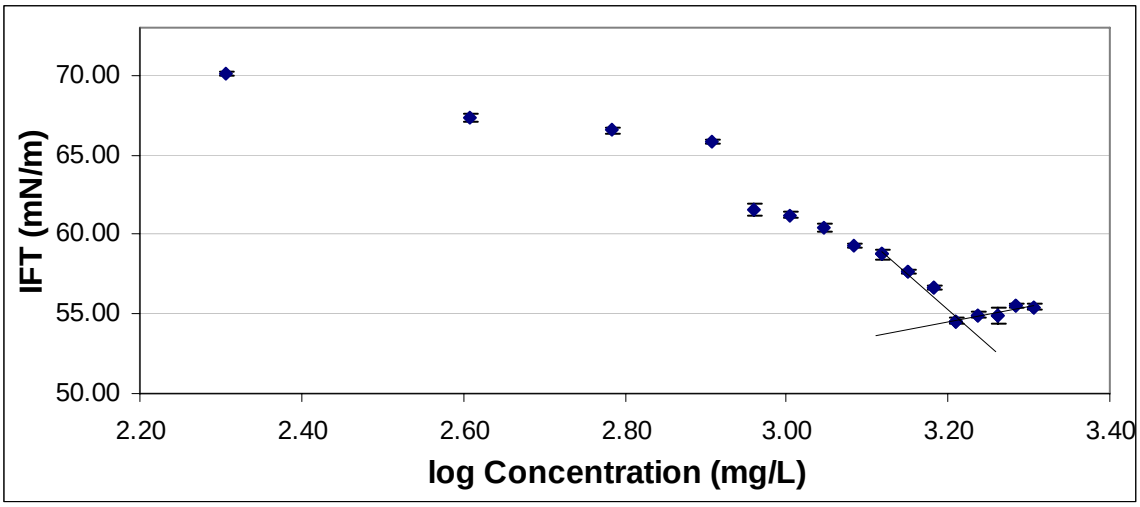

Figure 4-3 IFT vs. log [**3CAm19**]

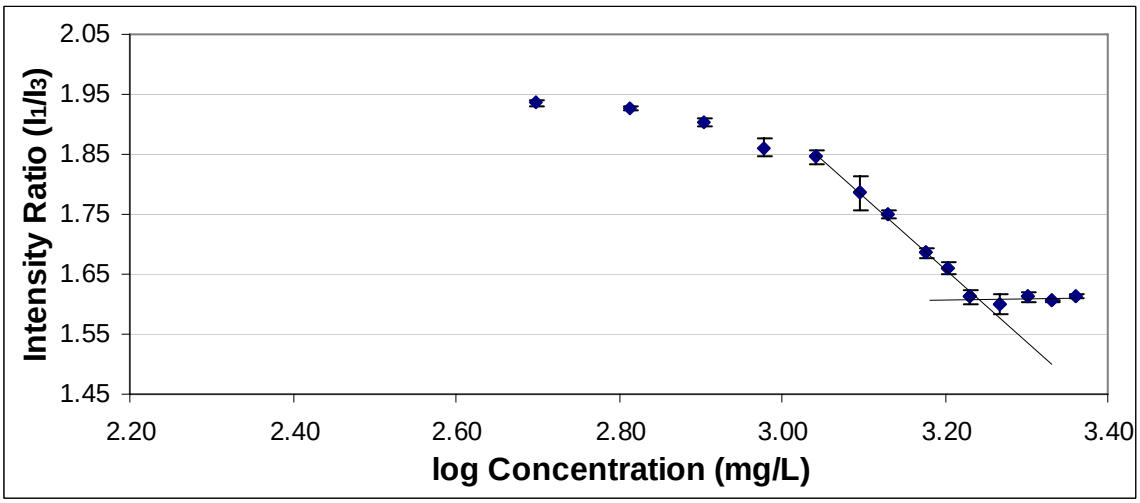

Figure 4-4 Fluorescence Intensity Ratio (I_1/I_3) vs. log [**3CAm19**]

Figure 4-5 is the IFT vs. log[amphiphile] data for **3CAm17**. Figure 4-6 is the pyrene fluorescence vs. log [amphiphile] data for **3CAm17**. This amphiphile demonstrates significantly different behavior from that of **3CAm21** and **3CAm19** (Figures 4-1 through 4-4). The IFT decreases to a minimum of ~ 49 mN/m and then rises again until leveling off at ~ 55 mN/m. The fluorescence intensity graph shows similar behavior, although the CMC point appears at lower concentration. The apparent CMC for **3CAm17** is determined to be 6,000 mg/L (0.01 M) by surface tension and 5,000 mg/L

(0.01 M) by pyrene fluorescence. The minimum that occurs will be discussed further in section 4.4.2.

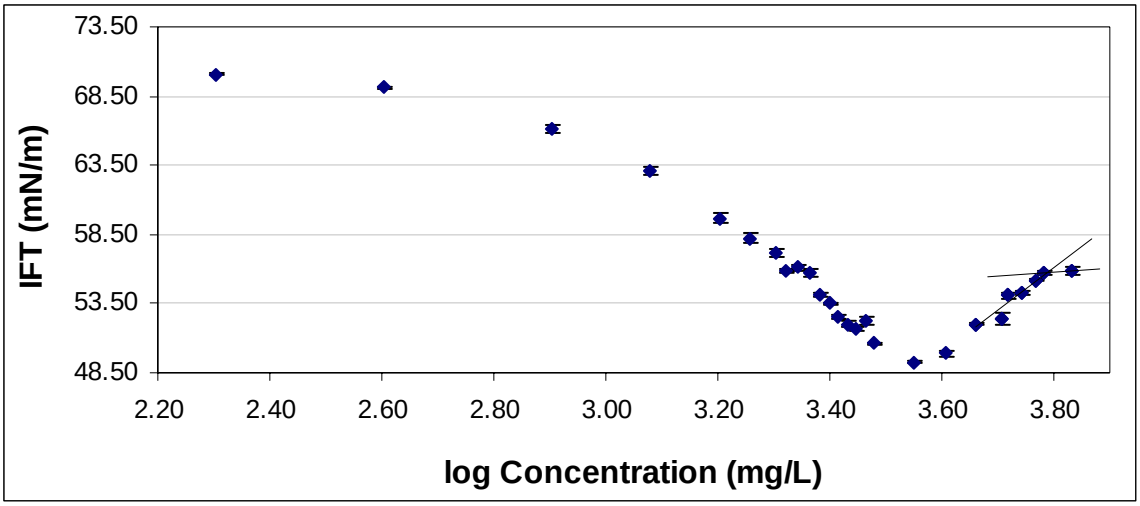

Figure 4-5 IFT vs. log [**3CAm17**]

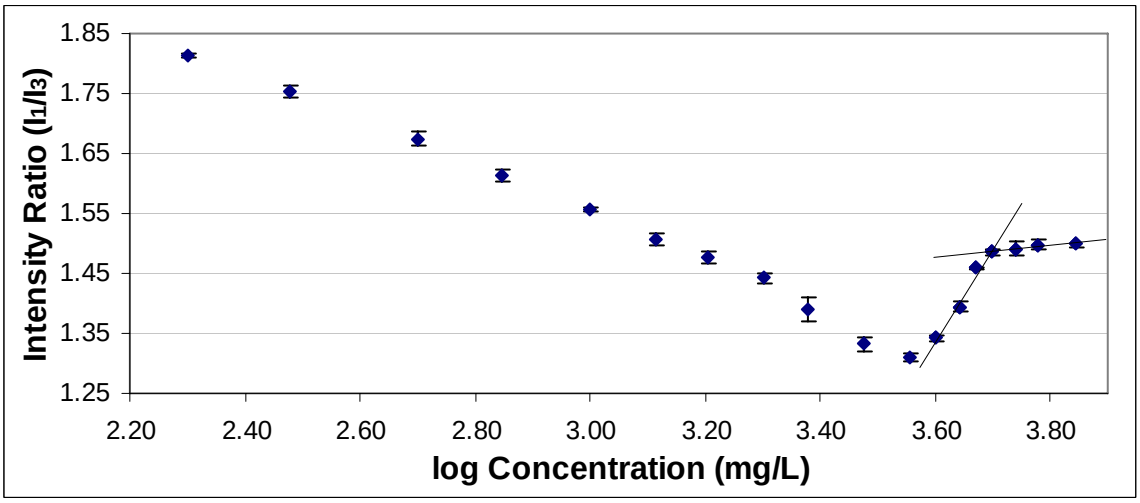

Figure 4-6 Fluorescence Intensity Ratio (I_1/I_3) vs. log [**3CAm17**]

Figure 4-7 is the IFT vs. log[amphiphile] data for **3CAm15** and Figure 4-8 is the pyrene fluorescence data. The pyrene fluorescence data shows a much sharper break than the surface tension data with less variation in the data points before the break occurs. Additionally, the pyrene data has more points after the break to make determination of

the linear regression line more accurate. The apparent CMC for **3CAm15** is 8,000 mg/L (0.02 M) by surface tension and 9,000 mg/L (0.02 M) by pyrene fluorescence.

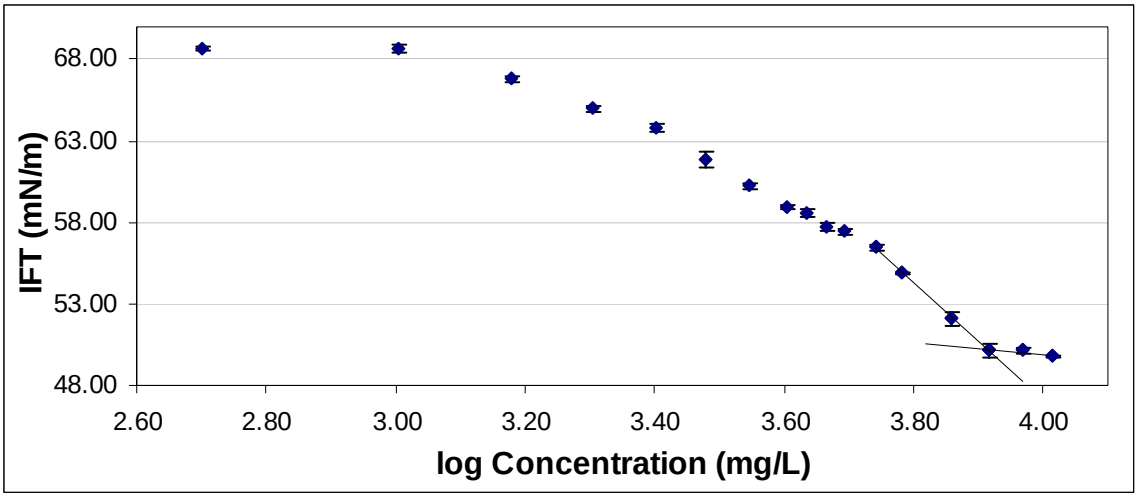

Figure 4-7 IFT vs. log [**3CAm15**]

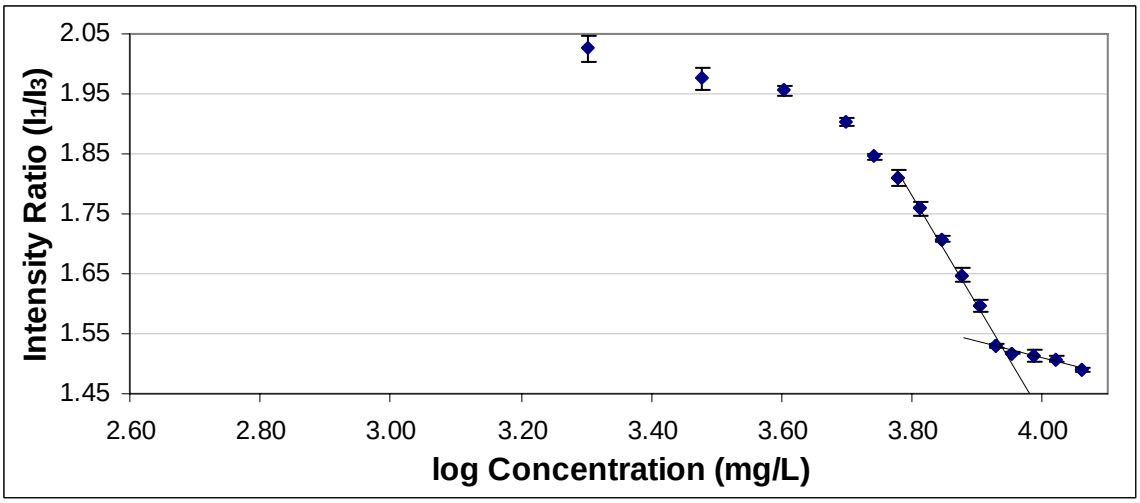

Figure 4-8 Fluorescence Intensity Ratio (I_1/I_3) vs. log [**3CAm15**]

Figure 4-9 is the IFT vs. log[amphiphile] data for **3CAm13** and Figure 4-10 is the pyrene fluorescence data. Neither method shows a CMC break before 10,000 mg/L. Additionally, the surface tension in Figure 4-9 drops far below the average surface tension value at which the previously tested amphiphiles begin to level off. This tends to

suggest that the **3CAm13** sample does not begin to aggregate below 10,000 mg/L concentration.

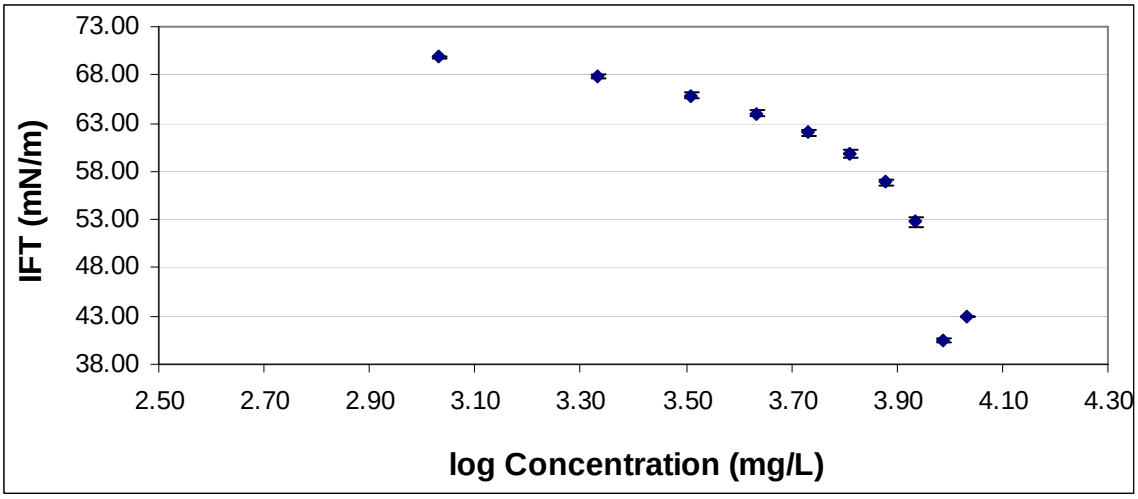

Figure 4-9 IFT vs. log [**3CAm13**]

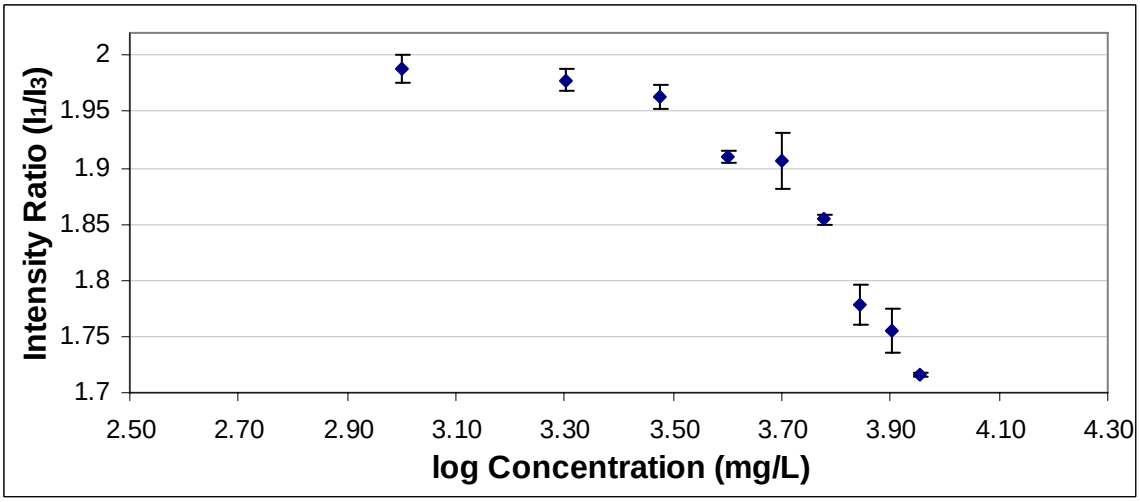

Figure 4-10 Fluorescence Intensity Ratio (I_1/I_3) vs. log [**3CAm13**]

4.3.3 – 3CCbn Data

Figure 4-11 is the IFT vs. log[amphiphile] data for **3CCb22** and Figure 4-12 is the pyrene fluorescence data. The surface tension data seems to show a small dip before the CMC, similar to what is seen in Figures 4-5 and 4-6. However, no corresponding dip in the fluorescence data is observed. This tends to indicate that the dip in the surface

tension measurements is due to scatter, making an accurate determination of the CMC more difficult. While the pyrene data does not break very sharply, it is much easier to make an accurate determination of the CMC using that data due to lack of the dip. The apparent CMC for **3CCb22** is 200 mg/L (0.4 mM) by surface tension and 200 mg/L (0.3 mM) by pyrene fluorescence.

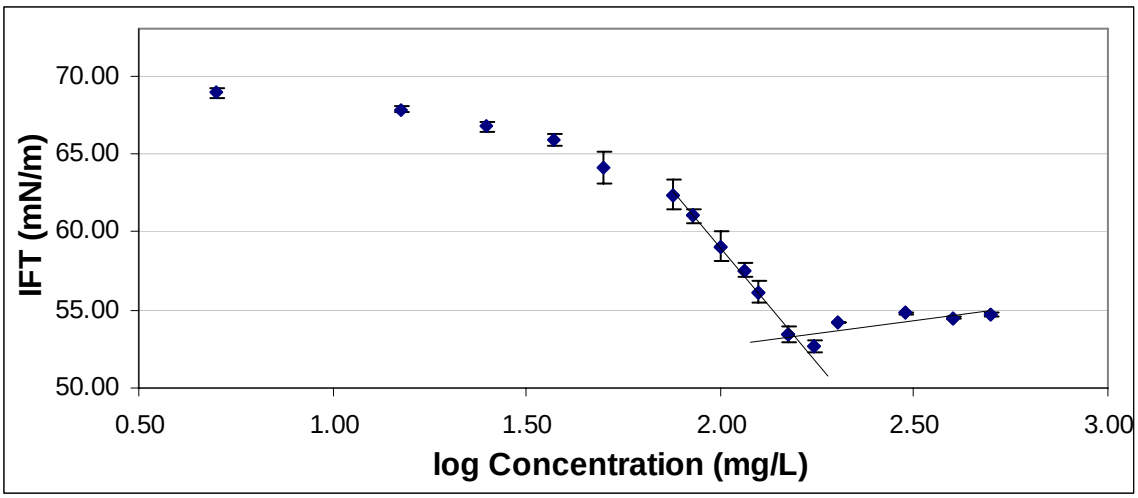

Figure 4-11 IFT vs. log [**3CCb22**]

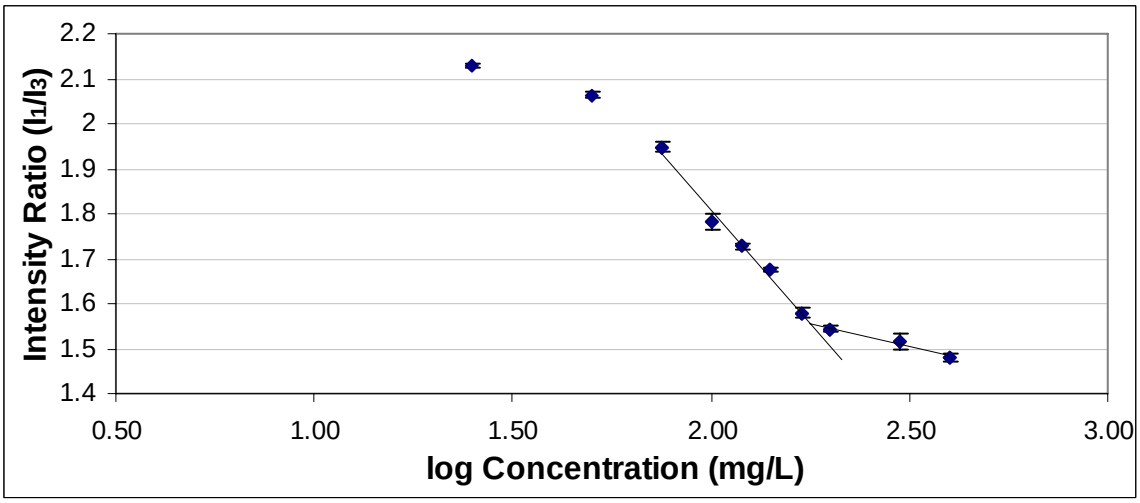

Figure 4-12 Fluorescence Intensity Ratio (I_1/I_3) vs. log [**3CCb22**]

Figure 4-13 is the IFT vs. log[amphiphile] data for **3CCb20** and Figure 4-14 is the pyrene fluorescence data. There is a significant discrepancy in the CMC determined

by the two methods. The surface tension curve of Figure 4-13 shows a break, but the data points leading up to and following the break are not linear, making an accurate CMC determination using the surface tension data difficult at best. The pyrene fluorescence data, on the other hand, shows very linear data, and the break is significantly clearer than the surface tension break. This indicates that the CMC determined by pyrene fluorescence is much more accurate than the CMC determined by surface tension. The apparent CMC for **3CCb20** is 300 mg/L (0.5 mM) by surface tension and 500 mg/L (0.8 mM) by pyrene fluorescence.

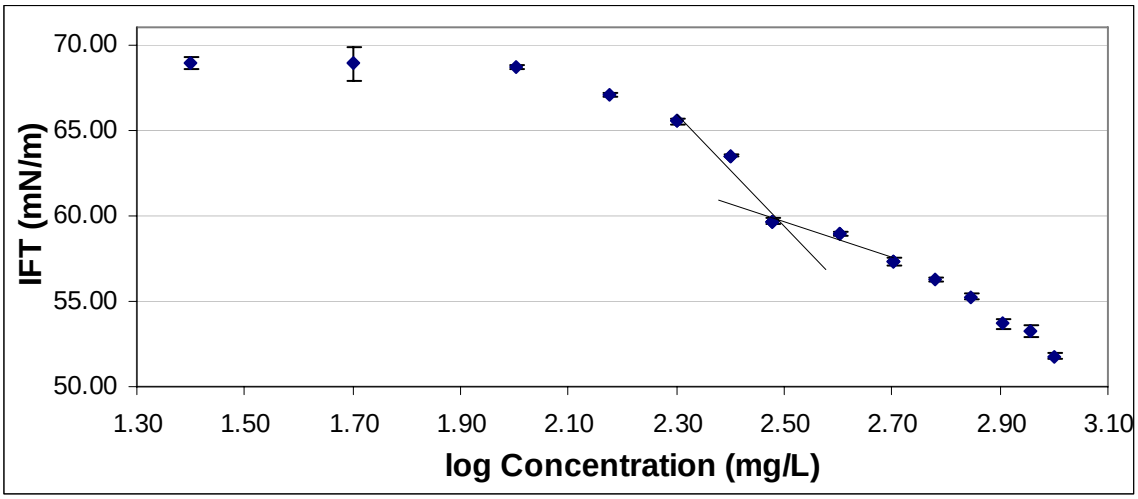

Figure 4-13 IFT vs. log [**3CCb20**]

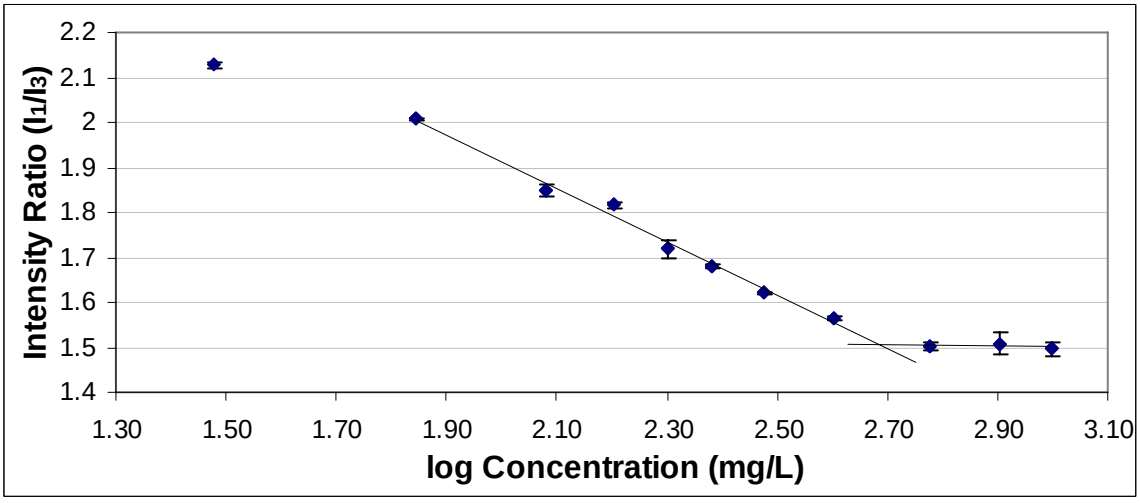

Figure 4-14 Fluorescence Intensity Ratio (I_1/I_3) vs. log [**3CCb20**]

Figure 4-15 is the IFT vs. log[amphiphile] data for **3CCb18** and Figure 4-16 is the pyrene fluorescence data. Both curves show very shallow breaks, making accurate determination of the CMC by either method problematic. There is good agreement between the two methods, but without a clearer break no comment can me made as to the accuracy of the measurement. The apparent CMC for **3CCb18** is 1,000 mg/L (3 mM) by surface tension and 1,000 mg/L (3 mM) by pyrene fluorescence.

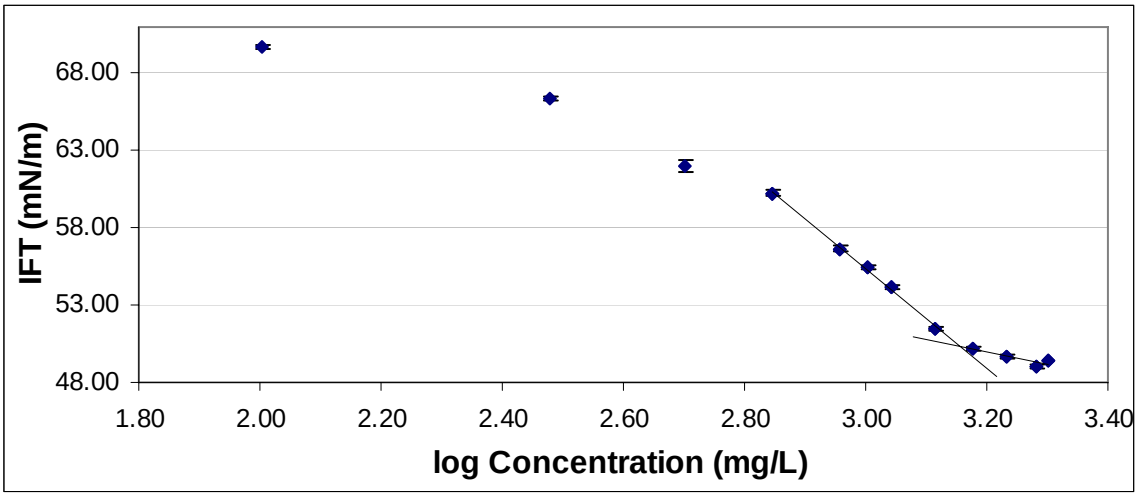

Figure 4-15 IFT vs. log [**3CCb18**]

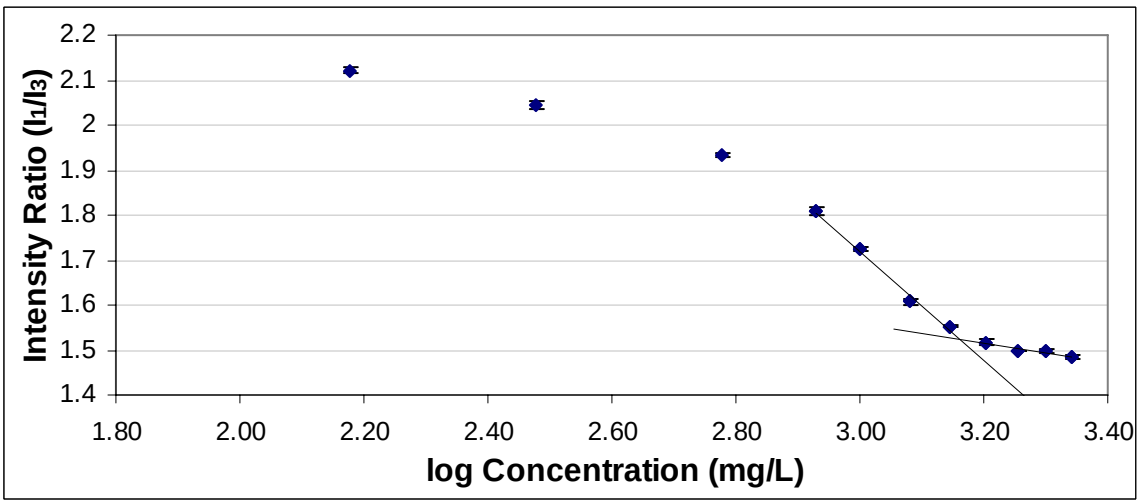

Figure 4-16 Fluorescence Intensity Ratio (I_1/I_3) vs. log [**3CCb18**]

Figure 4-17 is the IFT vs. log[amphiphile] data for **3CCb16** and Figure 4-18 is the pyrene fluorescence data. Again, there appears to be a dip in the surface tension graph with no corresponding dip in the fluorescence data, as seen with the **3CCb22** compound. This tends to indicate that the CMC measured by pyrene fluorescence will be more accurate. The apparent CMC for **3CCb16** is 4,00 mg/L (7 mM) by surface tension and 3,00 mg/L (7 mM) by pyrene fluorescence.

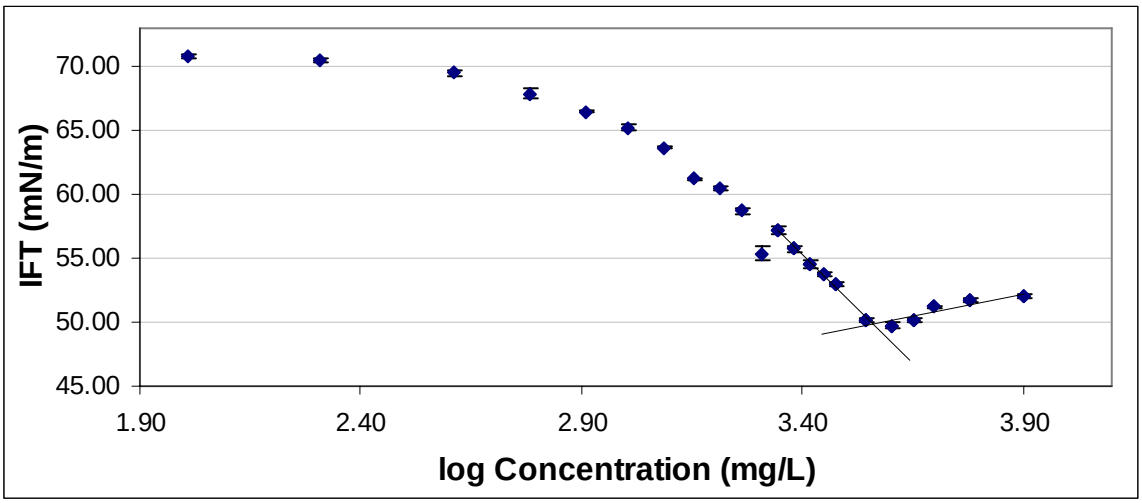

Figure 4-17 IFT vs. log [**3CCb16**]

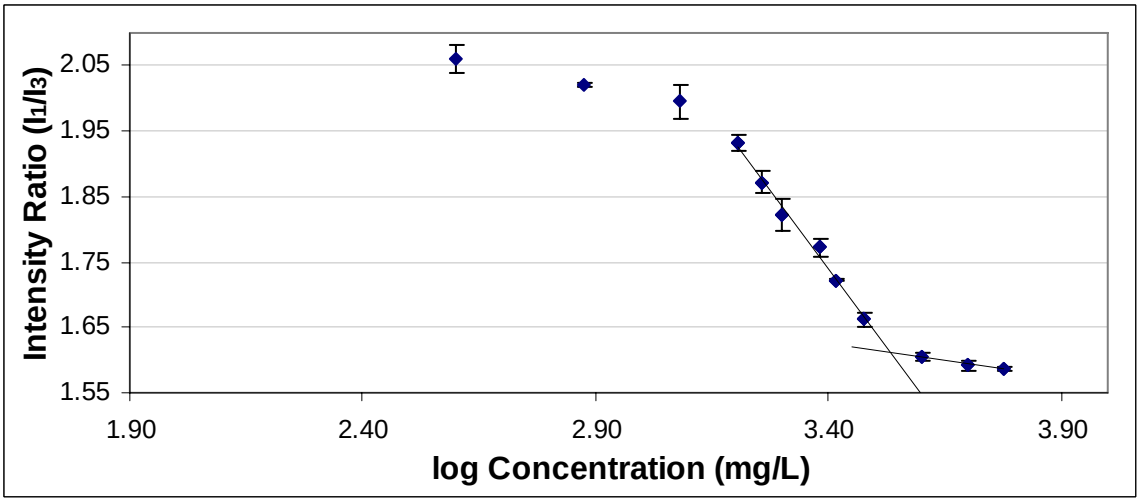

Figure 4-18 Fluorescence Intensity Ratio (I_1/I_3) vs. log [**3CCb16**]

Figure 4-19 is the IFT vs. log[amphiphile] data for **3CCb14** and Figure 4-20 is the pyrene fluorescence data. Again, we see that the data points directly before the break are either not particularly straight (surface tension) or are scattered (pyrene fluorescence), hindering our ability to accurately measure the CMC. As an example, if we include the data point at log concentration ~ 3.6 in the pyrene fluorescence measurements, it increases the apparent CMC from 6,700 mg/L up to 7,100 mg/L. Either point produces CMC values that are not very similar to the CMC obtained via surface tension. Du experienced decreasing amphiphile solubility with the higher concentration solutions, which may also point towards this not being an actual break but an artifact arising from lower solubility. Because there are so few data points before and after the apparent break in either measurement set of data, it is difficult to make an accurate determination of the CMC.

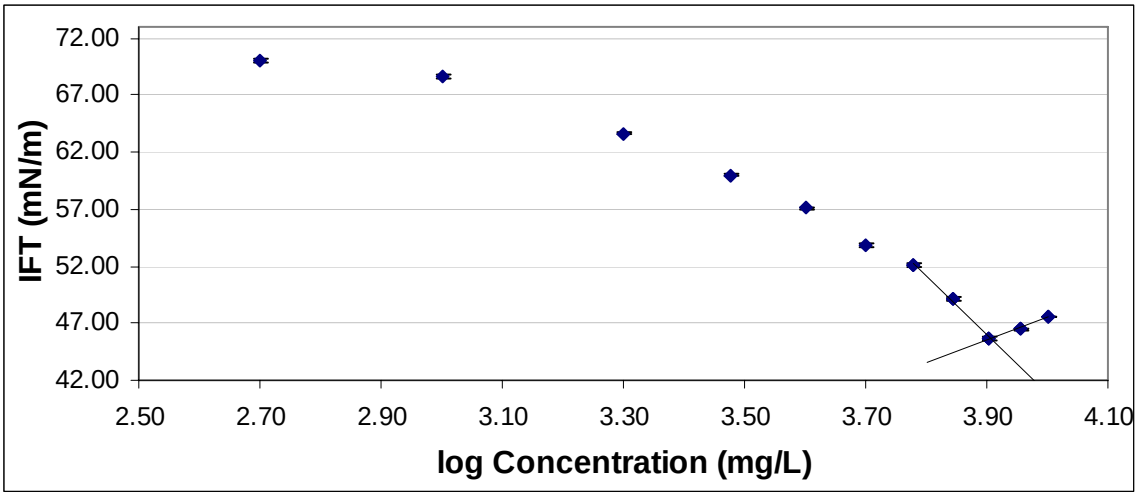

Figure 4-19 IFT vs. log [**3CCb14**]

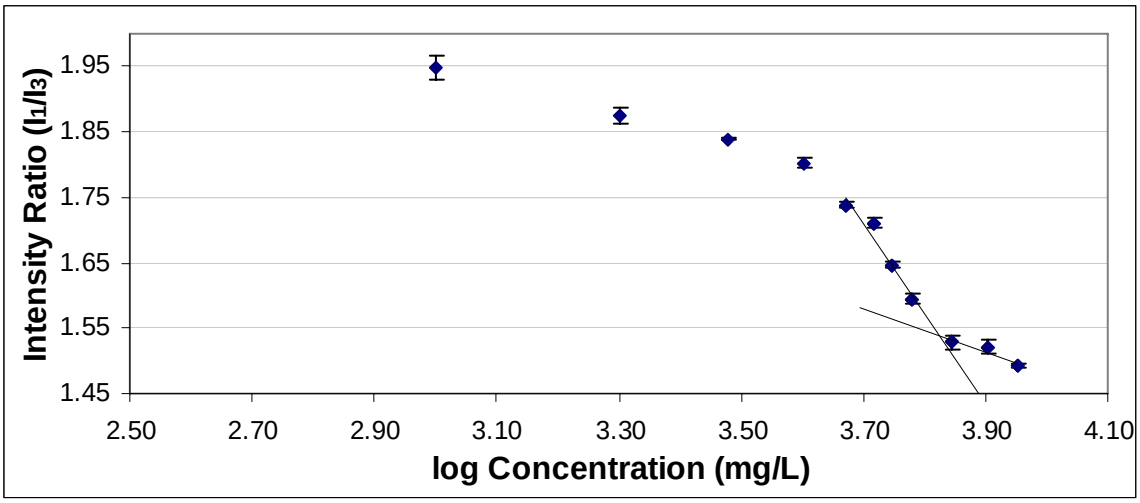

Figure 4-20 Fluorescence Intensity Ratio (I_1/I_3) vs. log [**3CCb14**]

4.3.4 – 3CUrn Data

Figure 4-21 is the IFT vs. log[amphiphile] data for **3CUr22** and Figure 4-22 is the pyrene fluorescence data. There is an extremely large discrepancy in the apparent CMC values between the two measurement techniques. The CMC break via surface tension is not very sharp, nor are the data very linear either before or after the break. The CMC break via pyrene fluorescence is much sharper, and tends to indicate that the pyrene fluorescence data are more accurate. The apparent outlier in the surface tension data at ~ 2.3 roughly corresponds with the CMC value indicated by the pyrene fluorescence measurements. However, it is not possible to accurately declare that single point as the CMC break. A second and third set of measurements of the surface tension would have to be made in order to accurately gauge what is occurring. The apparent CMC for **3CUr22** is 600 mg/L (1 mM) by surface tension and 100 mg/L (0.2 mM) by pyrene fluorescence.

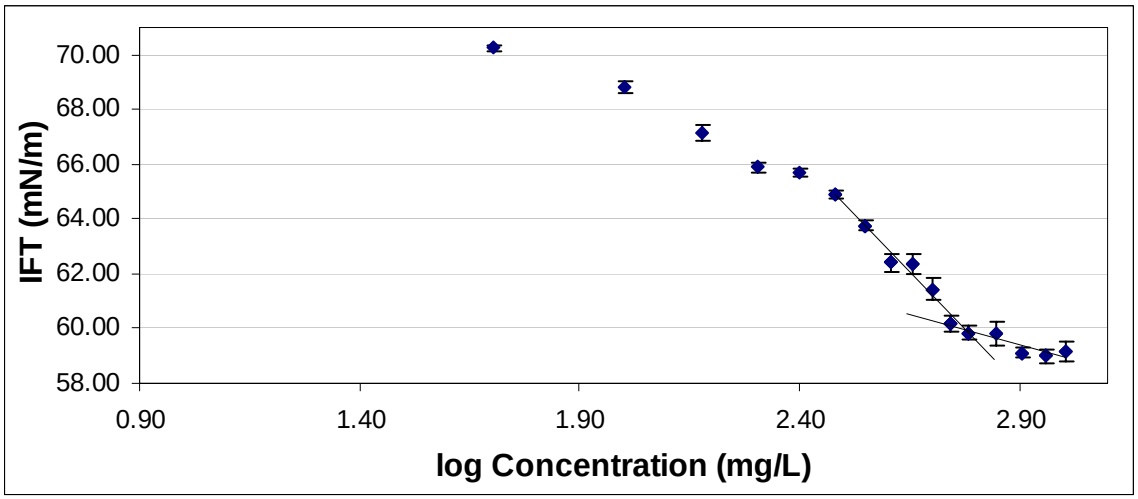

Figure 4-21 IFT vs. log [**3CUr22**]

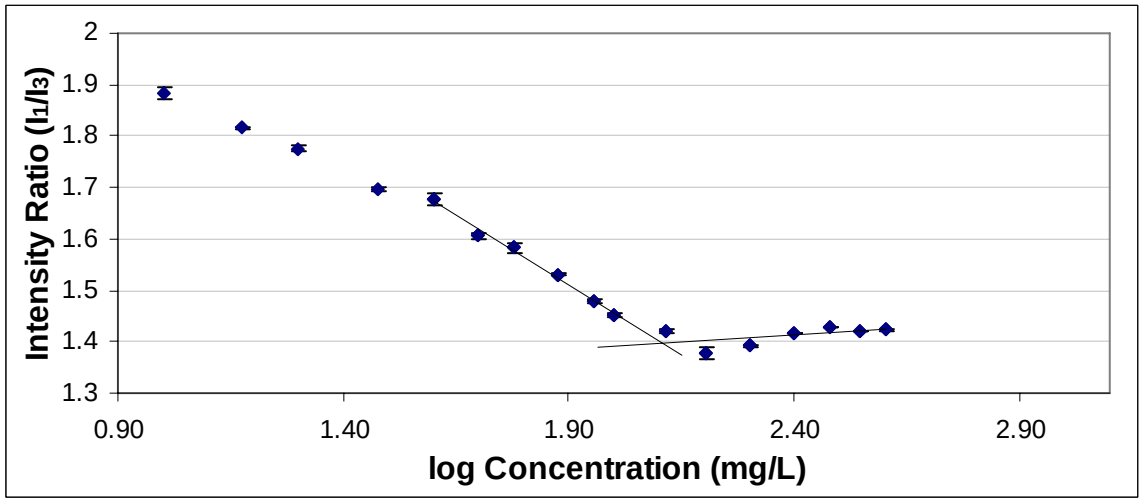

Figure 4-22 Fluorescence Intensity Ratio (I_1/I_3) vs. log [**3CUr22**]

Figure 4-23 is the IFT vs. log[amphiphile] data for **3CUr20** and Figure 4-24 is the pyrene fluorescence data. The scatter in the surface tension data preceding the break point makes accurate determination of the CMC difficult. The data are much more linear in the pyrene fluorescence data, which tends to indicate increased accuracy. The apparent CMC for **3CUr20** is 800 mg/L (1 mM) by surface tension and 800 mg/L (1 mM) by pyrene fluorescence.

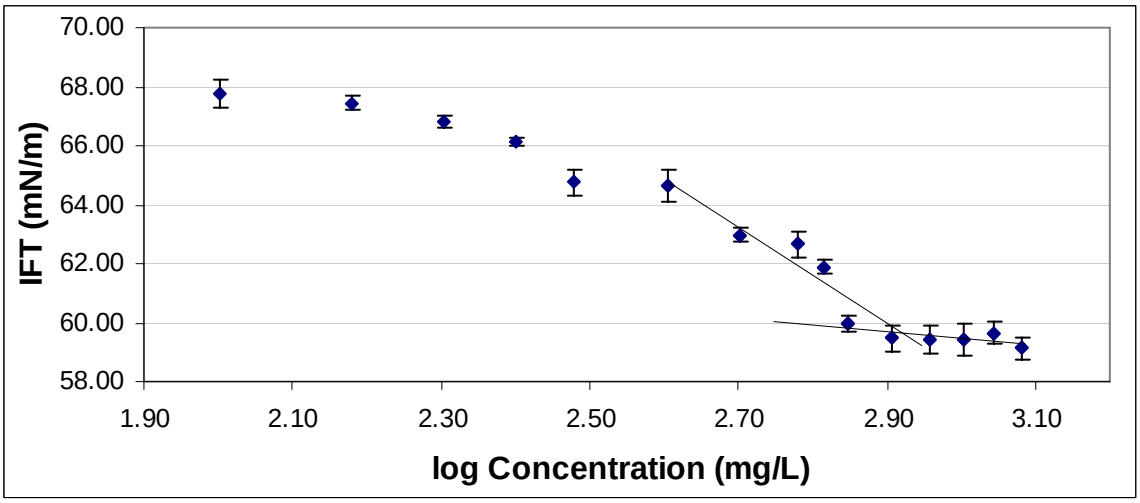

Figure 4-23 IFT vs. log [**3CUr20**]

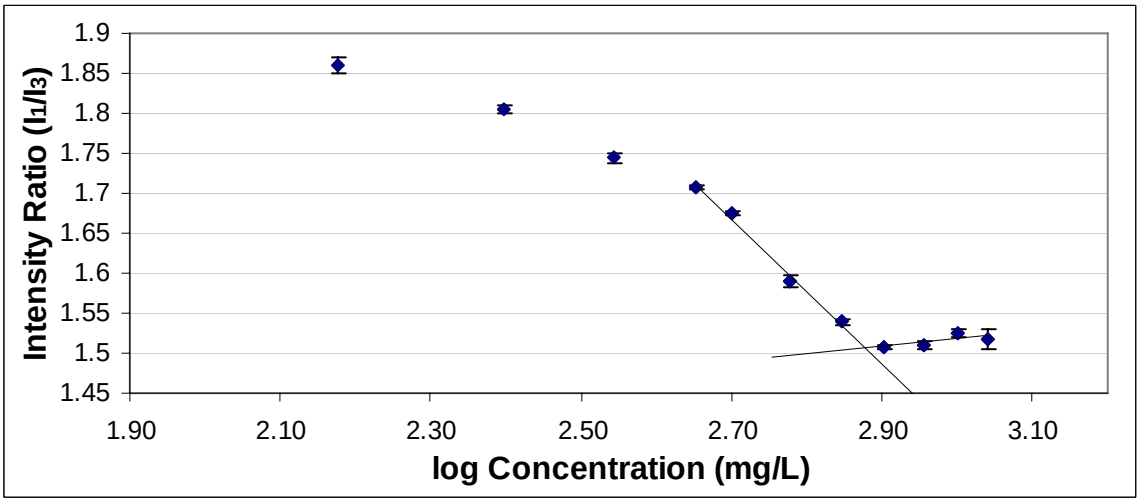

Figure 4-24 Fluorescence Intensity Ratio (I_1/I_3) vs. log [**3CUr20**]

Figure 4-25 is the IFT vs. log[amphiphile] data for **3CUr18** and Figure 4-26 is the pyrene fluorescence data. The data from the pyrene fluorescence measurements are much more linear, with a much sharper break, indicating that determination of the CMC from these data is probably more accurate than from the surface tension data. The apparent CMC for **3CUr18** is 1,000 mg/L (2 mM) by surface tension and 1,000 mg/L (2 mM) by pyrene fluorescence.

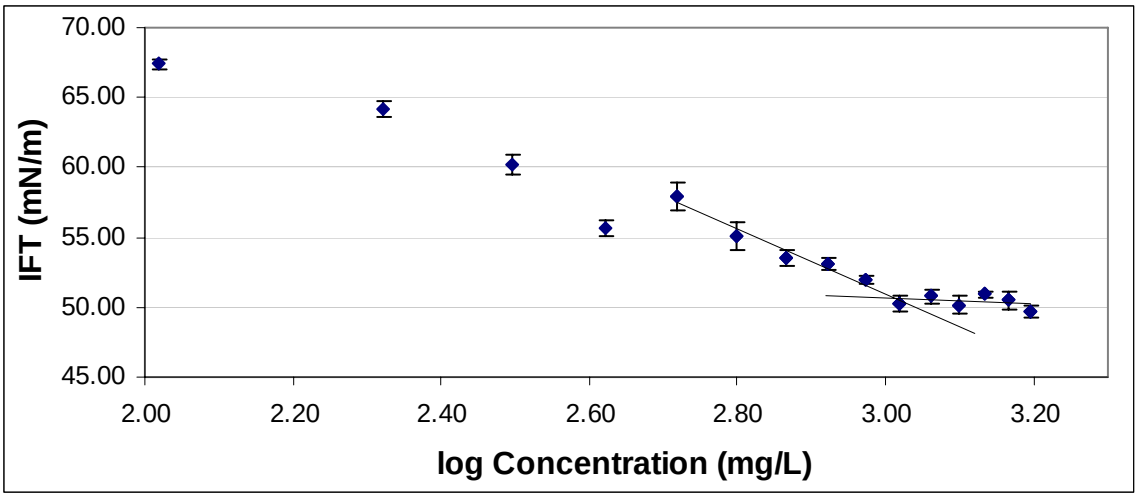

Figure 4-25 IFT vs. log [**3CUr18**]

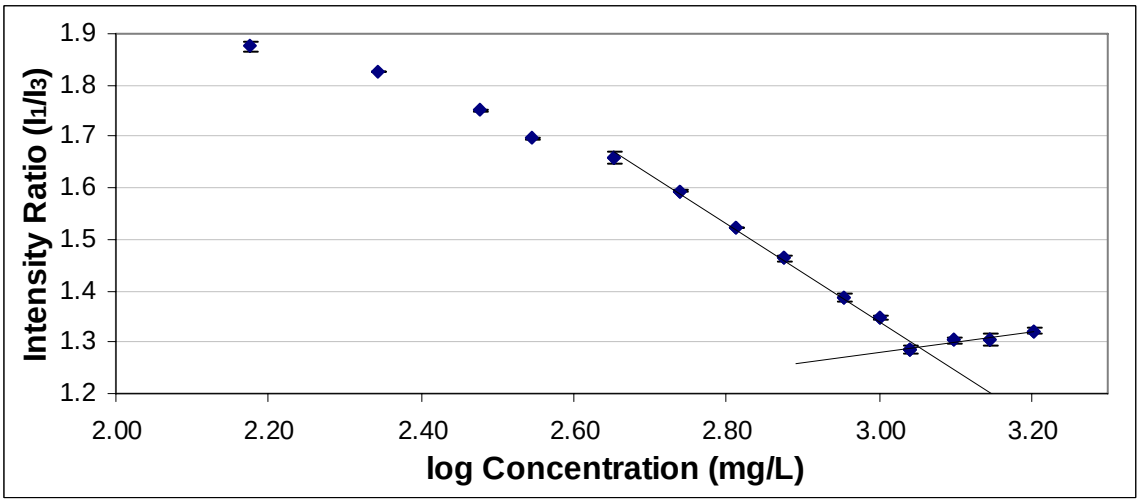

Figure 4-26 Fluorescence Intensity Ratio (I_1/I_3) vs. log [**3CUr18**]

Figure 4-27 is the IFT vs. log[amphiphile] data for **3CUr16** and Figure 4-28 is the pyrene fluorescence data. The determination of the CMC by surface tension measurements is problematic at best. The apparent break in the curve looks sharp, but the surface tension continues to decrease sharply after leveling off, indicating that this could be either a true break or simply scatter in the data. Comparison to the pyrene fluorescence data tends to indicate that this is scatter, and that the CMC has not been reached by the final data point at log concentration of ~ 3.40 in the surface tension

measurements. The determination of the CMC from the pyrene fluorescence data is better, but the lack of a sharp break point makes accurate determination of the CMC questionable. The apparent CMC for **3CUr16** is 3,000 mg/L (7 mM) by pyrene fluorescence.

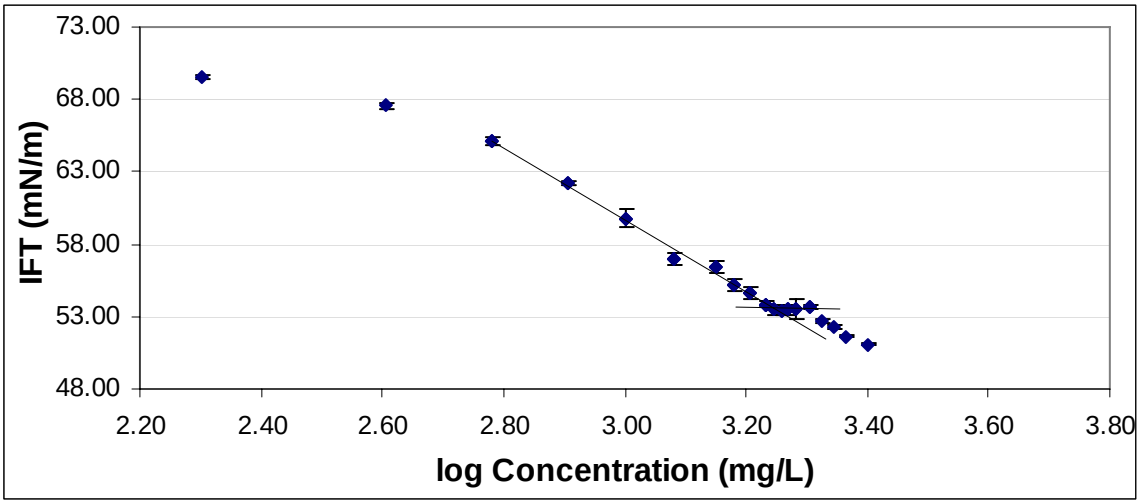

Figure 4-27 IFT vs. log [**3CUr16**]

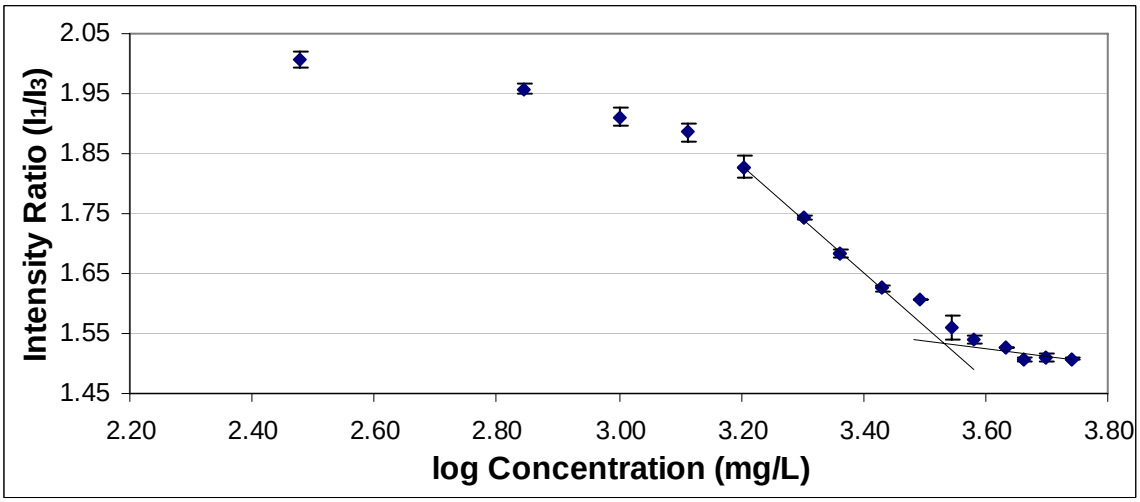

Figure 4-28 Fluorescence Intensity Ratio (I_1/I_3) vs. log [**3CUr16**]

Figure 4-29 is the IFT vs. log[amphiphile] data for **3CUr14** and Figure 4-30 is the pyrene fluorescence data. The pyrene fluorescence data shows the beginning of a break at log concentration of ~ 3.85. The surface tension data stops before this apparent break,

so no corroborating evidence of a break is present. Further tests to higher concentrations via surface tension and pyrene fluorescence may indicate a definite break in the curve.

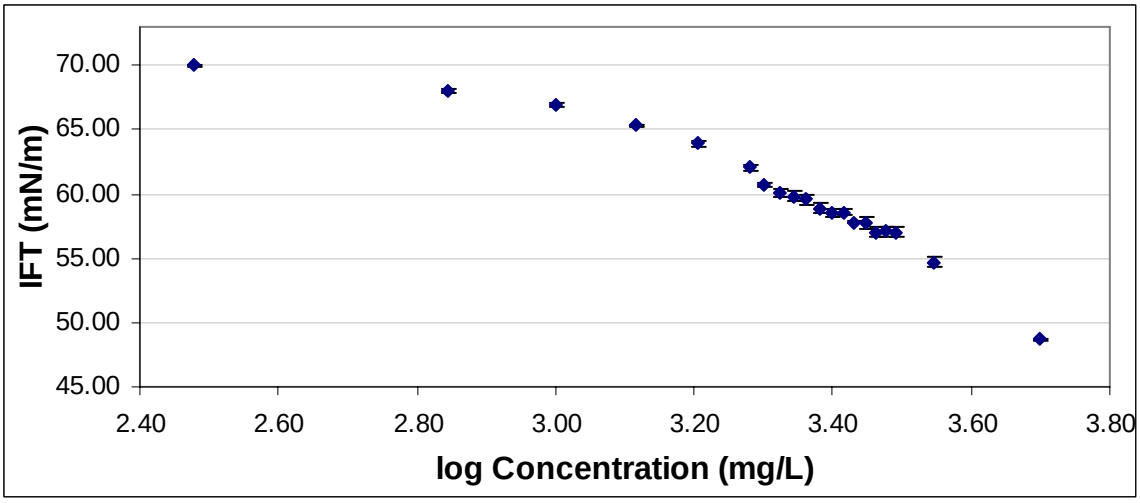

Figure 4-29 IFT vs. log [**3CUr14**]

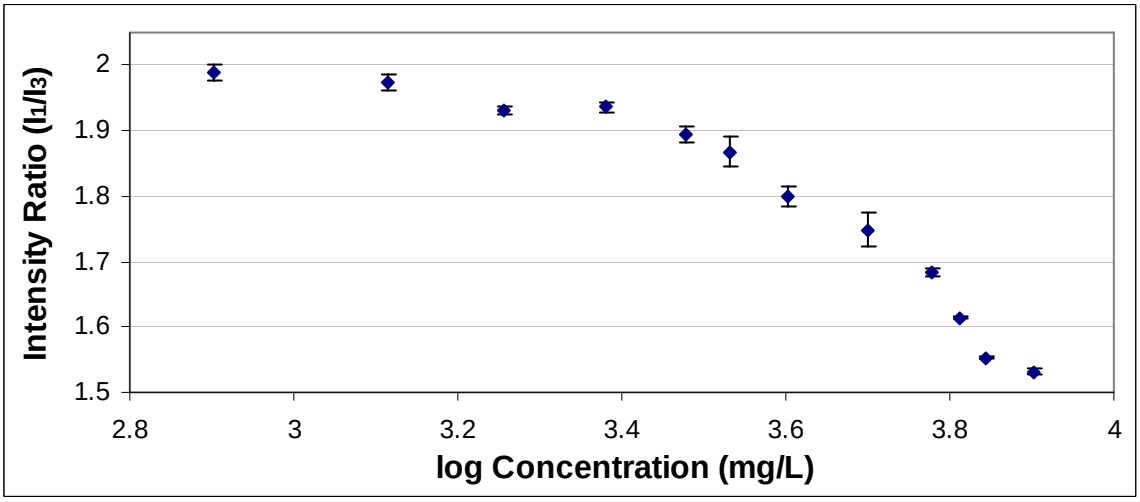

Figure 4-30 Fluorescence Intensity Ratio (I_1/I_3) vs. log [**3CUr14**]

4.4 – Discussion of Surface Tension and Pyrene Fluorescence Measurements

4.4.1 – General Comments

The error bars associated with the pyrene fluorescence graphs represent the standard deviation in the I_1/I_3 ratio from three separate measurements of the same

solution. Error bars on the surface tension graphs indicate the standard deviation in interfacial tension from 5 separate measurements of the same solution. Variation in the surface tension measurements is typically due to inadequate equilibration time or excessive drop movement. Recall that the movement of the surfactant molecule from the bulk to the surface is an equilibrium process, and by attempting to take the measurements too early an inaccurate reading will typically result. Proper equilibration time was determined for each sample by allowing the instrument to record IFT as a function of time and determining where the change in interfacial tension over a 10-second period is less than 0.05 mN/m. Outlying data points, as seen in Figures 4-3, 4-17, and 4-25, are typically due to minor errors in solution preparation. As the concentrations of surfactant and the amount of solution used to prepare each dilution for measurement are so small, any minor variation in solution preparation can cause large changes in the observed surface tension.

We note that for all these amphiphiles, the surface tension does not decrease nearly as much as it does for fatty-acid derived amphiphiles, such as SDS (typical values for the surface tension of SDS solutions at the CMC are on the order of 35 – 40 mN/m). This indicates that these dendritic amphiphiles are much less surface active than SDS. This should be true since the three-headed amphiphiles are typically less hydrophobic than single-headed amphiphiles. The increased hydrophilicity of the headgroup in the three-headed amphiphiles means that moving the amphiphile to the surface does not have as great an effect on energy minimization as is seen for single-headed amphiphiles. Therefore a decrease in surface activity is the expected result.

The CMC as determined by surface tension versus pyrene fluorescence measurement is significantly different in some cases. Differences of up to 500 mg/L can be seen between the techniques (Figures 4-21 and 4-22).

4.4.2 – Error Associated with Proper Determination of the CMC

As indicated in section 4.3, the error associated with determination of the correct concentration to use for the CMC is variable for each graph, and is mainly indeterminate human error that arises from the selection or rejection of any given data point used to generate the linear regression lines. By way of example, we consider the plots of the CMC curves for **3CUr20** using surface tension and pyrene fluorescence measurements.

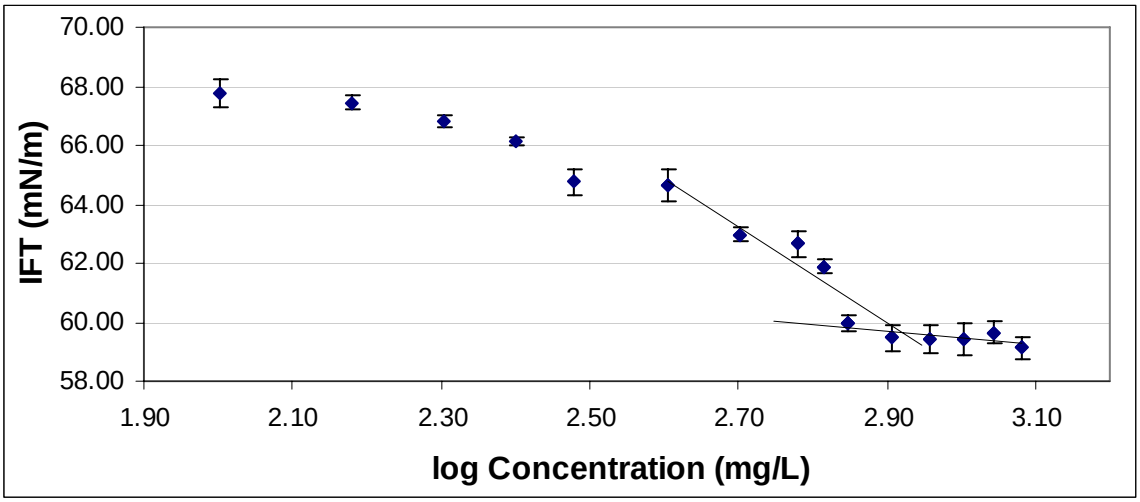

Figure 4-31 IFT vs. log [**3CUr20**]

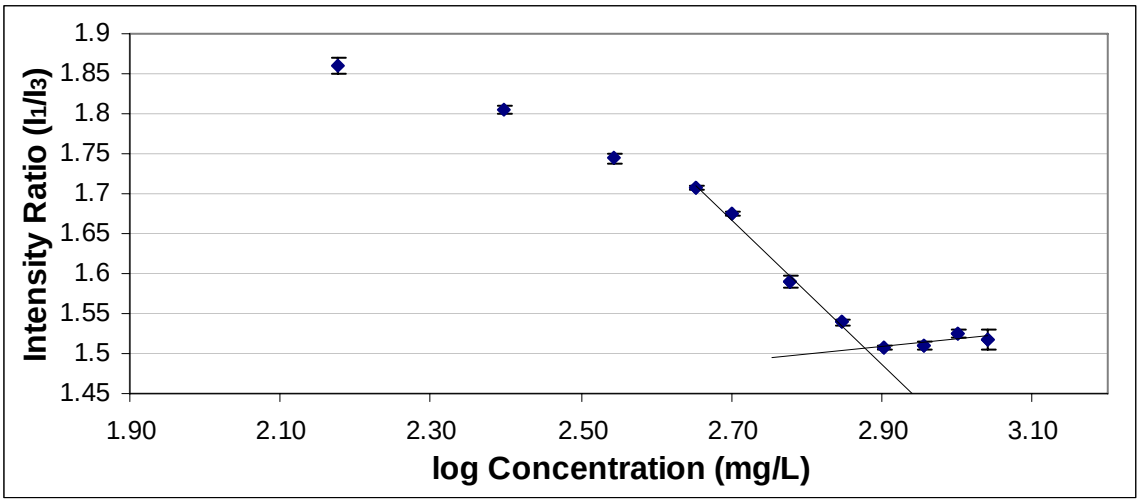

Figure 4-32 Fluorescence Intensity Ratio (I_1/I_3) vs. log [**3CUr20**]

The points used to generate the linear regression lines for the fluorescence data (four points before the break and four points after in Figure 4-32) are fairly linear in nature, indicating that the intersection of these two lines is probably a fairly accurate representation of the actual CMC (800 mg/L, 1 mM),. However, the same cannot be said for the surface tension data. There is far too much scatter in the data before the break to say with any certainty that the linear regression line from those points is accurate enough to use them to predict the CMC. The plot of the surface tension data for the **3CUr20** compound should represent the largest extent of the error in determining the CMC, since this data has the worst linear fit of all the collected samples. Therefore, if the maximal error in the CMC for **3CUr20** can be determined then the error associated with the measurements of the remaining compounds should be lower.

By examining the error associated with the generation of the trendlines, it should be possible to determine an error limit of the concentration into which the CMC should fall.

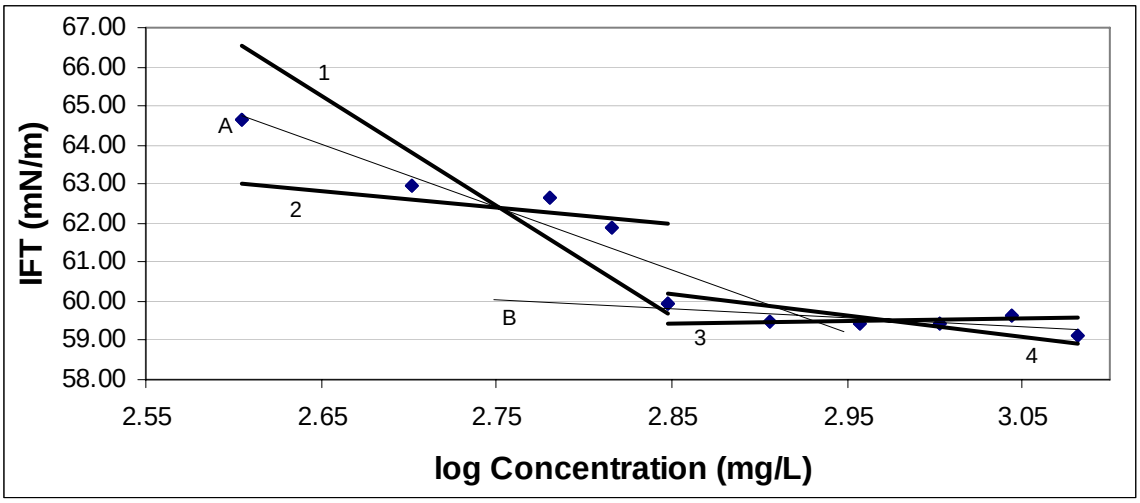

Figure 4-33 Trendlines of maximal error at 95% confidence interval for surface tension measurements of **3CUr20**

For the upper trend line (**A**), $y = (-16.15 \pm 12.07)x + (106.84 \pm 33.20)$ and for the lower trend line (**B**), $y = (-2.32 \pm 3.00)x + (66.42 \pm 8.92)$. The heavy trendlines in Figure 4-33 (labeled **1–4**) represent the 95% confidence interval for the error in the trendlines of the data, constructed as shown in Table 4-2.

Table 4-2 Data Used in Construction of Trendlines 1–4 in Figure 4-33

Trend line	Slope	y-intercept
1	-28.21 (-16.15 – 12.07)	140.04 (106.84 + 33.20)
2	-4.08 (-16.15 + 12.07)	73.64 (106.84 – 33.20)
3	0.68 (-2.32 + 3.00)	57.49 (66.42 – 8.92)
4	-5.32 (-2.32 – 3.00)	75.34 (66.42 + 8.92)

From the maximum extent of these error trendlines over the range of the data, we can construct an approximation of the error in the concentration in determining the CMC.

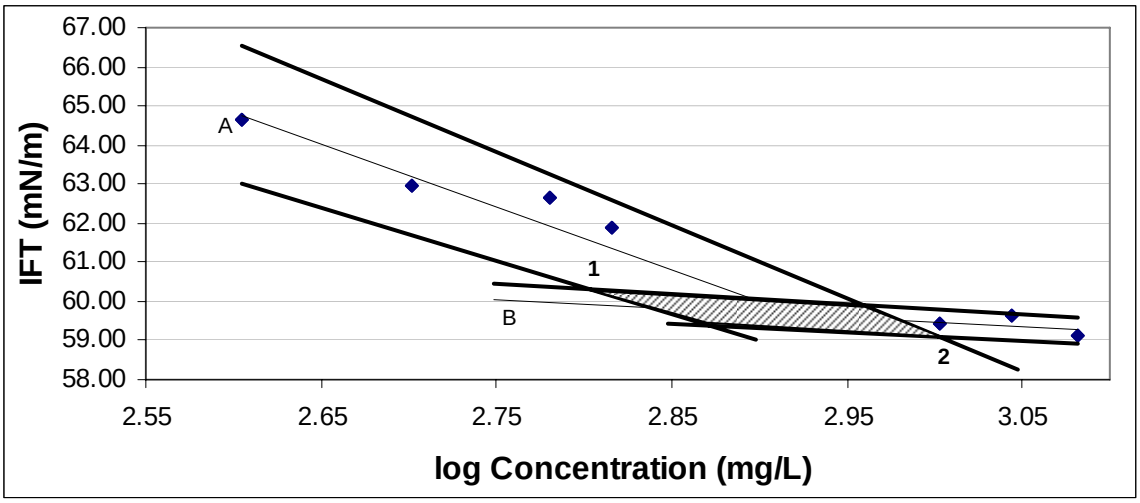

Figure 4-34 Determining error range for the concentration of the CMC for **3CUr20**

The shaded region in Figure 4-34 should represent the maximal extent of the error in determining the actual concentration of the CMC based off the linear regression lines of the data.

This is not a rigorous mathematical treatment of the error; instead this represents an attempt to derive an estimate of the possible amount of maximum error that can be expected when determining the CMC by linear regression for these compounds using surface tension measurements. The log concentration values at points 1 and 2 in Figure 4-34, which are the maximum extent of variation in x (the log concentration), are 2.8 and 3.0, respectively. This works out to actual concentrations of 600 mg/L and 1,000 mg/L, respectively. Therefore, the estimated error in concentration when trying to determine the CMC for **3CUr20** is approximately ± 200 mg/L. This error is quite large, but this represents a worst-case scenario for all the data collected by surface tension. Comparison of the surface tension ± error measurement to the pyrene fluorescence measurement of **3CUr20** shows that the CMC as determined by pyrene fluorescence (800 mg/L) falls within the limits of the error from the surface tension measurement (800 ± 200 mg/L).

4.4.3 – Effect of Impurities on the Determination of the CMC

We note in Figures 4-5 and 4-6 that the surface tension drops to a minimum and then rises again before leveling off. According to work done by Lin et al.[15] on SDS solutions, this minimum is due to impurities in the solution. Lin noted that laboratory-grade SDS shows a minimum in the graph of surface tension vs. concentration via the Wilhelmy-plate method and attributes this to the presence of lauryl alcohol. Lauryl alcohol is highly surface active—more so than SDS itself—and consequently drives the surface tension below the point at which the CMC would occur for pure SDS. When SDS begins to aggregate, the lauryl alcohol impurity becomes encapsulated inside the micellar structure, thereby allowing the surface tension to rise to its "true" value. This encapsulation of lauryl alcohol is energetically favorable because it is more hydrophobic in nature than SDS itself, which has a charged head group in comparison to the neutral alcohol moiety of lauryl alcohol.

Conductivity measurements were taken on these solutions and the results were compared to the surface tension measurements obtained initially by Wilhelmy-plate tensiometry. Because lauryl alcohol is a neutral molecule, it should theoretically have no effect on the CMC determined by conductivity measurements, which functions only for ionic species. This is exactly what is seen–the conductivity measurements agreed with the CMC values for pure SDS and match the point at which the surface tension rises and then levels off in the "contaminated" SDS/lauryl alcohol system.

Due to this physical phenomenon, surface tension measurements done via tensiometry or drop-shape analysis can also be used as a purity test. For SDS, an impurity of only 0.01% lauryl alcohol can cause a minimum in the surface tension vs. concentration graph.[1] Even though all materials passed elemental analysis, it is still

possible that during solution preparation and subsequent dilutions, an impurity was introduced.

Many of the surface tension vs. log concentration plots demonstrate much shallower breaks when compared to the pyrene fluorescence data or have a great deal of scatter prior to the break (see Figures 4-3, 4-13, 4-23, and 4-25 as notable examples). A possible explanation for this observation comes from our measurement conditions. In order to keep ionic strength from changing and to ensure complete deprotonation of the headgroup an excess of triethanolamine (TEA) was used in our solution preparation. This excess ranged from $32–46\times10^3$ molar equivalents of TEA. The difference in excess is because the concentration of TEA was kept steady at ~ 9 g/L, while the surfactant concentration changed during the creation of the dilution series.

A possible explanation is the excess TEA acted as a type of impurity and caused the variations seen in the surface tension plots. Because of the size of the headgroups, the micellar structure would already be fairly loose in nature. Additionally, the linker groups would also serve as a good hydrogen bonding sites in the interior of the micelle towards TEA (the amido carbonyl oxygen and carbamato linkers would function as hydrogen-bond acceptors, whereas the ureido linker can function as both donor and acceptor). We would not expect TEA to penetrate too deeply into the interior of the micelle due to its polar nature in comparison with the long-chain alkyl tails of the amphiphile that make up the micelle interior.

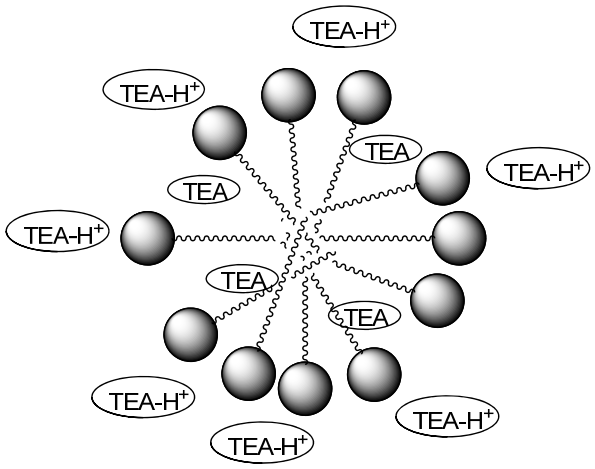

Figure 4-35 Effect of excess TEA on micellar structure; TEA is $N(CH_2CH_2OH)_3$ and TEA-H+ is $^{+}HN(CH_2CH_2OH)_3$

The main problem with this theory is the lack of this effect in Du's pyrene fluorescence measurements. Almost all of Du's data are very linear before and after the CMC, and almost none of the pyrene fluorescence curves continue to decrease after the CMC as seen most noticeably in Figure 4.13. As pyrene is much less soluble in water than TEA (0.135 mg/L, 0.667 μM vs. infinite solubility) due to its completely nonpolar structure (Figure 4-23), it would preferentially be encapsulated into the micelle when the CMC is reached, thereby preventing TEA incorporation.

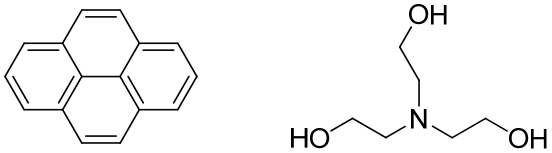

Figure 4-36 Chemical structures of pyrene (left) and TEA (right)

Since TEA could not be incorporated into the micelle during these experiments, we are hypothesizing that the micelle formed is actually much tighter in nature than that seen for the experiments run via pendent-drop where there was no pyrene present. The appearance of the bumps in the data for the surface tension measurements occurs because, as the concentration of amphiphile continues to increase, the TEA is eventually

forced out of the micelle during the natural equilibrium processes that form the micelle. The micelle then preferentially incorporates more molecules of amphiphile in place of the expelled TEA molecules as the amphiphile is more hydrophobic in nature than TEA. This pre-micellar equilibrium process of attempting to exclude excess TEA could be responsible for the scatter in the data before the CMC seen in some of the surface tension measurements.

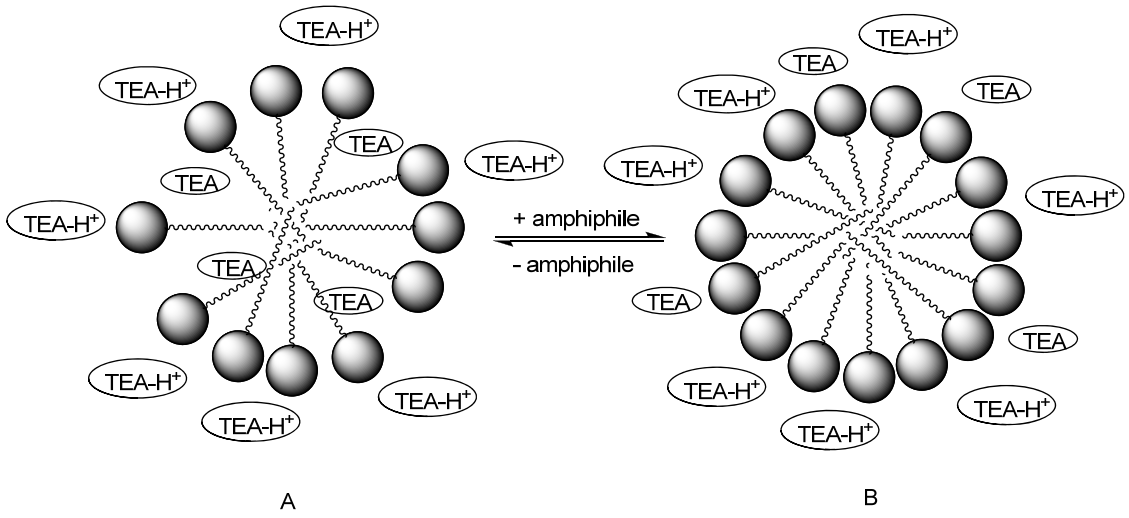

Figure 4-37 Theorized micellar structural changes incorporating TEA at low concentrations (A) and excluding TEA at high concentrations (B) of amphiphile

4.4.4 – Comparison of Single-Tailed Dendritic Amphiphiles

Figures 4-35 and 4-36 compare the log CMC vs. number of carbons for the surface tension and pyrene fluorescence measurement techniques, respectively.

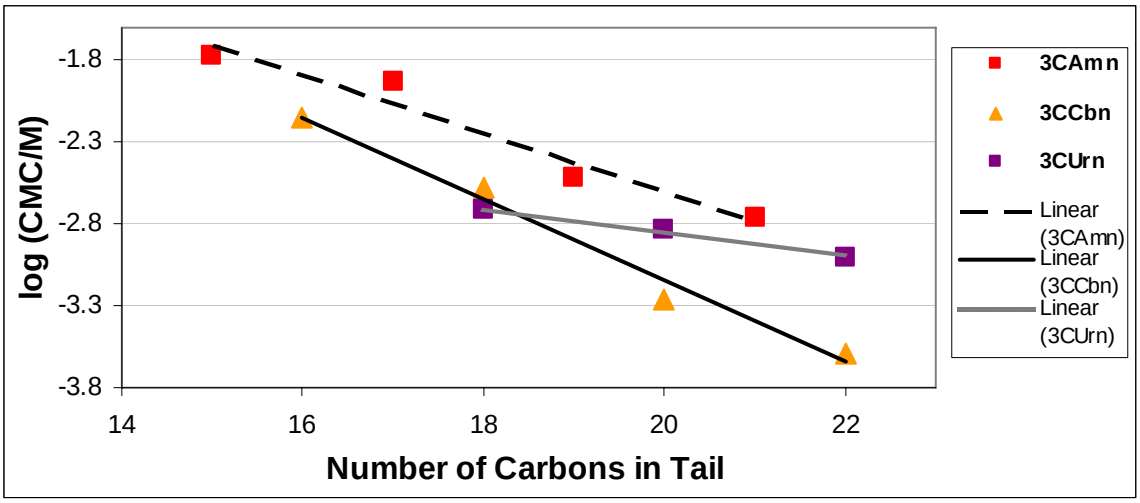

Figure 4-38 Plot of log CMC vs. number of carbons from surface tension measurements. **3CAmn**: y = -0.18 ± 0.03x + 1.0 ± 0.5; **3CCbn**: y = -0.25 (±0.02)x + 1.8 (±0.3); **3CUrn**: y = -0.071 (±0.009)x - 1.4 (±0.2). Error values are standard error.

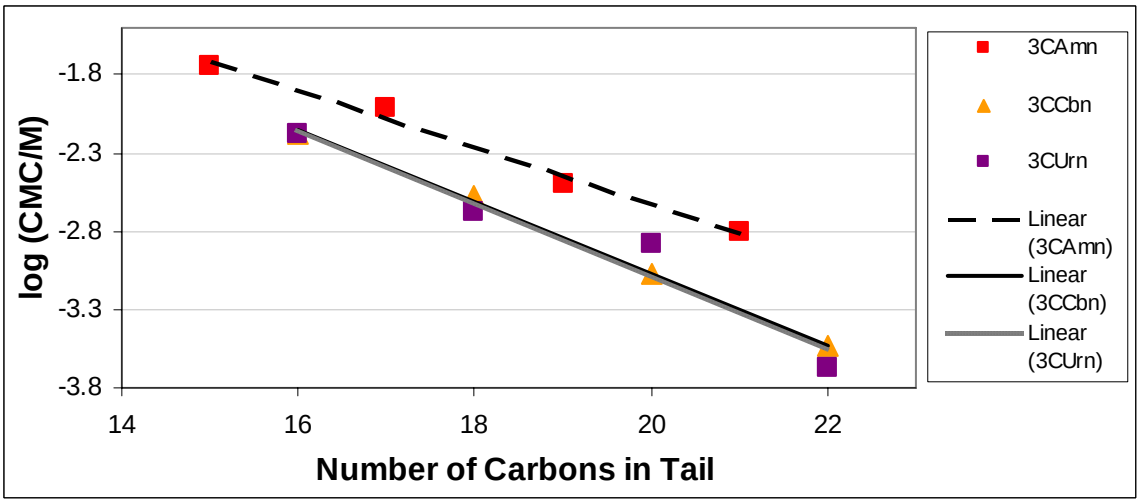

Figure 4-39 Plot of log CMC vs. number of carbons from pyrene fluorescence. **3CAmn**: y = -0.18 (±0.01)x + 1.0 (±0.3); **3CCbn**: y = -0.23 (±0.01)x + 1.5 (±0.2); **3CUrn**: y = -0.23 (±0.04)x + 1.6 (±0.8). Error values are standard error.

There is generally good agreement between the two techniques for both the **3CAmn** and the **3CCbn** series. In general, the determination of the CMC was easier from the pyrene fluorescence data because this data was typically much more linear and had sharper breaks, making the placement of the trendlines for CMC determination easier and more accurate. The **3CUrn** series, however, shows wildly differing slopes between

the two techniques. Upon first inspection, it appears as though the surface tension data shown in Figure 4-35 gives a better linear fit, and are therefore more accurate. However, recall that determination of the CMC for the **3CUr16** amphiphile is inconclusive, as the surface tension continued to decrease after the apparent break, and the pyrene fluorescence data showed that the break occurred at higher concentrations than tested for the surface tension measurements (Figures 4-27 and 4-28). Additionally, the **3CUr22** amphiphile data collected via surface tension showed a much shallower break and had less linear data both before and after the CMC than the pyrene fluorescence data. The difference in break points is substantial (100 mg/L for pyrene vs. 600 mg/L for surface tension, Figures 4-21 and 4-22), and the CMC determined from the surface tension data is suspect because of these discrepancies. Due to these differences it is more likely that the slope given by the pyrene fluorescence technique is actually the more accurate of the two sets.

Comparison of the **2CAmn** amphiphiles (data from Marcelo Actis[16]) to the **3CAmn** series in Figure 4-37 shows that the **2CAmn** series presents a steeper slope (-0.28 vs. -0.18) in addition to more negative log CMC values, indicating that the **2CAmn** series aggregates at lower concentrations. This also indicates that the addition of each methylene group has a greater effect on the CMC for the two-headed amphiphile than it does for the three. This trend agrees with expected theoretical behavior because the two-headed amphiphiles should form micelles at lower concentrations than the three-headed series because there is one less headgroup that contributes to ionic repulsion during micelle formation and the tails are not as soluble for a given chain length with only two headgroups.

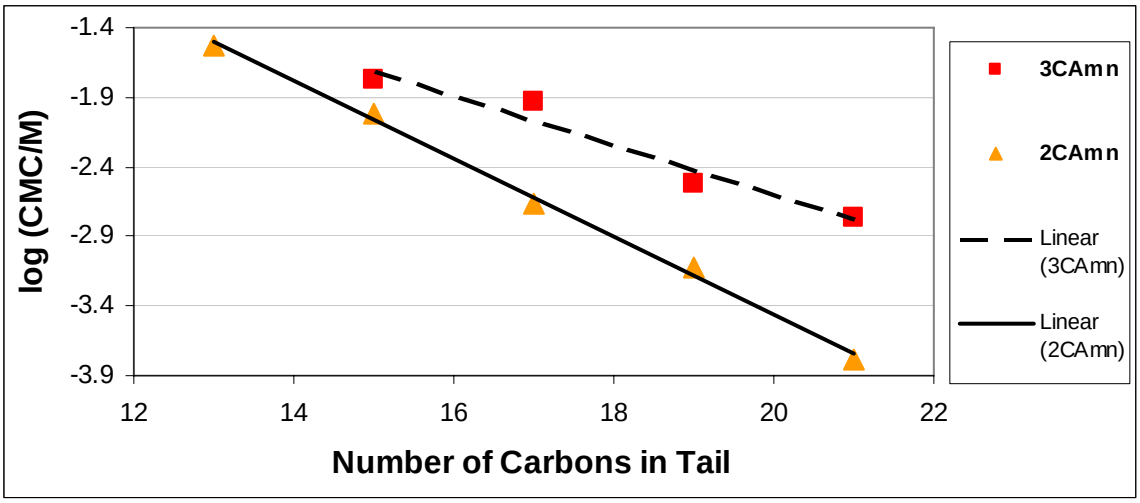

Figure 4-40 Comparison of **2CAmn** and **3CAmn** series amphiphiles log CMC vs. number of carbons. **2CAmn**: y = -0.281 (±0.008)x + 2.2 (±0.1); **3CAmn**: y = -0.18 (±0.01)x + 1.0 (±0.3)

One of the main avenues of exploration for this project was to observe the effect of making small modifications to the linker group in the series (Figure 4-28).

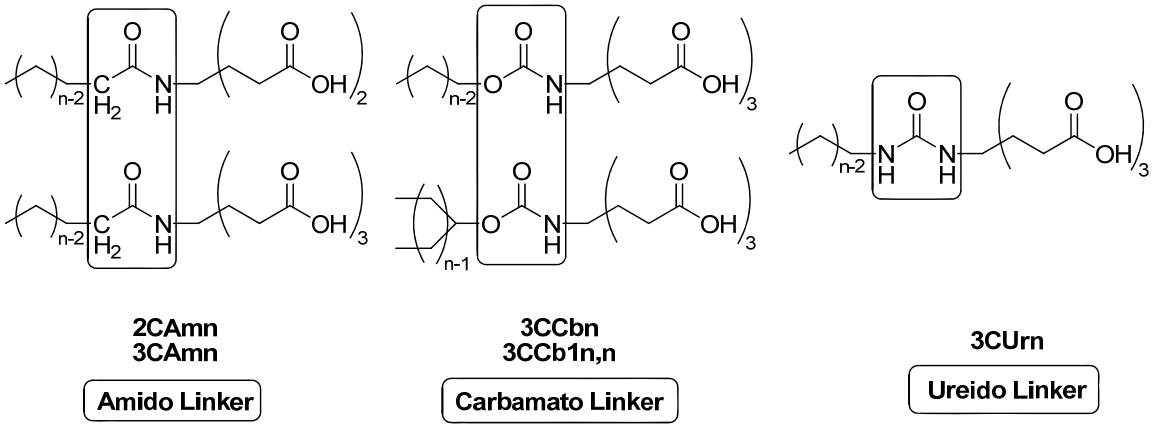

Figure 4-41 Differences in amphiphilic series linker groups

The Klevens equation[17] (eq 1) gives the relationship between log CMC and carbon chain length of an amphiphile, such that

$$\log CMC = A - Bn_c \qquad (1)$$

where A is dependent on the surfactant head group, solution temperature, and inert electrolytes, and B is an empirical constant, approximately equal to log 2 (0.301),

representing the effect of each methylene group of the tail on the CMC. A relatively large value of B indicates that the addition of each methylene group has a large effect in lowering the CMC. Shinoda[18] has indicated that the slope of the lines in plots of log CMC vs. number of carbons in the tail is due to the number and types of polar groups involved in the molecule. This can be seen to be true for these amphiphiles by comparing the **2CAmn** and **3CAmn** series, in which the slope does indeed change when the only difference is the removal of one ionizable head group (**2CAmn** slope = -0.28 vs. **3CAmn** slope = -0.18). All three three-headed amphiphiles show relatively similar slopes, indicating that the change in linker group is not having a noticeable effect on the aggregation properties. Recall that micellar aggregation is a function of the hydrophobic tails attempting to minimize their energy, while the headgroups act to resist aggregation by ionic repulsion (cf. section 1.3).

4.4.5 – Effect of Changes in Counterion

The CMC of the three-headed, single-tail amphiphiles were determined in potassium hydroxide solution (pH 10–11).[19] The comparison of these data to the surface tension/pyrene fluorescence data allows determination of the effect of changing counterion on the CMC for these dendritic amphiphiles.

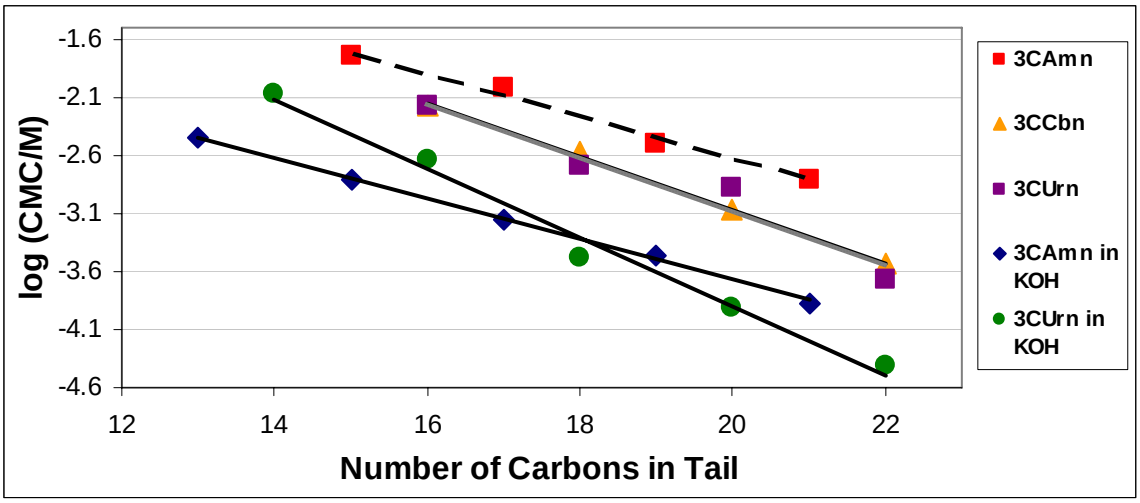

Figure 4-42 The effect of changing the counterion on CMC. Unless specified, triethanolamine (as triethanolammonium ion) was used as the counterion.

Figure 4-42 shows the effect of changing the counterion on the CMC. The CMC has decreased for both amphiphilic series measured in potassium hydroxide solution. Additionally, the **3CAm13** and **3CUr14** amphiphiles are now exhibiting a CMC, indicating that they are not as soluble in KOH solution as they are in triethanolamine solution.

Recall from section 1.3.2.3 that the counterion will decrease hydrophilic repulsion, thereby decreasing the CMC.[20] This is a screening effect, where the positively charged counterion screens the negative charges on the headgroup from each other. The CMC and the degree of binding of the counterion to the amphiphile are related such that as the degree of binding of the counterion increases, the CMC will decrease. The degree of binding of the counterion to the micelle is related to the hydrated radius, polarizability, and charge of the counterion. Counterions with larger hydrated radii show weaker degrees of binding to the micelle, so that $NH_4^+ > K^+ > Na^+ > Li^+$ for anionic amphiphiles.[21] The triethanolammonium counterion will have a larger hydrated radius than the potassium ion, and we would therefore expect the degree of binding to decrease

and the CMC to increase in the triethanolammonium salts of the amphiphiles versus the potassium salts of the amphiphiles. This is exactly what is seen in examining the data in Figure 4-42.

Counterions with increased polarizability and charge show increased degrees of binding. The charge is the same on both the triethanolammonium and the potassium counterions. However, the polarizability is not. The triethanolammonium counterion is much more polarizable than the potassium ion, and we would expect to see the CMC of the triethanolammonium salts of the amphiphiles decrease in relation to the potassium salts of the amphiphiles. The data in Figure 4-42 indicate an overall increase in the CMC of the triethanolammonium salt amphiphiles over the potassium salt amphiphiles, which tends to indicate that the hydrated radius of the triethanolammonium salt amphiphiles has a greater net effect on the CMC than the polarizability.

4.4.6 – Comparison to Natural Fatty Acids

Figure 4-40 shows the comparison of these amphiphiles to those measured by Shinoda[18] (**1 – 3**) and Bashura[7] (**4**). Compounds **1 – 4**, shown in Figure 4-27, are all derived from natural fatty acids. Compounds **2** and **3** are synthetic derivatives of malonic ester, whereas compounds **1** and **4** are the basic natural fatty acids with differing counterions.

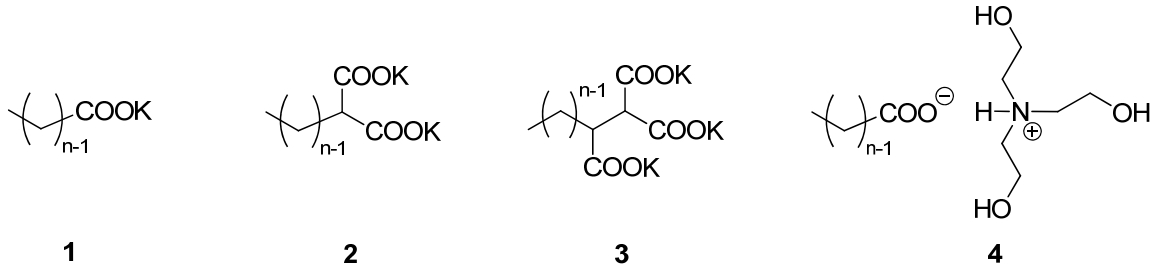

1 **2** **3** **4**

Figure 4-43 Structures shown in Figure 4-41

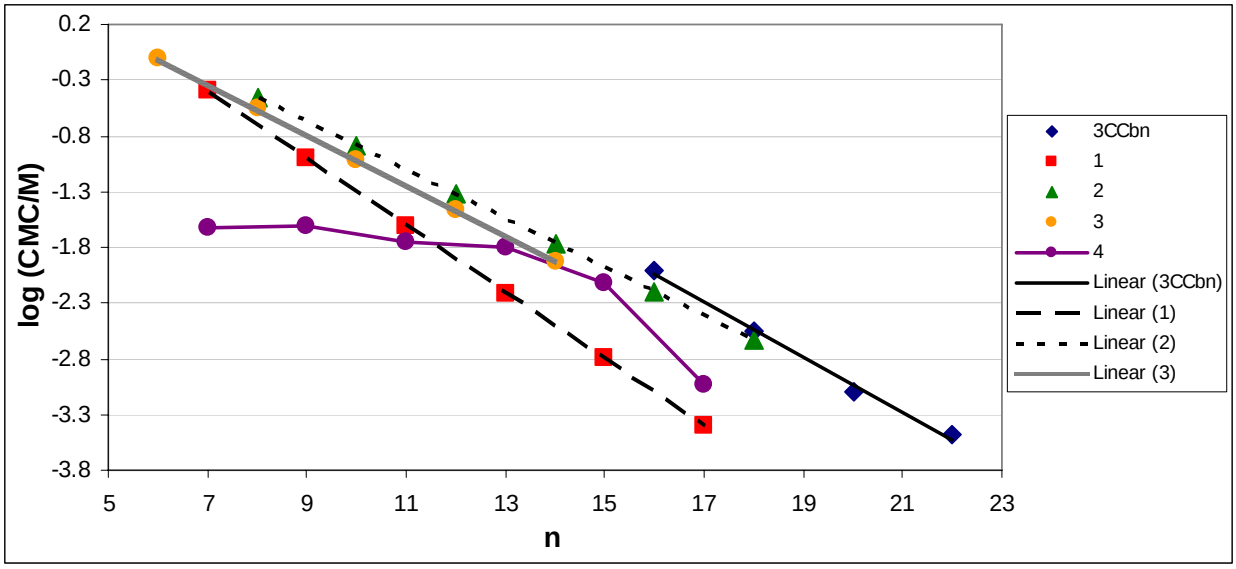

Figure 4-44 Comparison of fatty acid CMC vs. chain length to dendritic amphiphiles. Only **3CCbn** of the dendritic amphiphiles is included for clarity. The line for **4** is an eye-guide.

For all fatty acid compounds the CMC lies at a lower value compared to the same chain length dendritic amphiphile. This is the expected trend, as a compound with only one or two ionizable headgroups should form micelles sooner than the dendritic amphiphiles that have three heads. The fatty-acid derived compounds therefore form micelles at lower concentrations than the corresponding chain-length dendritic amphiphile. The CMC of amphiphile **1** decreases more rapidly than any of the others (as noted by the steeper slope). Again this is the expected trend, as an amphiphile with less headgroups will tend to form micelles sooner as chain length increases. There is no given data for fatty acid CMCs above 18 total carbons, most likely due to the CMC of these compounds being below their Krafft temperature. The rigid structure of surfactants **1–3** may make the formation of the crystal hydrate much more likely than for the dendritic amphiphiles, which have a very flexible headgroup that may have trouble crystallizing

and so lower the Krafft temperature. It is unknown whether **4(17)** is an extreme outlier or an example of some type of biphasic micellar structural change.

4.5 – CMC MEASUREMENTS OF TWO-TAILED AMPHIPHILES

The CMCs of the two-tailed amphiphiles, **3CCb1(n,n)**, were measured by surface tension experiments as previously described for the **3CAmn**, **3CCbn**, and **32CUrn** series (cf. section 4.3). Figure 4-45 shows the IFT vs. log[amphiphile] data for **3CCb1(12,12)**. The break is extremely sharp, occurring over a very narrow concentration range (~ 2.2 mg/L). There is considerable scatter in the data after the break. This is most likely due to errors in solution preparation due to the extremely small concentrations involved in making these solutions. The apparent CMC for **3CCb1(12,12)** is 12 mg/L (2×10^{-2} mM).

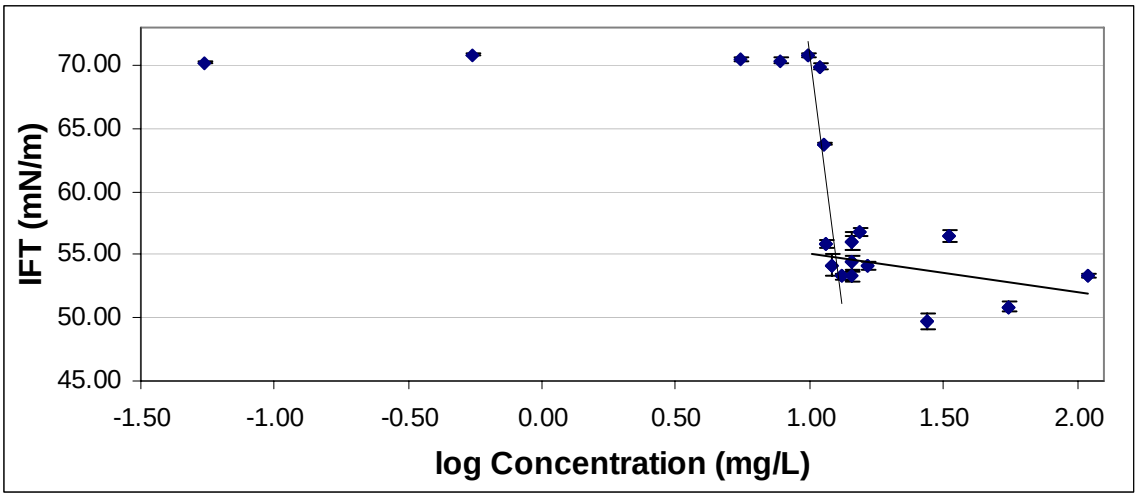

Figure 4-45 IFT vs. log [**3CCb1(12,12)**]

Figure 4-46 shows the IFT vs. log[amphiphile] data for **3CCb1(11,11)**. The decrease in the surface tension resembles the experiments of the single-tail series. The break is fairly sharp; however there is a fair amount of scatter in the data points before the CMC, and the trend line of the points after the CMC is only composed of 3 data

points. The surface tension also decreases to values not previously seen with these dendritic amphiphiles. The apparent CMC for **3CCb1(11,11)** is 500 mg/L (0.9 mM).

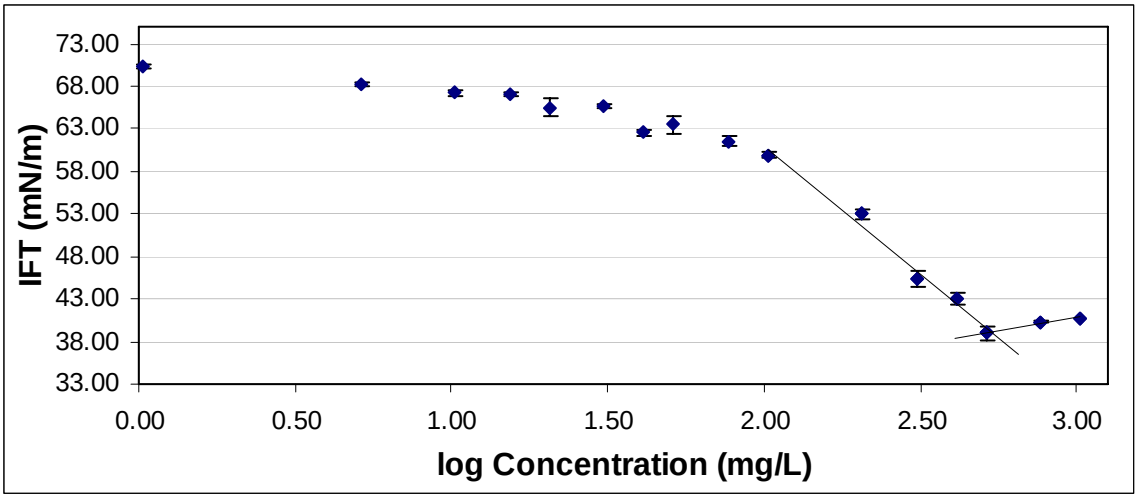

Figure 4-46 IFT vs. log [**3CCb1(11,11)**]

Figure 4-47 shows the IFT vs. log[amphiphile] data for **3CCb1(10,10)**. There is a fair amount of non-linearity in the data before the break occurs. Additionally, there are not enough data points in the linear portion after the break to make an accurate trend line. The data after the break continues to show a rather severe decrease in surface tension. The apparent CMC for **3CCb1(10,10)** is 80 mg/L (0.1 mM).

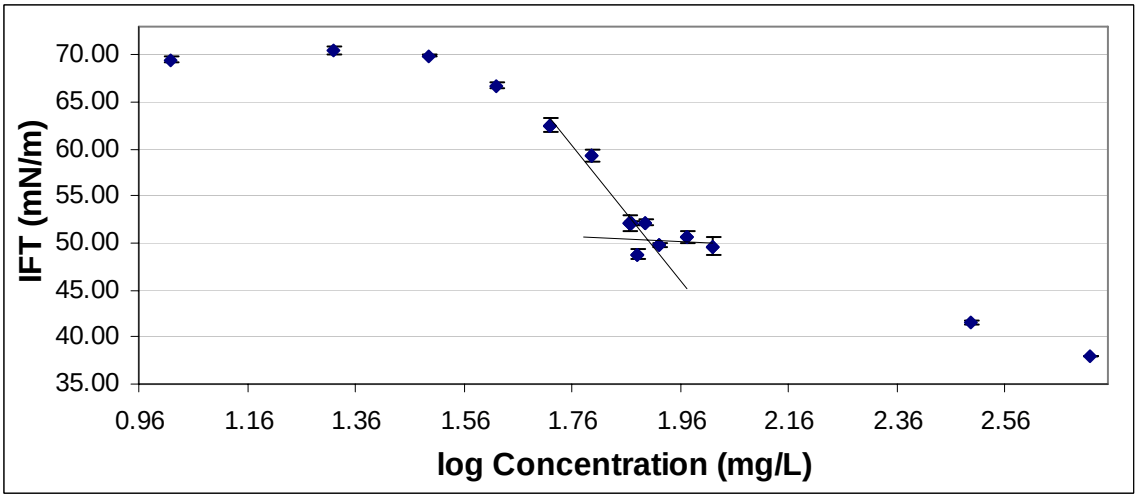

Figure 4-47 IFT vs. log [**3CCb1(10,10)**]

Figure 4-48 shows the IFT vs. log[amphiphile] data for **3CCb1(9,9)**. The data before the break are fairly linear, however, the surface tension continues to decrease after the break, making an accurate determination of the CMC difficult. The apparent CMC for **3CCb1(9,9)** is 300 mg/L (0.5 mM).

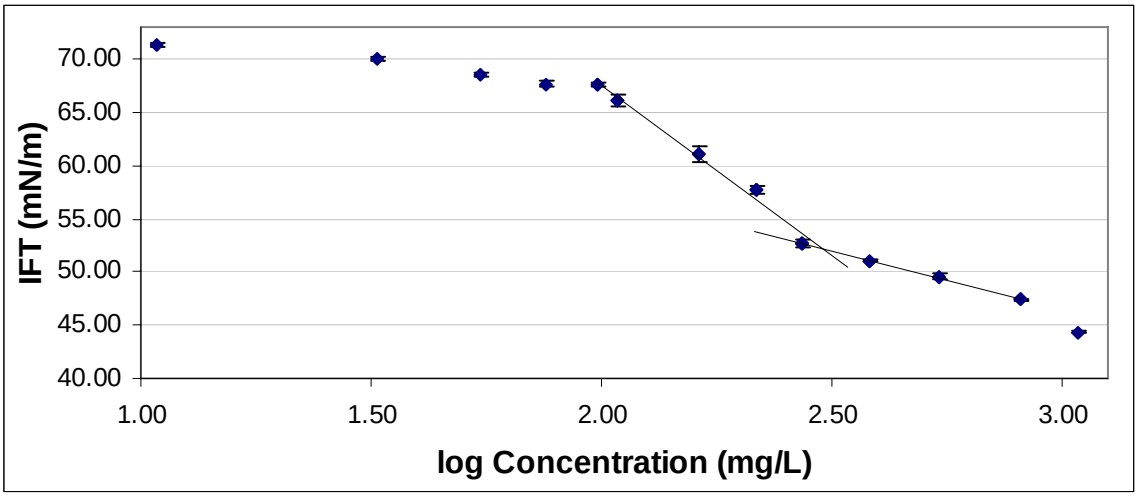

Figure 4-48 IFT vs. log [**3CCb1(9,9)**]

Figure 4-49 shows the IFT vs. log[amphiphile] data for **3CCb1(8,8)**. There is no apparent break in the surface tension measurements indicating a CMC up to 10,000 mg/L, which is the limit of our testing.

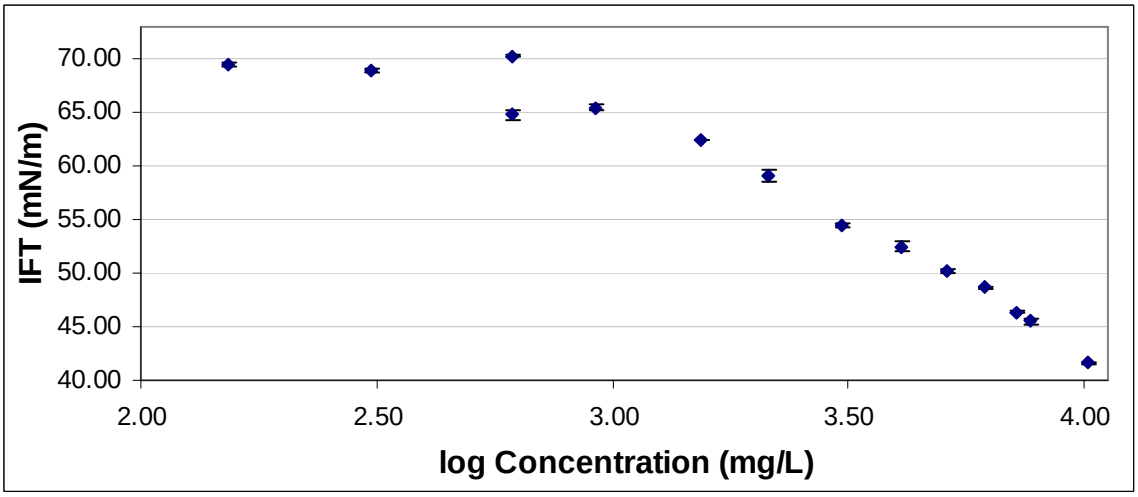

Figure 4-49 IFT vs. log [**3CCb1(8,8)**]

Figure 4-50 shows the IFT vs. log[amphiphile] data for **3CCb1(7,7)**. Even though it appears as though there is a break of some sort, the fact that the **3CCb1(8,8)** amphiphile does not show a break tends to suggest that this is not a true break, but rather a spurious data point. There is no apparent break in the surface tension measurements indicating a CMC up to 10,000 mg/L, which is the limit of our testing.

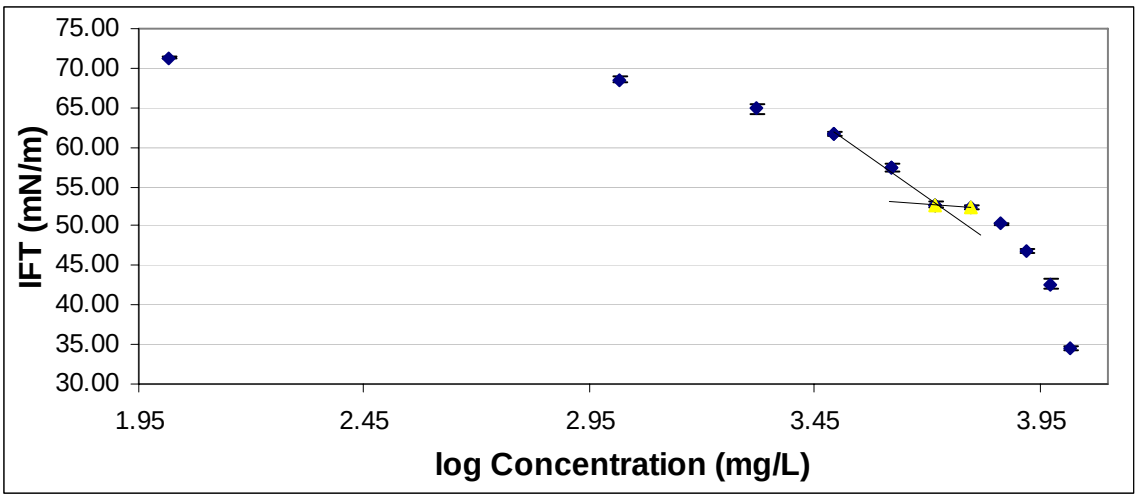

Figure 4-50 IFT vs. log [**3CCb1(7,7)**]

4.6 – Discussion of Two-Tailed Amphiphile CMC Measurements

4.6.1 – General Comments

The most noticeable difference in the surface tension data when compared to the single-tail amphiphiles is the sharpness of the break for the **3CCb1(12,12)** amphiphile. The surface tension decreases by ~ 20 mN/m over a very narrow concentration range of ~ 2 mg/L. A possible explanation for this sharp break is the concentration at which the **3CCb1(12,12)** amphiphile starts to form micelles is very small (12.5 mg/L). It is therefore possible that the instrument is not able to detect any decrease in the surface tension before the CMC occurs. Therefore the only change in the data occurs with the

onset of micelle formation. A different technique such as fluorescence or conductivity may show a more gradual decrease, depending on experimental sensitivity.

Another interesting trend is that starting with the **3CCb1(10,10)** amphiphile, the surface tension continues to decrease rather sharply after the apparent break. Additionally, there are a few cases (Figures 4-46 and 4-47) where the apparent CMC occurs at surface tension values below what was seen for the single-tail amphiphiles, indicating that these two-tailed amphiphiles may be more surface active than their single-tail counterparts.

4.6.2 – Comparison of Two-Tailed Amphiphiles to Single-Tail Amphiphiles

Figure 4-51 shows a plot of log CMC versus the total number of carbons in the tail for the **3CCb1(n,n)** amphiphiles. The surface tension data of the **3CCbn** series is shown for comparison.

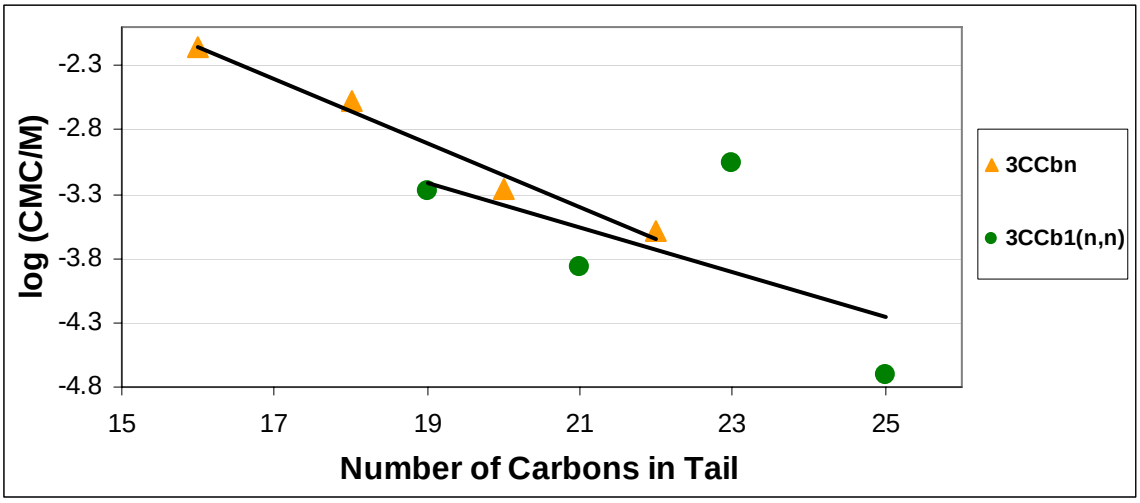

Figure 4-51 Comparison of single-tail and two-tail amphiphiles log CMC vs. number of carbons in the tail

The most noticeable feature is the scatter in the data for the **3CCb1(n,n)** series, specifically **3CCb1(11,11)**. A second measurement technique, such as pyrene fluorescence, must be used to determine the CMC for these two-tailed compounds to

determine if the scatter in the data is real or is a product of using surface tension as the measurement technique. No real information can be gleaned from this data as it is now. A Q test indicates that the **3CCb1(11,11)** datum is not able to be discarded as a spurious data point.

The **3CCb1(9,9)**, **3CCb1(10,10)**, and **3CCb1(12,12)** amphiphiles lie below the trend line of the **3CCbn** series, indicating that these two-tailed amphiphiles form micelles at concentrations below those seen for the single-tail, three-headed series. This tendency to form micelles at lower concentrations is probably due to the volume of the hydrophobic tail. It is more energetically favorable for the **3CCb1(n,n)** series to undergo micellization and remove the large volume tails from the aqueous environment than for a comparable chain length single-tailed surfactant. Additionally, because these two-tailed amphiphiles have surfactant numbers close to 1 (section 1.4.2.3, eq 2), they most likely form planar bilayers instead of spherical micelles. It is possible that it is energetically more favorable for bilayer formation than spherical micelle formation, and therefore the two-tail amphiphiles aggregate at lower concentrations.

4.7 – CONCLUSIONS AND FUTURE WORK

The CMC measurements of the dendritic amphiphiles by using pendent-drop analysis are accomplished relatively easily in comparison with the Wilhelmy plate method, and require far less material to obtain the data. However, it has been shown through a second measurement technique that surface tension may not be the best way to obtain the CMC data. The breaks in the surface tension data are typically either not very sharp, or there is a loss of linearity before and/or after the break, making accurate determination of the CMC by surface tension measurements difficult.

As expected, the three-headed amphiphiles show higher CMC values due to increased water solubility as compared to the fatty acid and malonic acid derivatives measured by Shinoda and Bashura and the two-headed amphiphiles measured by Marcelo Actis. We do not note any differences in plots of log CMC vs. carbon chain length from changes in the linker group, which suggests that this structural difference among the three homologous series of amphiphiles does not affect the micellization point. The relatively high CMCs of the dendritic amphiphiles in comparison with the fatty acid analogs suggest that these amphiphiles may not have a detergency effect when antimicrobial studies are performed, as the MICs are not likely to be higher than the CMCs. The ability to solubilize ultra long-chain hydrocarbons ($n \geq 20$) with the dendritic headgroup suggests that studies with even longer chain hydrocarbon tails can be undertaken to see if CMC can be further increased.

The CMCs for the **3CCb1(n,n)** series needs to be measured via a second method to verify the accuracy of the data. The **3CCb1(11,11)** amphiphile, specifically, seems to show too high of a CMC in relation to the **3CCb1(9,9)**, **3CCb1(10,10)**, and

3CCb1(12,12) amphiphiles. In several cases, as seen with the single-tail amphiphiles, it is too difficult to determine whether a break has occurred, which makes accurate assignment of a CMC problematic, and therefore limits any analysis of the data. The **3CCb1(12,12)** amphiphile showed a precipitous drop in the surface tension over a very narrow concentration range. Further studies of the surface tension of the **3CCb1(13,13)** and longer chain length amphiphiles are warranted to determine if this effect is specific to this particular amphiphile or is a function of all the amphiphiles of this structure over a given carbon chain length.

4.8 – EXPERIMENTAL

4.8.1 – Fluorescence Measurements.

Aliquots of pyrene in methanol were first transferred to empty vials, then the solutions of amphiphiles at given concentrations were added to vials after the methanol was evaporated. All of the mixtures were shaken gently for at least 24 h. The emission fluorescence spectra of pyrene were recorded by a spectrometer with the excitation wavelength = 334 nm. Excitation bandpasses were set at 5 nm with that of emission as 2.5 nm. The emission intensities of the first (I_1=373 nm) and third (I_3=384nm) peaks were used to determine the CMC value. Plots of the fluorescence intensity ratio (I_1/I_3) vs. log concentration of amphiphile were made. The value of the CMC was estimated by linear least-squares regression of the points immediately before and after the break, taken as the point where a distinct change in the decrease of I_1/I_3 occurred.

4.8.2 – Conductivity Measurements.

The dry dendritic amphiphile was added to the KOH solution. The dispersion was heated to 60 °C, vortex-mixed, and supplemented by KOH powder until obtaining transparent solution. For each solution pH at 30 °C was determined, before starting and after finishing of conductivity dependences measurement. The conductivity measurements were made with the digital WTW inoLab conductometer (Wissenschaftlich Technische Werkstätten, Weilheim, Germany), equipped with electrode WTW Tetra Con 325 (Wissenschaftlich Technische Werkstätten, Weilheim, Germany), at 30.0 ± 0.1 °C. The solutions were stirred during measurement. The value of CMC was estimated by linear least-squares analyses, as the intersection of two linear parts, before and after the break in the conductivity dependence.

4.8.3 – Surface Tension Measurements

A video system (mounted on a vibration isolation table) that measures the surface tension of a pendent drop from an 18-gauge stainless-steel needle (1.27 mm) was used to measure the critical micelle concentration (CMC) of the amphiphiles. To help maintain humidity levels and ensure that the drop size did not vary significantly during the measurements, the pendent drop was enclosed in a standard glass cuvette that contained 0.5 mL of aqueous triethanolamine (~9 mg/mL) dissolved in ultrapure (Type I) water. A hole (2.54 mm) was drilled in the Teflon™ lid to accommodate the needle. Calibration of the instrument entailed measuring the tip width of the needle with a micrometer and using that measurement to perform an initial calibration of the video camera's magnification. The calibration was further refined by then adjusting the magnification to produce a surface tension value of 72.8 mN/m with a ~ 15 μL drop of ultrapure (Type 1) water at an ambient air temperature of 20.0 °C. Surface tension value was adjusted if the water temperature varied from 20.0 °C by more than ± 0.1 °C.

Surface tension measurements were carried out on each solution via drop-shape analysis, with each drop being measured 20 times (one measurement was made by the software every 0.5 seconds) to produce an average surface tension. Reproducibility of the measurements was determined by performing the drop-shape analysis on five different drops of the same solution to obtain values with standard deviations of approximately ± 0.3 mN/m. Plots of surface tension vs. log [amphiphile] were made; linear least-square analyses of the points before and the points after the break were used to determine the CMC.

4.8.4 – 3CAmn Series CMC Methodology

4.8.4.1 – CMC Determination of 3CAm21

Amphiphile **3CAm21** (50.5 mg) was combined with triethanolamine (TEA, 458.7 mg) in a 50-mL volumetric flask, diluted to the mark with ultrapure (Type I) water, and sonicated for 1 h to produce a stock solution. The stock solution that was used to generate a series of dilutions for determining the CMC was prepared in the following manner. The stock solution (0.50 mL), measured with an autopipettor, was placed in a 20-mL scintillation vial and diluted with an aqueous solution (4.50 mL) comprised of TEA (9.003 mg/mL) in ultrapure (Type I) water. This produced a dilute solution with an amphiphile (**3CAm21**) concentration of 101.0 mg/L. Similar dilutions were made to produce the amphiphile concentrations shown in the table. Measurements of interfacial tension (IFT) were made immediately after dispensing the drop.

Soln Label	Amphiphile Concentration (mg/L)	Mean IFT (mN/m)	Std. Dev.
Water	0	72.58	0.05
Water/TEA	0	71.51	0.05
100	101.0	69.49	0.08
200	202.0	68.63	0.12
300	303.0	67.14	0.10
400	404.0	65.69	0.11
500	505.0	64.40	0.11
600	606.0	63.21	0.07
700	707.0	61.96	0.08
800	808.0	60.82	0.14
900	909.0	59.94	0.08
1000	1010.0	59.22	0.06
1100	1141.1	59.44	0.11
1200	1244.8	59.12	0.07
1300	1348.5	59.01	0.06
1400	1452.3	58.84	0.08
1500	1556.0	58.93	0.08

4.8.4.2 – CMC Determination of 3CAm19

Amphiphile **3CAm19** (101.2 mg) was combined with TEA (463.3 mg) in a 50 mL volumetric flask to produce a stock solution, which was made in a manner analogous to that of **3CAm21**. The stock solution was diluted with an aqueous solution comprised of TEA (9.003 mg/mL) in ultrapure (Type I) water to give the amphiphile (**3CAm19**) concentrations as shown in the table. Measurements of IFT were made after letting each drop equilibrate for 24 min.

Soln Label	Amphiphile Concentration (mg/L)	Mean IFT (mN/m)	Std. Dev.
Water	0	72.65	0.10
Water/TEA	0	71.22	0.14
200	202.4	70.15	0.12
400	404.8	67.37	0.24
600	607.2	66.54	0.17
800	809.6	65.85	0.11
900	910.8	61.57	0.36
1000	1012.0	61.22	0.16
1100	1113.2	60.46	0.29
1200	1214.4	59.30	0.13
1300	1315.6	58.77	0.33
1400	1416.8	57.63	0.14
1500	1518.0	56.66	0.09
1600	1619.2	54.58	0.24
1700	1720.4	54.92	0.21
1800	1821.6	54.94	0.48
1900	1922.8	55.53	0.12
2000	2024.0	55.46	0.13

4.8.4.3 – CMC Determination of 3CAm17

Amphiphile **3CAm17** (78.5 mg) was combined with TEA (461.5 mg) in a 50-mL volumetric flask to produce a stock solution, which was made in a manner analogous to that of **3CAm21**. The stock solution was diluted with an aqueous solution comprised of TEA (9.134 mg/mL) in ultrapure (Type I) water to give the amphiphile (**3CAm17**) concentrations as shown in the table. Measurements of IFT were made after letting each drop equilibrate for 10 min.

Soln Label	Amphiphile Concentration (mg/L)	Mean IFT (mN/m)	Std. Dev.
Water	0	72.63	0.08
Water/TEA	0.00	71.18	0.12
200	200.4	70.07	0.07
400	400.8	69.11	0.07
800	801.6	66.14	0.35
1200	1202.4	63.10	0.25
1600	1603.2	59.68	0.32
1800	1803.6	58.25	0.40
2000	2004.0	57.16	0.30
2100	2104.2	55.86	0.18
2200	2204.4	56.09	0.17
2300	2304.6	55.72	0.30
2400	2404.8	54.12	0.09
2500	2505.0	53.51	0.08
2600	2605.2	52.57	0.12
2700	2705.4	52.00	0.20
2800	2805.6	51.64	0.13
2900	2905.8	52.24	0.33
3000	3006.0	50.62	0.11
3500	3552.5	49.28	0.10
4000	4060.0	49.89	0.21
4500	4567.5	52.01	0.09
5000	5075.0	52.38	0.44
5200	5238.5	54.09	0.23
5500	5540.7	54.30	0.15
5800	5843.0	55.19	0.11
6000	6044.4	55.72	0.12
6750	6800.0	55.88	0.22

4.8.4.4 – CMC Determination of 3CAm15

Amphiphile **3CAm15** (301.8 mg) was combined with TEA (451.2 mg) in a 50-mL volumetric flask to produce a 6 g/L stock solution, which was made in a manner analogous to that of **3CAm21**. An additional stock solution of 10 g/L was made by combining amphiphile **3CAm15** (103.4 mg) with TEA (98 mg) in a 10 mL volumetric flask. The stock solution was diluted with an aqueous solution comprised of TEA (9.054 mg/mL) in ultrapure (Type I) water to give the amphiphile (**3CAm15**) concentrations as shown in the table. Measurements of IFT were made after letting each drop equilibrate for 8 min.

Soln Label	Amphiphile Concentration (mg/L)	Mean IFT (mN/m)	Std. Dev.
Water	0	72.64	0.04
Water/TEA	0	70.82	0.06
500	503.0	68.66	0.13
1000	1006.0	68.70	0.26
1500	1509.0	66.79	0.21
2000	2012.0	64.96	0.20
2500	2515.0	63.78	0.25
3000	3018.0	61.89	0.51
3500	3521.0	60.24	0.18
4000	4024.0	58.98	0.14
4300	4325.8	58.59	0.22
4600	4627.6	57.73	0.25
4900	4929.4	57.46	0.19
5500	5533.0	56.46	0.14
6000	6036.0	54.90	0.07
7000	7238.0	52.07	0.44
8000	8272.0	50.15	0.41
9000	9306.0	50.14	0.14
10000	10340.0	49.80	0.07

4.8.4.5 – Attempted CMC Determination of 3CAm13

Amphiphile **3CAm13** (269.2 mg) was combined with TEA (226.3 mg) in a 25-mL volumetric flask to produce a stock solution, which was made in a manner analogous to that of **3CAm21**. The stock solution was diluted with an aqueous solution comprised of TEA (9.045 mg/mL) in ultrapure (Type I) water to give the amphiphile (**3CAm13**) concentrations as shown in the table. Measurements of IFT were made after letting each drop equilibrate for 5 min.

Soln Label	Amphiphile Concentration (mg/L)	Mean IFT (mN/m)	Std. Dev.
Water	0	72.88	0.07
Water/TEA	0	71.52	0.14
1000	1076.8	69.89	0.09
2000	2153.6	67.90	0.23
3000	3230.4	65.88	0.30
4000	4307.2	63.99	0.29
5000	5384.0	62.03	0.28
6000	6460.8	59.76	0.38
7000	7537.6	56.85	0.33
8000	8614.4	52.76	0.57
9000	9691.2	40.48	0.13
10000	10768.0	43.00	0.04

4.8.5 – 3CCbn Series CMC Solution Preparation Methodology

4.8.5.1 – CMC Determination of 3CCb22

Amphiphile **3CCb22** (50.1 mg) was combined with triethanolamine (TEA, 456.9 mg) in a 50-mL volumetric flask, diluted to the mark with ultrapure (Type I) water, and sonicated for 1 h to produce a stock solution. Dilutions for determining the CMC were prepared from the stock solution in the following manner. The stock solution (0.05 mL), measured with an autopipettor, was placed in a 20-mL scintillation vial and diluted with an aqueous solution (9.95 mL) comprised of TEA (9.024 mg/mL) in ultrapure (Type I) water. This produced a dilute solution with an amphiphile (**3CCb22**) concentration of 5.0 mg/L. Similar dilutions were made to produce the amphiphile concentrations shown in the table. Measurements of interfacial tension (IFT) were made immediately after dispensing the drop.

Soln Label	Amphiphile Concentration (mg/L)	Mean IFT (mN/m)	Std. Dev.
Water	0	72.74	0.05
Water/TEA	0	72.12	0.09
5	5.0	68.89	0.31
15	15.0	67.85	0.15
25	25.1	66.74	0.34
37	37.1	65.86	0.39
50	50.1	64.12	1.06
75	75.2	62.37	0.94
85	85.2	61.03	0.46
100	100.2	59.06	0.99
115	115.2	57.56	0.45
125	125.3	56.15	0.70
150	150.3	53.42	0.55
175	175.4	52.69	0.35
200	200.4	54.17	0.04
300	300.6	54.82	0.06
400	400.8	54.51	0.11
500	501.0	54.70	0.18

4.8.5.2 – CMC Determination of 3CCb20

Amphiphile **3CCb20** (50.2 mg) was combined with TEA (455.1 mg) in a 50-mL volumetric flask to produce a stock solution, which was made in a manner analogous to that of **3CCb22**. The stock solution was diluted with an aqueous solution comprised of TEA (9.011 mg/mL) in ultrapure (Type I) water to give the amphiphile (**3CCb20**) concentrations as shown in the table. Measurements of IFT were made after letting each drop equilibrate for 23.5 min.

Soln Label	Amphiphile Concentration (mg/L)	Mean IFT (mN/m)	Std. Dev.
Water	0	72.95	0.06
Water/TEA	0	71.43	0.10
25	25.1	68.88	0.34
50	50.2	68.86	0.97
100	100.4	68.67	0.09
150	150.6	67.09	0.11
200	200.8	65.52	0.20
250	251.0	63.52	0.06
300	301.2	59.65	0.19
400	401.6	58.98	0.13
500	502.0	57.28	0.26
600	602.4	56.22	0.11
700	702.8	55.25	0.17
800	803.2	53.66	0.24
900	903.6	53.23	0.35
1000	1004.0	51.78	0.20

4.8.5.3 – CMC Determination of 3CCb18

Amphiphile **3CCb18** (100.4 mg) was combined with TEA (226.7 mg) in a 25-mL volumetric flask to produce a stock solution, which was made in a manner analogous to that of **3CCb22**. The stock solution was diluted with an aqueous solution comprised of TEA (8.999 mg/mL) in ultrapure (Type I) water to give the amphiphile (**3CCb18**) concentrations as shown in the table. Measurements of IFT were made after letting each drop equilibrate for 12 min.

Soln Label	Amphiphile Concentration (mg/L)	Mean IFT (mN/m)	Std. Dev.
Water	0	72.75	0.05
Water/TEA	0.00	71.23	0.11
100	100.4	69.75	0.15
500	502.0	61.97	0.37
1000	1004.0	55.48	0.13
1500	1506.0	50.22	0.14
2000	2008.0	49.39	0.23
300	301.2	66.37	0.11
700	702.8	60.26	0.24
900	903.6	56.66	0.24
1100	1104.4	54.16	0.14
1300	1305.2	51.47	0.17
1700	1706.8	49.63	0.15
1900	1907.6	49.04	0.08

4.8.5.4 – CMC Determination of 3CCb16

Amphiphile **3CCb16** (101.5 mg) was combined with TEA (450.6 mg) in a 50-mL volumetric flask to produce a 2 g/L stock solution, which was made in a manner analogous to that of **3CCb22**. An additional stock solution of 6 g/L was made by combining amphiphile **3CCb16** (149.9 mg) with TEA (232.8 mg) in a 25 mL volumetric flask. The stock solution was diluted with an aqueous solution comprised of TEA (8.996 mg/mL) in ultrapure (Type I) water to give the amphiphile (**3CCb16**) concentrations as shown in the table. Measurements of IFT were made after letting each drop equilibrate for 5 min.

Soln Label	Amphiphile Concentration (mg/L)	Mean IFT (mN/m)	Std. Dev.
Water	0	72.84	0.06
Water/TEA	0	71.26	0.24
100	101.5	70.78	0.14
200	203.0	70.49	0.20
400	406.0	69.50	0.20
600	609.0	67.89	0.40
800	812.0	66.47	0.08
1000	1015.0	65.25	0.23
1200	1218.0	63.68	0.13
1400	1421.0	61.25	0.09
1600	1624.0	60.50	0.17
1800	1827.0	58.70	0.28
2000	2030.0	55.38	0.58
2200	2198.5	57.23	0.32
2400	2398.4	55.74	0.26
2600	2598.3	54.55	0.28
2800	2798.1	53.72	0.15
3000	2998.0	53.00	0.16
3500	3497.7	50.12	0.15
4000	3997.3	49.77	0.30
4500	4497.0	50.17	0.10
5000	4996.7	51.20	0.11
6000	5996.0	51.73	0.13
8000	7994.7	52.09	0.18

4.8.5.5 – Attempted CMC Determination of 3CCb14

Amphiphile **3CCb14** (250.1 mg) was combined with TEA (232.3 mg) in a 25-mL volumetric flask to produce a stock solution, which was made in a manner analogous to that of **3CCb22**. The stock solution was diluted with an aqueous solution comprised of TEA (8.999 mg/mL) in ultrapure (Type I) water to give the amphiphile (**3CCb22**) concentrations as shown in the table. Measurements of IFT were made after letting each drop equilibrate for 5 min.

Soln Label	Amphiphile Concentration (mg/L)	Mean IFT (mN/m)	Std. Dev.
Water	0	72.88	0.07
Water/TEA	0	71.52	0.14
1000	1076.8	69.89	0.09
2000	2153.6	67.90	0.23
3000	3230.4	65.88	0.30
4000	4307.2	63.99	0.29
5000	5384.0	62.03	0.28
6000	6460.8	59.76	0.38
7000	7537.6	56.85	0.33
8000	8614.4	52.76	0.57
9000	9691.2	40.48	0.13
10000	10768.0	43.00	0.04

4.8.6 – 3CUrn Series CMC Solution Preparation Methodology

4.8.6.1 – CMC Determination of 3CUr22

Amphiphile **3CUr22** (50.4 mg) was combined with triethanolamine (TEA, 452.2 mg) in a 50-mL volumetric flask, diluted to the mark with ultrapure (Type I) water, and sonicated for 1 h to produce a stock solution. Dilutions for determining the CMC were prepared from the stock solution in the following manner. The stock solution (0.25 mL), measured with an autopipettor, was placed in a 20-mL scintillation vial and diluted with an aqueous solution (4.75 mL) comprised of TEA (9.076 mg/mL) in ultrapure (Type I) water. This produced a dilute solution with an amphiphile (**3CUr22**) concentration of 50.4 mg/L. Similar dilutions were made to produce the amphiphile concentrations shown in the table. Measurements of interfacial tension (IFT) were made immediately after dispensing the drop.

Soln Label	Amphiphile Concentration (mg/L)	Mean IFT (mN/m)	Std. Dev.
Water	0	73.00	0.11
Water/TEA	0	71.48	0.14
50	50.4	70.27	0.10
100	100.8	68.83	0.24
150	151.2	67.16	0.28
200	201.6	65.89	0.17
250	252	65.70	0.14
300	302.4	64.90	0.17
350	352.8	63.77	0.16
400	403.2	62.40	0.31
450	453.6	62.38	0.36
500	504	61.45	0.37
550	554.4	60.19	0.31
600	604.8	59.85	0.24
700	705.6	59.79	0.44
800	806.4	59.11	0.20
900	907.2	58.98	0.23
1000	1008	59.16	0.38

4.8.6.2 – CMC Determination of 3CUr20

Amphiphile **3CUr20** (75.5 mg) was combined with TEA (456.2 mg) in a 50-mL volumetric flask to produce a stock solution, which was made in a manner analogous to that of **3CUr22**. The stock solution was diluted with an aqueous solution comprised of TEA (9.016 mg/mL) in ultrapure (Type I) water to give the amphiphile (**3CUr20**) concentrations as shown in the table. Measurements of IFT were made immediately after dispensing the drop.

Soln Label	Amphiphile Concentration (mg/L)	Mean IFT (mN/m)	Std. Dev.
Water	0	72.76	0.20
Water/TEA	0	71.39	0.15
100	100.7	67.76	0.46
150	151.0	67.45	0.26
200	201.3	66.84	0.20
250	251.7	66.15	0.14
300	302.0	64.75	0.43
400	402.7	64.64	0.53
500	503.3	62.98	0.23
600	604.0	62.66	0.42
650	654.3	61.87	0.23
700	704.7	59.96	0.25
800	805.3	59.48	0.45
900	906.0	59.43	0.48
1000	1006.7	59.42	0.53
1100	1107.3	59.64	0.38
1200	1208.0	59.12	0.37

4.8.6.3 – CMC Determination of 3CUr18

Amphiphile **3CUr18** (78.5 mg) was combined with TEA (461.5 mg) in a 50-mL volumetric flask to produce a stock solution, which was made in a manner analogous to that of **3CCb22**. The stock solution was diluted with an aqueous solution comprised of TEA (9.134 mg/mL) in ultrapure (Type I) water to give the amphiphile (**3CUr18**) concentrations as shown in the table. Measurements of IFT were made after letting each drop equilibrate for 20 min.

Soln Label	Amphiphile Concentration (mg/L)	Mean IFT (mN/m)	Std. Dev.
Water	0	72.79	0.13
Water/TEA	0.00	71.00	0.14
100	104.7	67.44	0.35
200	209.3	64.20	0.55
300	314.0	60.18	0.76
400	418.7	55.71	0.57
500	523.3	57.91	0.98
600	628.0	55.13	1.02
700	732.7	53.51	0.62
800	837.3	53.10	0.48
900	942.0	51.97	0.26
1000	1046.7	50.30	0.56
1100	1151.3	50.76	0.55
1200	1256.0	50.18	0.62
1300	1360.7	50.90	0.21
1400	1465.3	50.47	0.66
1500	1570.0	49.73	0.44

4.8.6.4 – CMC Determination of 3CUr16

Amphiphile **3CUr16** (100.6 mg) was combined with TEA (453.5 mg) in a 50-mL volumetric flask to produce a 2 g/L stock solution, which was made in a manner analogous to that of **3CUr22**. An additional stock solution of 2.5 g/L was made by combining amphiphile **3CUr16** (25.2 mg) with TEA (195.7 mg) in a 10 mL volumetric flask. The stock solutions were diluted with an aqueous solution comprised of TEA (9.134 mg/mL) in ultrapure (Type I) water to give the amphiphile (**3CCb16**) concentrations as shown in the table. Measurements of IFT were made after letting each drop equilibrate for 12 min.

Soln Label	Amphiphile Concentration (mg/L)	Mean IFT (mN/m)	Std. Dev.
Water	0	72.75	0.19
Water/TEA	0	69.55	0.30
200	201.2	69.58	0.11
400	402.4	67.55	0.18
600	603.6	65.14	0.26
800	804.8	62.22	0.17
1000	1006.0	59.78	0.64
1200	1207.2	57.00	0.40
1400	1408.4	56.46	0.39
1500	1509.0	55.23	0.41
1600	1609.6	54.62	0.37
1700	1710.2	53.84	0.24
1750	1760.5	53.46	0.36
1800	1810.8	53.38	0.21
1850	1861.1	53.48	0.38
1900	1911.4	53.56	0.67
2000	2016.0	53.63	0.11
2100	2116.8	52.66	0.14
2200	2217.6	52.28	0.10
2300	2318.4	51.64	0.07
2500	2520.0	51.05	0.06

4.8.6.5 – Attempted CMC Determination of 3CUr14

Amphiphile **3CUr14** (175.2 mg) was combined with TEA (453.4 mg) in a 50-mL volumetric flask to produce a stock solution, which was made in a manner analogous to that of **3CUr22**. An additional stock solution of 5 g/L was made by combining amphiphile **3CUr16** (25.0 mg) with TEA in ultrapure (Type I) water (5 mL of 9.089 mg/mL solution, measured with an autopipettor). The stock solution was diluted with an aqueous solution comprised of TEA (9.089 mg/mL) in ultrapure (Type I) water to give the amphiphile (**3CUr22**) concentrations as shown in the table. Measurements of IFT were made after letting each drop equilibrate for 8 min.

Soln Label	Amphiphile Concentration (mg/L)	Mean IFT (mN/m)	Std. Dev.
Water	0	72.81	0.21
Water/TEA	0	71.24	0.13
300	300.3	69.99	0.08
700	700.8	68.07	0.18
1000	1001.1	66.92	0.20
1300	1301.5	65.31	0.06
1600	1601.8	63.92	0.27
1900	1902.2	62.04	0.29
2000	2002.3	60.74	0.19
2100	2102.4	60.07	0.36
2200	2202.5	59.85	0.34
2300	2302.6	59.57	0.36
2400	2402.7	58.85	0.39
2500	2502.9	58.53	0.26
2600	2603.0	58.60	0.29
2700	2703.1	57.80	0.08
2800	2803.2	57.75	0.43
2900	2903.3	57.04	0.32
3000	3003.4	57.08	0.39
3100	3103.5	56.99	0.39
3500	3504.0	54.71	0.36
5000	5000.0	48.68	0.10

4.8.7 – 3CCb1(n,n) Series CMC Solution Preparation Methodology

4.8.7.1 – CMC Determination of 3CCb1(12,12).

Amphiphile **3CCb1(12,12)** (27.5 mg) was combined with triethanolamine (TEA, 240.5 mg) in a 25-mL volumetric flask, diluted to the mark with ultrapure (Type I) water, and sonicated for 1 h to produce a stock solution. This stock solution was used to prepare a second stock solution (110 mg/L concentration) by diluting 1 mL of the original stock into 9 mL TEA (9.111 mg/mL) in ultrapure (Type I) water. Dilutions for determining the CMC were prepared from this second stock solution in the following manner. The second stock solution (0.10 mL), measured with an autopipettor, was placed in a 20-mL scintillation vial and diluted with an aqueous solution (1.90 mL) comprised of TEA (9.111 mg/mL) in ultrapure (Type I) water. This produced a dilute solution with an amphiphile (**3CCb1(12,12)**) concentration of 5.50 mg/L. Similar dilutions were made to produce the amphiphile concentrations shown in the table. Measurements of IFT were made after letting each drop equilibrate for 20 min.

Soln Label	Amphiphile Concentration (mg/L)	Mean IFT (mN/m)	Std. Dev.
Water	0	72.67	0.06
Water/TEA	0	70.41	0.18
0.05	0.06	70.24	0.15
0.50	0.55	70.85	0.08
5.00	5.50	70.50	0.18
7.00	7.70	70.39	0.21
9.00	9.90	70.77	0.15
10.00	11.00	69.87	0.23
10.25	11.28	63.75	0.10
10.50	11.55	55.89	0.29
11.00	12.10	54.20	0.93
12.00	13.20	53.31	0.22
13.00	14.30	56.08	0.74
14.00	15.40	56.80	0.28
15.00	16.50	54.17	0.31
25.00	27.50	49.72	0.57
30.00	33.00	56.49	0.42
50.00	55.00	50.86	0.37
100.00	110.00	53.36	0.15
13.00	14.30	53.30	0.40
13.00	14.30	54.38	0.57
13.00	14.30	55.94	0.49

4.8.7.2 – CMC Determination of 3CCb1(11,11).

Amphiphile **3CCb1(11,11)** (25.7 mg) was combined with TEA (227.5 mg) in a 25-mL volumetric flask to produce a stock solution, which was made in a manner analogous to that of **3CCb1(12,12)**. The stock solution was diluted with an aqueous solution comprised of TEA (9.152 mg/mL) in ultrapure (Type I) water to give the amphiphile (**3CCb1(11,11)**) concentrations as shown in the table. Measurements of IFT were made after letting each drop equilibrate for 30 min.

Soln Label	Amphiphile Concentration (mg/L)	Mean IFT (mN/m)	Std. Dev.
Water	0	72.72	0.07
Water/TEA	0	71.04	0.07
1	1.0	70.38	0.30
5	5.1	68.21	0.15
10	10.3	67.27	0.33
15	15.4	67.15	0.26
20	20.6	65.54	1.12
30	30.8	65.59	0.24
40	41.1	62.55	0.37
50	51.4	63.49	1.09
75	77.1	61.55	0.51
100	102.8	59.88	0.31
200	205.6	52.97	0.60
300	308.4	45.38	0.87
500	514.0	38.96	0.89
1000	1028.0	40.79	0.32
400	411.2	42.93	0.69
750	771.0	40.32	0.15

4.8.7.3 – CMC Determination of 3CCb1(10,10).

Amphiphile **3CCb1(10,10)** (52.3 mg) was combined with TEA (232.2 mg) in a 25-mL volumetric flask to produce a stock solution, which was made in a manner analogous to that of **3CCb1(12,12)**. The stock solution was diluted with an aqueous solution comprised of TEA (9.028 mg/mL) in ultrapure (Type I) water to give the amphiphile (**3CCb1(10,10)**) concentrations as shown in the table. Measurements of IFT were made after letting each drop equilibrate for 20 min.

Soln Label	Amphiphile Concentration (mg/L)	Mean IFT (mN/m)	Std. Dev.
Water	0	72.72	0.07
Water/TEA	0.00	71.46	0.15
10	10.5	69.52	0.29
20	20.9	70.48	0.43
30	31.4	69.88	0.10
40	41.8	66.73	0.29
50	52.3	62.51	0.71
60	62.8	59.36	0.63
70	73.2	52.11	0.88
71	74.3	52.05	0.23
73	75.8	48.78	0.51
75	78.5	52.17	0.32
80	83.7	49.85	0.19
90	94.1	50.58	0.64
100	104.6	49.64	0.92
300	313.8	41.59	0.18
500	523.0	37.97	0.04

4.8.7.4 – CMC Determination of 3CCb1(9,9).

Amphiphile **3CCb1(9,9)** (54.4 mg) was combined with TEA (239.7 mg) in a 25-mL volumetric flask to produce a stock solution, which was made in a manner analogous to that of **3CCb1(12,12)**. The stock solutions were diluted with an aqueous solution comprised of TEA (9.039 mg/mL) in ultrapure (Type I) water to give the amphiphile (**3CCb1(9,9)**) concentrations as shown in the table. Measurements of IFT were made after letting each drop equilibrate for 20 min.

Soln Label	Amphiphile Concentration (mg/L)	Mean IFT (mN/m)	Std. Dev.
Water	0	72.84	0.04
Water/TEA	0	70.72	0.16
10	10.9	71.29	0.14
30	32.6	70.02	0.13
50	54.4	68.54	0.23
70	76.2	67.69	0.36
90	97.9	67.60	0.16
100	108.8	66.04	0.58
150	163.2	61.13	0.76
200	217.6	57.72	0.40
250	272.0	52.63	0.39
350	380.8	51.07	0.15
500	544.0	49.58	0.30
750	816.0	47.40	0.09
1000	1088.0	44.33	0.08

4.8.7.5 – CMC Determination of 3CCb1(8,8).

Amphiphile **3CCb1(8,8)** (76.6 mg) was combined with TEA (102.2 mg) in a 10-mL volumetric flask to produce a stock solution, which was made in a manner analogous to that of **3CCb1(12,12)**. An additional stock solution of ~10 g/L was made by combining amphiphile **3CCb1(8,8)** (10.2 mg) with TEA in ultrapure (Type I) water (1 mL of 9.090 mg/mL solution, measured with an autopipettor). The initial stock solution was diluted with an aqueous solution comprised of TEA (9.090 mg/mL) in ultrapure (Type I) water to give the amphiphile (**3CCb1(8,8)**) concentrations as shown in the table. Measurements of IFT were made after letting each drop equilibrate for 20 min.

Soln Label	Amphiphile Concentration (mg/L)	Mean IFT (mN/m)	Std. Dev.
Water	0	72.80	0.04
Water/TEA	0	70.72	0.16
150	153.2	69.49	0.22
300	306.4	68.94	0.23
600	612.8	64.81	0.48
900	919.2	65.41	0.28
1500	1532.0	62.44	0.09
2100	2144.8	59.11	0.55
3000	3064.0	54.46	0.26
4000	4085.3	52.50	0.40
5000	5106.7	50.25	0.18
6000	6128.0	48.68	0.10
7000	7149.3	46.37	0.14
7500	7660.0	45.49	0.29
10000	10200.0	41.59	0.11
600	612.8	70.31	0.09

4.8.7.6 – CMC Determination of 3CCb1(7,7).

Amphiphile **3CCb1(7,7)** (104.0 mg) was combined with TEA (98.9 mg) in a 10-mL volumetric flask to produce a stock solution, which was made in a manner analogous to that of **3CCb1(12,12)**. The stock solution was diluted with an aqueous solution comprised of TEA (9.090 mg/mL) in ultrapure (Type I) water to give the amphiphile (**3CCb1(7,7)**) concentrations as shown in the table. Measurements of IFT were made after letting each drop equilibrate for 15 min.

Soln Label	Amphiphile Concentration (mg/L)	Mean IFT (mN/m)	Std. Dev.
Water	0	72.77	0.06
Water/TEA	0	70.66	0.08
100	104.0	71.32	0.20
1000	1040.0	68.48	0.37
2000	2080.0	64.84	0.55
3000	3120.0	61.66	0.18
4000	4160.0	57.41	0.47
5000	5200.0	52.69	0.35
6000	6240.0	52.40	0.28
7000	7280.0	50.27	0.19
8000	8320.0	46.84	0.18
9000	9360.0	42.64	0.60
10000	10400.0	34.44	0.23

4.9 – REFERENCES

(1) Evans, D. F.; Wennerstrom, H. In *The Colloidal Domain: Where Physics, Chemistry, and Biology Meet*; 2nd ed.; Wiley-VCH: New York, 1999, p 7-10.

(2) D'Cruz, O. J.; Uckun, F. M. *Curr. Pharm. Des.* **2004**, *10*, 315-336.

(3) Williams, A. A.; Sugandhi, E. W.; Macri, R. V.; Falkinham, J. O., III; Gandour, R. D. *J. Antimicrob. Chemother.* **2007**, *59*, 451-458.

(4) Vorum, H.; Brodersen, R.; Kragh-Hansen, U.; Pedersen, A. O. *Biochim Biophys Acta* **1992**, *1126*, 135-142.

(5) Kaneko, D.; Olsson, U.; Sakamoto, K. *Langmuir* **2002**, *18*, 4699-4703.

(6) Bates, R. G.; Allen, G. F. *J Research Natl. Bur. Standards* **1960**, *64A*, 343-346.

(7) Bashura, A. G.; Klimenko, O. I.; Nurimbetov, K. N.; Gladukh, E. V. *Farmatsevtichnii Zhurnal (Kiev)* **1989**, *3*, 57-58.

(8) Nichifor, M.; Lopes, S.; Bastos, M.; Lopes, A. *J. Phys. Chem. B* **2004**, *108*, 16463-16472.

(9) Mohr, A.; Talbiersky, P.; Korth, H.-G.; Sustmann, R.; Boese, R.; Blaser, D.; Rehage, H. *J. Phys. Chem. B* **2007**, *111*, 12985-12992.

(10) Wintgens, V.; Daoud-Mahammed, S.; Gref, R.; Bouteiller, L.; Amiel, C. *Biomacromolecules* **2008**, *9*, 1434-1442.

(11) Kalyanasundaram, K.; Thomas, J. K. *J. Am. Chem. Soc.* **1977**, *99*, 2039-2044.

(12) Nakajima, A. *Bull. Chem. Soc. Jpn.* **1971**, *44*, 3272.

(13) Nakajima, A. *Spectrochim. Acta, Part A* **1974**, *30*, 860.

(14) Nakajima, A. *J. Mol. Spectrosc.* **1976**, *61*, 467.

(15) Lin, S.-Y.; Lin, Y.-Y.; Chen, E.-M.; Hsu, C.-T.; Kwan, C.-C. *Langmuir* **1999**, *15*, 4370.

(16) Actis, M. L. Synthesis, Characterization, Critical Micelle Concentration and Biological Activity of two-Headed Amphiphiles. M.S., Chemistry, Virginia Polytechnic Institute and State University, Blacksburg, 2008.

(17) Klevens, H. B. *J. Am. Oil Chem. Soc.* **1953**, *30*, 74-80.

(18) Shinoda, K. *J. Phys. Chem.* **1956**, *60*, 1439.

(19) Macri, R. V.; Karlovská, J.; Doncel, G. F.; Du, X.; Maisuria, B. B.; Williams, A. A.; Sugandhi, E. W.; III, J. O. F.; Esker, A. R.; Gandour, R. D. *Bioorg. Med. Chem.* **2009**, *17*, 3162-3168.

(20) Lomax, E. G. In *Amphoteric Surfactants*; Lomax, E. G., Ed.; Marcel Dekker, Inc.: New York, 1996; Vol. 59, p 13-14.

(21) Rosen, M. J. In *Surfactants and Interfacial Phenomena*; 3 ed.; John Wiley & Sons, Inc.: Hoboken, New Jersey, 2004, p 139-144.

CHAPTER 5 – BIOLOGICAL ASSAY DATA FOR DENDRITIC AMPHIPHILES

5.1 – INTRODUCTION

The overarching project goal is developing safe, highly effective topical microbicides that can be used as broad spectrum anti-infectives. These microbicides should function against a wide a range of pathogens while presenting virtually no deleterious side effects to the user. We have previously discussed how an amphiphilic compound tends to show signs of cytotoxicity as the concentration of that amphiphile nears the CMC (cf. chapter 1). In this chapter, we will look at the structure-activity relationships of MIC to chain length, single-tail versus two-tail amphiphiles, and hydrophobicity (clogP) to describe these compounds' ability to inhibit the growth of several pathogens. We will also compare MICs to CMCs for individual homologues. If MIC $\geq$ CMC, then detergency as a mechanism of inhibition is possible; if MIC < CMC, detergency is less likely to be a mechanism of inhibition and some other mechanism(s) of inhibition is (are) occurring. Furthermore, the ratio of MIC/CMC is a measure of safety for use as an antimicrobial.[1]

All biological data were collected by other researchers. The reported MIC_{99} measurements were made by (Dr.) Andre Williams, (Dr.) Eko Sugandhi, Ms. Myra Williams, and Ms. Shauntrece Hardrict in Dr. Falkingham's laboratory in the Department of Biological Sciences at Virginia Tech. HIV and epithelial cell cytotoxicity measurements (listed as half maximal effective concentration, EC_{50}) were made by Dr. Gustavo Doncel's research group in the Department of Obstetrics and Gynecology at the Eastern Virginia Medical School.

After determining the proper counterion for optimal solution solubility, a broad spectrum screening against various bacteria, fungi, and yeasts demonstrated that the compounds possessed antimicrobial activity.[2] The next study[3] demonstrated the value of the inoculum effect[4-6] (cf. 5.5.1) in measuring the intrinsic susceptibility of *Mycobacterium smegmatis* to **3CUrn**. Both published results led us to focus on three different therapeutic areas for additional exploration with regards to the efficacy of these amphiphiles. The first study entailed exploration of the possible use of these compounds as vaginal microbicides. The second study involved the potential of using these compounds as anti-infectives against various mycobacteria. The third study probed effectiveness of these compounds as nasal anti-infectives against *Staphylococcus aureus* and methicillin-resistant *S. aureus* (MRSA).

5.2 – INITIAL BROAD-SCREEN TESTING OF TRICARBOXYLATO AMPHIPHILES FOR ANTIMICROBIAL ACTIVITY

Tables 5-1 and 5-2 show the results of the broad spectrum testing of these tricarboxylato amphiphiles.

Table 5-1 Comparison of bacterial activities of dendritic tricarboxylato amphiphiles

Amphiphile	MIC_{99} (μM)				
	E. coli	***K. pneumoniae***	***S. aureus***	**MRSA**	***M. luteus***
3CAm13	610	1200	14000	1200[a]	>14000
3CAm15	280-570	1200	13000	1200[a]	>13000
3CAm17	270	1100	12000	1100[a]	>12000
3CAm19	130	1100	1400	66	>12000
3CAm21	120	490	700	120	>11000
3CCb14	290	290	13000	2300[a]	>13000
3CCb16	270	70[a]	12000	2200[a]	>12000
3CCb18	260	130[a]	1400	520	>12000
3CCb20	120	120[a]	1400	490	>11000
3CCb22	230	120[a]	330	230	>11000
3CUr14	290	290[a]	6400	6400[a]	>13000
3CUr16	140	270[a]	760	6000[a]	>12000
3CUr18	130	260[a]	1400	700[a]	>12000
3CUr20	63	240[a]	1400	1400[a]	>11000
3CUr22	120	470[a]	1300	1300[a]	>11000

[a] Incomplete inhibition, approximately MIC_{50}
All data in this table from Reference 2
Error is ± one twofold dilution where multiple determinations of the MIC gave the same value.

Table 5-2 Comparison of mycobacterial and fungal activities of dendritic tricarboxylato amphiphiles

	MIC_{99} (μM)			
Amphiphile	***M. smegmatis***	***S. cerevisiae***	***C. neoformans***	***A. niger***
3CAm13	610	1200	310	14000
3CAm15	290	580	290	6400
3CAm17	70	270	140–270	270
3CAm19	33	66	33–66	130
3CAm21	63	7.7	250	120
3CCb14	290[a]	570	1600	13000
3CCb16	140[a]	540	47	6000[a]
3CCb18	16[a]	66	180	5700[a]
3CCb20	31[a]	16	1400	1400
3CCb22	60[a]	1.8	2700	1300
3CUr14	580[a]	580	1600	6400
3CUr16	140[a]	540	47	3100
3CUr18	33[a]	130	90	1400
3CUr20	63[a]	120	2800	680
3CUr22	120[a]	30	5200	5200

[a] Incomplete inhibition, approximately MIC_{50}
All data in this table from Reference 2
Error is ± one twofold dilution where multiple determinations of the MIC gave the same value.

The dendritic amphiphiles were tested against a range of microbes in a series of broad spectrum tests. The best activity seen in the broad spectrum tests for the **3CCbn** series occurs against the organisms *Klebsiella pneumoniae*, *Mycobacterium smegmatis*, *Saccharomyces cerevisiae*, *Candida albicans*, and *Cryptococcus neoformans* (Figures 5-2

through 5-6, data from Tables 5-1 and 5-2). For each microorganism discussed, the MIC and structure of a currently used antibiotic is provided for reference.

5.2.1 – Background on Microbes

K. pneumoniae—a Gram-negative bacterium found in the normal flora of the mouth, skin, and intestines[7]—is considered an opportunistic pathogen commonly contracted as a nosocomial infection. *M. smegmatis is* a Gram-positive mycobacterium that is not typically considered as a human pathogen – indeed, most mycobacteria are harmless and are found in soil samples where they break down organic matter.[8] *M. smegmatis* is relatively non-pathogenic in comparison to its more virulent cousins such as *M. tuberculosis, M. africanum, M. bovis* (tuberculosis), and *M. leprae* (leprosy). It is also a relatively fast-growing form of mycobacterium. Because *M. smegmatis* is non-pathogenic and rapid-growing it is typically used in applications such as gene cloning[8] and serves here as a model for the more virulent forms of mycobacteria.

S. cerevisiae is a form of budding yeast used for baking and brewing. It is not considered a pathogenic organism and is used in this study as a model of pathogenic forms of yeast.[9] *C. albicans* is a diploid fungus (a form of yeast) that occurs in 80% of the human population with no deleterious side effects, existing in a commensal state in the mouth and gastrointestinal tract of the host.[9] However, pathogenic overgrowth of the various *Candida* species leads to candidiasis, or yeast infections. This is also known as "thrush" – a common infection in infants due to weaker immune systems. The various *Candida* species present especially intractable infections to immunocompromised patients (e.g. those who are HIV-positive, or are undergoing cancer chemotherapy or organ/bone marrow transplantation), and can lead to potentially fatal systemic fungal infections.[7] *C. neoformans* is another yeast-like fungus. Contraction of *C. neoformans*

leads to cryptococcosis, a serious and potentially fatal fungal infection.[10] Cryptococcosis is a defining opportunistic infection in AIDS patients and for patients with certain lymphomas (e.g. Hodgkin's lymphoma), potentially leading to cryptococcal meningitis.

5.2.2 – Activity against *K. pneumoniae*

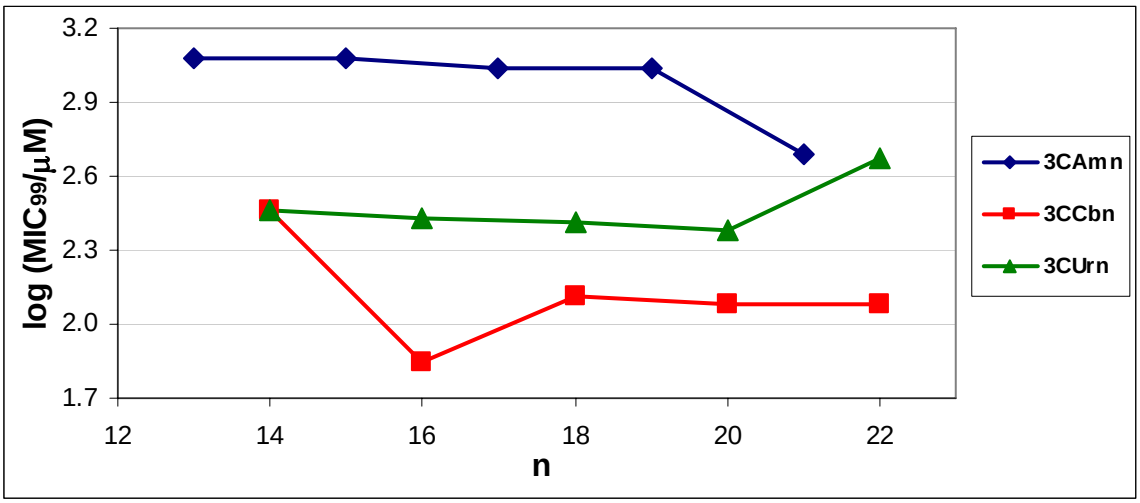

Figure 5-1 log MIC_{99} vs. carbon chain length against *K. pneumoniae*. Lines are eye-guides. Error is ± 0.3.

The difference in activity of the **3CCbn** and **3CUrn** series when compared to the **3CAmn** series is striking, and may indicate that the linker group is playing some role in the inhibition process, as that is the only structural difference between the three series of compounds. Figure 5-2 shows that there is a cutoff effect (cf. chapter 1) at **3CCb16**, which is most active (MIC_{99} = 70 μM). Longer chain homologues of the **3CAmn** series may show increasing activity with increasing chain length. Imipenem (Fig 5-2) MIC_{50} = 0.84 μM vs. *K. pneumoniae* strain C2 @ 10^5 CFU/mL inoculum.[11]

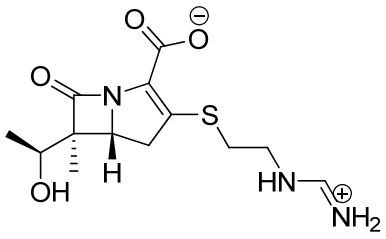

Figure 5-2 Chemical structure of Imipenem

5.2.3 – Activity against *M. smegmatis*

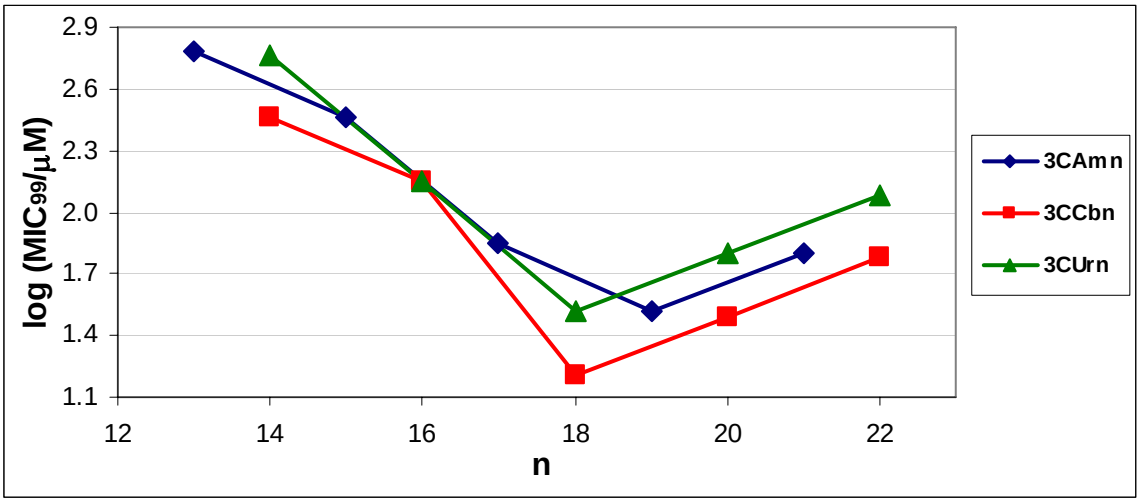

Figure 5-3 log MIC_{99} vs. carbon chain length against *M. smegmatis*. Lines are eye-guides. Error is ± 0.3.

We note in Figure 5-3 that all three of the tested amphiphiles show a cutoff effect at 18 (**3CCb18** MIC_{99} = 16 μM and **3CUr18** MIC_{99} = 33 μM) and 19 (**3CAm19** MIC_{99} = 33 μM) carbons in the tail, indicating that a specific chain length of amphiphile is the most effective in inhibiting growth of *M. smegmatis*. Further, the isosteric changes do not appear to make a significant difference, although the **3CCbn** series appears more effective than the others. Ethambutol MIC_{99} = 0.88 μM vs. *M. smegmatis* strain MTCC 6 @ 10^5 CFU/mL inoculum.[12]

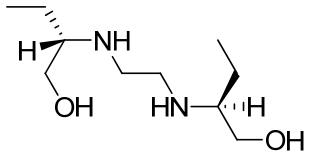

Figure 5-4 Chemical structure of (S,S)-Ethambutol

5.2.4 – Activity against *S. cerevisiae*

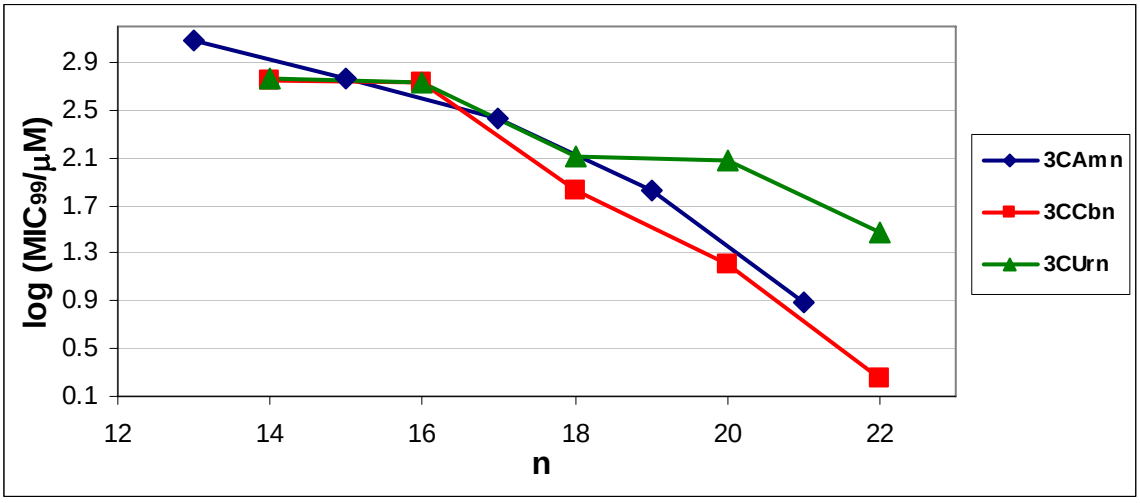

Figure 5-5 log MIC_{99} vs. carbon chain length against *S. cerevisiae*. Lines are eye-guides. Error is ± 0.3.

From the data in Figure 5-4, we see that the synthesis and testing of longer-chain homologues (> 22 carbons) against *S. cerevisiae* in each series is potentially warranted, as the MIC is still decreasing up to the longest chain homologue tested. Additionally, the **3CCb22** homologue (MIC_{99} = 1.8 μM) already has comparable potency to the current clinical antibiotic, Amphotericin B MIC_{90} = 1.1 μM against *S. cerevisiae* @ 10^3 CFU/mL inoculum.[13]

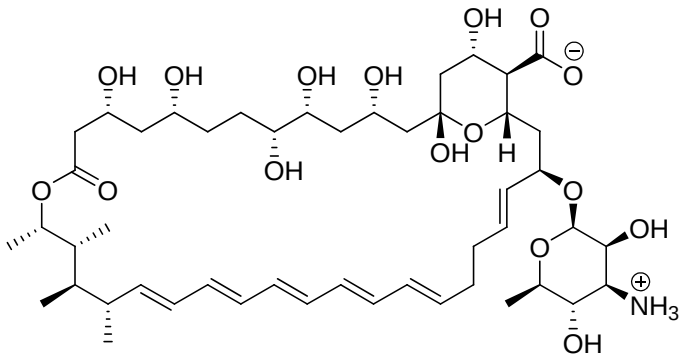

Figure 5-6 Chemical structure of Amphotericin B

5.2.5 – Activity against *C. albicans*

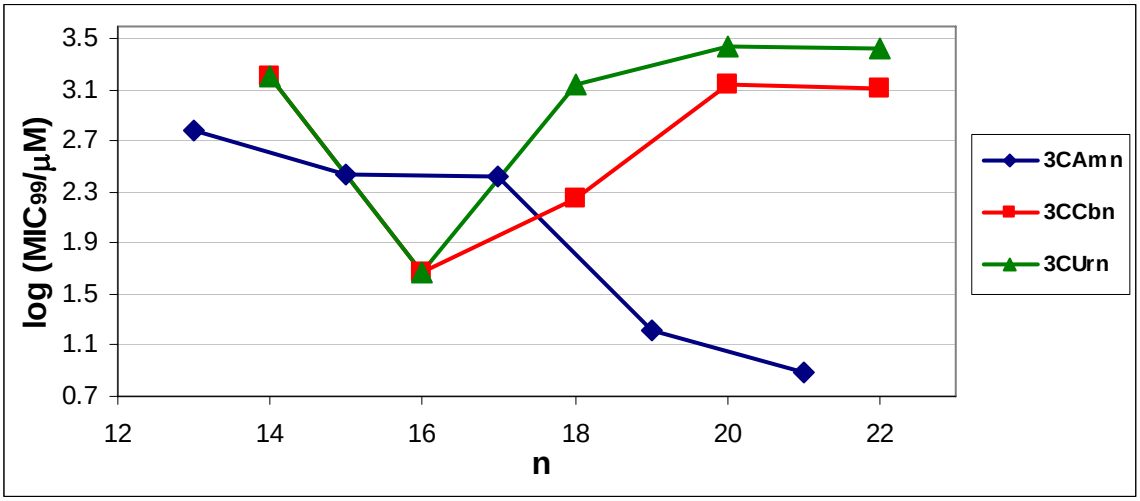

Figure 5-7 log MIC_{99} vs. carbon chain length against *C. albicans*. Lines are eye-guides. Error is ± 0.3.

The most notable feature in Figure 5-7 is that the **3CCbn** and **3CUrn** series reach a cutoff at n = 16, (MIC_{99} = 47 μM) while the **3CAmn** is still continuing to decrease at n = 21 carbons (MIC_{99} = 7.7 μM). Again, potential further studies are possibly warranted to determine at what chain length, if any, the **3CAmn** series will show a cutoff. Fluconazole MIC_{50} = 0.41 μM against *C. albicans* strain ATCC 90029 @ 10^3 CFU/mL inoculum.[14]

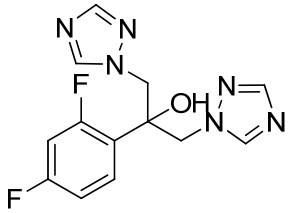

Figure 5-8 Chemical structure of Fluconazole

5.2.6 – Activity against *C. neoformans*

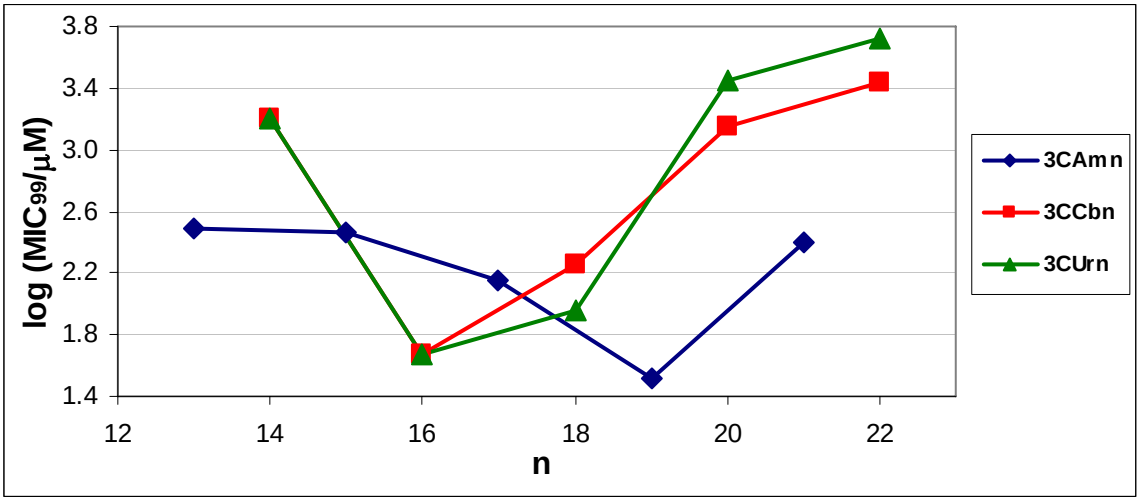

Figure 5-9 log MIC_{99} vs. carbon chain length against *C. neoformans*. Lines are eye-guides. Error is ± 0.3.

Figure 5-9 shows that all three homologous series show cutoff effects; these occur at **3CCb16** (MIC_{99} = 47 μM) and **3CUr16** (MIC_{99} = 47 μM), and **3CAm19** (MIC_{99} = 33 μM). We also note that the MICs of these amphiphiles are on par with the effectiveness of the comparison antibiotic. Fluconazole MIC_{80} = 13 μM against *C. neoformans* @ 10^4 CFU/mL inoculum.[15] (See Figure 5-8 for structure).

5.2.7 – General Discussion

The three homologous series of amphiphiles show extremely good solution solubility, due to the multiple ionizable carboxyl moieties in the headgroup as well as the choice of a counterion that imparts maximum water solubility. The initial series of amphiphiles tested show good activity against several microorganisms in the study. For several microbes, the activity rivaled that of current clinical drugs. Maximal activity was often seen from one member of a homologous series (e.g. **3CCb18, 3CUr18,** and **3CAm19** against *M. smegmatis*), indicating that a specific mechanism of action was potentially at work as opposed to detergency, where amphiphiles dissolve membranes.

Detergency should occur for all members of a homologous series and would not produce a cutoff effect, but rather parallel the values of the CMC for all homologues. Consequently, as chain length increases, both CMC and MIC decrease. The good activity and the prospect of a non-detergent mechanism of action suggests that further investigating how these amphiphiles inhibit the growth of the susceptible organisms through both studying the mechanism and synthesizing new amphiphiles is warranted. The following sections examine subsequent work to this broad-screen testing[2] and our recognition of the inoculum effect.[3]

These published results led us to focus on three different therapeutic areas for additional exploration with regards to the efficacy of these amphiphiles. The first study (run concurrently with the broad spectrum testing) looked at these compounds' abilities to act as topical anti-infectives against HIV and *Neisseria gonorrhoeae*, two sexually transmitted pathogens. In conjunction with these data, we tested the ability of these amphiphiles to inhibit the growth of *Lactobacillus plantarum*, a critical part of normal vaginal flora that helps maintain vaginal pH and is an indicator of overall vaginal health. Finally, as an indicator of safety, we tested the cytotoxicity of these compounds towards epithelial cells. The second study involved exploring the potential of these compounds as topical anti-infectives against various mycobacteria (e. g. *M. smegmatis, M. marinum*, and *M. chelonae*). The third study focused on the effectiveness of these compounds as anti-infectives against *Staphylococcus aureus* and methicillin-resistant *S. aureus* (MRSA), two pathogens of recent increased scientific focus due to diminishing effectiveness of current antibiotics toward these bacteria.

5.3 – TESTING OF TRICARBOXYLATO AMPHIPHILES FOR POTENTIAL USE AS TOPICAL VAGINAL MICROBICIDES

The first study focused on these amphiphiles' activity as potential topical vaginal microbicides (Table 5-3). The anti-HIV and cytotoxicity data were collected during the same time frame as the broad spectrum tests.

Table 5-3 Comparison of biological activities of dendritic tricarboxylato amphiphiles

Amphiphile	EC_{50} (μM)		MIC_{99} (μM)		
	Anti-HIV activity	**Cytotoxicity**	***N. gonorrhoeae***	***L. plantarum*** [a,b]	***C. albicans*** [a,b]
3CAm13	740	300	12000	610	610
3CAm15	230	940	12000	570	280
3CAm17	n/d	n/d	2700	540	270
3CAm19	170	340	130	520	16
3CAm21	130	250	120	490	7.7
3CCb14	370	620	580	6400	1600
3CCb16	170	440	280	6000	47
3CCb18	130	350	65	1400	180
3CCb20	130	280	120	1400	1400
3CCb22	110	360	120	1300	1300
3CUr14	270	290	12000	6400	1600
3CUr16	180	350	2800	6000	47
3CUr18	240	280	130	1400	1400
3CUr20	130	210	120	1400	2800
3CUr22	120	260	120	940	2700
Triethanolamine	>6700	>4100	>270000	>270000	>270000

[a] incomplete inhibition, approximately MIC_{50}
[b] data from Reference 2
n/d = not determined
MIC_{99} error is ± one twofold dilution where multiple determinations of the MIC gave the same value. EC_{50} standard deviation is ± 10%.

5.3.1 – Background on Microbes

Since the identification of HIV in December, 1981, this retrovirus has become a pandemic infection in humans. It is estimated that 25 million people have died from the opportunistic infections that HIV/AIDS has caused, with 2.8 million deaths in 2005 alone.[16] One-third of the HIV/AIDS related deaths occur in sub-Saharan Africa, retarding economic growth and increasing poverty.

Sexually transmitted bacteria and fungi can enhance HIV infections,[17-19] therefore inhibiting the growth of these microbes is desirable. One such bacterium, *N. gonorrhoeae*, is a Gram-negative bacterium responsible for the sexually transmitted disease gonorrhoea.[7] This bacterium is typically encountered as a co-infection with Chlamydia (*Chlamydia trachomatis)*, and if left untreated in females leads to PID (pelvic inflammatory disease) and potential infertility.[20]

L. plantarum is a beneficial bacterium found colonizing in the human intestinal tract and vaginal walls. It self-aggregates and adheres to epithelial vaginal walls, thereby displacing vaginal pathogens. Studies *in vitro* demonstrate that colonized lactobacilli inhibit growth of organisms such as *Escherichia coli* and *Streptococcus agalactiae*.[21]

5.3.2 – Activity against *N. gonorrhoeae*

The most striking feature of the data presented for inhibiting growth of *Neisseria gonorrhoeae* is activity of the **3CCbn** series in comparison to those of the **3CAmn** and **3CUrn** series (Table 5-3).

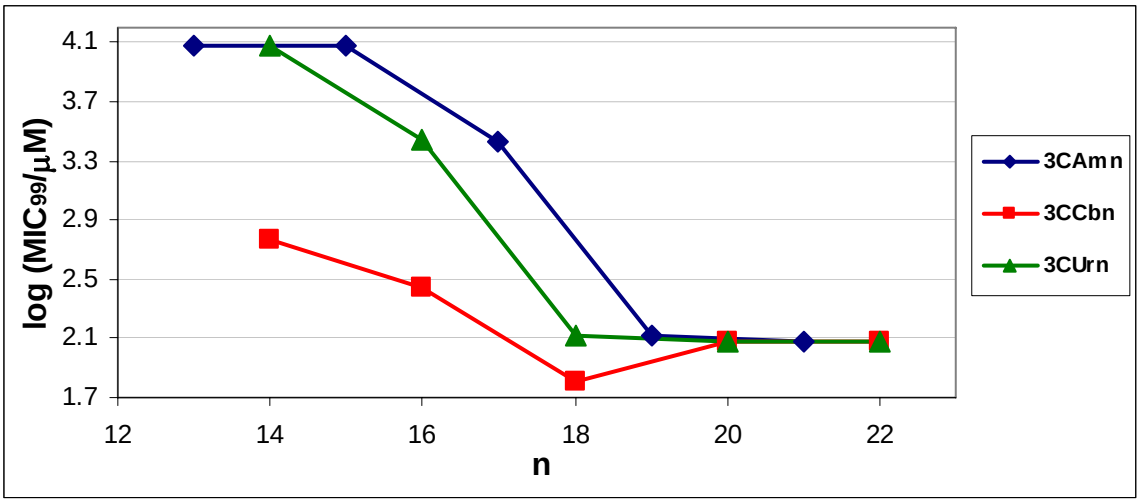

Figure 5-10 log MIC_{99} vs. carbon chain length against *N. gonorrhoeae.* Lines are eye-guides. Error is ± 0.3.

Figure 5-10 shows the data for these three series against *N. gonorrhoeae*. While all three series reach approximately equal values of inhibitory activity at n = 18 carbons in the tail (19 for the **3CAm** series), the activity of the **3CCbn** series at shorter chain lengths is much greater than the others, where the **3CCb14** amphiphile is almost 21 times more effective at inhibiting growth (**3CCb14** CMC = 580 μM vs. **3CUr14** and **3CAm15** CMC = 12,000 μM). We note a possible cutoff effect for the **3CCbn** series at n = 18 carbons in the tail, indicating that **3CCb18** (MIC_{99} = 65 μM) may indicate a specificity for this chain length and/or linker.

5.3.3 – Activity against HIV

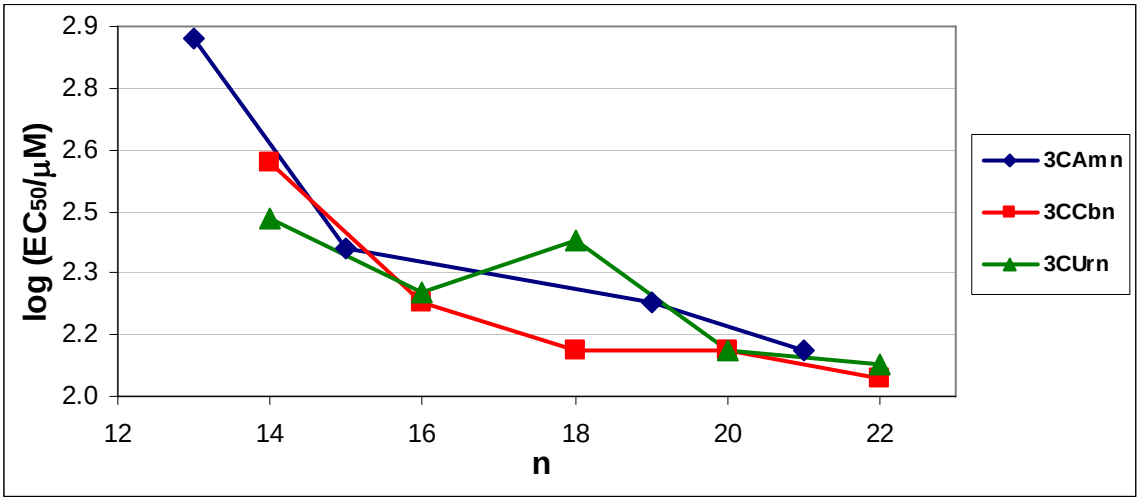

Figure 5-11 log EC_{50} vs. carbon chain length against HIV. Lines are eye-guides. **3CAm17** EC_{50} was not determined. Standard deviation ±10%.

The data indicate that these compounds are effective at inhibiting HIV to some extent. All three compounds continue to show decreasing activity up to the longest chain length homologue tested. The **3CUrn** series shows an interesting trend as it reaches a minimum at **3CUr16**, rises to **3CUr18**, and then begins falling again for the **3CUr20** and **3CUr22** homologues.

While the anti-HIV activity is not particularly compelling, it should be noted that current antiretroviral therapies for HIV/AIDS treatments use three or four different Nucleoside and Non-Nucleoside Reverse Transcriptase Inhibitors (NRTI and NNRTI, respectively) concurrently that function in a synergistic manner. A typical drug therapy regimen used would include the NNRTI efavirenz, in conjunction with zidovudine and lamivudine (both NRTIs).[22] However, these current treatments have shown a host of side-effects, including teratogenicity in child-bearing mothers who are receiving antiretroviral drug therapies.[23] Additionally, the cost of these antiretroviral therapies can be prohibitive, costing in the thousands of dollars for a one-month supply. (e.g. the

combination of efavirenz with tenofovir and emtricitabine, sold under the brand name Atripla™ (Bristol-Myers Squibb & Gilead Sciences, LLC), retails for over $1,500 USD for a 30-day supply).

5.3.4 – Activity against *L. plantarum*, Cytotoxicity, and the Therapeutic Index

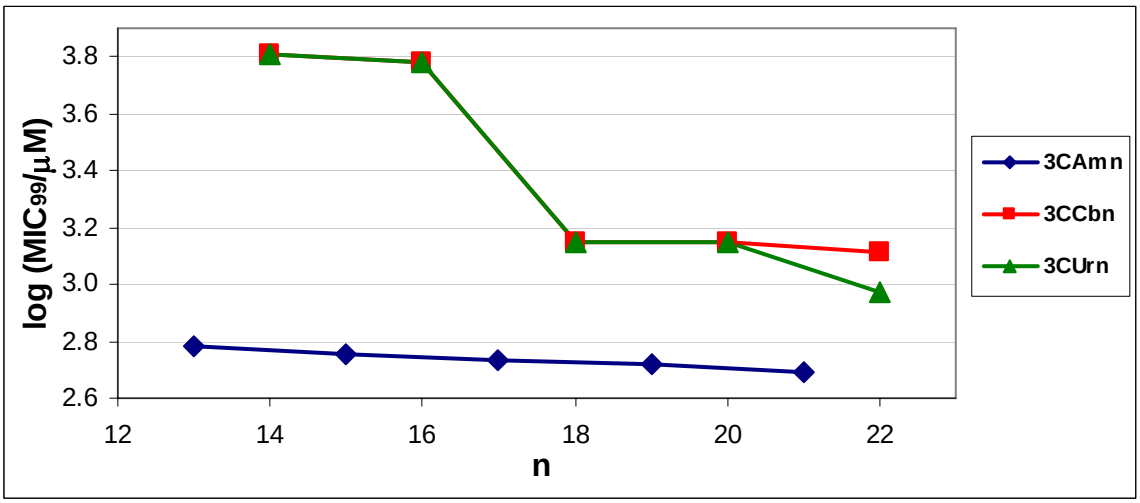

Figure 5-12 log MIC_{99} vs. chain length against *L. plantarum*. Lines are eye-guides. Error is ± 0.3.

The data collected for inhibition of *L. plantarum* shows that the **3CAmn** series is a much better inhibitor than either the **3CCbn** or **3CUrn** series. However, we do not want to inhibit the growth of *L. plantarum*, as this is a beneficial organism that is found in the natural ecosystem of the vagina (cf. 5.3.1). The change in activity is most likely due to the linker group, with the more hydrophilic -O- and -NH- linkers of the **3CCbn** and **3CUrn** series, respectively, affecting the growth less than that of the relatively hydrophobic $–CH_2-$ linker seen in the **3CAmn** series.

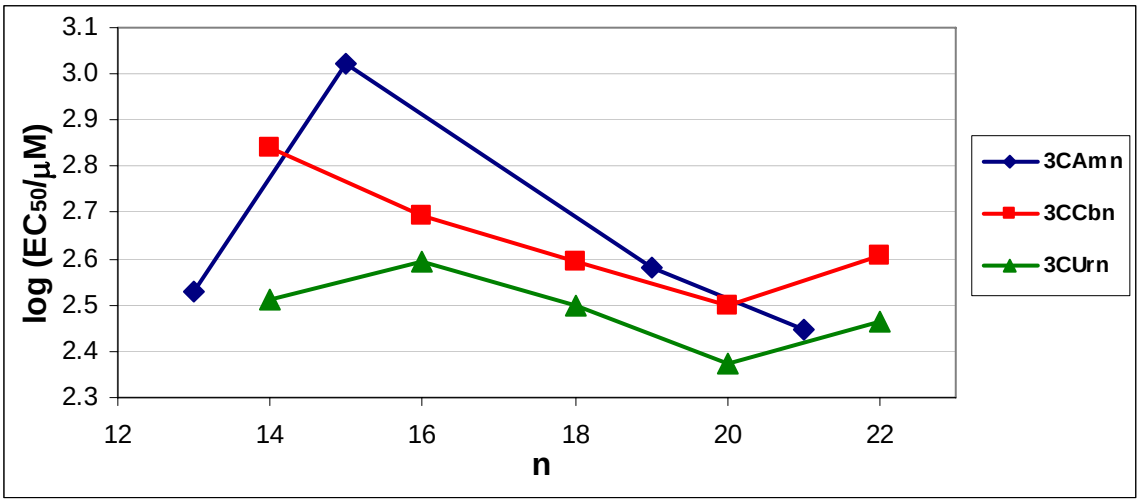

Figure 5-13 log EC_{50} vs. chain length for cytotoxicity data. Lines are eye-guides. **3CAm17** was not determined. Standard deviation ±10%.

The cytotoxicity data shows that all three homologous series of amphiphiles reach approximately the same EC_{50} values. The **3CCbn** and **3CUrn** series show a cutoff at n = 20 carbons in the tail. The **3CAmn** series continues to decrease, after rising sharply from n = 13 to n = 15, up to the longest chain homologue tested.

The Therapeutic Index (TI, also known as the Therapeutic Ratio) is given by the general formula,

$$TI = \frac{TD_{50}}{ED_{50}} \qquad (1)$$

where TD_{50} is the half maximal toxic dose, and ED_{50} is the half maximal effective dose. A large TI quotient is preferable to a small one, as this represents the case where it takes much more of the compound to cause deleterious effects than is necessary for effective therapeutic response. While a larger TI is preferable, there are examples of drugs with TIs that are fairly narrow (e.g. Amphotericin B TI ~ 9 for systemic *C. albicans* infections in rats[24]). In determining the Therapeutic Index for our system, the TD_{50} corresponds to

the cytotoxicity of these amphiphiles towards epithelial cells and the ED_{50} corresponds to either the MIC_{50} or EC_{50} values shown for the inhibition of the target organisms.

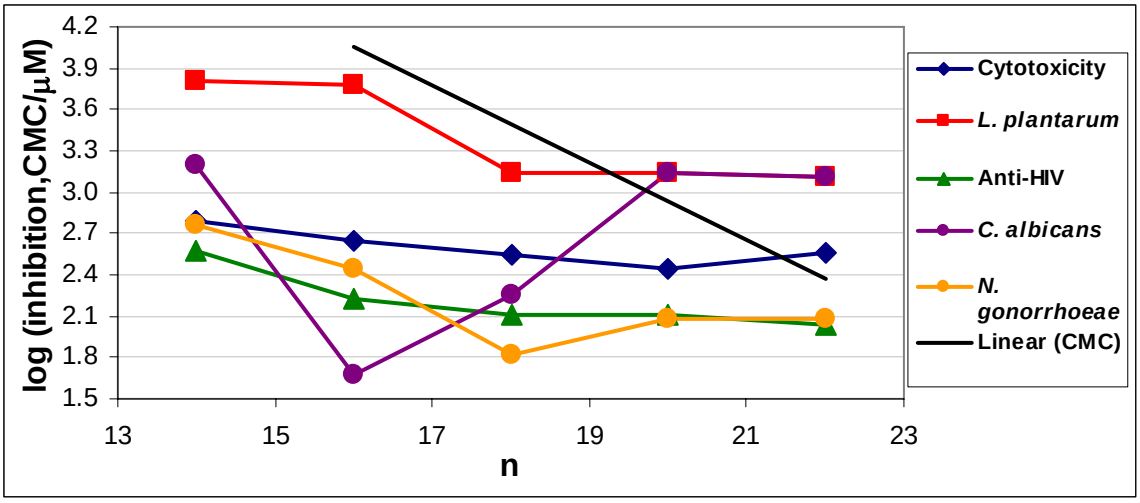

Figure 5-14 log inhibition vs. chain length for the **3CCbn** series (EC_{50} for HIV and Cytotoxicity data, MIC_{99} for *L. plantarum*, *C. albicans*, and *N. gonorrhoeae*). Lines are eye-guides. Error is ± 0.3 for MIC, standard deviation ±10% for HIV/cytotoxicity.

Figure 5-14 shows the data from Table 5-3 for only the **3CCbn** series to illustrate the effectiveness of this compound as a potential topical vaginal microbicide. **3CCb18** seems to be the most effective overall amphiphile. The concentrations required for activity against HIV (**3CCb18** EC_{50} = 130 μM) and *N. gonorrhoeae* (**3CCb18** MIC_{99} = 65 μM) shows lower cytotoxicity (**3CCb18** EC_{50} = 350 μM) and even lower activity against *L. plantarum* (**3CCb18** MIC_{99} = 1400 μM). This tends to indicate that **3CCb18** would be fairly safe as a topical microbicide against *N. gonorrhoeae*, with Therapeutic Indices for **3CCb18** of 5.4 with respect to the cytotoxicity. The anti-HIV TI of **3CCb18** is not as good, with an index of 2.7 with respect to the cytotoxicity.

5.3.5 – General Discussion

The data indicate that the **3CCbn** series – more specifically **3CCb18** – has the most potential for use as a topical vaginal microbicide of the three amphiphilic series

tested. As the TI is not ideal, it may be that these amphiphiles are better suited towards applications as a prophylactic agent, where concentrations would not need to be as high in order to prevent the onset of an infection, rather than being used to help clear an infection once the pathogen has been contracted. As the MIC_{99} data were collected before our discovery of the inoculum effect,[3] it is quite likely that retesting these organisms (*N. gonorrhoeae, L. plantarum,* and *C. albicans*) will yield lower MIC values and may show increases in the TI values.

5.4 – Results and Discussion of Testing of Tricarboxylato Amphiphiles for Potential Use as anti-Mycobacterial Agents

5.4.1 – The Inoculum Effect

After the publication of the broad-spectrum data, we discovered that we may have collected the MIC data at too high an inoculum density.[3] Inoculum density is simply the number of microbial agents (cells, colonies, etc) found per milliliter of solution being tested, expressed as Colony Forming Units/mL, or CFU/mL. If the inoculum density is too high it could potentially lead to inaccurate MIC values for the compound against the microorganism in question. The determination of the "intrinsic activity" became a major focus of the testing of these amphiphiles against mycobacteria and other pathogens.[3] The presence of a change in the MIC of a drug candidate against a microorganism based on the inoculum density is known as the inoculum effect.[4-6]

The inoculum effect can be thought of as an increased demand for the drug candidate as the initial inoculum density is increased.[5] As the inoculum density is increased, the available molecules of drug candidate have been used up and therefore an increase in the MIC results as there is not enough drug present to inhibit pathogen

growth. A mathematical treatment[25] of the inoculum effect describes the effect of increasing initial inoculum density as a function of the MIC,

$$\log MIC = \log MIC_0 + \left(e^{k(\log I - \log I_{tr})} - 1\right) \quad (1)$$

where *MIC* is the activity at a given inoculum density, MIC_0 is the baseline MIC (the "intrinsic activity"), *k* is a constant that describes the rate of increase of log MIC at high inoculum density, *log I* is the size of the test inoculum, and *log* I_{tr} is the inoculum threshold immediately before the rise of the MIC. What eqn. 1 tells us is that, at low inoculum density (log I < log I_{tr}), the MIC is equal to the intrinsic activity (MIC_0) of the drug candidate being tested, and a graph of log MIC vs. log inoculum shows a constant value. As log I increases above log I_{tr}, the MIC increases exponentially.

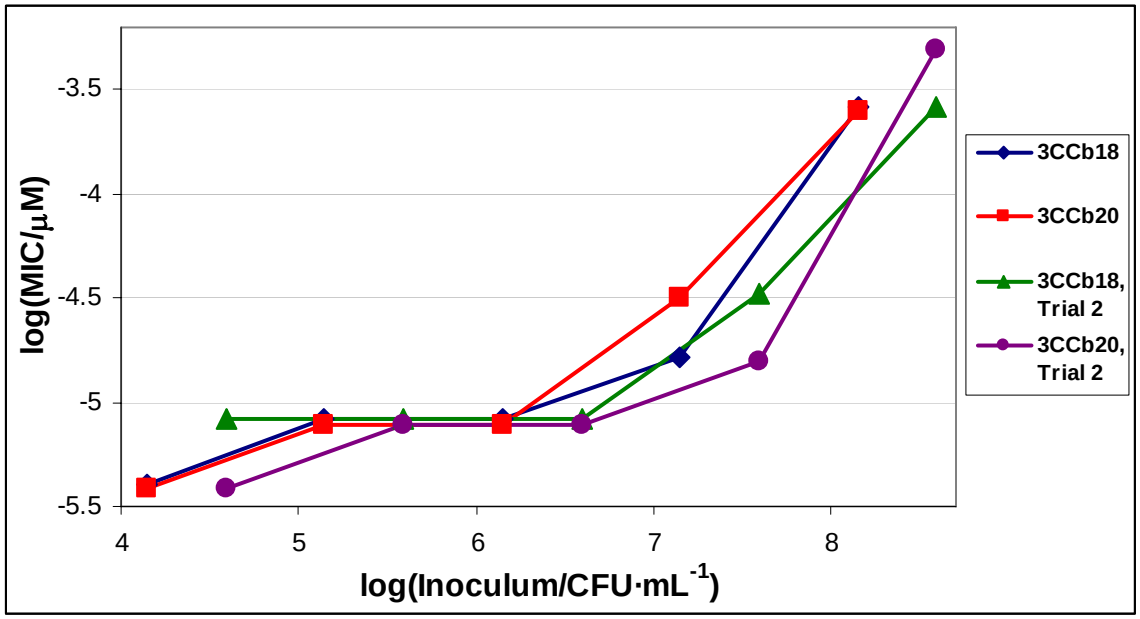

Figure 5-15 log MIC_{99} vs. log CFU/mL of *M. smegmatis* plot demonstrating the Inoculum Effect. Lines are eye-guides. Error is ±0.3.

5.4.2 – Results and Discussion of Focused anti-Mycobacterial Testing

Based on this discovery of an inoculum effect from the study of the **3CUrn** homologues[3], the MICs were re-determined for these amphiphiles in a focused study at

lower initial inoculum density (10^5 CFU/mL), which is the inoculum recommended by the American Society of Microbiology. The data from the focused study of these amphiphiles as potential anti-mycobacterial agents is presented in Table 5-4.

Table 5-4 MIC and MBC (μM) of two- and three-headed dendritic amphiphiles against *M. smegmatis* strain mc2155, *M. marinum* strain ATCC 927, and *M. chelonae* strain EO-P-1[c]

	M. smegmatis			***M. marinum***		***M. chelonae***	
Amphiphile	**MIC_{99}**[b]	**MIC_{99}**	**MBC**	**MIC_{99}**	**MBC**	**MIC_{99}**	**MBC**
3CAm13	610	79		630		59	
3CAm15	290	74		590		74	
3CAm17	70	53		560		35	
3CAm19	33	6.3	8.3	50		17	
3CAm21	63	47		95		130	
3CCb14	290[a]	74		440		55	
3CCb16	140[a]	52		420		70	
3CCb18	16[a]	8.3	8.3	83	520	17	
3CCb20	31[a]	7.9	7.9	16	500	31	
3CCb22	60[a]	120		360		240	
3CUr14	580[a]	37		440		74	
3CUr16	140[a]	35		420		70	
3CUr18	33[a]	6.3	8.3	42	520	17	
3CUr20	63[a]	63		63		47	
3CUr22	120[a]	60		180		480	

[a] Incomplete inhibition – approximately MIC_{50}

[b] Data in this column from reference 2

[c] Average of duplicate measurements of two different cultures. Error is ± one twofold dilution.

We note that the MICs for *M. smegmatis* have been reduced from the original broad screen data,[2] which was run at an initial inoculum density of 10^8 CFU/mL. In one case

(**3CCb22**) the MIC actually increased, although this is within experimental error. Additionally, the incomplete inhibition seen in the majority of the cases in the original study[2] are now absent. Presumably the incomplete inhibition was caused by the initial inoculum density being too high for the amount of amphiphile needed for complete inhibition. All three homologous series show cutoff effects at n = 18 (**3CUr18** CMC = 6.3 μM), n = 19 (**3CAm19** CMC = 6.3 μM), and n = 20 (**3CCb20** CMC = 7.9 μM) carbons in the tail. The **3CCb20** homologue appears to be the most effective general anti-infective against the three different species of mycobacteria tested. *M. marinum* appears to be particularly resistant to these amphiphiles in comparison to the other mycobacteria tested. This is especially true for the **3CAmn** series.

The MBC (Minimum Bactericidal Concentration) is the concentration required to kill the organism, as opposed to just preventing growth. For the **3CCbn** series, the MBC is equal to the MIC, indicating that these amphiphiles (**3CCb18** and **3CCb20**, respectively) are particularly effective in controlling *M. smegmatis*. The **3CAm19** and **3CUr18** amphiphiles show similar behavior. Similar results were seen against *M. marinum*, however the MBC is 6- to 31-times higher than the MIC, indicating that these amphiphiles may control growth effectively (thereby preventing the spreading of an infection), but may not be effective in removing an infection of *M. marinum* (**3CCb20** MIC_{99} = 16 μM, MBC = 500 μM; **3CUr18** MIC_{99} = 42 μM, MBC = 520 μM).

5.5 – Discussion of Testing of Tricarboxylato Amphiphiles for Potential Use As Inhibitors of *S. aureus* and MRSA

While the data from the broad screen testing shown in Table 5-1 for *S. aureus* and MRSA is not nearly as impressive as the previous studies discussed, we note that there are several good candidates among the compounds tested, most notably **3CAm19** (MIC_{99}

= 66 μM)**, 3CAm21** (MIC_{99} = 120 μM)**,** and **3CCb22** (MIC_{99} = 230 μM). For reference, the drug Vancomycin (Figure 5-7) has a MIC_{50} value of 0.5 μg/mL (0.3μM) against MRSA @ $10^4 – 10^6$ CFU/mL.[26]

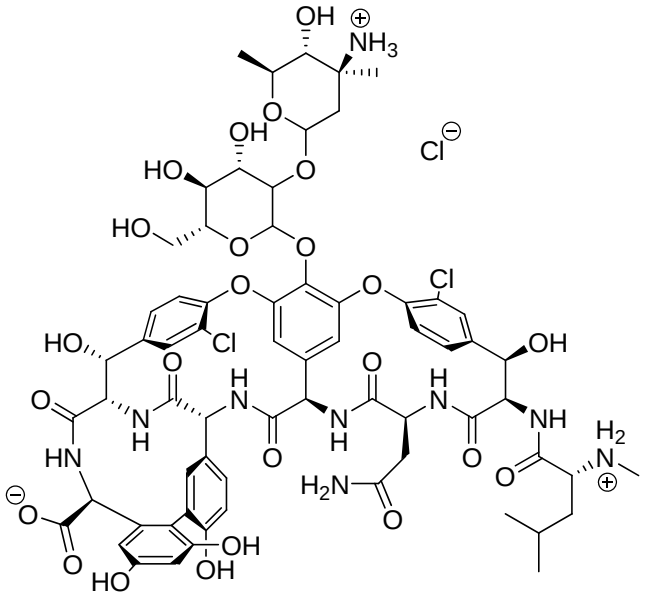

Figure 5-16 The chemical structure of Vancomycin

The authors conclude[26], however, that not all MRSA strains are susceptible to Vancomycin treatment, and for those strains with higher resistance the treatment success rate is very low (55.6% success rate for strains with MIC_{50} values at 0.5 μg/mL; but for strains with MIC_{50} values between 1–2 μg/mL, the treatment success rate drops to 9.5%).

Because the initial measurements from the broad screen testing[2] were made at high inoculum densities [i.e., 10^8 CFU/mL] these measurements could have also been susceptible to an inoculum effect (cf. 5.5.1).[4,25,27] This inoculum effect may have clinical relevance,[6,28-32] especially for *S. aureus* and MRSA, because infections caused by these organisms can result in abscesses and biofilms where cell numbers of up to $10^{9\text{-}10}$ CFU/gram have been reported.[33] Increasing the inoculum density from 10^6 to 10^8 CFU/mL increased the MICs of several drugs against *S. aureus*.[34]

Based on this information, a new study was undertaken with lower inoculum densities against strains of *S. aureus* and MRSA. The results of these tests are presented in Table 5-5.

Table 5-5 MICs of dendritic amphiphiles against *S. aureus* strain ATCC 6358 and MRSA strain ATCC 43330

	MIC_{99} (μM)	
Amphiphile	***S. aureus***	**MRSA**
3CAm13	1200	1200
3CAm14	1200	1200
3CAm15	1200	1200
3CAm16	1100	1100
3CAm17	550	520
3CAm19	66	39
3CAm21	19	15
3CCb14	1200	1200
3CCb16	230	600
3CCb18	60	43
3CCb20	9.7	2.9
3CCb22	11	3.5
3CUr14	1200	1200
3CUr16	690	520
3CUr18	66	36
3CUr20	17	4.2
3CUr22	18	4.0

Error (±0.3) represents one twofold dilution where multiple determinations of the MIC gave the same value.

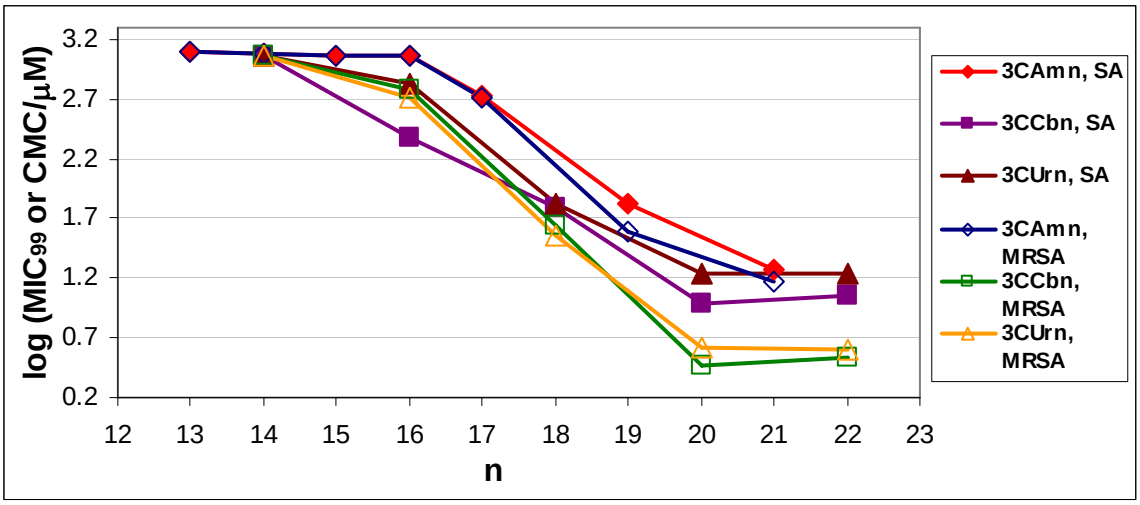

Figure 5-17 MIC_{99} vs. # of carbons in the tail for dendritic amphiphiles against *S. aureus* (SA) and MRSA. Lines are eye-guides. Error is ± 0.3.

We immediately note the reduction in MIC for the tested compounds in comparison to the data given in Table 5-1. This demonstrates that, as theorized, an inoculum effect was indeed occurring. Figure 5-14 demonstrates that the most active amphiphiles tested are the **3CCb20** and **3CCb22** homologues, with MIC_{99} values ranging from 2.9 to 3.5 μM for MRSA and from 9.7 to 11 μM for *S. aureus*. The longer chain homologues of the ureido isosteric series also show comparable activity against MRSA (**3CUr 20** MIC_{99} = 4.2 μM and **3CUr22** MIC_{99} = 4.0 μM). The **3CCbn** and **3CUrn** series are also more effective inhibitors of MRSA than *S. aureus*.

These data, when compared to the initial data from Table 5-1, also suggest that these amphiphiles may not be very effective in treating already established *S. aureus* and MRSA infections, especially those in which an abscess has formed due to the high inoculum density found under such conditions. These amphiphiles would be better suited as prophylactic agents to prevent the spread of these organisms to patients in the first place, or as initial treatment options in surface skin infections. Due to the recent surge of

antibiotic-resistant strains of *S. aureus* and the potential of this bacterium to pose a major health threat, we feel that further investigations into improving the efficacy of these compounds towards *S. aureus* and MRSA are warranted. These compounds already show good to outstanding safety indices (**3CCb20** TI = 29 vs. *S. aureus* and 97 vs. MRSA. **3CCb22** TI = 33 vs. *S. aureus* and 103 vs. MRSA) when cytotoxicity is compared to MIC.

5.6 – Effect of Hydrophobicity on MIC

The low water solubility of the natural fatty acids prevents the use of long-chain fatty acids to study their antimicrobial activity. The fatty acids above C12 are not very water soluble, and for all intents and purposes the fatty acids above C18 are completely insoluble at physiological pH (cf. Table 4-1). The synthesis of these dendritic amphiphiles coupled with the proper choice of counterion has enabled us to overcome these solubility issues with chain lengths up to 22 carbons and beyond. However, it is possible that these dendritic amphiphiles are too hydrophilic, and do not partition well into the microbial membrane. In support of this theory, we note that the activity of the **3CCbn** amphiphiles against *S. aureus* and *MRSA* (Table 5-1) continued to increase as chain length increased (i.e. the amphiphile became more hydrophobic). In the following sections we will examine how amphiphilic hydrophobicity is determined and in what direction this information drove our research.

5.6.1 – Measuring Hydrophobicity

Two common methods for reporting the preference of a compound for dissolution into a hydrophobic or hydrophilic phase are the log of the partition coefficient and the log of the distribution coefficient. The partition coefficient (P), is defined as the ratio of

concentrations of a compound between two immiscible solutions.[35] Typically, 1-octanol is used as the hydrophobic phase and water is used as the hydrophilic phase,

$$\log P = \log\left(\frac{[solute]_{octanol}}{[solute]_{water}}\right) \quad (1)$$

where *logP* is the log of the partition coefficient, $[solute]_{octanol}$ is the concentration of the compound in the hydrophobic (1-octanol) phase, and $[solute]_{water}$ is the concentration of the compound in the hydrophilic (water) phase. From eq. 1, it follows that logP > 0 indicates that the compound is more soluble in the hydrophobic phase, and logP < 0 indicates a preference for the hydrophilic phase. logP = 0 indicates an equal preference for both phases. When the data are calculated instead of physically measured the calculated logP, or clogP, value is reported.

The determination of logP, however, is only valid for a single microspecies, as the charge on any given microspecies will affect the affinity of that compound for the hydrophobic or hydrophilic phase. In the case of compounds with ionizable groups (such as the dendritic amphiphiles), the log of the distribution coefficient (logD) is typically a more useful measurement. The distribution coefficient (D) is defined as the ratio of the sum of the concentrations of all species of the compound in octanol to the sum of the concentrations of all species of the compound in water.[35]

$$\log D = \log\left(\frac{[solute]^{ionized}_{octanol} + [solute]^{unionized}_{octanol}}{[solute]^{ionized}_{water} + [solute]^{unionized}_{water}}\right) \quad (2)$$

where *logD* is the log of the distribution coefficient, $[solute]^{ionized}_{octanol}$ is the portion of the ionized compound in the hydrophobic phase, $[solute]^{unionized}_{octanol}$ is the portion of the unionized compound in the hydrophobic phase, $[solute]^{ionized}_{water}$ is the portion of the ionized

compound in the hydrophilic phase, and $[solute]_{water}^{unionized}$ is the portion of the unionized compound in the hydrophilic phase. As would be expected the logD value is pH dependent, and reporting of the logD must be accompanied by the pH at which the determination is made.

As an example (Figure 5-18) the following expressions are derived for logP and logD using an acid dissociation reaction of a general acid AH:

$$AH \rightleftharpoons H^{\oplus} + A^{\ominus}$$

$$P_0 = \frac{[AH]_{octanol}}{[AH]_{water}} \qquad P_1 = \frac{[A^-]_{octanol}}{[A^-]_{water}} \qquad D = \frac{[HA]_{octanol} + [A^-]_{octanol}}{[HA]_{water} + [A^-]_{water}}$$

Figure 5-18 Partition and Distribution coefficients for a general acid dissociation reaction. P_0 is the partition coefficient for the neutral acid AH, P_1 is the partition coefficient for the conjugate base A^-, and D is the dissociation constant for all the microspecies present. Recreated from reference 35.

5.6.2 – Determination of the Distribution Coefficient for Dendritic Amphiphiles

Calculation[36] of logD at physiological pH (7.4) for these amphiphiles produces values from -3.26 (**3CCb14**) to -0.65 (**3CCb22**), indicating that these dendritic amphiphiles preferentially favor the hydrophilic phase. It is possible that reducing the hydrophilicity of these amphiphiles may lead to lower MICs, as the amphiphiles would then be more likely to interact with the hydrophobic cell membrane of the microbe in question. There are two ways to accomplish this: reducing the number of ionizable headgroups, or increasing the number of carbons in the tail. To test this hypothesis a series of two-headed, single-tail amphiphiles (**2CCbn)** and three-headed, two-tail amphiphiles (**3CCb1(n,n,)**) were synthesized and have been tested against mycobacteria (shown in Figure 5-19). Additionally, a precedence for activity of two-tailed amphiphiles against *Mycobacterium leprae* exists from the work of Adams.[37]

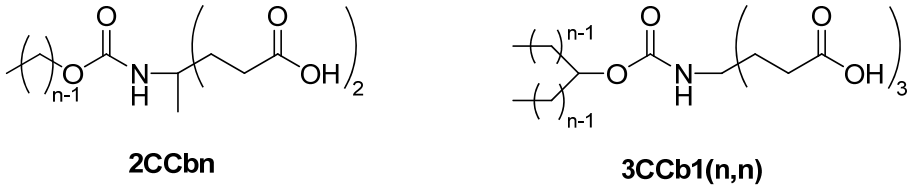

Figure 5-19 Chemical structures of **2CCbn** and **3CCb1(n,n)**

The logD data for these compounds range from 0.30 (**2CCb14**) to 4.05 (**2CCb22**) for the **2CCbn** series, and from -2.78 (**3CCb1(7,7)**) to 1.91 (**3CCb1(12,12)** for the **3CCb1(n,n)** series. From the calculated logD data, the **2CCbn** series is more hydrophobic than either of the **3CCb** series, and the **3CCb1(n,n)** series falls between that of the **2CCbn** and **3CCbn** series in terms of hydrophobicity. From these calculated logD, we see that the removal of one of the headgroups has a larger effect on the hydrophobicity of the amphiphile at pH 7.4 than adding a second tail. Additionally, the question arises as to whether the addition of the second tail in the **3CCb1(n,n)** series will change the way the amphiphile partitions into the cell membrane, as the two-tailed amphiphiles structurally resemble the phospholipids that make up the natural structure of a cell membrane.

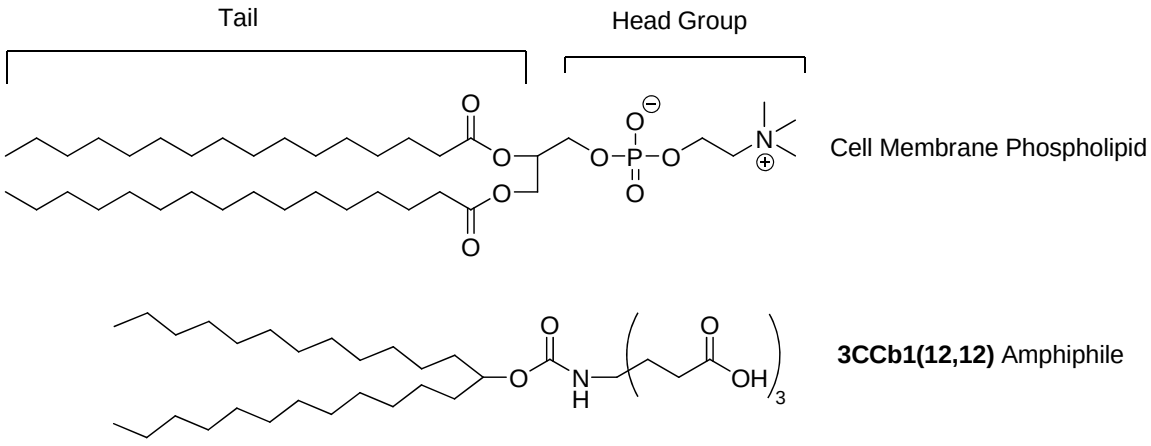

Figure 5-20 Structural comparison of cell membrane phospholipids and **3CCb1(n,n)** amphiphiles

It should be noted that while logD can be predictive for structure-activity relationships,[38] the data is only valid within a given structural template. Therefore, the change in number of headgroups (**3CCbn** vs. **2CCbn**) prevents the comparison of the three homologous series to one another using a logD calculation. As logP values deal with one specific microspecies, we can compare MIC vs. logP values of a given microspecies to determine if hydrophobicity is playing a role in growth inhibition (i.e. does logP (hydrophobicity) correlate with MIC). Figure 5-21 shows the ionization equilibria for **3CCbn** and **2CCbn** at pH 7.4 in water, including the percent microspecies present and the clogP values in parentheses.

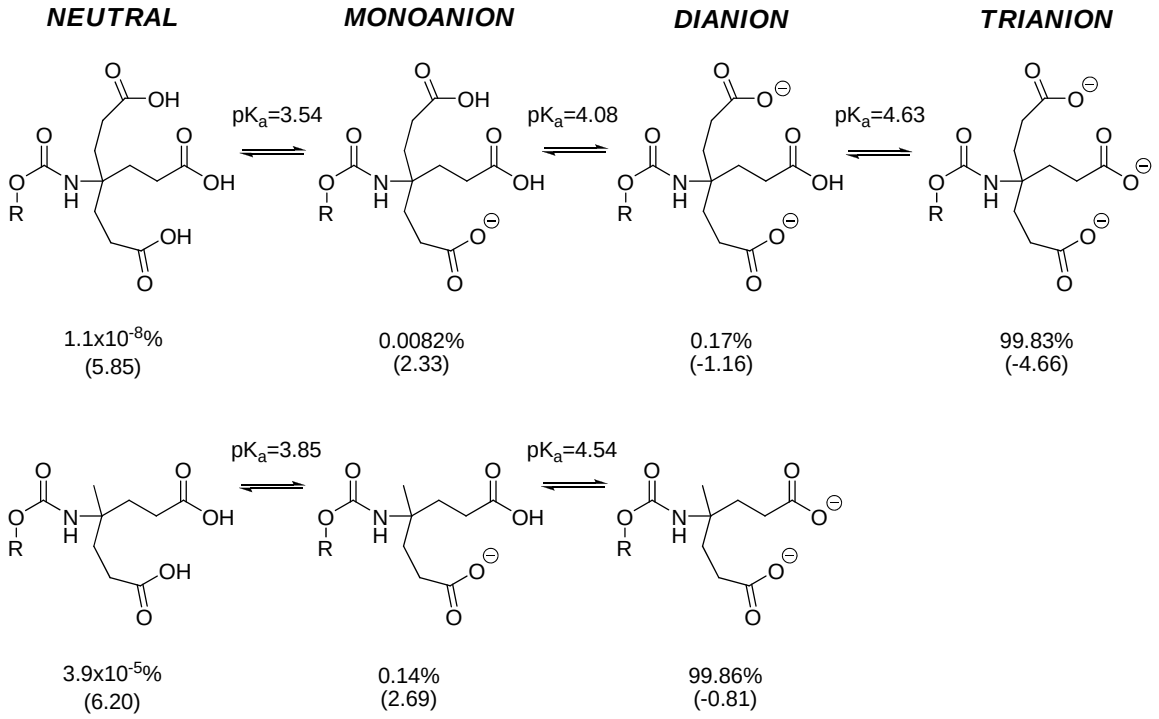

Figure 5-21 Ionization equilibria of **3CCb22** and **2CCb22** in water at pH 7.4. Numbers below the structures are the percent microspecies present and (clogP) values. Data calculated with MarvinSketch 5.1.4.[36]

At physiological pH (7.4), the trianion of the **3CCbn** and **3CCb1(n,n)** series is the dominant microspecies, whereas the dianion is the dominant microspecies for the **2CCbn** series. The clogP values for the dianion microspecies are 3.09 for **2CCb22** and 2.73 for **3CCb22**. The monoanionic and neutral microspecies have similar values of clogP among the two series. The neutral microspecies are hydrophobic (clogP > 3.0) and will partition into a membrane. The most hydrophilic microspecies is the trianion (clogP = -4.66). Any microspecies that partition into a cell and do not return to solution will be regenerated to maintain the equilibrium concentration of the microspecies (LeChâtelier's Principle). Therefore, it does not matter which clogP values we use to compare to the MIC. The following comparison of MIC vs. clogP will use the values for the nonionic microspecies, the standard used for such comparisons.

5.6.3 – Results of anti-Mycobacterial Testing—Correlation of Hydrophobicity with MIC

The collected data for mycobacteria is shown in Table 5-6.

Table 5-6 MIC_{99} and MBC (μM) of two- and three-headed dendritic amphiphiles against *M. smegmatis* strain mc^2155, *M. marinum* strain ATCC 927, and *M. chelonae* strain EO-P-1 [a]

	M. smegmatis		***M. marinum***		***M. chelonae***	
Amphiphile	**MIC_{99}**	**MBC**	**MIC_{99}**	**MBC**	**MIC_{99}**	**MBC**
2CAm19	29	29	30	590	300	
2CAm21	70	53	8.8	550	560	
3CAm13	79		630		59	
3CAm14	110		460		38	
3CAm15	74		590		74	
3CAm16	54		580		72	
3CAm17	53		560		35	
3CAm19	6.3	8.3	50		17	
3CAm21	47		95		130	
3CAm23	90		90		240	

2CCb16	120		320		15
2CCb18	140		280		19
2CCb20	350		830		18
2CCb22	1200		730		180
2CCb30	110		160		210
3CCb14	74		440		55
3CCb16	52		420		70
3CCb18	8.3	8.3	83	520	17
3CCb20	7.9	7.9	16	500	31
3CCb22	120		360		240
3CCb1 (7, 7)	210		840		26
3CCb1 (8, 8)	130		530		25
3CCb1 (9, 9)	97		510		32
3CCb1 (10, 10)	46		180		24
3CCb1 (11, 11)	120		350		240
3CCb1 (12, 12)	110		440		220
3CUr14	37		440		74
3CUr16	35		420		70
3CUr18	6.3	8.3	42	520	17
3CUr20	63		63		47
3CUr22	60		180		480
3CUr (7,7)	110		110		47
3CUr (8,8)	100		35		27
3CUr (9,9)	190		64		48
3CUr (10,10)	95		120		32
3CUr (11,11)	120		120		720
3CUr 1 (7,7)	72		290		54
3CUr 1 (10,10)	46		370		46
3CUr 1 (11,11)	170		690		86

[a] Average of duplicate measurements of two different cultures. Error is ± one twofold dilution where multiple determinations of the MIC gave the same value.

5.6.3.1 – Activity against *M. smegmatis*

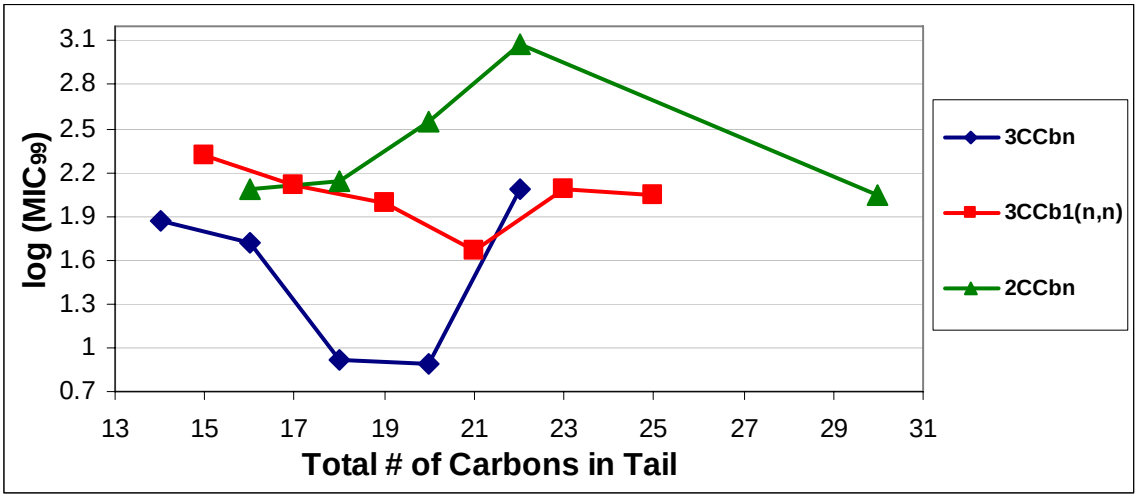

Figure 5-22 Comparison of **3CCbn, 3CCb1(n,n),** and **2CCbn** series MIC_{99} vs. total carbons in tail against *M. smegmatis* strain mc^2155. Lines are eye-guides. Error is ± 0.3.

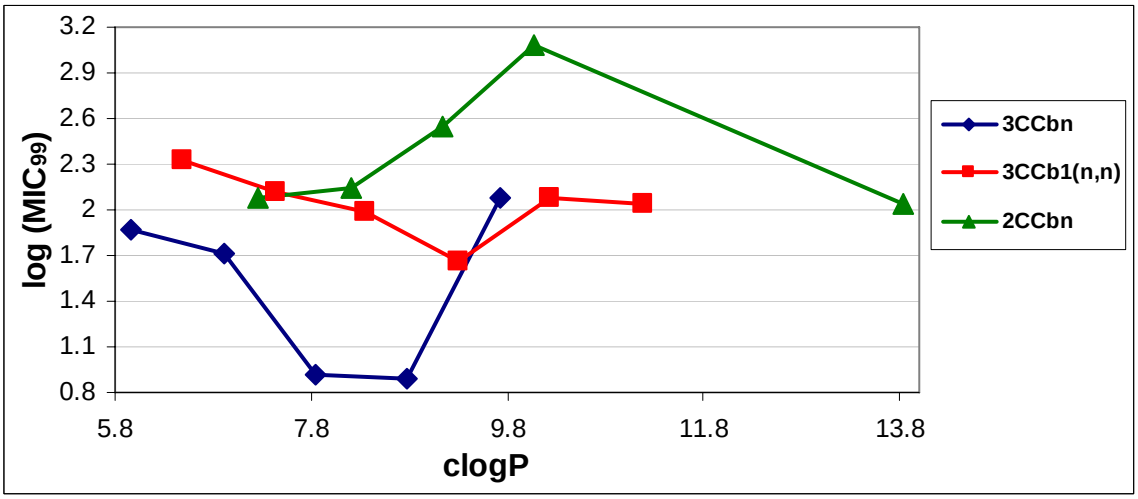

Figure 5-23 Comparison of **3CCbn, 3CCb1(n,n),** and **2CCbn** series MIC_{99} vs. clogP against *M. smegmatis* strain mc^2155. Lines are eye-guides. Error is ± 0.3.

Figure 5-23 shows that the less hydrophilic series are actually weaker inhibitors of growth against *M. smegmatis*. The most effective amphiphiles are **2CCb16** (MIC_{99} = 120 μM, clogP = 7.26), **3CCb20** (MIC_{99} = 7.9 μM, clogP = 8.78) and **3CCb1(10,10)** (MIC_{99} = 46 μM, clogP = 9.30). The **2CCbn** shows a rather strange trend as chain length increases. The MIC rises until **2CCb22** (MIC_{99} = 1200 μM), and then drops 10-fold at

2CCb30 (MIC_{99} = 110 μM). It is possible that there is a minimum occurring between the two amphiphiles. Further synthesis and testing is necessary to confirm this possibility. The other series show similar trends in comparing the three-headed amphiphiles against either the two-headed amphiphiles or the two-tailed amphiphiles.

The comparison of Figures 5-22 and 5-23 also demonstrates that there is no correlation between activity and chain length or hydrophobicity – a stark contrast to the data shown in Figures 5-24 and 5-25.

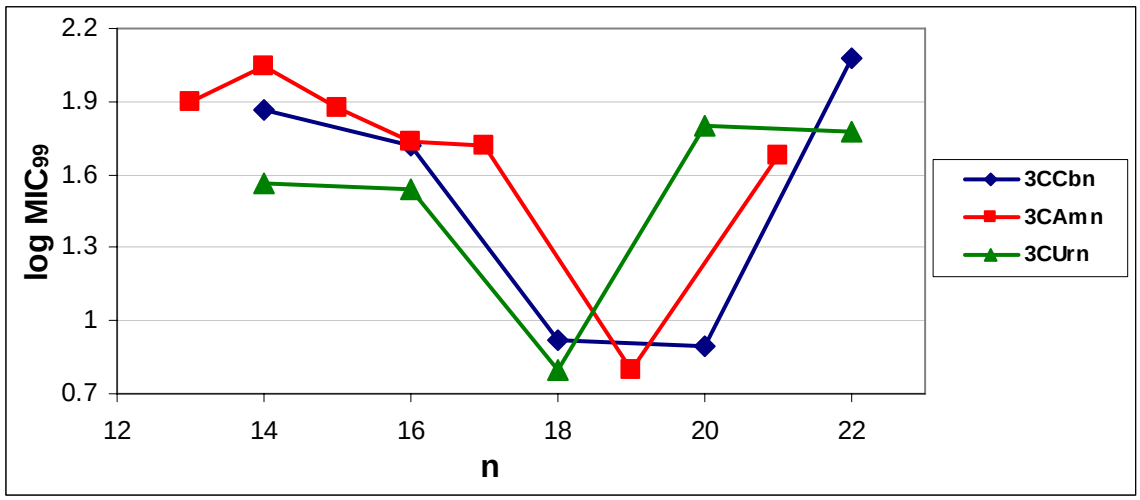

Figure 5-24 log MIC_{99} vs. chain length for the **3CCbn**, **3CAmn,** and **3CUrn** series against *M. smegmatis* strain MC^2 155. Lines are eye-guides. Error is ± 0.3.

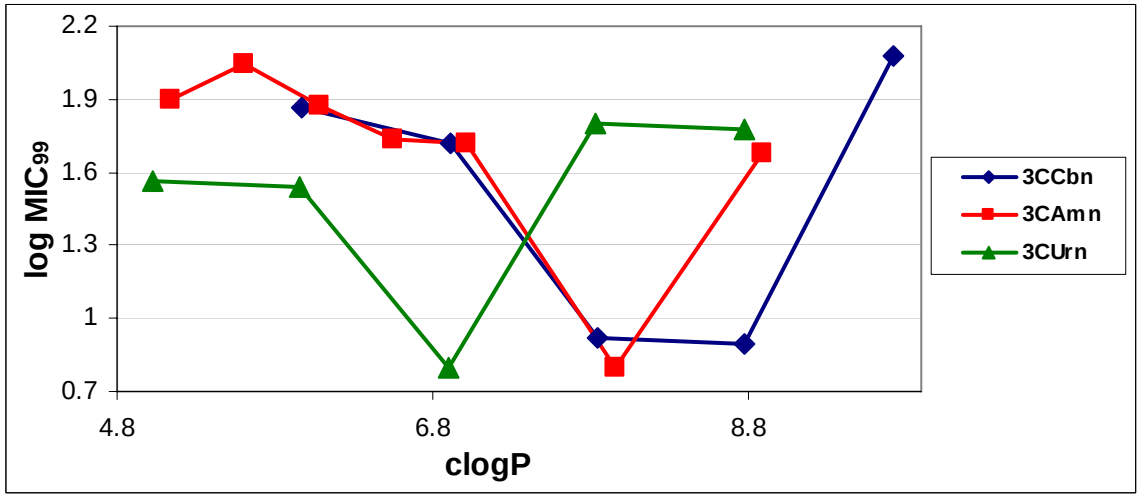

Figure 5-25 log MIC_{99} vs. clogP for the **3CCbn**, **3CAmn,** and **3CUrn** series against *M. smegmatis* strain MC^2 155. Lines are eye-guides. Error is ± 0.3.

The data shown in Figures 5-24 and 5-25 indicate that chain length, not hydrophobicity, are better indicators of activity for these amphiphilic series against *M. smegmatis*. There is a tighter correlation between the series when MIC is compared against chain length as opposed to hydrophobicity, indicating that the linker group is not the dominant factor for determining activity. This seems to indicate the specific chain length of the amphiphile plays some role in inhibition and that the type of linker is of secondary importance.

5.6.3.2 – Activity against *M. marinum*

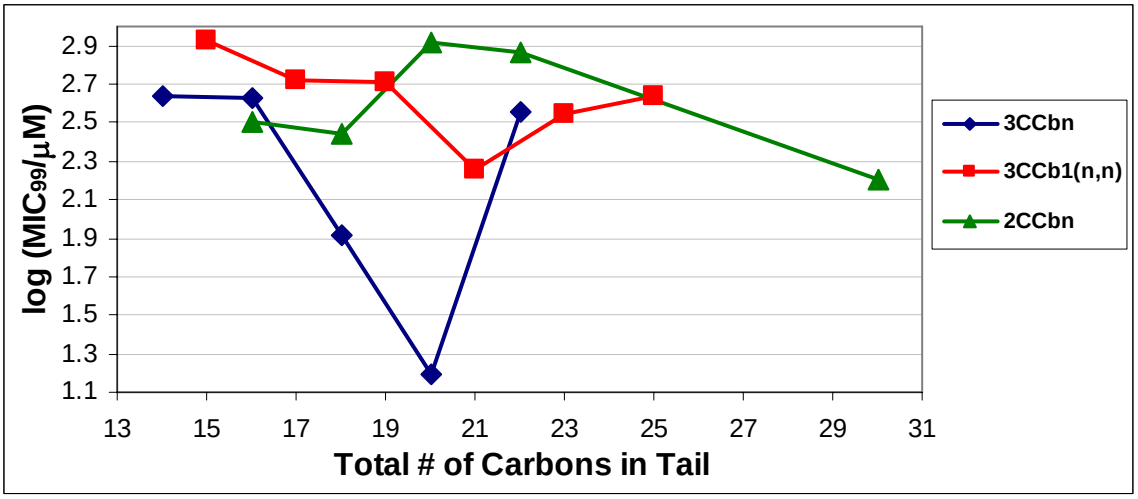

Figure 5-26 Comparison of **3CCbn, 3CCb1(n,n),** and **2CCbn** series MIC_{99} vs. total carbons in tail against *M. marinum* strain ATCC 927. Lines are eye-guides. Error is ± 0.3.

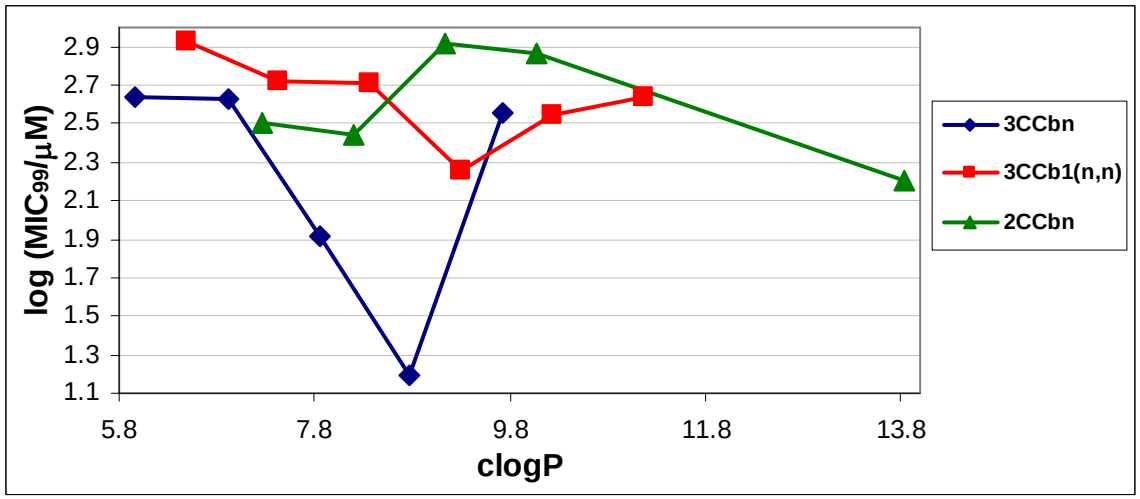

Figure 5-27 Comparison of **3CCbn, 3CCb1(n,n),** and **2CCbn** series MIC_{99} vs. clogP against *M. marinum* strain ATCC 927. Lines are eye-guides. Error is ± 0.3.

Figures 5-26 and 5-27 show the comparison of the **3CCbn** series against the two-tailed (**3CCb1(n,n)**) and two-headed (**2CCbn**) series amphiphiles. The **3CCbn** series clearly gives the best activity (**3CCb20** MIC_{99} = 16μM). The **3CCb1(n,n)** and **2CCbn** series are approximately 10 times less effective at growth inhibition (**3CCb1(10,10)** MIC_{99} = 180 μM, **2CCb30** MIC_{99} = 160 μM). As with the *M. smegmatis* data, we note no correlation between number of carbons in the tail and hydrophobicity.

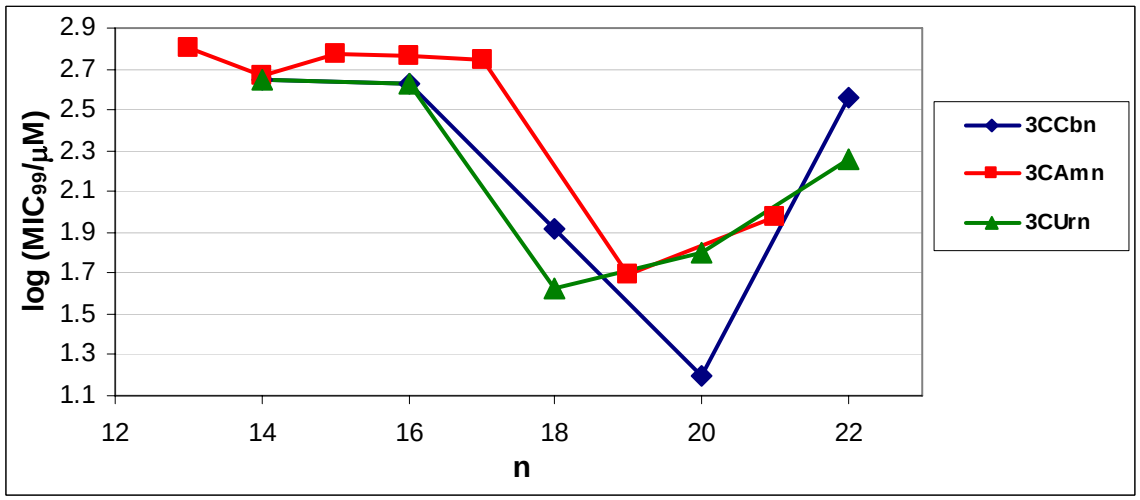

Figure 5-28 log MIC_{99} vs. chain length for the **3CCbn**, **3CAmn,** and **3CUrn** series against *M. marinum* strain ATCC 927. Lines are eye-guides. Error is ± 0.3.

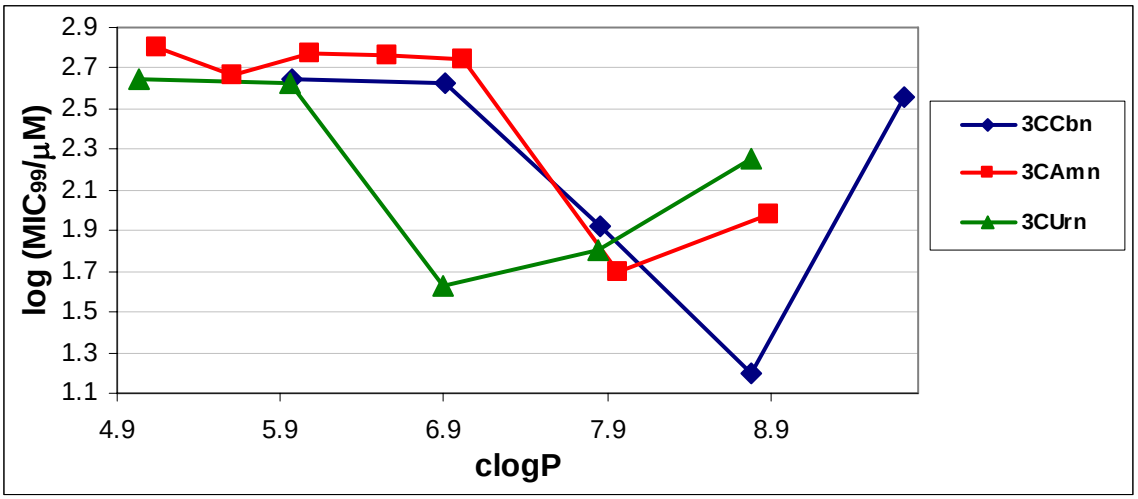

Figure 5-29 log MIC_{99} vs. chain length for the **3CCbn**, **3CAmn,** and **3CUrn** series against *M. marinum* strain ATCC 927. Lines are eye-guides. Error is ± 0.3.

Figures 5-28 and 5-29 show the data for the triheaded amphiphiles against *M. marinum*. The **3CCb20** amphiphile shows the most activity (MIC_{99} = 16μM), followed by **3CUr18** (MIC_{99} = 42μM) and **3CAm19** (MIC_{99} = 50μM). All three series show cutoff effects. As with the *M. smegmatis* data, there is a tighter data correlation when log MIC is compared to chain length, as opposed to clogP.

5.6.3.3 – Activity against *M. chelonae*

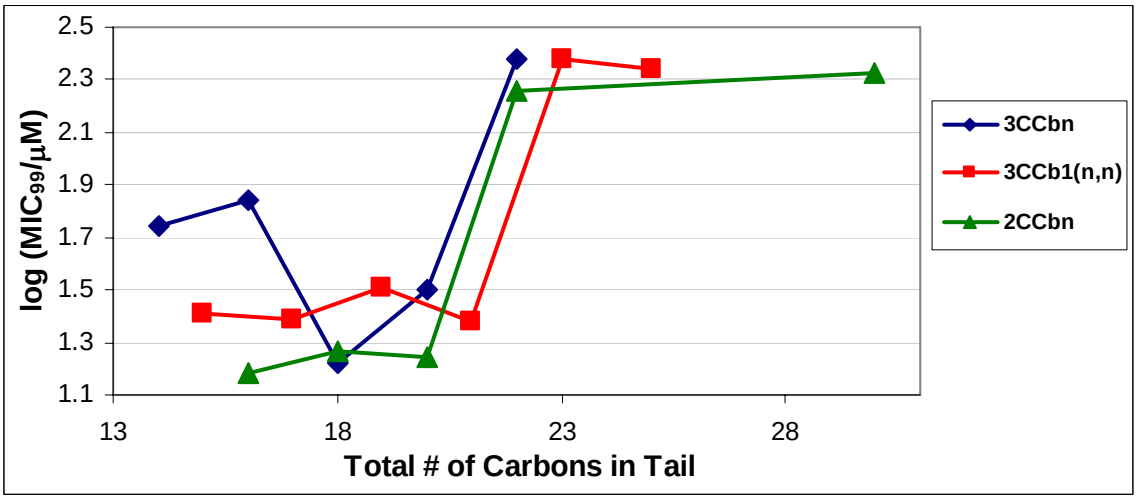

Figure 5-30 Comparison of **3CCbn, 3CCb1(n,n),** and **2CCbn** series MIC_{99} vs. total carbons in tail against *M. chelonae* strain EO-P-1. Lines are eye-guides. Error is ± 0.3.

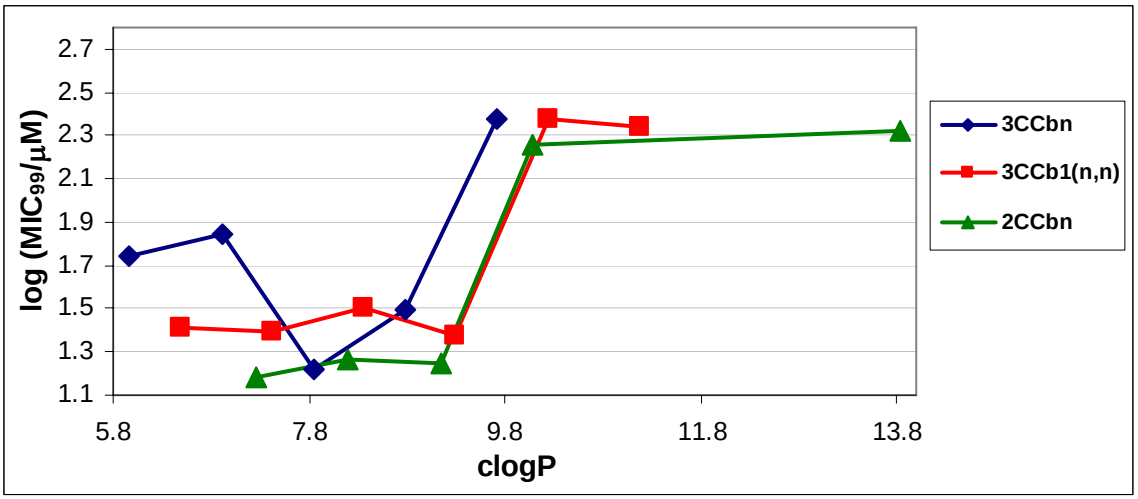

Figure 5-31 Comparison of **3CCbn, 3CCb1(n,n),** and **2CCbn** series MIC_{99} vs. clogP against *M. chelonae* strain EO-P-1. Lines are eye-guides. Error is ± 0.3.

Figures 5-30 and 5-31 present the inhibition data of the various **Cb** series against *M. chelonae*. Against this organism, the **3CCb18** (MIC_{99} = 17μM) and **2CCb16** (MIC_{99} = 15μM) show approximately equivalent activity. The **3CCbn** series shows a definite cutoff at **3CCb18**, whereas the **2CCbn** and **3CCb1(n,n)** series both show a relatively linear response to increasing carbons in the tail until **3CCb1(10,10)** and **2CCb20** are reached, at which time the MIC increases by approximately 10-fold (**3CCb1(11,11)** MIC_{99} = 240μM, **2CCb22** MIC_{99} = 180μM). Again we notice no discernable correlation between MIC and either number of carbons in the tail or hydrophobicity.

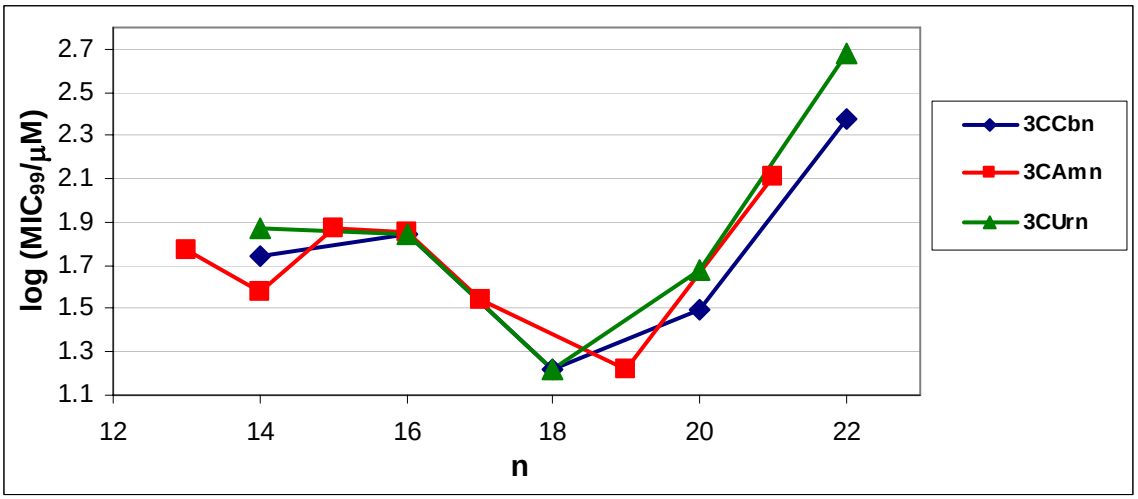

Figure 5-32 log MIC_{99} vs. chain length for the **3CCbn**, **3CAmn,** and **3CUrn** series against *M. chelonae* strain EO-P-1. Lines are eye-guides. Error is ± 0.3.

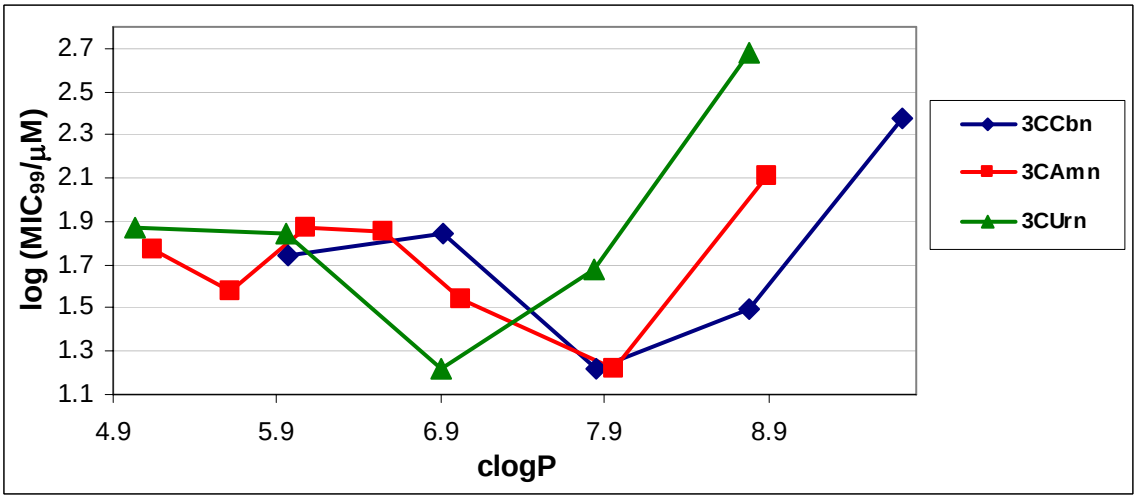

Figure 5-33 log MIC_{99} vs. chain length for the **3CCbn**, **3CAmn,** and **3CUrn** series against *M. chelonae* strain EO-P-1. Lines are eye-guides. Error is ± 0.3.

Figures 5-32 and 5-33 display the inhibition data for the triheaded amphiphiles against *M. chelonae*. All three amphiphilic series show cutoffs for **3CCb18**, **3CAm19**, and **3CUr18** (MIC_{99} = 17µM for all 3). The **3CAmn** series shows an apparent second cutoff at **3CAm14**, however this is within experimental error for the measurement. As with the previous two mycobacteria tested, we note a much tighter data correlation when MIC is compared to carbon chain length instead of hydrophobicity.

5.6.4 – Results of anti-*S. aureus*/MRSA testing—Correlation of Hydrophobicity with MIC

The collected data for inhibition of *S. aureus*/MRSA is shown in Table 5-7.

Table 5-7 MIC_{90} data for **3CCbn**, **2CCbn**, and 2- tailed series against *S. aureus* and MRSA

	MIC_{90} (mM)	
Amphiphile	***S. aureus***	**MRSA**
2CCb16	59	> 1250
2CCb18	4.5	4.5
2CCb20	8.6	4.3
2CCb22	260	260
2CCb30	> 870	> 870
3CCb14	1200 [a]	1200 [a]
3CCb16	230 [a]	600 [a]
3CCb18	60 [a]	43 [a]
3CCb20	9.7 [a]	2.9 [a]
3CCb22	11 [a]	3.5 [a]
3CCb 1 (7, 7)	> 890	> 890
3CCb 1 (8, 8)	> 890	> 890
3CCb 1 (9, 9)	> 890	> 890
3CCb 1 (10, 10)	> 890	> 890
3CCb 1 (11, 11)	> 890	> 890
3CCb 1 (12, 12)	> 890	> 890
3CUr (7,7)	150	1200
3CUr (8,8)	140	1100
3CUr (9,9)	260	530
3CUr (10,10)	500	750
3CUr (11,11)	950	950
3CUr 1 (7,7)	140	1100
3CUr 1 (10,10)	980	980
3CUr 1 (11,11)	930	930

[a] Data from Table 5-5

Error is ± one twofold dilution where multiple determinations of the MIC gave the same value.

The data from Table 5-7 indicates that, unlike the mycobacteria data, the more hydrophobic series (**2CAmn, 2CCbn**) are more active against *S. aureus* and MRSA. The

two-tailed amphiphiles [**3CCb1(n,n), 3CUr(n,n),** and **3CUr1(n,n)**] are extremely ineffective inhibitors in comparison to the other tested amphiphiles. It is clear that the structure of the two-tailed amphiphiles contributes to the inactivity.

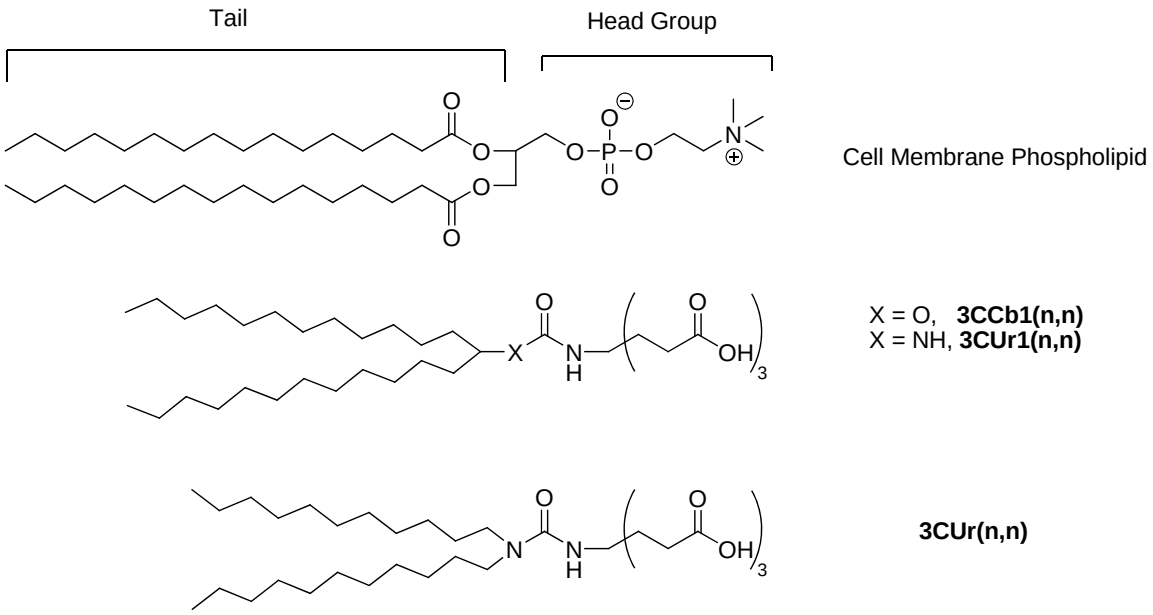

Figure 5-34 Structural comparison of cell membrane phospholipids (DPPC shown) and two-tailed amphiphiles.

As Figure 5-34 shows, the longest chain homologues of the two-tailed compounds (**3CCb1(12,12), 3CUr1(12,12)**, and **3CUr(11,11)** are still "shorter" in length than the example phospholipid shown (dipalmitoylphosphatidylcholine, DPPC). This could possibly create dead space in the cell membrane, referred to as free volume (cf. Chapter 1),[39,40] which would lead to decreased inhibitory activity. There is also a difference in the way the tails are connected to the "linker" atoms when these amphiphiles are compared to phospholipids. The phospholipid tails are attached to the headgroup via a glycerol (1,2,3-trihydroxypropyl) backbone. This allows the tails to pack as closely together as possible, forming parallel chains. The way the tails are connected to the linker group in the amphiphilic series prevents the formation of the parallel chains seen in phospholipids,

instead forming a "V" shape. This would create free volume, as the tails would not be able to pack as closely together, and may completely prevent the tails of the amphiphiles from inserting into the membrane due to steric bulk.

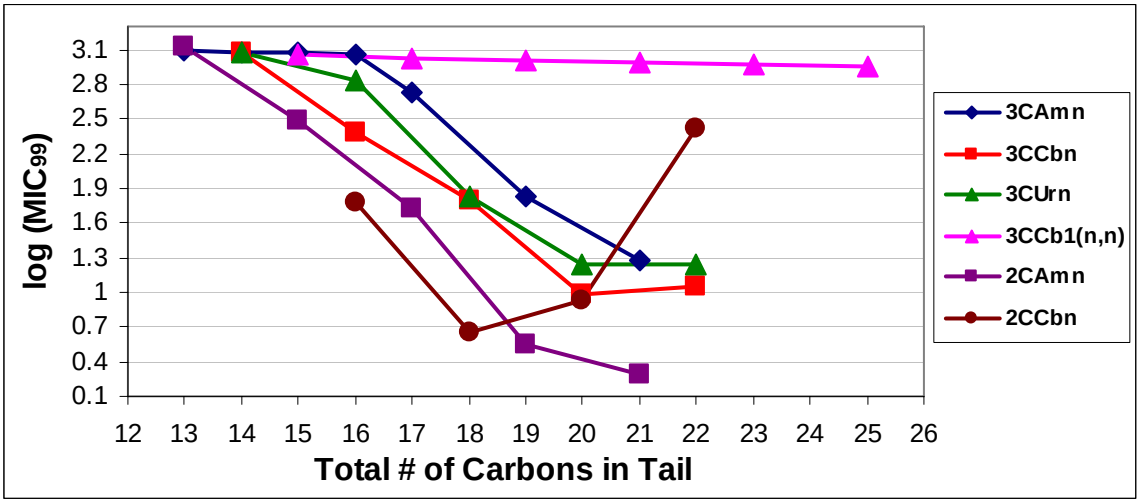

Figure 5-35 log MIC_{90} vs. number of carbons in the tail group for various amphiphiles against *S. aureus*. Lines are eye-guides. Error is ± 0.3.

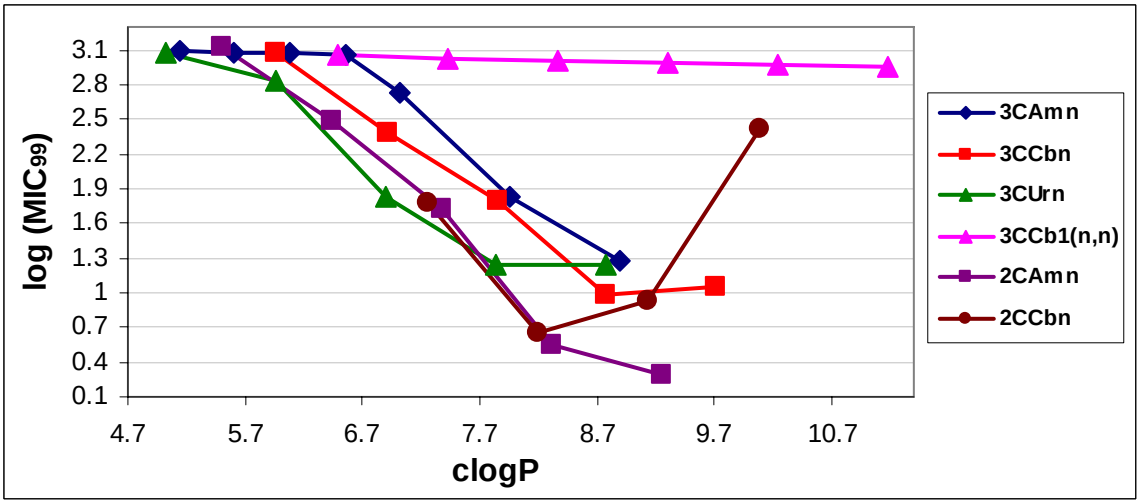

Figure 5-36 log MIC_{90} vs. clogP for various amphiphiles against *S. aureus*. Lines are eye-guides. Error is ± 0.3.

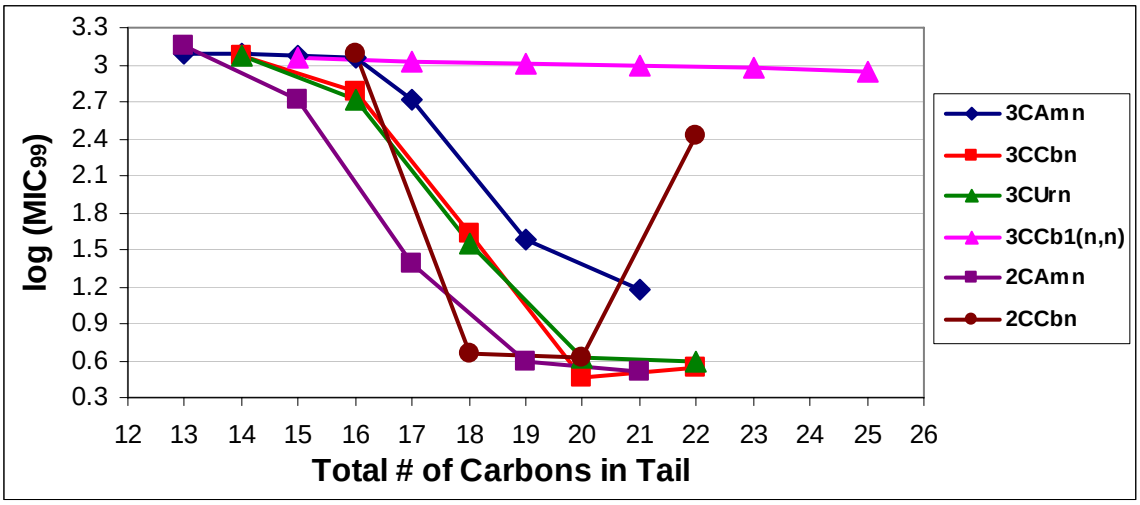

Figure 5-37 log MIC_{90} vs. number of carbons in the tail group for various amphiphiles against MRSA. Lines are eye-guides. Error is ± 0.3.

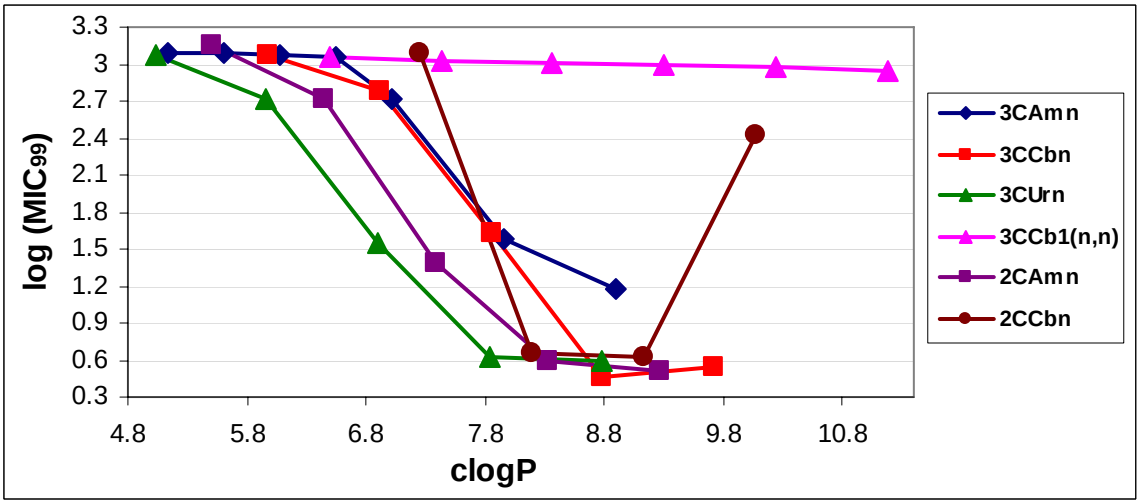

Figure 5-38 log MIC_{90} vs. clogP for various amphiphiles against MRSA. Lines are eye-guides. Error is ± 0.3.

Figures 5-35 – 5-38 show that, in contrast to the mycobacteria data, the inhibition of *S. aureus* and MRSA are more dependent on hydrophobicity than chain length. The data has greater scatter in the log MIC vs. chain length graphs with no apparent correlation. When the log MIC_{90} vs. clogP data is plotted we see that the more hydrophobic amphiphiles (**3CAmn** and **3CCbn**) cluster together – and at higher clogP values – than the more hydrophilic amphiphiles (**3CUrn** and **2CAmn**). The **2CCbn**

series clusters with the hydrophilic series for *S. aureus* and with the hydrophobic series for MRSA. Once again, most single-tail amphiphiles reach maximal activity when clogP ranges from 7.8 to 9.8. The **3CAmn** series is still decreasing for the longest chain homologue for *S. aureus* and MRSA and the **2CAmn** series is still decreasing for *S. aureus*. This suggests that longer chain homologues of the amido isostere – especially the **2CAmn** series – may show greater activity than what has been observed.

5.7 – COMPARISON OF CMC TO MIC

5.7.1 – Effect of Solution pH Changes Between CMC and MIC Measurements

In order to compare the CMC data to the MIC data, we need to ensure that the ionization of the headgroups is constant across the pH range at which the CMC and MIC testing is conducted. If at pH 9–10 (the pH of the solution used for CMC testing) all the headgroups are fully ionized, but at pH 7.4 (the pH used for biological testing) only one or two of the headgroups are ionized, then it follows that the CMC should be lower at the lower pH of the MIC tests due to decreased solubility. This would limit our ability to determine if the CMC is actually higher than the MIC and would hinder a determination as to whether the amphiphile is acting via detergency or some specific interaction. Recent work in our group has shown that at pH 7.4 the CMCs of the **3CUr16** and **3CAm21** decrease by two- and four-fold (respectively) from that seen at pH 9.[41] For this discussion, we assume that the other members of the amphiphilic series will show similar pH dependencies.

5.7.2 – Discussion of MIC/CMC Relationship

Figure 5-39 shows a comparison of CMC and MIC vs. chain length for the **3CCbn** series for the vaginal microbicide focused study. The CMC data presented have been corrected to pH 7.4 by lowering the CMC obtained at pH 9 three-fold.

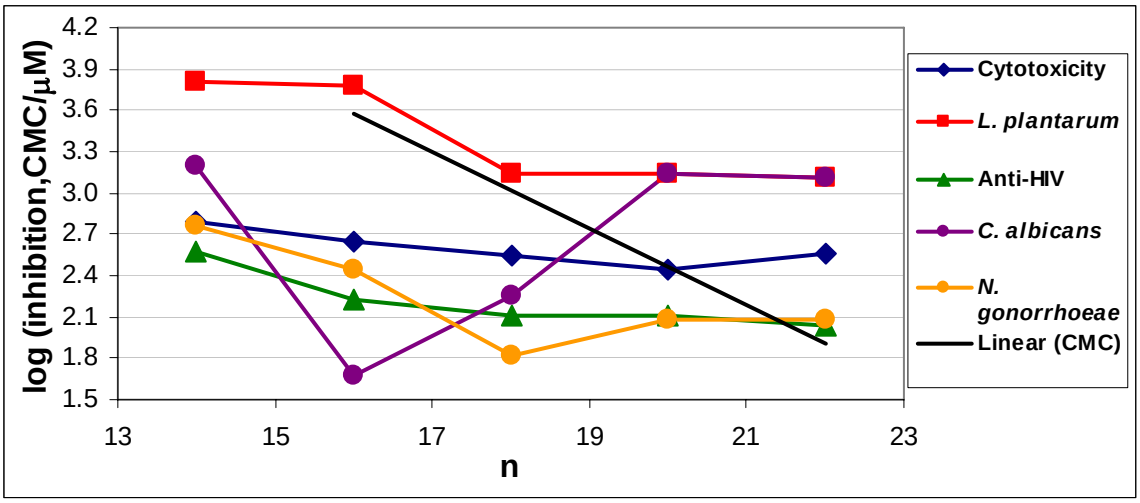

Figure 5-39 Comparison of CMC and MIC_{99} vs. chain length for **3CCbn** series. Lines are eye-guides. Error is ± 0.3 for MIC data.

Activity against *N. gonorrhoeae* and HIV remains below the CMC for all homologues except **3CCb22**. Activity against *C. albicans* is below the CMC for homologues up to 18 carbons in the tail, at which point the activity rises above the CMC for the **3CCb20** and **3CCb22** homologues. Cytotoxicity is below the CMC for all homologues except **3CCb22**. Given that the activity does not generally parallel the CMC (activity does not increase as CMC decreases) and there is a cutoff effect for some homologues (e.g. *N. gonorrhoeae* for **3CCb18**), this tends to suggest that the amphiphilic activity is not due to detergency. As a measure of safety, Vieira *et al.* note that target values for the CMC/MIC ratio should be ≥ 100 for optimal safety.[1] For *N. gonorrhoeae*, this ratio is ~ 16 for **3CCb18**. Against *C. albicans* **3CCb16** has a CMC/MIC ratio of ~82.

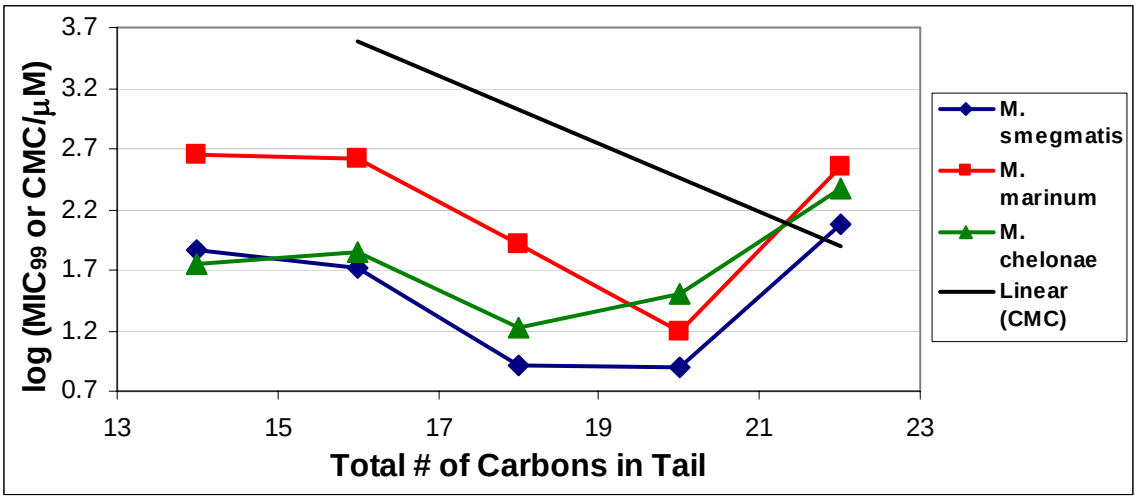

Figure 5-40 MIC_{99} and CMC vs. chain length for **3CCbn** series against various species of mycobacteria. Lines are eye-guides. Error is ± 0.3 for MIC data.

Figure 5-40 shows a similar trend for the **3CCbn** series against various mycobacteria as that seen in the anti-HIV study. For all three mycobacteria studied, the activity lies well below the CMC up to n = 20 carbons, and rises to the CMC for the 22 carbon chain homologue (**3CCb22**). The CMC/MIC ratio is best for **3CCb18** against *M. smegmatis* (~ 126) and *M. chelonae* (~ 63). The best CMC/MIC ratio for *M. marinum* is seen for **3CCb20** (~17).

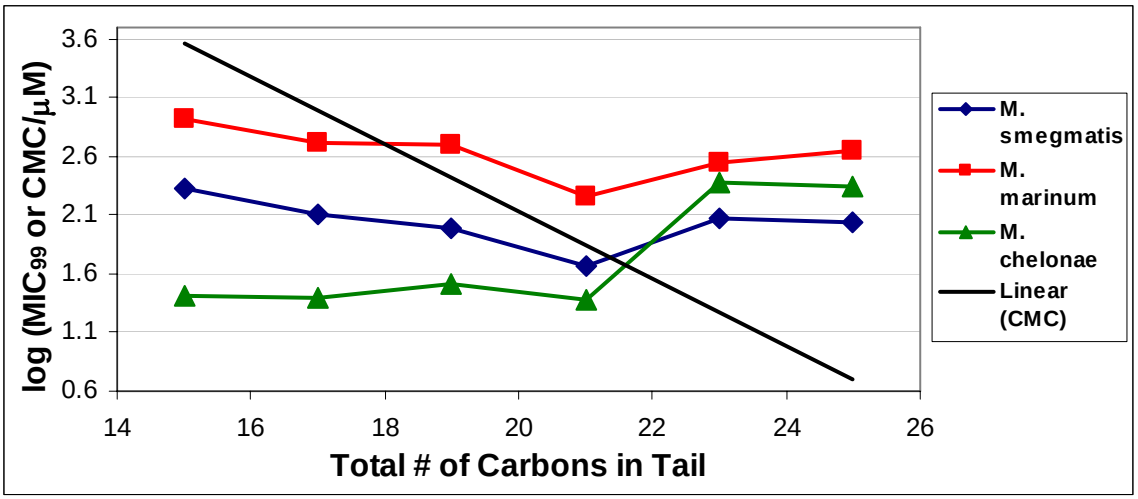

Figure 5-41 MIC_{99} and CMC vs. chain length for **3CCb1(n,n)** series against various species of mycobacteria. Lines are eye-guides. Error is ± 0.3 for MIC data.

Figure 5-41 presents the mycobacteria/CMC data for the **3CCb1(n,n)** series. The most active compound of the series, **3CCb1(10,10)**, shows CMC/MIC ratios of ~1.5 for *M. smegmatis*, ~2.9 for *M. chelonae*, and 0.39 for *M. marinum*. The proximity of the CMC to the MIC of the **3CCb1(n,n)** series could indicate that the inhibition is caused by detergency.

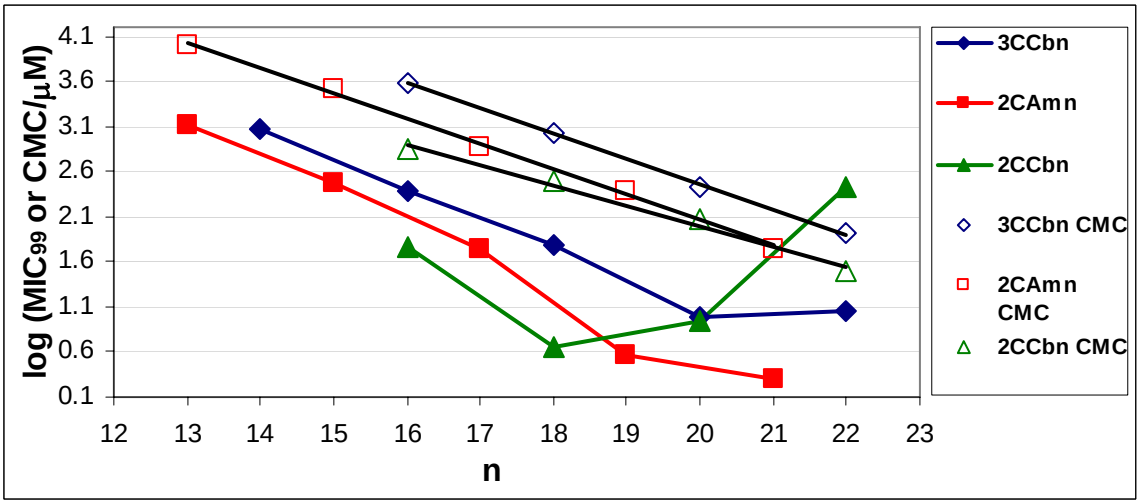

Figure 5-42 MIC_{99} and CMC vs. chain length for various amphiphiles against *S. aureus*. Lines are eye-guides. Error is ± 0.3 for MIC data.

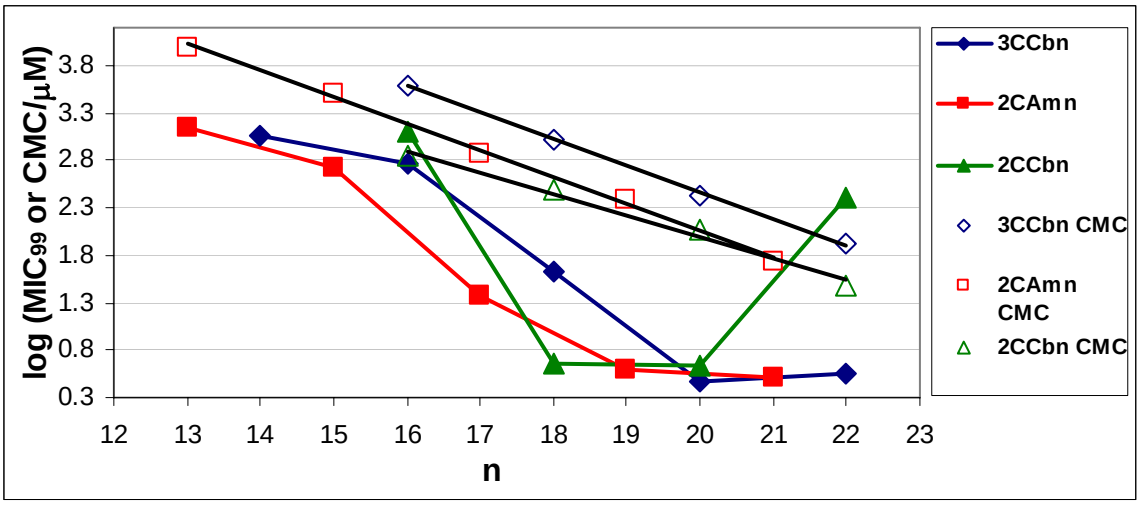

Figure 5-43 MIC_{99} and CMC vs. chain length for various amphiphiles against MRSA. Lines are eye-guides. Error is ± 0.3 for MIC data.

Figures 5-42 and 5-43 show MIC/CMC relationships for two- and three-headed amphiphiles against *S. aureus* and MRSA. Activity for the most active amphiphiles in each series lies well below the CMC, with CMC/MIC ratios for *S. aureus* of ~68 for **2CCb18**, ~68 for **2CAm19**, and ~14 for **3CCb20**. CMC/MIC ratios for MRSA are ~68 for **2CCb18**, ~27 for **2CAm19**, and ~93 for **3CCb20**. Only the **2CCbn** series shows a cutoff, with **3CCbn** and **2CAmn** either no longer changing or continuing to decrease up to the longest chain length homologue.

5.8 – EXPERIMENTAL

5.8.1 – Broad Screen Testing

Determination of MICs for the broad screen testing have been previously described.[2]

5.8.2 – Amphiphiles as Potential Vaginal Microbicides

HIV inhibition, cytotoxicity assays, and MIC measurements against *N. gonorrhoeae* have been previously described.[41]

5.8.3 – Amphiphiles as Potential anti-Mycobacterial Agents

MIC measurements against *mycobacteria* from the study of the inoculum effect have been previously described.[3]

5.8.4 – Amphiphiles as Potential anti-Infectives against *S. aureus* and MRSA.

5.8.4.1 – Stock Solutions of Dendritic Amphiphiles

Stock solutions (12,500 mg/L) for all homologues were prepared by vortexing the di- and tricarboxylic acids in the aqueous triethanolamine solution (5% w/v). Final stock concentrations ranged from 20,800 to 31,300 μM depending on the formula weight of the homologue.

5.8.4.2 – Bacterial Strains.

S. aureus strain ATCC 6358 and an unrelated MRSA strain ATCC 43330 were acquired from Danville Community Hospital. Six recent patient isolates of MRSA (523000, 522870, 34864, 36361, 53016, 34380) were obtained from Georgetown University Medical Center Hospital. Collection of MRSA from adults was approved by the Institutional Review Board of Georgetown University Medical Center.

5.8.4.3 – Measurement of MIC

MIC measurements were performed as described,[2] with the single modification of dilution of cultures in growth medium (ten- to 100000-fold). Undiluted cultures and dilutions were used as inocula for MIC measurements.

5.8.4.4 – Quality Assurance

All cultures used as inocula were uncontaminated and the colonies had the expected morphologies. Cultures used for inoculation were stored up to 4 d at 4 °C until used without any differences in experimental results.

5.9 – REFERENCES

(1) Vieira, O. V.; Hartmann, D. O.; Cardoso, C. M. P.; Oberdoerfer, D.; Baptista, M.; Santos, M. A. S.; Almeida, L.; Ramalho-Santos, J. o.; Vaz, W. L. C. *PLoS ONE* **2008**, *3*, e2913.

(2) Williams, A. A.; Sugandhi, E. W.; Macri, R. V.; Falkinham, J. O., III; Gandour, R. D. *J. Antimicrob. Chemother.* **2007**, *59*, 451-458.

(3) Sugandhi, E. W.; Macri, R. V.; Williams, A. A.; Kite, B. L.; Slebodnick, C.; Falkinham, J. O.; Esker, A. R.; Gandour, R. D. *J . Med. Chem.* **2007**, *50*, 1645-1650.

(4) Brook, I. *Rev. Infect. Dis.* **1989**, *11*, 361-368.

(5) Gehrt, A.; Peter, J.; Pizzo, P. A.; Walsh, T. J. *J. Clin. Microbiol.* **1995**, *33*, 1302-1307.

(6) Soriano, F. *J. Antimicrob. Chemother.* **1992**, *30*, 566-569.

(7) Sherris, J. C.; 4th ed.; Ryan, K. J., Ray, C. G., Eds.; McGraw-Hill Professional: New York, 2004.

(8) Kieser, T., *Mycobacterium smegmatis*, 2009, http://www.jic.ac.uk/SCIENCE/molmicro/Myco.html, last accessed February 19th, 2009

(9) *SGD project. "Saccharomyces Genome Database"*, http://www.yeastgenome.org/, last accessed February 19th, 2009

(10) King, J. W.; Dasgupta, A., *Cryptococcosis*, 2007, http://emedicine.medscape.com/article/215354-overview, last accessed February 19th, 2009

(11) Pichardo, C.; Rodrıguez-Martınez, J. M.; Pachon-Ibanez, M. E.; Conejo, C.; Ibanez-Martınez, J.; Martınez-Martınez, L.; Pachon, J.; Pascual, A. *Antimicrob. Agents Chemother.* **2005**, *49*, 3311-3316.

(12) Kaur, D.; Khuller, G. K. *Int. J. Antimicrob. Agents* **2001**, *17*, 51-55.

(13) Zerva, L.; Hollis, R. J.; Pfaller, M. A. *J. Clin. Microbiol.* **1996**, *34*, 3031-3034.

(14) Barchiesi, F.; Spreghini, E.; Baldassarri, I.; Marigliano, A.; Arzeni, D.; Giannini, D.; Scalise, G. *Antimicrob. Agents Chemother.* **2004**, *48*, 4056-4058.

(15) Aller, A. I.; Martin-Mazuelos, E.; Lozano, F.; Gomez-Mateos, J.; Steele-Moore, L.; Holloway, W. J.; Gutierrez, M. J.; Recio, F. J.; Espinel-Ingroff, A. *Antimicrob. Agents Chemother.* **2000**, *44*, 1544-1548.

(16) *OVERVIEW OF THE GLOBAL AIDS EPIDEMIC: 2006 REPORT ON THE GLOBAL AIDS EPIDEMIC*, Joint United Nations Programme on HIV/AIDS, 2006, http://data.unaids.org/pub/GlobalReport/2006/2006_GR_CH02_en.pdf, last accessed February 27th, 2009

(17) Fichorova, R. N.; Bajpai, M.; Chandra, N.; Hsiu, J. G.; Spangler, M.; Ratnam, V.; Doncel, G. F. *Biol. Reprod.* **2004**, *71*, 761-769.

(18) Hillier, S. L.; Moench, T.; Shattock, R.; Black, R.; Reichelderfer, P.; Veronese, F. J. *J. Acquir. Immune Defic. Syndr.* **2005**, *39*, 1-8.

(19) Van Damme, L.; Ramjee, G.; Alary, M.; Vuylsteke, B.; Chandeying, V.; Rees, H.; Sirivongrangson, P.; Mukenge-Tshibaka, L.; Ettiegne-Traore, V.; Uaheowitchai, C.; Karim, S. S.; Masse, B.; Perriens, J.; Laga, M. *Lancet* **2002**, *360*, 971-977.
(20) Robbins, S. L. In *Robbins Basic Pathology*; 8th ed.; Kumar, V., Abbas, A. K., Fausto, N., Mitchell, R., Eds.; Saunders Publishing: Philadelphia, PA, 2007.
(21) Boris, S.; Suárez, J. E.; Vázquez, F.; Barbés, C. *Infect Immun.* **1998**, *66*, 1985-1989.
(22) *HIV and Its Treatment: What You Should Know - Health Information for Patients*, U.S. Department of Health and Human Services, 2008, http://aidsinfo.nih.gov/ContentFiles/HIVandItsTreatment_cbrochure_en.pdf, last accessed January 31st, 2009
(23) Saitoh, A.; Hull, A. D.; Franklin, P.; Spector, S. A. *J. Perinatol.* **2005**, *25*, 555-556.
(24) Souza, L. C.; Campa, A. *J. Antimicrob. Chemother.* **1999**, *44*, 77-84.
(25) Li, R. C.; Ma, H. H. M. *J. Chemother.* **1998**, *10*, 203-207.
(26) Sakoulas, G.; Moise-Broder, P. A.; Schentag, J.; Forrest, A.; Robert C. Moellering, J.; Eliopoulos, G. M. *J. Clin. Microbiol.* **2004**, *42*, 2398–2402.
(27) Chapman, S. W.; Steigbigel, R. T. *J. Infect. Dis.* **1983**, *147*, 1078-1089.
(28) LaPlante, K. L.; Rybak, M. *J. Antimicrob. Agents Chemother.* **2004**, *48*, 4665-4672.
(29) Cantoni, L.; Glauser, M. P.; Bille, J. *Antimicrob. Agents Chemother.* **1990**, *34*, 2348-2353.
(30) Sullam, P. M.; Drake, T. A.; Tauber, M. G.; Hackbarth, C. J.; Sande, M. A. *Antimicrob. Agents Chemother.* **1985**, *27*, 320-323.
(31) Stevens, D. L.; Gibbons, A. E.; Bergstrom, R.; Winn, V. *J. Infect. Dis.* **1988**, *158*, 23-28.
(32) Stevens, D. L.; Maier, K. A.; Laine, B. M.; Mitten, J. E. *J. Infect. Dis.* **1987**, *155*, 220-228.
(33) Scheld, W. M.; Sande, M. A. In *Principles and Practice of Infectious Diseases*; 4th ed.; Mandell, G. L., Bennett, J. E., Dolin, R., Eds.; Churchill Livingstone: New York, 1995, p 740-782.
(34) Mizunaga, S.; Kamiyama, T.; Fukuda, Y.; Takahata, M.; Mitsuyama, J. *J. Antimicrob. Chemother.* **2005**, *56*, 91-96.
(35) *MarvinSketch User's Guide - logP and logD Calculation*, http://chem.sis.nlm.nih.gov/chemidplus/applet/marvin/chemaxon/marvin/help/logPlogD.html#Ref1, last accessed March 27th, 2009
(36) *Marvin Sketch (pKa, logP, and logD calculator), v.* 5.1.4, ChemAxon, http://intro.bio.umb.edu/111-112/OLLM/111F98/newclogp.html, last accessed February 13, 2009
(37) Stanley, W. M.; Coleman, G. H.; Greer, C. M.; Sacks, J.; Adams, R. *J. Pharm. Exper. Ther.* **1932**, *45*, 121-162.
(38) Scherrer, R. A.; Howard, S. M. *J. Med. Chem.* **1977**, *20*, 53-58.
(39) Balgavy, P.; Devinsky, F. *Adv. Colloid Interface Sci.* **1996**, *66*, 23-63.

(40) Williams, A. A. Syntheses, Characterization, Physical and Biological Properties of Long-chain, Water-soluble, Dendritic Amphiphiles. PhD Dissertation, Department of Chemistry, Virginia Polytechnic Institute and State University, Blacksburg, VA, 2008.
(41) Macri, R. V.; Karlovská, J.; Doncel, G. F.; Du, X.; Maisuria, B. B.; Williams, A. A.; Sugandhi, E. W.; III, J. O. F.; Esker, A. R.; Gandour, R. D. *Bioorg. Med. Chem.* **2009**, *17*, 3162-3168.

CHAPTER 6 – CONCLUSIONS AND FUTURE WORK

6.1 – SUMMARY

Synthesis of the target amphiphiles, **3CCbn** and **3CCb1(n,n)**, was achieved in two steps from Weisocyanate™ and the single or two-tailed symmetric alcohol, respectively. We have synthesized 10 new single-tail amphiphiles and precursors (**3ECbn** and **3CCbn** series) and 12 new two-tail amphiphiles and precursors (**3ECb1(n,n)** and **3CCb1(n,n)** series). Synthesis of the **3CCb1(n,n)** series was improved over that of the **3CCbn** series by changing from formic to trifluoroacetic acid during the solvolysis of the *tert*-butyl groups in **3ECb1(n,n)**. Final product yields of the **3CCbn** and **3CCb1(n,n)** series were good (59–84% from Weisocyanate™ and either alkan-1-ol or the two-tailed symmetric alcohol, respectively), and all compounds were fully characterized by melting point, 1H and 13C NMR, IR, high res. Mass Spec, and elemental analysis.

The CMC measurements of the dendritic amphiphiles by using pendent-drop analysis are accomplished relatively easily in comparison with the Wilhelmy plate method, and require far less material to obtain the data. However, it has been shown through a pyrene fluorescence technique that surface tension may not be the best way to obtain the CMC data. In comparison to pyrene fluorescence, the breaks in the surface tension data are typically either not very sharp, or there is a loss of linearity before and/or after the break, making accurate determination of the CMC by surface tension measurements difficult.

As expected, the three-headed amphiphiles show higher CMC values due to increased water solubility as compared to the fatty acid and malonic acid derivatives

measured by Shinoda[1,2] and Bashura[3] and the two-headed amphiphiles measured by Marcelo Actis.[4] We do not note any differences in plots of log CMC vs. carbon chain length from changes in the linker group, which suggests that this structural difference among the three homologous series of amphiphiles does not affect the micellization point. The relatively higher CMCs of the dendritic amphiphiles in comparison with the fatty acid analogs suggest that these amphiphiles may not have a detergency effect when antimicrobial studies are performed, as the MICs are not likely to be higher than the CMCs. The ability to solubilize ultra long-chain hydrocarbons ($n \geq 20$) with the dendritic headgroup suggests that studies with even longer chain hydrocarbon tails can be undertaken to see if CMC can be further increased.

The CMCs for the **3CCb1(n,n)** series needs to be measured via a second method to verify the accuracy of the data. The **3CCb1(11,11)** amphiphile, specifically, seems to show too high of a CMC in relation to the **3CCb1(9,9)**, **3CCb1(10,10)**, and **3CCb1(12,12)** amphiphiles. In several cases, as seen with the single-tail amphiphiles, it is too difficult to determine whether a break has occurred, which makes accurate assignment of a CMC problematic, and therefore limits any analysis of the data. The **3CCb1(12,12)** amphiphile showed a precipitous drop in the surface tension over a very narrow concentration range. Further studies of the surface tension of the **3CCb1(13,13)** and longer chain length amphiphiles are warranted to determine if this effect is specific to this particular amphiphile or is a function of all the amphiphiles of this structure over a given carbon chain length.

The relatively high CMCs of these dendritic amphiphiles in comparison with the fatty acid analogs suggest that these amphiphiles do not have a detergency effect, as the MICs are typically not higher than the CMCs. The ability to solubilize ultra long-chain hydrocarbons ($n \geq 20$) with the dendritic headgroup suggests that studies with even longer chain hydrocarbon tails can be undertaken to see if CMC can be further increased.

The proper choice of counter-ion has enabled us to overcome solubility issues and produce long-chain amphiphiles that are effective against a variety of microorganisms. From the initial broad screen testing and our discovery of the inoculum effect, we determined that these amphiphiles show promise as anti-infectives. The 18–20 carbon chain homologue of each series appears to be the most active of the series. Additionally, most of the active amphiphiles show some type of cutoff effect. These two observations point toward some specific mechanism of inhibition where the 18–20 carbon chain homologue has the greatest effect. This theory is supported when MIC is compared to CMC and no observable correlation between activity and micelle formation appears.

We have explored the effect of changing hydrophobicity by reducing the number of headgroups or increasing the number of tails. Reducing the number of headgroups had mixed effects—either increasing or decreasing the MIC from that of the three-headed homologue—depending on the type of organism. The two-tailed amphiphiles showed generally less ability to inhibit organism growth.

The comparison of MIC to CMC gives a potential measure of safety of these compounds. All of the most active amphiphiles showed good MIC/CMC ratios, indicating that detergency was probably not a factor in organism growth inhibition. While the efficacy of these amphiphiles toward individual organisms varied, the data

collected indicate that further efforts into improving the MICs of these amphiphiles are warranted.

6.2 – REFERENCES

(1) Shinoda, K. *J. Phys. Chem.* **1954**, *58*, 1136-1141.

(2) Shinoda, K. *J. Phys. Chem.* **1955**, *59*, 432-435.

(3) Bashura, A. G.; Klimenko, O. I.; Nurimbetov, K. N.; Gladukh, E. V. *Farmatsevtichnii Zhurnal (Kiev)* **1989**, *3*, 57-58.

(4) Actis, M. L. Synthesis, Characterization, Critical Micelle Concentration and Biological Activity of two-Headed Amphiphiles. M.S., Chemistry, Virginia Polytechnic Institute and State University, Blacksburg, 2008.